Development and validation of bubble dynamics models for Hydrodynamic Ram event in fuel tanks

Thomas Fourest

▶ **To cite this version:**

Thomas Fourest. Development and validation of bubble dynamics models for Hydrodynamic Ram event in fuel tanks. Materials. Université de Bretagne occidentale - Brest, 2015. English. NNT : 2015BRES0054 . tel-01264361v2

HAL Id: tel-01264361
https://hal.science/tel-01264361v2

Submitted on 11 Dec 2018

HAL is a multi-disciplinary open access archive for the deposit and dissemination of scientific research documents, whether they are published or not. The documents may come from teaching and research institutions in France or abroad, or from public or private research centers.

L'archive ouverte pluridisciplinaire **HAL**, est destinée au dépôt et à la diffusion de documents scientifiques de niveau recherche, publiés ou non, émanant des établissements d'enseignement et de recherche français ou étrangers, des laboratoires publics ou privés.

THÈSE / UNIVERSITÉ DE BRETAGNE OCCIDENTALE
sous le sceau de l'Université européenne de Bretagne

pour obtenir le titre de
DOCTEUR DE L'UNIVERSITÉ DE BRETAGNE OCCIDENTALE
Mention : Mécanique des Fluides
École Doctorale des Sciences de la Mer

présentée par

Thomas Fourest

Préparée à L'Onera et l'ENSTA-Bretagne

Development and validation of bubble dynamics models for Hydrodynamic Ram event in fuel tanks

Thèse soutenue le 05/11/15

devant le jury composé de :

Bruno Blanke
Chercheur CNRS, LPO / Président du jury

Ashwin Chinnayya
Professeur de l'ISAE-ENSMA de Poitiers / Rapporteur

Michel Boustie
Directeur de recherche (HDR), CNRS / Rapporteur

Vincent Faucher
Expert Senior (HDR), CEA Cadarache / Examinateur

Daniel Fuster
Chercheur CNRS, UPMC / Examinateur

David Varas
Maitre de conférence, Universidad Carlos III / Examinateur

Jean-Marc Laurens
Maitre de conférence (HDR), ENSTA-Bretagne / Directeur de thèse

Eric Deletombe
Maître de recherche (HDR), Onera / Co-encadrant

"Light thinks it travels faster than anything but it is wrong.
No matter how fast light travels,
it finds the darkness has always got there first,
and is waiting for it."

Terry Pratchett

Acknowledgement

At the beginning of my thesis, my supervisors told me that the three years of the thesis would pass in the blink of an eye, I did not believe them at that time, but looking back it would seem so, and it is now time for me to express my thanks to all those who played a role in this thesis.

Firstly, I want to thank my defence committee for letting my defence be an enjoyable moment, and for your brilliant comments and suggestions. I would like to express my sincere gratitude to Ashwin Chinnayya and Michel Boustie, for accepting the task of reviewing this thesis work and for their interesting questions, comments and nice words during the defence. Then I would also like to thank the rest of my thesis committee for their interest in my work: Bruno Blanke and David Varas for accepting to be part of the defence committee and Vincent Faucher and Daniel Fuster for their kind remarks on my work during the thesis and for their advice.

Then, I would like to thank the funders of this thesis work: the French Ministry of Defence and DGA (French Armament Procurement Directorate) and Onera in the persons of Jean-Pierre Grisval, Head of the Department and Laurent Lefebvre, Head of the Research Unit.

Then, obviously my sincere thanks go to my supervising team. First I would like to thank Jacques Dupas for giving me the opportunity of doing my master's internship at Onera and for the confidence that he entrusted in me during that internship, which led to this PhD subject.

I would also like to thank my thesis director Jean-Marc Laurens for accepting to take the responsibility of this thesis and for making it possible.

I would like to thank Michel Arrigoni, who manage to stay available and to keep a close contact in spite of the large distance separating us. Thank you for your sympathy and your usual good mood, for inviting me to your home, and for making me come to Brest and Bucharest.

My deepest gratitude goes to Eric Deletombe, who really was my main support during this thesis. You manages to always stay available in spite of his numerous responsibilities. I really learned a lot working with you.

In addition, in my daily work I have been blessed with a friendly and cheerful group of fellow students: Julien, Vincent, Claire, Nicolas and Magali. I also want to thank my colleagues from Onera and in particular from the Design and Dynamic Resistance Research Unit: Roland, Jean-Luc, Jean-François, David, Steve Alain, Jean-Michel, Jacky, Gérald, Matthieu, Nicolas, Loïc, Florence, Didier, Bernard, Hughes. A special mention for Bertrand, with whom I basically shared an office for three years, for his time, his always helpful comments, and for the role of mentor that he played during these three years. I also want to thank Arnaud and Benjamin that I had a lot of pleasure to supervise in project and in internship.

Last but not the least, I would like to thank my family, my parents, my brother Simon, and finally Maryse simply for being here.

Contents

Acknowledgement **i**

Nomenclature **vii**

Bibliographie et synthèse des travaux en français **1**
I Introduction . . . 3
II Utilisation d'équations de type Rayleigh Plesset pour l'analyse des bulles créées lors d'un coup de bélier hydrodynamique. . . . 7
II.1 Présentation des cas d'étude . . . 7
II.2 Rappels généraux sur l'équation de Rayleigh-Plesset . . . 10
II.3 Estimation analytique du paramètre de confinement dans l'équa-tion de Rayleigh-Plesset confinée . . . 15
III Étude de l'influence de la compressibilité du liquide sur la dynamique de bulles confinées . . . 18
III.1 Simulations éléments-finis compressibles de dynamiques de bulles confinées 19
III.2 Résultats des simulations compressibles de dynamique de bulles confinées 22
IV Développement et validation d'un modèle compressible de type Keller-Miksis confiné . . . 23
IV.1 Formulation du modèle de Keller-Miksis . . . 24
IV.2 Application des équations dans le cas d'un conteneur sphérique élastique 26
V Conclusions et perspectives . . . 31

Introduction **35**

1 Context of the research and state of the art **39**
1.1 Hydrodynamic Ram . . . 41
1.2 State of the art of Hydrodynamic Ram simulations . . . 43
1.2.1 Analytical models . . . 43
1.2.2 Numerical models . . . 45

2 Analysis of bubbles dynamics created by hydrodynamic ram in confined geometries using the Rayleigh-Plesset equation **49**
2.1 Introduction . . . 51
2.2 Studied cases . . . 53
2.2.1 Description of the ballistic experiments . . . 53
2.2.2 Exploitation of the test results for Rayleigh-Plesset simulation . . . 53
2.3 Rayleigh-Plesset modelling . . . 55
2.3.1 Derivation of Rayleigh-Plesset equation . . . 55

2.3.2 Application of Rayleigh-Plesset equation for HRAM events 56
2.4 Confined Rayleigh-Plesset equation 58
2.4.1 Modification of RP equation to take confinement effect into account. . . 58
2.4.2 Confined Rayleigh-Plesset equation for bubble created by HRAM events 60
2.4.3 Influence of gas modelling in numerical simulations 61
2.5 Discussion 62
2.6 Conclusion 63

3 Confined Rayleigh-Plesset equation for Hydrodynamic Ram analysis in thin-walled containers under ballistic impacts 65
3.1 Introduction 67
3.2 Studied cases 68
3.2.1 Description of the ballistic experiment 69
3.2.2 Use of the test results for Rayleigh-Plesset simulation 69
3.3 Confined Rayleigh-Plesset equation 70
3.4 Application of the confined Rayleigh-Plesset equation for bubbles created by HRAM events 71
3.4.1 Experimental calibration of α 72
3.4.2 Use of elasticity formula for the structure response 72
3.5 Conclusion 76

4 Cross validation of analytical and finite element models for Hydrodynamic Ram loads prediction in thin walled liquid filled containers 79
4.1 Introduction 81
4.2 Studied cases 83
4.3 Confined Rayleigh-Plesset equation 83
4.4 Quasi-incompressible confined bubble dynamics finite element simulations 85
4.4.1 Description of the quasi-incompressible confined bubble problem 85
4.4.2 Material Laws used in quasi-incompressible confined bubble dynamics simulations 86
4.4.3 Convergence study for the quasi-incompressible simulations 86
4.4.4 Simulation results of quasi-incompressible confined bubble dynamics . . 87
4.5 Compressible confined bubble dynamics finite element simulations 88
4.5.1 Description of the compressible confined bubble problem 88
4.5.2 Convergence study for the compressible simulations 90
4.5.3 Simulation results of compressible confined bubble dynamics 91
4.6 Discussion 93
4.7 Conclusion 94

5 Development and validation of a confined Keller-Miksis model for Hydrodynamic Ram loads prediction in liquid-filled containers. 97
5.1 Introduction 99
5.2 Formulation of the Keller-Miksis model 100
5.2.1 Basic fluid mechanics equations 101
5.2.2 Simplifications introduced in the Keller-Miksis model 102
5.2.3 Derivation of the Keller-Miksis differential equation 102
5.2.4 Determination of g 103

5.3 Application to a rigid wall case . . . 103
5.3.1 Verification of the consistency of analytical models for rigid containers . . 104
5.3.2 Finite element modelling . . . 105
5.3.3 Comparison of the confined Keller-Miksis and finite element simulations for bubbles in rigid containers . . . 107
5.4 Application to an elastic wall case . . . 107
5.4.1 Verification of the consistency of analytical models for elastic containers . 109
5.4.2 Comparison of the confined Keller-Miksis and finite element simulations for bubbles in elastic containers . . . 111
5.4.3 Evaluation of the improvement in prediction using the confined Keller-Miksis model . . . 112
5.5 Discussion . . . 113
5.6 Conclusion and outlooks . . . 114

General conclusion and outlooks **117**

A Study of the capabilities of an ALE bi-material fluid simulation for solving cavity expansion and collapse during an Hydrodynamic Ram event **121**
A.1 State of the art of HRAM modelling . . . 122
A.2 Importance of the cavitation phase simulation . . . 123
A.3 Numerical simulation of the water entry of the projectile . . . 123
A.4 Finite Element model . . . 124
A.4.1 Description . . . 124
A.4.2 Material laws . . . 124
A.4.3 Fluid structure interaction . . . 125
A.5 Results . . . 126
A.5.1 May's experiment (water entry 10.6 $m.s^{-1}$) . . . 126
A.5.2 Water entry with confinement tank . . . 127
A.6 Conclusion . . . 127
A.7 Acknowledgement . . . 128

B Thermal effects in cavitation **129**
B.1 Characteristics of usual aeronautic fuel materials . . . 129
B.2 Indicator of thermal effects . . . 130

C Confinement effects of a spherical container on the dynamic of a single bubble created by optic cavitation **133**
C.1 Experimental setup . . . 133
C.1.1 Laser source . . . 133
C.1.2 Optical system . . . 134
C.1.3 Containers description . . . 134
C.1.4 High-speed camera and lighting system . . . 135
C.1.5 Millimetric grid . . . 135
C.2 Experimental results . . . 135
C.2.1 Time history of bubble radius . . . 137
C.3 Conclusion . . . 139

D Demonstration of the relation between κ and α **141**

Nomenclature

Subscripts, superscripts and other qualifiers

On any variable, Ω:

$\dot{\Omega}$	Time derivative of Ω
$\ddot{\Omega}$	Second time derivative of Ω
$\partial\Omega$	Partial derivative of Ω
Ω_0	Quantity Ω at initial time
Ω_∞	Quantity Ω at the infinite
Ω_b	Quantity Ω at the liquid/gas bubble interface
Ω_s	Quantity Ω at the interface between liquid and container
Ω_l	Quantity Ω of the liquid
Ω_p	Quantity Ω of the projectile
Ω_{vap}	Saturated vapour value
Ω_{amt}	Atmospheric value

Coordinates

r	Radial coordinate
t	Time coordinate
θ	Orthoradial coordinate

Variables

α	Volumetric confinement parameter
γ	Ratio of specific heats of gas
ϵ	Strain in the material
κ	Radial confinement parameter
Λ	Ratio of the container radius to the bubble radius

ν	Poisson coefficient or dynamic viscosity
ρ	Density
σ	Stress in the material
ϕ	Velocity potential
a, b	Dimensions of the plate
$c_p l$	Specific heat at constant pressure
D	Stiffness of the plate to bending
e	Thickness of the spherical shell
E	Young modulus
E_k	Kinetic energy of the liquid
Imp	Impulse transmitted to the structure
k	Polytropic constant
L_{ev}	Latent heat of vaporisation
M_x, M_y	Momentum on the sides of the plates
N	Membrane flux
P	Pressure
R	Radius
S	surface tention
T	Temperature
V	Volume
w	Bending of the plate

Bibliographie et synthèse des travaux en français

Contents

I	Introduction	**3**
II	Utilisation d'équations de type Rayleigh Plesset pour l'analyse des bulles créées lors d'un coup de bélier hydrodynamique.	**7**
III	Étude de l'influence de la compressibilité du liquide sur la dynamique de bulles confinées	**18**
IV	Développement et validation d'un modèle compressible de type Keller-Miksis confiné	**23**
V	Conclusions et perspectives	**31**

Ce chapitre consiste en une bibliographie et une synthèse des travaux de thèse en français. Cette synthèse a été soumise en tant que : T. Fourest, J.-M. Laurens, E. Deletombe, M. Arrigoni, and J. Dupas. Développement et validation de modêles de dynamique de bulles confinées pour la simulation du coup de bélier hydrodynamique dans les réservoirs de carburants. *Comptes Rendus Mecanique*, 2015b. (submitted).

I Introduction

La conception de réservoirs de carburant au regard des pressions générées par des phénomènes de coup de bélier hydrodynamique est un enjeu majeur pour les aéronefs Civils et Militaires, afin d'en réduire la vulnérabilité. Le phénomène du "coup de bélier hydrodynamique" est particulièrement dangereux pour les structures à parois fines, qui ne peuvent pas être blindées à cause de contraintes de poids. Dans ce contexte il est admis que des modélisations numériques du phénomène de coup de bélier hydrodynamique permettraient d'améliorer la survivabilité des structures à cette menace.

Le phénomène de coup de bélier hydrodynamique se produit lors de la pénétration d'un projectile ou d'un fragment haute vitesse/énergie dans un réservoir empli de liquide. Ball (1985) décrit le phénomène du coup de bélier hydrodynamique en trois phases : la phase de choc, la phase de traînée, et la phase de cavitation. A ces phases de nombreux auteurs dont Varas et collab. (2009a) ont ajouté une éventuelle phase de sortie du projectile. Ces phases sont illustrées en Figure I.

Phase :	Pénétration du projectile	Trainé du projectile	Croissance de la cavité	Implosion de la cavité
Charge :	Choc dans le liquide	Pression de traînée	Pression due à la croissance	Choc dans le liquide
Sans retournement :	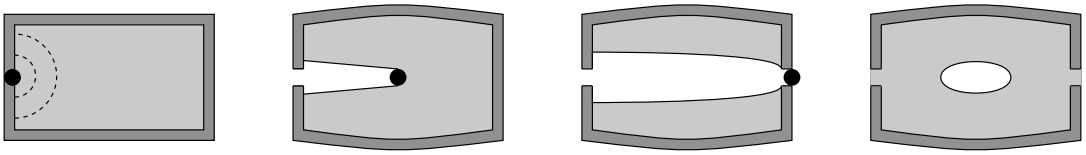			
Avec retournement :	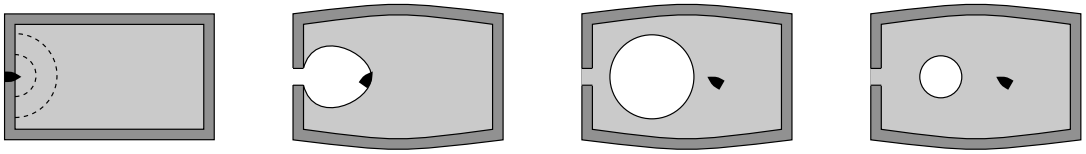			

FIGURE I – Scénarios généraux de coups de bélier hydrodynamiques dans les cas extrêmes de non-retournement du projectile et de retournement violent du projectile.

La phase de choc commence lorsque le projectile perfore la paroi du réservoir et impacte le liquide. A ce moment le projectile génère dans le liquide une onde de choc hémisphérique centrée sur le point d'impact. Les premières observations expérimentales en ont été faites par McMillen (1945) et McMillen et Harvey (1946), qui ont étudié l'onde de choc produite par la pénétration de sphères métalliques à hautes vitesses (de 610 $m.s^{-1}$ à 1500 $m.s^{-1}$) dans de l'eau, en utilisant une méthode d'ombroscopie. Ils se sont particulièrement intéressés aux caractéristiques de l'onde de choc produite dans le liquide. En effet, cette onde génère un chargement impulsif de la structure dans le voisinage du point d'impact, ce qui peut causer des dommages dans la paroi d'entrée (rupture en pétales, propagation de fissures, ...). Ils ont établi que le projectile était rapidement freiné par le liquide et que la vitesse de l'onde de choc convergeait rapidement vers la vitesse du son dans le liquide. Plus tard, Disimile et collab.

(2009) ont observé que les pressions mesurées lors de cette phase n'étaient pas toujours les plus intenses.

Durant la phase de traînée, le projectile perd de la vitesse en traversant le liquide, à cause de la résistance offerte par celui-ci. L'énergie cinétique perdue par le projectile est transmise au liquide qui se met en mouvement. Cela génère parallèlement des champs de pression transitoire qui se propagent dans le liquide et chargent les parois du réservoir. May (1952) fut le premier à avoir observé le mouvement de la cavité créée, jusqu'à sa fermeture (en surface ou en profondeur) lors d'impacts de projectiles à faible vitesse (8 $m.s^{-1}$). Par la suite Shi et collab. (2000) ; Shi et Kume (2001; 2004) ; Shi et Takami (2001) ; Shi et Itoh (2009) ont fait les mêmes observations pour des projectiles à plus hautes vitesses (342 $m.s^{-1}$). Contrairement à la phase de choc, le liquide est mis en mouvement de manière graduelle et non impulsionnelle lors de la phase de traînée. De ce fait, les pressions sont plus faibles mais durent un temps considérablement plus long. Ce mouvement du fluide et les pressions qui y sont associées peuvent continuer après la sortie (où l'arrêt) du projectile.

La phase de cavitation se produit simultanément à la phase de traînée et continue après le passage du projectile. Durant ce passage, on a vu que le projectile transmet son énergie au liquide et crée dans son sillage une cavité. Cette cavité est constituée de l'air entrant lors de l'impact et de vapeur de liquide, si la pression dans la cavité devient inférieure à la pression de vapeur saturante de celui-ci. Elle peut parfois osciller avant que le liquide ne retrouve son état initial. Selon les conditions d'impact cette cavité peut rester ouverte comme dans Varas et collab. (2009a) ou peut se refermer comme dans Deletombe et collab. (2013). Lors de l'implosion de la cavité, une onde de choc secondaire est émise dans le liquide, qui peut créer tout comme l'onde de choc primaire, de la cavitation sur les parois du réservoir en s'y réfléchissant (voir Deletombe et collab. (2013)), et donner lieu à un autre mécanisme d'endommagement du réservoir. Disimile et collab. (2009) ont observé des pressions qui pouvaient être plus élevées lors de cette phase que lors du choc initial, en fonction de la masse du projectile (son matériau). Généralement, la cavité n'étant pas sphérique, elle subit une fission lors de son implosion et génère de nombreuses bulles qui vont à leur tour éventuellement pulser.

La phase de sortie commence lors de l'impact du projectile sur la paroi de sortie. Contrairement à l'impact sur la paroi d'entrée, le projectile heurte une paroi qui est pré-contrainte, voire déjà endommagée par les phases précédentes (voir l'impact dans le réservoir AIRBUS-Group Innovation dans Deletombe et collab. (2013)). Dans les réservoirs métalliques, une forme caractéristique de rupture en pétales est généralement observée comme dans Stepka (1966).

Il existe de nombreux paramètres qui affectent le phénomène de coup de bélier hydrodynamique, tels que ceux mentionnés par Morse et Stepka (1966) ; Stepka et Morse (1963) ; Stepka et collab. (1964; 1965) ; Stepka (1966), qui dépendent des trois éléments impliqués (le projectile, le réservoir et le liquide). Les effets de deux autres paramètres, le retournement du projectile et le taux de remplissage du réservoir, sont discutés ci-après.

La partie de l'énergie cinétique transférée durant les phases de traînée et de croissance de la cavité dépend de la forme du projectile, de sa masse, de sa vitesse et de son éventuel retournement. Le retournement du projectile se produit lorsque ces projectiles hautes vitesses/hautes énergies sont stables dans l'air mais pas dans l'eau. De plus, l'angle d'impact influence fortement l'occurrence et l'intensité du retournement (Sareen et Smith, 1996). Lorsque le projectile se retourne, il transmet son énergie cinétique plus rapidement au milieu liquide. Un cas extrême de retournement mènerait à un transfert instantané et à une cavité sphérique (cas de l'explosion sous marine). Au contraire si le projectile ne se retourne pas, le transfert d'énergie cinétique est plus lent et cela crée une cavité plus allongée dans le sillage du projectile. Bless (1979) a

observé que les pressions qui résultaient d'un impact avec retournement du projectile pouvaient être cinq fois plus intenses que celles observées lors d'un même impact sans retournement.

Plus récemment Deletombe et collab. (2013) ont présenté des essais d'impacts dans l'eau de projectiles non académiques (munitions 7.62 mm NATO) à hautes vitesses (850 $m.s^{-1}$). Ils ont observé l'effet du retournement du projectile sur la forme de la cavité et sur sa dynamique. Les différences induites dans le comportement du liquide dues au retournement du projectile sont illustrées dans la Figure I.

Un autre paramètre influant sur la sévérité d'un évènement de coup de bélier hydrodynamique est le taux de remplissage du réservoir. Varas et collab. (2009a; 2012b) se sont intéressés expérimentalement et numériquement à l'influence de ce paramètre dans des cas d'impacts de billes en acier, donc sans retournement du projectile. Ils ont mesuré dans chaque cas des déformations maximales pour un taux de remplissage de 100%. Cependant, en diminuant le taux de remplissage, ils ont également observé des concentrations de déformation dans les zones proches de la trajectoire du projectile, liées à l'impact de la surface libre sur les parois. Il est possible que cet impact ne puisse pas toujours être négligé au regard de la vulnérabilité du réservoir, en fonction du matériau constituant les parois.

En ce qui concerne l'étude quantitative des chargements générés lors du phénomène de coup de bélier hydrodynamique, les premiers travaux ont été réalisés par Morse et Stepka (1966) ; Stepka et Morse (1963) ; Stepka et collab. (1964; 1965) ; Stepka (1966). Ces auteurs ont effectué de nombreuses mesures expérimentales durant l'impact de projectiles hautes vitesse sur des réservoirs emplis de liquide, et ont identifié les différents facteurs qui affectaient les chargements durant un tel événement. Ils ont essayé de déterminer leur influence sur la survivabilité du réservoir, mais n'ont pas pu établir in fine de relation simple capable de différencier les effets de ces paramètres.

Par la suite, la première méthode numérique utilisée pour étudier l'interaction entre le fluide et la structure, qui simplifiait grandement le problème, fut la *théorie du piston*. Cette théorie fut utilisée dans (Ball, 1974) pour simuler des essais finalement publiés dans (Ball, 1976). Cependant cette approche unidimensionnelle sous-estimait les pressions transmises lors du coup de bélier hydrodynamique aux parois du réservoir, et couplée à des codes d'analyses par éléments-finis, donnait des déplacements et des déformations inférieurs à ceux observés expérimentalement. L'utilisation de cette théorie a constitué néanmoins un premier pas vers une résolution couplée des équations non-linéaires des fluides et des solides.

Pour améliorer ces prédictions numériques, Lundstrom (1977) a proposé l'utilisation de la méthode de l'image variable (Variable Image Method). Dans cette méthode, le champ de pression est décrit grâce à une fonction potentielle qui satisfait l'équation des ondes. Cette méthode permet de traiter des problèmes bidimensionnels et fournit un couplage plus réaliste entre le fluide et la structure. Cependant son utilisation n'a pas été particulièrement couronnée de succès et est restée limitée à des géométries simples.

Par la suite, des méthodes éléments-finis lagrangiennes ont été utilisées entre autres par Kimsey (1980). Pour étudier le phénomène de coup de bélier dans les réservoirs, cet auteur a simulé la phénoménologie de la propagation de l'onde de choc initiale et la phase de traînée d'un projectile cylindrique (ne se retournant pas) dans un réservoir axi-symétrique en effectuant une simulation bidimensionnelle lagrangienne. Cependant, l'utilisation de cette formulation n'étant pas adaptée au traitement des grandes déformations subies par le liquide, ces simulations sont restée limitées à des trajectoires de projectile simples et à l'étude des premières phases du phénomène.

Plus tard, Varas et collab. (2009a; 2009b; 2012a; 2012b) ont fait des essais d'impact et de pénétration de projectiles sphériques hautes vitesses (600 and 900 $m.s^{-1}$) dans des réservoirs en aluminium. Ils ont enregistré l'évolution de la cavité et des pressions mesurées en plusieurs positions dans le réservoir. Ils ont alors effectué des simulations numériques éléments-finis Couplées Euler Lagrange et particulaires (SPH) et ont comparé les résultats calculés aux résultats expérimentaux. Ils ont obtenu un bon accord sur la forme des bulles et sur les pressions prédites dans le liquide. Cependant ils ne se sont pas intéressés à l'intégralité du phénomène et ont limité leur étude aux phases de traînée de la sphère et de traversée du réservoir. De plus ils n'ont pas modélisé le phénomène de vaporisation dans leurs simulations (cette hypothèse manquant de justification dans la littérature).

Plus récemment, Deletombe et collab. (2011; 2013) ont testé l'impact de projectiles 7.62 mm NATO dans un réservoir générique et dans un bassin de grandes dimensions. Dans ces essais, la séquence complète de la dynamique de bulles créées par le retournement d'un projectile a pu être enregistrée. Ces essais ont fourni des données intéressantes pour la validation de simulations numériques de l'impact d'un projectile réel dans un réservoir et dans un bassin, sur toute la durée du phénomène. Les auteurs ont conclu qu'aucune des phases du phénomène de coup de bélier ne pouvait être négligée pour le dimensionnement des structures, car elles pouvaient toutes induire une impulsion significative. Cependant au vu de la complexité des phénomènes se produisant lors du retournement du projectile, ces tests n'ont pas pu être intégralement simulés numériquement.

La synthèse de ces études met en évidence qu'il existe des modèles numériques capables de simuler les premières étapes du phénomène de coup de bélier hydrodynamique, validés par rapport à des résultats expérimentaux. De plus il existe des données expérimentales relatant la séquence complète des phénomènes pour des bulles créées lors d'essais avec retournement du projectile, mais aucun modèle n'a été publié qui s'avère capable de simuler l'ensemble des événements associées au coup de bélier hydrodynamique, jusqu'à la phase d'implosion. Enfin ces modèles, même limités, sont trop coûteux pour être utilisés dans des processus de conception et d'optimisation de réservoirs durant leur phase de développement.

Le présent travail de thèse est réalisé dans le contexte décrit précédemment. Il consiste a développer un modèle semi-analytique et des outils capables de simuler la phase de croissance et d'écroulement de la cavité créée lors d'un coup de bélier hydrodynamique pour des projectiles se retournant. Ce modèle est ensuite utilisé pour statuer sur les paramètres influant au premier et second ordres sur les prédictions numériques des chargements hydrodynamiques lors de coups de bélier dans les réservoirs de carburant.

Pour ce faire, une modification de l'équation dite de Rayleigh-Plesset, utilisée traditionnellement pour modéliser la dynamique de bulles consécutives à des situations d'explosion sous-marines dans un milieu infini (voir Brennen (1995) pour un résumé des travaux menés avec cette équation), est proposée afin de tenir compte du comportement élastique linéaire d'un réservoir sur la dynamique de la cavité. Cette nouvelle équation est appliquée aux cas expérimentaux présentés dans (Deletombe et collab. 2013), en procédant à la calibration d'un paramètre de confinement (qui traduit la réponse de la structure). Pour déterminer les conditions initiales de cette équation, une méthode originale basée sur un critère énergétique est développée. Ce critère est choisi pour garantir la cohérence énergétique du modèle avec les essais d'impacts haute vitesse.

L'étape suivante consiste à évaluer la capacité d'un modèle analytique linéaire élastique de réservoir à prédire la valeur du paramètre de confinement introduit (et précédemment calibré) dans le modèle de Rayleigh-Plesset modifié. Pour ce faire, la relation qui lie les pressions appliquées sur la structure à sa déformation est réécrite pour différentes géométries de manière à y faire intervenir la variation de volume interne de la structure. Puis la valeur numérique du paramètre de confinement est évaluée à l'aide de la théorie des plaques appliquée à la modélisation du comportement linéaire d'un réservoir multi-matériaux parallélépipédique. Finalement les dynamiques de bulles prédites lorsque le paramètre de confinement est calibré et évalué analytiquement avec une formulation plaque sont comparées.

L'étape suivante consiste à comparer le modèle de Rayleigh-Plesset confiné à des modélisations par éléments-finis unidimensionnelles qui incluent l'effet de compressibilité du liquide. L'objectif de cette comparaison est d'estimer l'erreur commise dans les prédictions (de la dynamique de bulles et de chargements hydrodynamiques appliqués à la structure) en négligeant l'effet de compressibilité, donc de propagation des ondes. Les simulations éléments-finis sont retenues pour obtenir cette comparaison car il a été montré par Baras et collab. (2012) qu'elles permettaient d'effectuer ces cas de simulation en prenant en compte la compressibilité du liquide. Pour comparer le modèle de Rayleigh-Plesset à des simulations compressibles, des conditions initiales en surpression sont utilisées de manière à avoir cette fois un domaine de liquide au repos initialement, ce qui permet de ne pas introduire de biais dans l'étude.

Comme un effet notable de compressibilité du liquide est relevé, un modèle analytique de dynamique de bulles confinées dans un liquide compressible est enfin développé. Sa formulation est basée sur l'équation de Keller et Miksis (1980) qui décrit la dynamique d'une bulle de gaz dans un domaine de liquide compressible infini. Ce modèle est étendu pour être appliqué dans un réservoir élastique. Pour cela une formulation dynamique est utilisée pour la réponse de la structure, basée sur l'approximation de Reissner (1944) (pour les coques). La cohérence du modèle est vérifiée, puis il est validé de nouveau par rapport à des simulations éléments-finis. Les rayons de bulles, mouvements et pressions à la paroi de la structure prédits avec ce modèle sont comparés à ceux prédits avec le modèle de Rayleigh-Plesset confiné pour estimer l'amélioration obtenue dans ces prédictions en utilisant un modèle compressible.

Finalement une analyse critique et une conclusion générale des travaux sont proposées puis quelques perspectives possibles de ces travaux identifiées.

II Utilisation d'équations de type Rayleigh Plesset pour l'analyse des bulles créées lors d'un coup de bélier hydrodynamique.

II.1 Présentation des cas d'étude

Les modèles de type Rayleigh-Plesset sont appliqués sur deux cas très différents : le premier est un impact d'un projectile NATO 7.62 mm dans un réservoir générique AIRBUS-Group Innovation de dimensions 0.3x0.54x0.66 m^3 empli d'eau (testé dans le cadre du projet EUCLID RTP 3.32). Le second est un tir balistique réalisé dans la piscine du département ONERA/ DAAP de dimensions plus importantes, 22x1.5x1.5 m^3. Dans les deux cas l'impact est normal à la paroi d'entrée ou à la surface libre du liquide. Ces essais ont été publiés dans Deletombe et collab. (2013), et correspondent respectivement à un cas de réservoir confiné et à un cas quasi

non-confiné.

Description des essais balistiques

Seule la description générale de l'évolution de la cavité est présentée ci-dessous. Plus de détails sur les essais expérimentaux peuvent être trouvés dans Deletombe et collab. (2013). Les Figures II et IV montrent respectivement les dynamiques des bulles observées pour les essais dans la piscine et dans le réservoir. La Figure III montre le torque d'air et le nuage de gaz qui sont observés à la fin de l'essai dans la piscine.

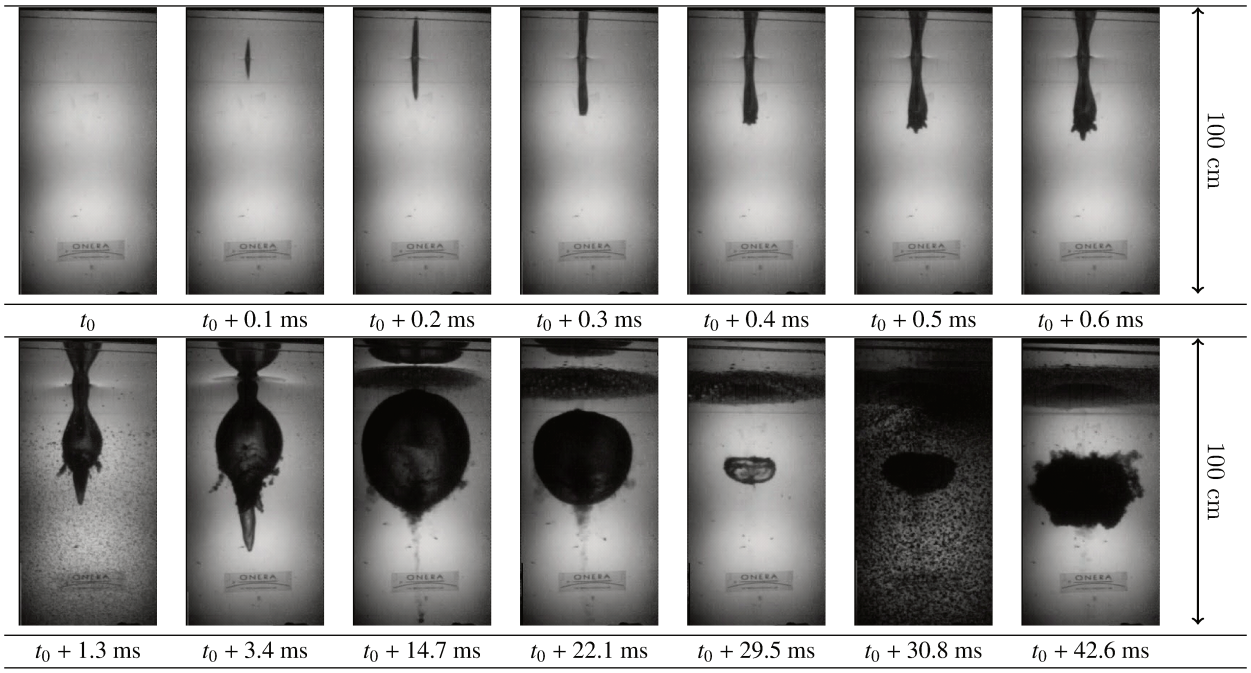

FIGURE II – Images de la cavité créée lors de l'impact d'un projectile 7.62 mm à 850 m.s^{-1} dans la piscine de l'ONERA/DAAP (10000 images par seconde).

Exploitation des résultats expérimentaux pour les simulations de type Rayleigh-Plesset

Le rayon de la bulle ainsi que la vitesse de l'interface de la bulle sont obtenus à partir des images expérimentales en utilisant le même processus que Deletombe et collab. (2013). La seule différence concerne l'utilisation d'une approximation du second ordre pour calculer la vitesse de croissance de la bulle :

1. une ellipse 2D est projetée sur les parties sombres des images correspondant à la bulle, ensuite un outil est utilisé pour calculer cette surface (pix^2) ;

2. cette surface est convertie en m^2 à partir de la correspondance entre pixels et mètres qui a été obtenue précédemment en plaçant une grille dans les réservoir (0.01x0.01 m pour le réservoir AIRBUS-Group Innovation et 0.05x0.1 m pour la piscine hydrodynamique) ;

3. la mesure de la surface est utilisée pour calculer le rayon d'un disque de même surface ;

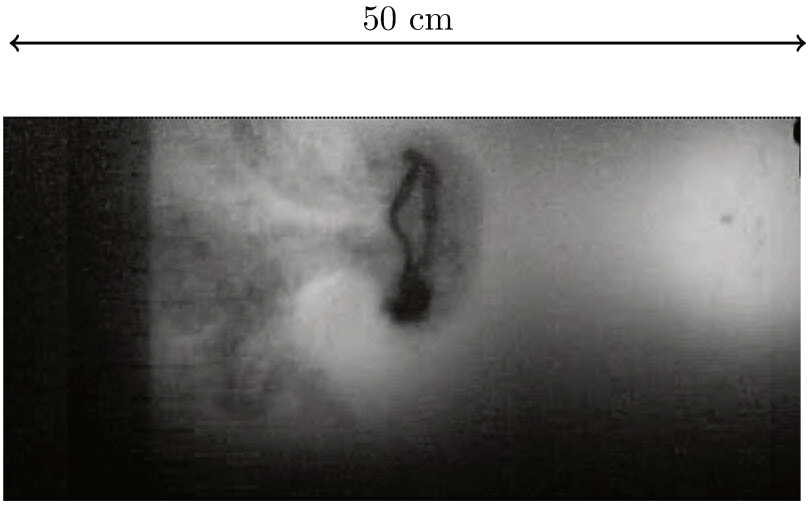

FIGURE III – Image du torque d'air observé à la fin de l'essai d'impact d'un projectile 7.62 mm à 850 m.s^{-1} dans la piscine de l'ONERA/DAAP (10000 images par seconde).

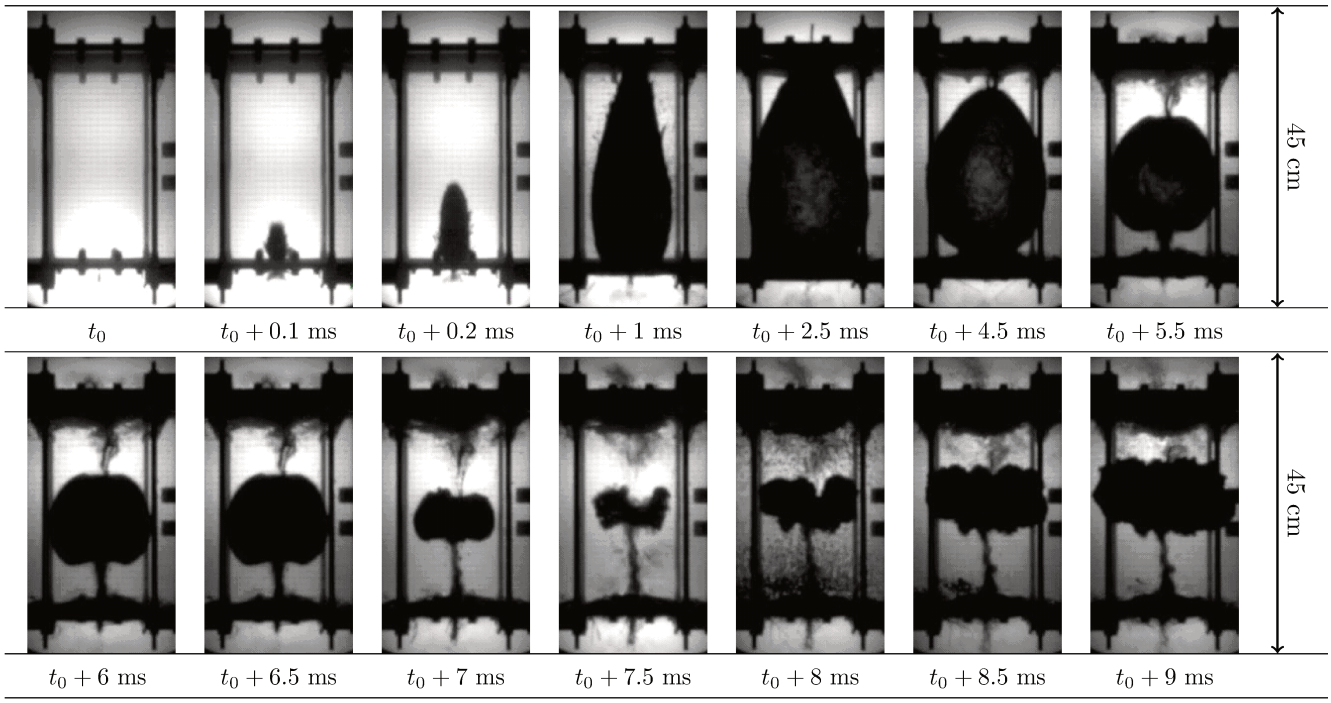

FIGURE IV – Images de la cavité créée lors de l'impact d'un projectile 7.62 mm à 850 m.s^{-1} dans un réservoir générique AIRBUS-Group Innovation (10000 images par seconde).

4. la vitesse "moyenne" de croissance de la bulle est ensuite calculée en utilisant une approximation polynomiale du second ordre du rayon obtenu durant la première milliseconde du phénomène.

II.2 Rappels généraux sur l'équation de Rayleigh-Plesset

Une grande quantité d'études sur la dynamique des bulles peut être trouvée dans la littérature. Ces études se révèlent utiles pour comprendre la physique du processus d'évolution de la cavité observée durant le phénomène de coup de bélier hydrodynamique. Elles ont commencé avec Rayleigh (1917) qui travailla à la prédiction des pressions durant l'implosion d'une bulle sphérique, en supposant le liquide incompressible, non-visqueux et la tension de surface négligeable. Son travail a ensuite été étendu par Plesset (1949), qui dériva l'équation différentielle ordinaire non linéaire d'évolution du rayon d'une telle bulle, devenue la célèbre *équation de Rayleigh-Plesset pour la dynamique des bulles*. Des améliorations de cette équation ont été proposées depuis par de nombreux auteurs tels que Keller et Miksis (1980), ou des extensions : Gilmore (1952), Fujikawa et Akamatsu (1980) et Prosperetti et Lezzi (1986). Ces améliorations concernent principalement la prise en compte d'effets qui sont influants à la fin de l'implosion de la bulle : la compressibilité du liquide, des effets thermiques et l'effet de non-équilibre du processus de condensation de la vapeur.

L'équation classique de Rayleigh-Plesset a prouvé son efficacité pour l'analyse physique de dynamiques de bulles à différentes échelles (flux cavitants, explosions sous-marines, ...). Cette équation est un modèle simple permettant l'étude préliminaire des phénomènes impliquant des dynamiques de bulles.

Derivation du modèle de Rayleigh-Plesset confiné

Une modification de l'équation de Rayleigh-Plesset est proposée pour prendre en compte les effets de confinement sans changer la méthode de résolution originelle de l'équation. Ces travaux ont été publiés dans Fourest et collab. (2014), voir le Chapitre 2. Pour obtenir cette équation et l'utiliser pour prédire la dynamique de bulles créées lors de coups de bélier hydrodynamiques, une bulle de gaz sphérique dans un domaine fini de liquide est considérée, et les hypothèses suivantes sont faites :

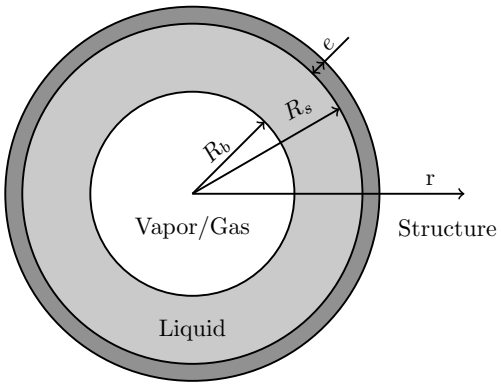

FIGURE V – Description du système considéré pour prendre en compte les effets de confinement dans l'équation de Rayleigh-Plesset.

- le liquide est incompressible,

- l'interface de la bulle reste sphérique,
- le transfert de l'énergie cinétique du projectile au liquide est instantané,
- l'effet de la gravité est négligeable,
- il n'y a pas de transfert de masse au travers de l'interface de la bulle,
- les effets de la viscosité du liquide et de la tension de surface sont négligés. Les effets visqueux sont influants pour des bulles ayant un rayon inférieur à 10^{-3} m (Chapman et Plesset 1971) mais ils sont généralement négligeables pour des bulles de rayon 10^{-1} m ou plus,
- le processus est supposé isotherme puisque il n'y a pas d'effets thermiques pour la cavitation dans l'eau à température ambiante (Brennen, 1995)[1],
- en plus de la vapeur d'eau, une quantité initiale de gaz non condensable (ici l'air) est considérée dans la bulle, son comportement est supposé adiabatique,
- l'effet du confinement structural est étudié en introduisant dans le modèle analytique un réservoir sphérique élastique équivalent (Figure V),
- le matériau est uniforme et isotrope, et le mouvement suffisamment lent pour que les effets d'inertie puissent être négligés et donc pour pouvoir utiliser une formulation statique de la réponse de la structure élastique.

L'équation de conservation de la masse pour un mouvement radial est exprimée en coordonnées sphériques. Grâce aux hypothèses précédentes, elle se réduit à (1) :

$$r^2\dot{r} = R_b^2\dot{R}_b \tag{1}$$

avec R_b le rayon de la bulle et $\dot{r}$ la vitesse radiale du liquide à la coordonnée r.

En utilisant les mêmes hypothèses, l'équation de conservation de la quantité de mouvement dans la direction radiale se réduit à (2) :

$$\ddot{r} + \dot{r}\frac{\partial \dot{r}}{\partial r} + \frac{1}{\rho_l}\frac{\partial P}{\partial r} = 0 \tag{2}$$

Il est considéré dans cet exercice que le centre de la bulle correspond au centre du réservoir. Le rayon externe initial de liquide R_{s_0} est défini comme le rayon qui contient le même volume de liquide que le réservoir testé (respectivement 50 m^3 pour la piscine et $7,7{\cdot}10^{-2}$ m^3 pour le réservoir AIRBUS-Group Innovation). Le comportement du liquide est supposé incompressible, donc le rayon du conteneur élastique R_s est directement relié au rayon de la bulle par (3) :

$$R_s = (R_{s_0}^3 + R_b^3 - R_{b_0}^3)^{1/3} \tag{3}$$

En intégrant (2) entre R_s et R_b, en utilisant (1) et en définissant $\Lambda = R_b/R_s$, la même équation que dans Obreschkow et collab. (2006) est trouvée en (4). Plus de détails sur la dérivation de l'équation standard de Rayleigh-Plesset, et sur son utilisation, peuvent être trouvés dans Franc et collab. (1995).

[1] L'importance des effets thermiques pour la cavitation dans un carburant aéronautique est discutée en Annexe B.

$$R_b\ddot{R}_b + \frac{3}{2}\dot{R_b}^2 + \frac{P_s(t) - P_b(t)}{\rho_l} - 2\dot{R_b}^2\Lambda - R_b\ddot{R}_b\Lambda + \frac{1}{2}\dot{R_b}^2\Lambda^4 = 0 \tag{4}$$

avec P_∞ la pression à $r = \infty$, P_b la pression dans la bulle, P_s la pression à l'interface entre le liquide et la structure sphérique et ρ_l la densité du liquide. Une équation similaire à celle de Rayleigh-Plesset est finalement obtenue avec l'addition de trois termes qui disparaissent quand $R_s = \infty$. Dans le cas d'un réservoir sphérique, la structure peut être modélisée en utilisant la théorie de l'élasticité pour une coque épaisse sphérique (5) :

$$P_s - P_{s_0} = (R_s - R_{s_0}).E.\left(\frac{(R_{s_0} + e)^3 - R_{s_0}^3}{R_{s_0}^3}\right)\left(\frac{2R_{s_0}^2}{2(1-2\nu)R_{s_0}^3 + (1+\nu)(R_{s_0} + e)^3}\right) \tag{5}$$

avec E le module de Young, ν le coefficient de Poisson et e l'épaisseur de la coque.

Application de l'équation de Rayleigh-Plesset au coup de bélier hydrodynamique avec calibration du paramètre de confinement

Dans le cas de bulles créées par coups de béliers hydrodynamiques, il est proposé de résoudre l'équation de Rayleigh-Plesset d'une manière non conventionnelle. Pour résoudre cette équation différentielle, des conditions initiales doivent être définies. Généralement pour des applications classiques de Rayleigh-Plesset, ces conditions initiales sont $R_{b_0} \neq 0$, $P_{b_0} > P_\infty$, et $\dot{R}_{b_0} = 0$. Dans le cas présent elles sont $R_{b_0} \neq 0$, $P_{b_0} < P_\infty$, et $\dot{R}_{b_0} \neq 0$, ce qui signifie que la dynamique de bulle n'est pas créée par une différence initiale entre la pression dans la bulle et dans le liquide à l'infini mais par une quantité de mouvement initiale donnée au liquide.

Les conditions initiales de l'équation de Rayleigh-Plesset sont déterminées à partir des essais effectués à l'ONERA et sont liées au temps initial choisi pour l'analyse (quand une bulle de cavitation apparait raisonnablement distinctement sur les images). Pour finir de déterminer les conditions initiales, une considération énergétique est utilisée, qui stipule que l'énergie cinétique du liquide dans le modèle de Rayleigh-Plesset doit être égale à l'énergie initiale théorique du projectile qui crée cette bulle (approximativement 3.5 kJ dans la piscine et 2.9 kJ dans le réservoir AIRBUS-Group Innovation). Comme la partition entre l'énergie cinétique du projectile transférée au liquide et l'énergie dissipée par déformation du projectile est inconnue, aucune dissipation n'est considérée dans cet exercice : toute l'énergie cinétique du projectile est estimée être transférée au liquide. L'énergie cinétique (6) du liquide est calculée sous hypothèse d'incompresibilité :

$$E_c = \frac{1}{2}\iiint_V \dot{r}^2\rho \, \mathrm{d}V = 2\pi\rho R_b^4\dot{R_b}^2\left(\frac{1}{R_b} - \frac{1}{R_s}\right) \tag{6}$$

Il est évident que les réservoirs dans les essais (voir Figure IV) ne sont pas sphériques et sont des assemblages de plusieurs matériaux. La rigidité globale d'un tel réservoir ne peut pas être obtenue avec un modèle de coque sphérique élastique monolithique d'aucun des matériaux constitutifs du réservoir. De plus, les parois du réservoir dans les essais travaillent en flexion alors qu'une coque sphérique soumise à une pression interne travaille en membrane. En fait la relation existant entre les pressions appliquées à la structure et ses déformations est complexe. Elle dépend des dimensions du conteneur, de ses matériaux, fixations, formes, et de la position

de la bulle. Obtenir cette relation nécessiterait l'utilisation de simulations numériques tridimensionnelles complètes. Pour éviter cela, il a été choisi d'introduire un facteur non dimensionnel κ pour obtenir une relation plus simple pour les déformations du réservoir élastique (7) qui remplace (5). Ce facteur est appelé paramètre de confinement dans la suite des travaux.

$$\frac{(P_s - P_{s_0})}{P_{s_0}} = \kappa \frac{(R_s - R_{s_0})}{R_{s_0}} \tag{7}$$

Le Tableau I résume les conditions initiales utilisées pour les simulations de type Rayleigh-Plesset dans le réservoir et la piscine. La pression initiale de l'air dans la piscine (après fermeture du sillage) : $P_{b0} = 8,1{\cdot}10^{-3}$ MPa, est calculée à partir d'une estimation du volume du torque d'air observé à la fin de l'essai (Figure III) : $V_{ring} = 4,5{\cdot}10^{-5}$ m^3. Puisque dans la vidéo le volume de cet anneau semble être constant en fin d'essai, il est supposé qu'il est à pression atmosphérique. En supposant que le gaz subit une compression adiabatique ($V_{ring}^{\gamma}.P_{\infty} = V_{b_0}^{\gamma}.P_{b_0}$) où γ est le coefficient polytropique du gaz et vaut 1.4. pour un gaz diatomique. une fois la cavité fermée (déconnectée de la surface), il est ainsi possible d'estimer la pression initiale dans la bulle dont on connait le volume. Pour le cas du réservoir, la quantité de gaz non-condensable piégé dans le sillage du projectile est inconnue, donc la bulle est supposée n'être initialement composée que d'air à la pression de vapeur saturante (début du processus de vaporisation). Il est intéressant de mentionner que le processus de transfert de masse entre le liquide et la vapeur est supposé instantané. A la fin de l'implosion, une condensation partielle se produit (Fujikawa et Akamatsu 1980 ; Fujikawa et collab. 1982) : la petite quantité de vapeur restante est compressée et stoppe l'effondrement du liquide. Cet effet, qui influence le rayon minimal de la bulle et l'onde de pression secondaire générée, est négligé car l'étude actuelle ne se concentre que sur la dynamique de bulle avant la phase terminale d'implosion. La pression minimale dans la bulle est donc prise égale à la pression de vapeur saturante du liquide, qui est supposée être constante (à température ambiante).

TABLE I – Valeurs numériques des conditions initiales utilisées pour les simulations des coups de bélier hydrodynamiques avec l'équation de Rayleigh-Plesset confinée.

Cas	P_{b_0} (MPa)	t_0 (ms)	R_{b_0} (mm)	$\dot{R}_{b_0}$ (mm.ms^{-1})	R_{s_0} (mm)	E_{k_0} (kJ)
Piscine	$P_{b_0} = 8,1{\cdot}10^{-3}$	0,51	42,3	86,44	2200	3500[a]
Réservoir	$P_{sat} = 2,23{\cdot}10^{-3}$	0,26	48,5	70,6	264	2900[a]

[a]Les énergies cinétiques initiales sont différentes car les vitesses initiales mesurées des projectiles sont différentes.

L'équation différentielle du second ordre de Rayleigh-Plesset est résolue numériquement en utilisant une méthode de Runge-Kutta du quatrième ordre. Les évolutions des rayons dans les deux cas sont présentées dans les Figures VI et VII pour plusieurs valeurs du paramètre de confinement. Les paramètres de confinement κ peuvent être calibrés pour obtenir un bon accord en amplitude entre les rayons de bulles expérimentaux et numériques : $\kappa = 2200$ et $\kappa = 400$ respectivement pour la piscine et le réservoir.

Les résultats obtenus dans cette partie des travaux tendent donc à confirmer la similarité supposée entre les dynamiques de bulles observées dans le phénomène de coup de bélier hydrodynamique et dans les explosions sous-marines. A noter que les phases associées au coup de bélier hydrodynamique sont aussi en accord avec celles décrites par Fuster et collab. (2009) pour d'autres processus cavitants : *phase d'expansion, phase de décélération et de compression initiale* (l'*implosion, le rebond et la génération d'onde secondaire* n'ont pas été examinés dans ce travail). Le processus de création des bulles est différent (impact de projectile pour le coup de bélier hydrodynamique et détonation pour les explosions sous-marines), mais une quantité de mouvement est impulsée au liquide dans les deux cas. L'équation de Rayleigh-Plesset est initialisée par cette quantité de mouvement donnée au liquide incompressible, et non par une surpression initiale dans la bulle. Cette approche est justifiée ici car la bulle est créée dans le sillage du projectile et il n'y a aucune raison pour que la pression de celle-ci excède la pression atmosphérique. La dynamique de bulle est donc principalement due à la quantité de mouvement transmise par le projectile au liquide. Si des projectiles explosifs étaient étudiés comme dans Anderson et collab. (1999) , la dynamique de bulle serait causée à la fois par la quantité de mouvement transmise par le projectile et par une suppression de la bulle due à la détonation. Dans ce cas, la pression de la bulle ne pourrait pas être négligée.

Dans cette section, l'effet de confinement dans l'équation de Rayleigh-Plesset dépend de deux paramètres : Λ et κ. Le premier quantifie une correction de l'équation de Rayleigh-Plesset due aux dimensions finies du domaine de liquide considéré. Le second définit la résistance opposée par la structure à l'expansion du liquide. Les résultats obtenus avec l'équation de Rayleigh-Plesset confinée semblent décrire de manière satisfaisante les dynamiques de bulles jusqu'à la phase d'implosion finale. A ce moment les rayons minimaux prédits sont notablement inférieurs aux rayons expérimentaux. Il faut noter qu'à ce stade, le modèle de Rayleigh-Plesset confiné ne peut pas être utilisé pour prédire les chargements sur la structure de réservoirs car il nécessite une initialisation à partir de données expérimentales, et la rigidité globale du réservoir n'est pas explicitement connue (excepté pour des réservoirs sphériques).

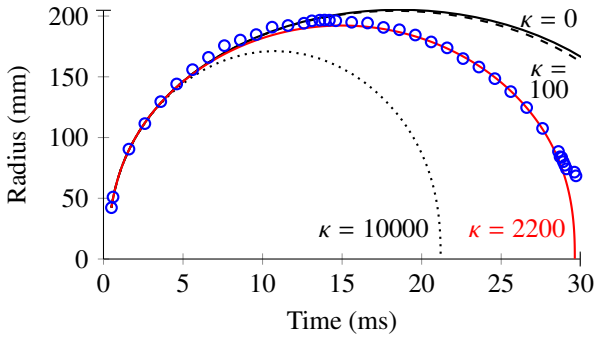

FIGURE VI – Évolution du rayon de bulle dans la piscine, expérimentale (o), et calculée avec le modèle de Rayleigh-Plesset confiné avec $\kappa = 0$ (—), $\kappa = 100$ (- - -), $\kappa = 10000$ (····), et avec $\kappa = 2200$ (—).

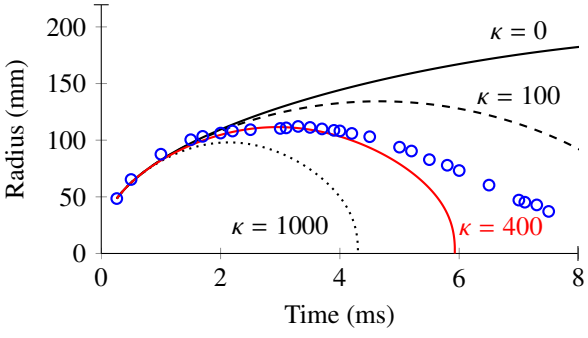

FIGURE VII – Évolution du rayon de bulle dans le réservoir, expérimentale (o), et calculée avec le modèle de Rayleigh-Plesset confiné avec $\kappa = 0$ (—), $\kappa = 100$ (- - -), $\kappa = 1000$ (····), et avec $\kappa = 400$ (—).

II.3 Estimation analytique du paramètre de confinement dans l'équation de Rayleigh-Plesset confinée

L'étape suivante consiste donc à évaluer la capacité d'un modèle analytique linéaire élastique de réservoir à prédire la valeur du paramètre de confinement dans le modèle de Rayleigh-Plesset modifié. Ces travaux ont été publiés dans Fourest et collab. (2015c) , voir le Chapitre 3.

Définition d'un paramètre de confinement pour réservoir de géométrie quelconque

Pour estimer la valeur du paramètre de confinement d'un réservoir de géométrie quelconque, une autre relation que (7) entre la pression appliquée à la surface de la coque sphérique et sa réponse est proposée pour ne plus faire apparaître le rayon du réservoir.

Il faut noter que durant un coup de bélier hydrodynamique, la structure subit des mécanismes de déformation complexes tels que de la plasticité ou de la rupture. Dans cette section, un comportement élastique linéaire de la structure est considéré en première étape. Une analyse inélastique ne pourrait être envisagée qu'une fois la pertinence et la validité du modèle analytique proposé suffisamment justifiées. Si le comportement du réservoir est supposé élastique et linéaire, une approximation de la relation entre la pression appliquée et le volume du réservoir est proposée en supposant la proportionnalité entre la variation de la pression appliquée à l'intérieur de la coque sphérique $P_s - P_{s_0}$ et la variation du volume interne de la sphère $V - V_0$. Ce coefficient de proportionnalité sera par la suite appelé paramètre de confinement volumique et noté α dans (8) :

$$P_s - P_{s_0} = \alpha(V - V_0) \tag{8}$$

Il peut être noté que l'utilisation de l'équation de Rayleigh-Plesset sur un réservoir de géométrie quelconque repose sur des hypothèses supplémentaires :

- la pression appliquée sur toutes les parois du réservoir est spatialement uniforme,
- la géométrie du réservoir n'affecte pas la géométrie de la bulle.

Détermination analytique du paramètre de confinement pour un réservoir parallélépipédique

Les résultats obtenus en calibrant le coefficient κ (ou indifféremment α[2]) au paragraphe précédent, $\kappa = 2200$ et $\kappa = 400$ pour avoir le même rayon maximal de bulle que observé expérimentalement respectivement dans la piscine et dans le réservoir, se sont avérés encourageants. Dans ce paragraphe la mesure dans laquelle la valeur numérique du coefficient α peut être prédite en utilisant des formules analytiques est étudiée. Le conteneur utilisé dans l'essai de référence n'est pas sphérique, et est un assemblage de plusieurs pièces avec plusieurs matériaux (principalement six plaques : deux en composite à matrice organique (CMO), deux en PMMA et deux en acier). Dans cette partie des travaux la valeur numérique du coefficient α est calculée avec des formules de plaques. Elle sera notée α_p.

La variation du volume du réservoir est obtenue par addition du volume libéré par la déformation de chaque paroi du réservoir : $\Delta V = 2(\Delta V_{p_{OMC}} + \Delta V_{p_{Acier}} + \Delta V_{p_{PMMA}})$. Les plaques sont considérées encastrées et soumises à une pression uniforme.

[2]La relation entre α et κ est $\alpha = \kappa\,(1/4\pi)\left(P_{s_0}/R_{s_0}^3\right)$. Cette relation est démontrée dans l'Annexe D.

II. UTILISATION D'ÉQUATIONS DE TYPE RAYLEIGH PLESSET POUR L'ANALYSE DES BULLES CRÉÉES LORS D'UN COUP DE BÉLIER HYDRODYNAMIQUE.

La variation de volume autorisée par la déformation d'une paroi (voir Figure VIII), est calculée (9) en utilisant la théorie des plaques et coques de Timoshenko et Woinowsky-Krieger (1959),

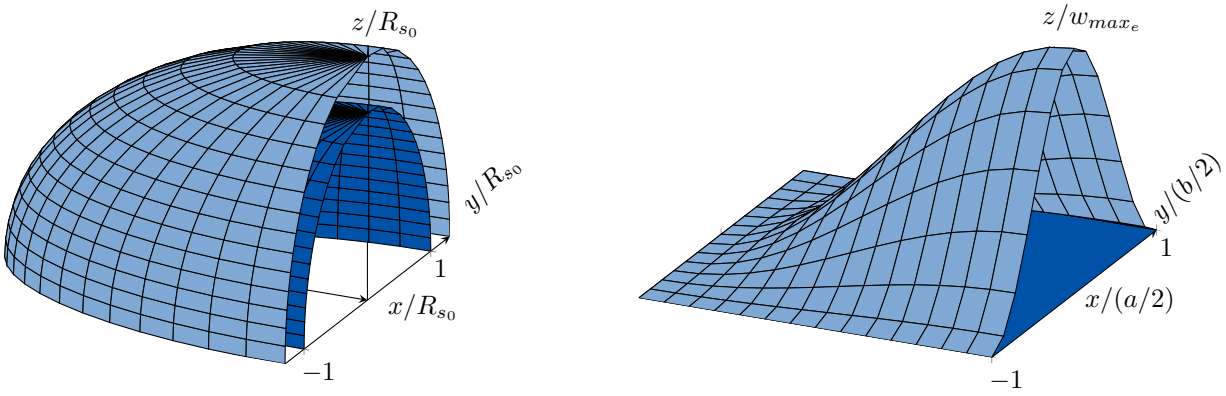

FIGURE VIII – Variation du volume interne d'un quart de conteneur sphérique (a) et de la moitié d'une plaque encastrée (b) soumis à une pression uniforme. Avant application de la pression (■) et après (■).

$$\Delta V_p = \iint_S w_{enc}.dS \tag{9}$$

La flexion de chaque plaque w_{enc} est calculée à partir de Timoshenko et Woinowsky-Krieger (1959) en utilisant (14-17) dans (11 - 13) pour obtenir les termes de (10) :

$$w_{enc} = w_{ss} + w_1 + w_2 \tag{10}$$

$$w_{ss} = \frac{4(P_w(t) - P_{w_0}).a^4}{\pi^5.D} \sum_{m=1,3,5...}^{\infty} \frac{(-1)^{(m-1)/2}}{m^5} cos\left(\frac{m\pi x}{a}\right) \left(1 - \frac{\beta_a tanh(\beta_a) + 2}{2cosh(\beta_a)} cosh\left(\frac{m\pi y}{a}\right) + \frac{1}{2cosh(\beta_a)} \frac{m\pi y}{a} sinh\left(\frac{m\pi y}{a}\right)\right) \tag{11}$$

avec a et b les dimensions de la plaque,et D la raideur en flexion de la plaque : $D = E.e^3/(12(1-\nu^2))$, $\beta_a = mb\pi/(2a)$ et $\beta_b = ma\pi/(2b)$.

$$w_1 = -\frac{a^2}{2\pi^2 D} \sum_{m=1,3,5...}^{\infty} E_m \frac{(-1)^{(m-1)/2}}{m^2 cosh(\beta_a)} cos\left(\frac{m\pi x}{a}\right) \left(\frac{m\pi x}{a} sinh\left(\frac{m\pi x}{a}\right) - \beta_a tanh(\beta_a) cosh\left(\frac{m\pi x}{a}\right)\right) \tag{12}$$

$$w_2 = -\frac{b^2}{2\pi^2 D} \sum_{m=1,3,5...}^{\infty} F_m \frac{(-1)^{(m-1)/2}}{m^2 cosh(\beta_b)} cos\left(\frac{m\pi y}{b}\right) \left(\frac{m\pi y}{b} sinh\left(\frac{m\pi y}{b}\right) - \beta_b tanh(\beta_b) cosh\left(\frac{m\pi y}{b}\right)\right) \tag{13}$$

avec :

$$(M_y)_{y=\pm b/2} = \sum_{m=1,3,5...}^{\infty} (-1)^{(m-1)/2} E_m cos\left(\frac{m\pi x}{a}\right) \tag{14}$$

$$(M_x)_{x=\pm a/2} = \sum_{m=1,3,5...}^{\infty} (-1)^{(m-1)/2} F_m cos\left(\frac{m\pi y}{b}\right) \tag{15}$$

et :

$$\left(\frac{\partial w}{\partial y}\right)_{y=\pm b/2} + \left(\frac{\partial w_1}{\partial y} + \frac{\partial w_2}{\partial x}\right)_{y=\pm b/2} = 0 \tag{16}$$

$$\left(\frac{\partial w}{\partial x}\right)_{x=\pm a/2} + \left(\frac{\partial w_1}{\partial x} + \frac{\partial w_2}{\partial y}\right)_{x=\pm a/2} = 0 \tag{17}$$

Pour obtenir les valeurs numériques de α_p tel que $\Delta P = \alpha_p \Delta V$, il est nécessaire de résoudre numériquement un système d'équations différentielles. Dans un premier temps, la variation de volume induite par une variation arbitraire de pression de $P_s - P_{s_0} = 1$ MPa est calculée pour chaque plaque. Les valeurs numériques obtenues sont présentées dans le Tableau II.

TABLE II – Variation de volume autorisée par les plaques pour une variation de pression de 1 MPa.

Material	E (MPa)	ν	a (mm)	b (mm)	ΔV_{plate} (m^3)
CMO	110000	0.3	540	660	$7{,}5{\cdot}10^{-3}$
PMMA	2600	0.3	300	540	$6{,}9{\cdot}10^{-5}$
Acier	210000	0.3	300	660	$6{,}0{\cdot}10^{-7}$

En utilisant (8) avec $P_s - P_{s_0} = 1$ MPa, $\Delta V = 1.52{\cdot}10^{-2}$ m^3, la valeur numérique obtenue pour le paramètre de confinement est : $\alpha_p = 66$ MPa.mm^{-3}. Elle est trouvée plus proche de celle calibrée (qui est $\alpha_{calib} = 150$ MPa.mm^{-3}) que la plus proche pouvant être obtenue avec un réservoir sphérique mono matériau ($\alpha_s = 5100$ MPa.mm^{-3}). Le ratio entre les valeurs calibrées et évaluées avec les formules analytiques de plaques est de 2.27 au lieu de 34 avec le conteneur sphérique. Les dynamiques de bulles prédites avec (4) en utilisant α_{calib} et α_p sont présentées dans la Figure IX.

La prédiction de la dynamique de bulle obtenue avec α_p est satisfaisante (la différence entre les rayons maximaux est de 11% et de 33% entre les temps d'implosion) sachant que le modèle n'est qu'une approximation de la réponse du conteneur réel. Les plaques dans le conteneur réel ne sont en effet pas parfaitement encastrées mais sont boulonnées et il y a des renforcements supplémentaires dans les coins du réservoir : les dimensions des plaques qui travaillent effectivement en flexion ne sont pas connues, et certaines parties ne sont simplement pas modélisées.

La relation entre la pression appliquée sur la structure et sa déformation est complexe. Elle dépend des dimensions, matériaux, fixations, formes du conteneur et de la position de la bulle. Dans cette partie des travaux, la mesure dans laquelle cette relation peut être approximée par des formules analytiques a été examinée. Le modèle analytique est basé sur une symétrie sphérique, alors que lors de l'essai, une bulle ellipsoïde a été créée dans un réservoir parallélépipédique. Les résultats tendent à démontrer que ce modèle permet néanmoins d'avoir une approximation intéressante de la dynamique de la bulle dans un cas aussi complexe. Des améliorations du modèle pourraient être obtenues en prenant en compte la forme elliptique de la bulle comme dans Wang et Blake (2010). Cependant le paramètre le plus important négligé dans ce modèle nous a semblé être la compressibilité du liquide.

III Étude de l'influence de la compressibilité du liquide sur la dynamique de bulles confinées

Les résultats obtenus précédemment sont prometteurs. Cependant le modèle analytique n'est pas complètement validé par comparaison avec des résultats expérimentaux ou des simulations numériques unidimensionnels pour l'instant. De plus le modèle utilisé dans cette approche est incompressible et l'effet de la compressibilité sur la dynamique des bulles dans un domaine de liquide fini n'est pas parfaitement connu.

Dans cette partie des travaux, le modèle de Rayleigh-Plesset confiné est comparé à des simulations éléments-finis de croissance de bulles confinées tenant compte de la compressibilité du liquide. L'objectif de cette comparaison est d'estimer l'erreur induite par le modèle analytique sur la dynamique de bulle, afin d'établir si un modèle analytique compressible confiné est nécessaire pour la prédiction des chargements mécaniques générés lors de l'occurrence d'un coup de bélier hydrodynamique. Cette étude se concentre sur le premier battement de bulles de grandes dimensions. L'implosion finale est réputée être un phénomène complexe et instable, durant lequel la bulle ne reste pas sphérique et peut fissionner (Frost et Strutevant 1986), sur lequel ce travail ne se concentre pas. Cette phase reste aujourd'hui un défi à simuler (Johnsen et Colonius 2009 ; Popinet et Zaleski 2002). Ces travaux ont été soumis à publication dans Fourest et collab. (accepté), voir le Chapitre 4.

Pour analyser l'influence de la compressibilité du liquide sur la dynamique des bulles confinées, il est choisi d'étudier les dynamiques de bulles comparables, en terme d'amplitude et de temps d'implosion, à celles observées dans les phénomènes de coups de bélier hydrodynamiques. La

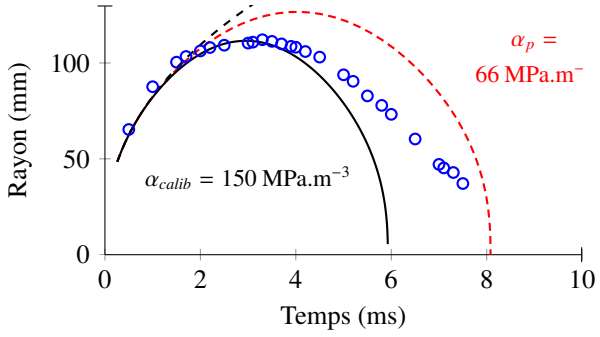

FIGURE IX – Évolution du rayon de bulle expérimentale (o) et prédite avec le modèle de Rayleigh-Plesset confiné avec α_{calib} (—), α_p (- - -) et $\alpha = 0$ (- - -).

Figure V rappelle le problème considéré. Les conteneurs sont emplis de liquide (ici de l'eau), et contiennent une bulle de gaz (ici de l'air) en leur centre. Il est choisi d'étudier les dynamiques de bulles dans trois réservoirs sphériques de rayon interne $R_{s_0} = 1$ m, avec une épaisseur de paroi de e = 6 mm, pour trois matériaux (acier, aluminium et PMMA), les caractéristiques de ces trois matériaux permettant de couvrir une variété de rigidités globales de la structure et donc une gamme de dynamiques de bulles confinées.

III.1 Simulations éléments-finis compressibles de dynamiques de bulles confinées

Le travail présenté dans ce paragraphe concerne la simulation par éléments-finis de dynamiques de bulles confinées en vue d'étudier les effets de la compressibilité du liquide sur celles-ci.

Description du problème de bulle confinée dans un liquide compressible

Dans cette partie des travaux, de nouvelles conditions initiales ont été choisies pour simuler une croissance de bulle causée par une surpression initiale dans bulle. C'est un cas plus standard à simuler, et le domaine liquide est au repos au début de la simulation, donc il n'y a pas de biais dans l'étude des effets de compressibilité (propagation des ondes). Ces conditions initiales sont les suivantes : $R_{b_0} = 40$ mm, $\dot{R}_{b_0} = 0$ m.s^{-1} et $P_{b_0} = 6$ MPa[3].

La théorie standard (18), utilisée dans Lauterborn et Vogel (2013), donne l'énergie de la bulle E_b dans un domaine liquide en fonction de son volume maximal. Comme les bulles étudiées dans le paragraphe 2 ont les mêmes rayons maximaux que celles étudiées avec les nouvelles conditions initiales, elles sont donc équivalentes en termes d'énergie.

$$E_b = \frac{4\pi}{3}(P_l - P_{vap})R_{b_{max}}^3 \tag{18}$$

La dynamique de bulle est alors créée par la différence initiale de pression entre le gaz dans la bulle et le liquide.

Au vu de la géométrie du problème, des simulations 2D axisymétriques sont réalisées. Le domaine maillé est réduit à un quart de disque avec des conditions de symétrie appliquées le long des axes x et y. Une méthode Euler-Lagrange Arbitraire est utilisée pour les grilles des domaines eau et air afin de conserver un maillage régulier au cours du calcul en évitant l'écroulement des éléments autour de la surface de la bulle et donc l'apparision d'instabilités numériques et la chute du pas de temps du calcul. La méthode Euler-Lagrange Arbitraire permet en effet de contrôler les déformations de la grille du maillage indépendamment de celles du matériaux Souli et collab. (2000). Les déplacements de l'interface de la bulle et des nœuds de la structure sont définis comme lagrangiens. De plus, la sphéricité de la surface de la bulle est imposée dans les simulations afin d'éviter l'apparition d'instabilités numériques durant la phase d'implosion, dûes à d'infimes déviations de maillage. L'interaction entre la structure et le liquide est traitée par utilisation d'un maillage conforme (nœuds communs). La Figure X ci-dessous décrit le problème considéré.

[3]Ces conditions initiales donnent la même dynamique de bulle que $R_{b_0} = 48.5$ mm, $\dot{R}_{b_0} = 70.6$ m.s^{-1} et $P_{b_0} = 0$ MPa, voir au chapitre 4

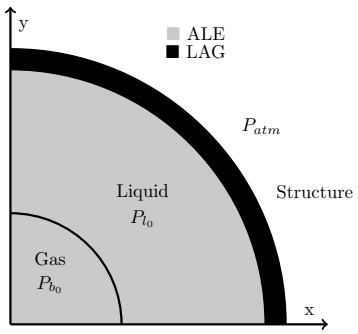

FIGURE X – Schéma du problème considéré dans les simulations compressibles de dynamique de bulles confinées.

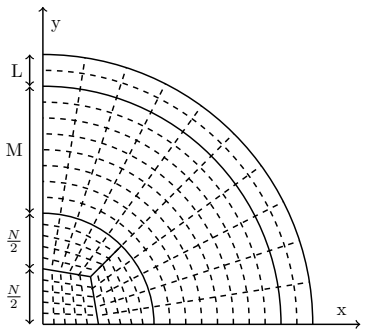

FIGURE XI – Principe de maillage dans les simulations compressibles de dynamique de bulles confinées.

Il est supposé que les dynamiques de bulles dans l'eau ne sont pas affectées par des effets thermiques à température ambiante (Brennen, 1995). Le comportement du liquide est supposé isotherme. L'équation d'état utilisée pour le liquide est (19) :

$$P_l = P_{l_0} + (\rho_l - \rho_{l_0})c_l^2 \tag{19}$$

avec $P_{l_0} = 0.1$ MPa, $\rho_{l_0} = 1000$ kg.m^{-3} et $c_l = 1500$ m.s^{-1}, les valeurs de pression, de densité et de vitesse du son de référence pour le liquide. Le comportement du gaz est supposé idéal et ses variables d'état sont liées par l'équation (20) :

$$P_g = P_{g_0}\left(\frac{\rho_g}{\rho_{g_0}}\right)^{n_g} \tag{20}$$

$P_{g0} = 0.1$ MPa et $\rho_{g0} = 1$ kg.m^{-3} sont les valeurs de référence de pression et de densité du gaz, et n_g est l'exposant polytropique. En considérant que le gaz à l'intérieur de la bulle est diatomique, la valeur $n_g = \gamma_g = 1.4$ est utilisé, ce qui correspond à une transformation adiabatique. Le matériau de la structure suit une loi de comportement élastique linéaire.

Étude de convergence pour les simulations éléments-finis compressibles

Les modèles éléments-finis sont composés d'éléments 4 nœuds axisymétriques. La Figure XI donne les paramètres utilisés pour la définition du maillage. N est le nombre d'éléments ortho-radiaux, M le nombre d'éléments de liquide dans la direction radiale et L le nombre d'éléments de réservoir dans la direction radiale. La précision des calculs éléments-finis étant liée à la finesse de maillage, et la méthode éléments-finis prouvée converger avec cette finesse de maillage, il est d'usage de procéder à une étude numérique de convergence des résultats avant de conclure sur les résultats de simulation. La Figure XII présente les résultats de cette étude de convergence qui porte sur le rayon de la bulle de gaz, dans le cas d'un réservoir en PMMA. Une convergence satisfaisante est obtenue pour le raffinement de maillage 55x636x4 (erreur relative <1%). Le Tableau III présente le coût CPU de chaque simulation.

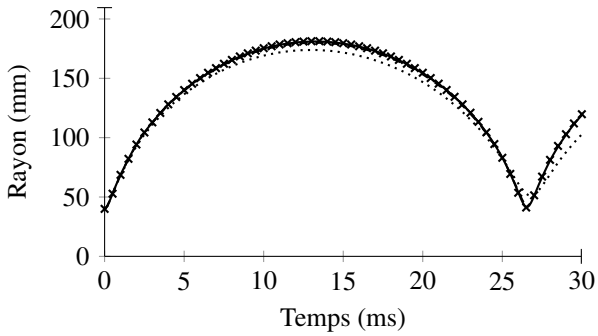

FIGURE XII – Rayon de la bulle en fonction du temps obtenu pour plusieurs raffinements du maillage NxMxL : 10x158x1 (···), 23x318x2 (- - -), 55x636x4 (—) and 110x1272x8 (x) dans les simulations éléments-finis.

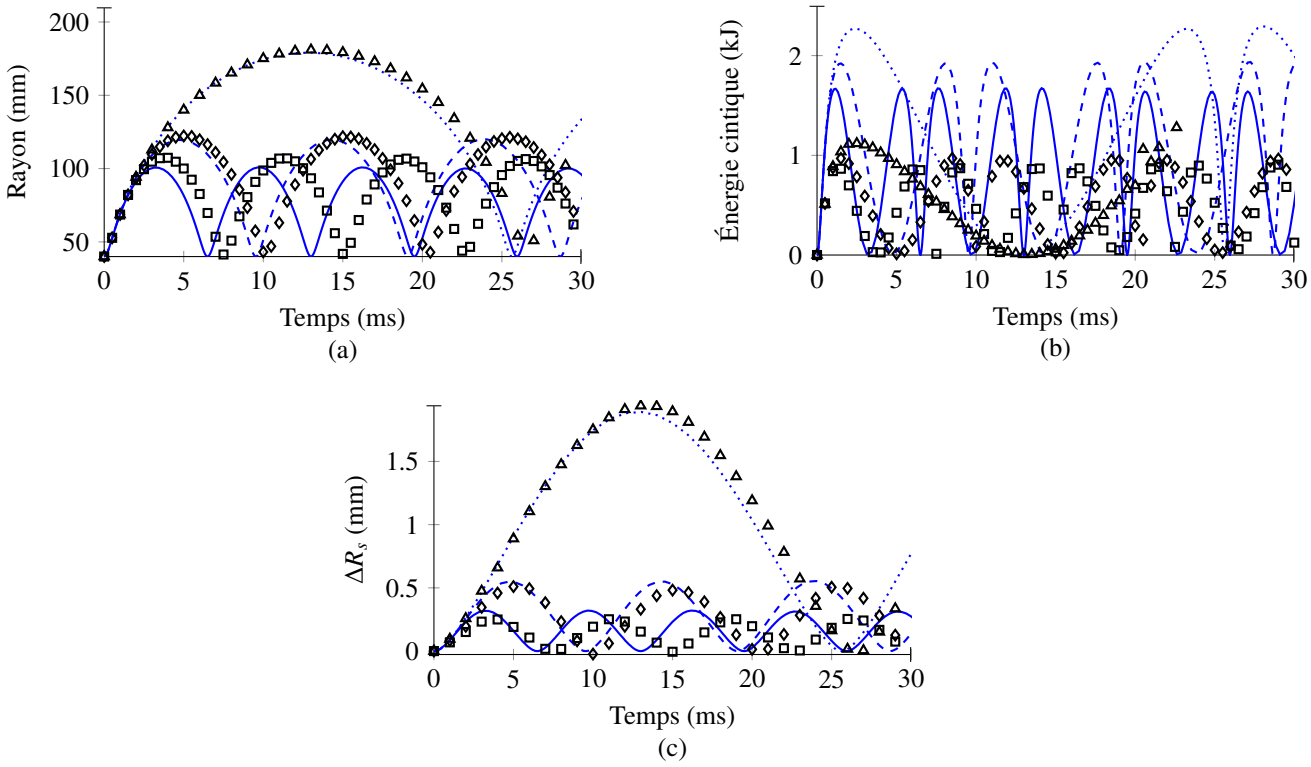

FIGURE XIII – Évolution des rayons de bulles (a), de l'énergie cinétique du liquide (b) et du mouvement de la paroi interne (c) prédites avec des simulations éléments-finis dans un réservoir en acier (□), en aluminium (◇) et en PMMA (△) et comparées au modèle de Rayleigh-Plesset confiné dans un réservoir en acier (—), en aluminium (- - -) et en PMMA (···).

TABLE III – Informations sur les modèles et performances des calculs compressibles sur un calculateur Intel® Ivy-Bridge E5-2667v2 ayant une fréquence d'horloge de 3.3 GHz.

model	Elements	Nodes	Δt_0 (ms)	CPU time (s)
10x158x1	1675	1851	$6{,}41{\cdot}10^{-4}$	42
24x318x2	8136	8494	$2{,}53{\cdot}10^{-4}$	205
56x636x4	38248	38974	$1{,}03{\cdot}10^{-4}$	2938
110x1280x8	150865	152320	$5{,}16{\cdot}10^{-5}$	12842

III.2 Résultats des simulations compressibles de dynamique de bulles confinées

Les bulles créées dans les conteneurs sphériques suivent la même dynamique que les bulles créées dans un domaine de liquide infini jusqu'à approximativement $t_1 = 1,25$ ms, qui est le temps nécessaire à l'onde initiale pour atteindre et être réfléchie par la surface du réservoir, puis revenir interagir avec la bulle. Après ce délai, les trois bulles développent des comportements différents. Les rayons maximaux et les temps d'implosion des bulles dans les réservoirs sphériques sont inférieurs à ceux prédit dans le cas non confiné. Contrairement aux dynamiques de bulle prédites avec le modèle de Rayleigh-Plesset, celles obtenues par calcul éléments-finis dans les conteneurs sphériques présentent une légère asymétrie entre les phases de croissance et d'effondrement.

La comparaison entre les dynamiques de bulles, dans la Figure XIII-(a), prédites avec le modèle de Rayleigh-Plesset confiné et les simulations éléments-finis, montre que le modèle de Rayleigh-Plesset confiné fournit une bonne approximation de la dynamique de bulle avec une erreur maximale sur l'amplitude du rayon inférieure à 6%.

La comparaison des énergies cinétiques du liquide prédites avec les deux méthodes dans la Figure XIII-(b), montre que celles calculées par éléments-finis sont significativement inférieures à celles prédites par le modèle de Rayleigh-Plesset confiné pour la même source (même pression de bulle initiale). De plus, le temps mis pour atteindre le maximum d'énergie cinétique dans les simulations éléments-finis est plus long. Ceci peut être expliqué par le fait que dans les simulations éléments-finis, le domaine d'eau est immobile initialement, alors que pour le modèle de Rayleigh-Plesset, il est initialement instantanément mis globalement en mouvement : cette mise en mouvement nécessite un certain temps dans le modèle éléments-finis compressible (propagation d'onde).

La Figure XIV compare les pressions dans le liquide en surface de la bulle et de la structure pour le cas d'un réservoir en acier. Les pressions appliquées à la structure sont intéressantes à relever dans ces simulations car cette information serait nécessaire pour le dimensionnement des structures au coup de bélier hydrodynamique. Dans le cas du réservoir en acier, les pressions prédites par le modèle analytique de Rayleigh-Plesset sont légèrement supérieures, et le battement de la bulle dure un temps légèrement plus court que ceux obtenus par simulation éléments-finis. L'impulsion transmise à la structure (21) est de $5.79{\cdot}10^4$ N.s pour le modèle analytique de Rayleigh-Plesset au lieu de $5.60{\cdot}10^4$ N.s dans la simulation éléments-finis com-

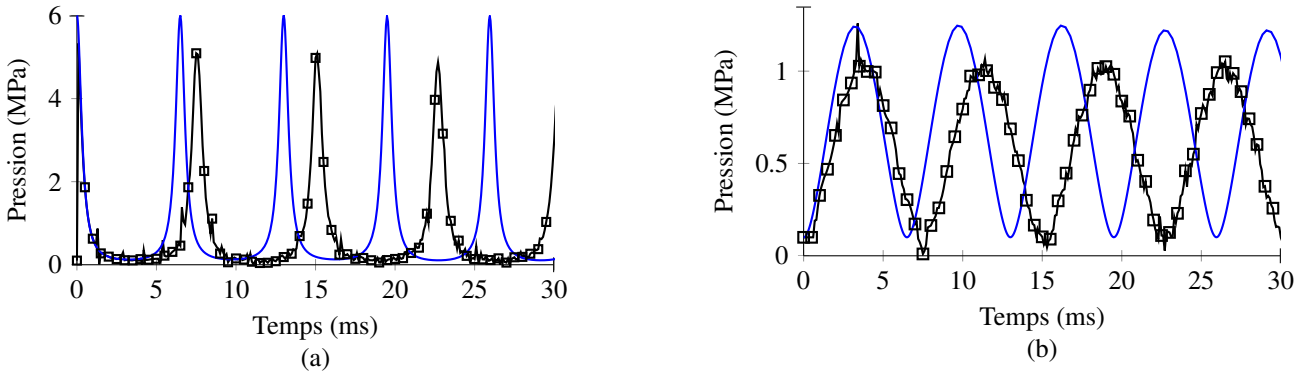

FIGURE XIV – Comparaison des pressions dans la bulle (a) et appliquées sur la paroi de la structure (b) prédites dans un réservoir d'acier avec des simulations éléments-finis (—□—) et avec le modèle de Rayleigh-Plesset confiné (—).

pressible, soit une différence de 3.3%. Le même ordre de grandeur est trouvé dans les trois cas étudiés. Cependant, comme cela peut être observé sur ces figures, le profil des courbes de pression appliquées sur la structure est significativement différent entre les deux modèles.

$$Imp = \int_{t_0}^{t_{implosion}} 4\pi R_s^2 P_s dt \tag{21}$$

Ces résultats montrent finalement que lorsque les rayons de bulles prédits avec les deux méthodes sont similaires, le modèle de Rayleigh-Plesset fournit également une approximation correcte des pressions appliquées à la structure et de l'impulsion qui lui est transmise. Cependant après la première implosion de bulle, le déphasage entre les deux modèles augmente. Même si les impulsions calculées avec les deux modèles sont proches, il est évident que les courbes de pressions calculées révèlent une différence significative en termes d'évolution temporelle, et ce même au cours du premier battement.

IV Développement et validation d'un modèle compressible de type Keller-Miksis confiné

L'effet de la compressibilité du liquide sur la dynamique de bulles de gaz oscillant dans un réservoir sphérique est évalué dans le paragraphe précédent. Il y est montré que sur les cas étudiés le modèle de Rayleigh-Plesset confiné donne une prédiction acceptable de la dynamique de la bulle et des chargements appliqués sur la structure (différence en impulsion inférieure à 3,5%). Cependant des différences significatives sont observées dans le profil temporel des courbes de pression appliquées à la structure, en comparant les modélisations analytiques incompressibles et les simulations éléments-finis compressibles. De plus, pour des réservoirs très rigides, le modèle de Rayleigh-Plesset peut prédire des résultats non-physiques dus à l'absence d'effet de compressibilité. Il ne permet pas non plus de prédire précisément les pressions de battement après le premier écroulement de la bulle.

Pour résoudre ces problèmes, une version confinée du modèle de Keller et Miksis (1980) est proposée dans cette partie des travaux. La cohérence du modèle avec les résultats précédents

est étudiée, puis le modèle est de nouveau validé par rapport à des simulations éléments-finis. Finalement l'amélioration apportée par ce modèle pour la prédiction des chargements hydrodynamiques est quantifiée sur un cas académique. Ces travaux ont été soumis à publication dans Fourest et collab. (soumis), voir le Chapitre 5.

IV.1 Formulation du modèle de Keller-Miksis

Une modification de l'équation classique de Rayleigh-Plesset a été proposée dans la section II pour prendre en compte un effet de confinement de la structure sur la dynamique de bulle. L'objectif des travaux présentés dans ce paragraphe est de proposer une amélioration de ce modèle pour prendre en compte l'effet de la compressibilité du liquide dans un modèle semi-analytique de dynamique de bulles confinées.

Équation de base de la mécanique des fluides

Le modèle proposé est basé sur le modèle de Keller et Miksis (1980) qui est une modification du modèle de Keller et Kolodner (1956) visant à inclure l'effet d'un potentiel de vitesse convergent sur la dynamique d'une bulle. L'équation de Keller-Miksis est écrite dans le cas présent sous les hypothèses suivantes :

- déformation sphérique de l'interface de la bulle (pas de fission),
- l'effet de la gravité est supposé nul,
- la viscosité et la tension de surface sont négligeables,
- la bulle est au centre d'un conteneur sphérique de rayon interne R_s,
- il n'y a aucune cavitation sur la paroi du réservoir.

La vitesse de l'interface de la bulle doit être égale à la vitesse du fluide à la surface de la bulle, ce qui donne l'équation (22) :

$$\dot{R}_b = \frac{\partial \phi(R_b, t)}{\partial r} \tag{22}$$

Le potentiel de vitesse ϕ, la pression P, et la densité du liquide ρ_l doivent satisfaire les équations de conservation de la masse (23), de Navier-Stokes (24), et d'état (25) (ici la loi des gaz parfaits),

$$\frac{\partial \rho_l}{\partial t} + \frac{\partial \phi}{\partial r}\frac{\partial \rho_l}{\partial r} + \rho_l \left(\frac{\partial^2 \phi}{\partial r^2} + \frac{2}{r}\frac{\partial \phi}{\partial r} \right) = 0 \tag{23}$$

$$\rho \left(\frac{\partial}{\partial t}\frac{\partial \phi}{\partial r} + \frac{\partial \phi}{\partial r}\frac{\partial^2 \phi}{\partial r^2} \right) + \frac{\partial P}{\partial r} = 0 \tag{24}$$

$$P_b = P_{b_0} \left(\frac{R_{b_0}}{R_b} \right)^{3\gamma} \tag{25}$$

L'équation de Navier-Stokes (24) est intégrée par rapport à r de r à l'infini, ce qui donne (26) :

$$-\dot{\phi} - \frac{1}{2}\frac{\partial \phi}{\partial r}^2 + \int_r^\infty \frac{dP}{\rho_l} = 0 \tag{26}$$

Ensuite, l'équation (26) est différentiée par rapport à t, avec $\frac{\partial P}{\partial t} = \frac{\partial P}{\partial \rho_l}\frac{\partial \rho_l}{\partial t} = c^2\frac{\partial \rho_l}{\partial t}$ avec $c^2 = \frac{\partial P}{\partial \rho_l}$ et c la vitesse du son dans le liquide, pour donner (27) :

$$\frac{\partial^2 \phi}{\partial t^2} + \frac{\partial \phi}{\partial r}\frac{\partial^2 \phi}{\partial t \partial r} + \frac{c^2}{\rho_l}\frac{\partial \rho_l}{\partial t} = 0 \tag{27}$$

Puis, (23) est utilisée dans (27) pour éliminer $\partial\rho_l/\partial t$, et divisée par c^2 pour obtenir (28) :

$$\frac{1}{c^2}\frac{\partial^2 \phi}{\partial t^2} - \frac{\partial^2 \phi}{\partial r^2} - \frac{2}{r}\frac{\partial \phi}{\partial r} = \frac{1}{\rho}\frac{\partial \rho_l}{\partial r}\frac{\partial \phi}{\partial r} - \frac{1}{c^2}\frac{\partial \phi}{\partial r}\frac{\partial \partial \phi}{\partial r \partial t} \tag{28}$$

L'équation de Keller-Miksis est écrite en faisant l'hypothèse que pour un fluide presque incompressible c^2 est grand et $\partial\rho/\partial r$ est petit. Cela mène à l'équation classique de propagation des ondes (29) :

$$\frac{1}{c^2}\frac{\partial^2 \phi}{\partial t^2} - \frac{\partial^2 \phi}{\partial r^2} - \frac{2}{r}\frac{\partial \phi}{\partial r} = 0 \tag{29}$$

Pour simplification, la densité du liquide ρ_l est fixée constante dans (26), ce qui donne (30) pour l'expression de la pression dans le liquide :

$$P(r,t) = P_\infty - \rho_l\left(\frac{\partial \phi}{\partial t} + \frac{1}{2}\left(\frac{\partial \phi}{\partial r}\right)^2\right) \tag{30}$$

Dérivation et résolution de l'équation différentielle de Keller-Miksis

En supposant que ϕ respecte l'équation de propagation des ondes (29), il peut être écrit dans (31) comme la somme d'un potentiel convergent et d'un potentiel divergent :

$$\phi = \frac{f(t - r/c)}{r} + \frac{g(t + r/c)}{r} \tag{31}$$

En définissant $\Delta(R_b)$ dans (32) comme la différence de pression divisée par la densité du liquide :

$$\Delta(R_b) = \frac{P_b - P_\infty}{\rho_l} = -\frac{\partial \phi}{\partial t} - \frac{1}{2}\left(\frac{\partial \phi}{\partial r}\right)^2 \tag{32}$$

et en utilisant (31) dans (32) et dans (22), on obtient pour exprimer R_b sans f (33) :

$$R_b\Delta(R_b) - cR_b\dot{R}_b = c\phi(R_b,t) - \frac{1}{2}R_b\dot{R}_b^2 - 2g'(t + \frac{R_b}{c}) \tag{33}$$

Finalement (33) est dérivée par rapport au temps et (32) est utilisée pour éliminer $\partial\phi/\partial t$, ce qui aboutit à l'équation différentielle classique de Keller-Miksis (34) :

$$-\ddot{R}_b R_b(\dot{R}b - c) = \frac{1}{2}\dot{R}_b{}^3 + \dot{R}_b\Delta(R_b) - c\left(\frac{3}{2}\dot{R}_b{}^2 - \Delta(R_b)\right) + R_b\dot{R}_b\Delta'(R_b) + 2\left(1 + \frac{\dot{R}_b}{c}\right)g''\left(t + \frac{R_b}{c}\right) = 0 \quad (34)$$

Pour résoudre cette équation différentielle, la fonction $g(t + R_b(t)/c)$ doit être exprimée. Dans cette partie des travaux, cette fonction est utilisée pour tenir compte de l'influence d'un conteneur sphérique sur la dynamique de la bulle. Pour cela il faut premièrement calculer f et f' qui sont exprimés dans (35) et (36) par combinaison de (22) et (32) pour $r = R_b$:

$$f(R_b, t) = -R_b^2\dot{R}_b + \frac{R_b^2}{c}\left(\Delta(R_b) + \frac{\dot{R}_b{}^2}{2}\right) - g(R_b, t) + \left(\frac{2R_b}{c}g'(R_b, t)\right) \quad (35)$$

$$f'(R_b, t) = -R_b\Delta(R_b) - g'(R_b, t) - \frac{1}{2}R_b\dot{R}_b{}^2 \quad (36)$$

Initialement $g = g' = 0$ puis pour $t > (R_{s_0} - R_{b_0})/c$, qui est le temps nécessaire au potentiel de vitesse pour atteindre l'interface de la structure depuis la surface de la bulle, g' est exprimé en utilisant (22) et (31) pour $r = R_s$, ce qui donne (37). g est alors obtenue par intégration numérique et g'' par différentiation numérique. Il faut être prudent lors de cette différentiation et s'assurer que cela ne génère pas de bruit numérique lors de la résolution.

$$g'(Rs, t) = R_s c\left(\dot{R}_s + \frac{1}{R_s^2}(f(R_s, t) + g(R_s, t)) + \frac{1}{R_s c}f'(R_s, t)\right) \quad (37)$$

Les relations entre f et g aux surfaces de la bulle et de la structure sont finalement obtenues en utilisant l'équation des ondes (29), ce qui donne $f(R_b, t_1) = f(R_s, t_2)$ avec $t_2 = (R_s(t_2) - Rb(t_1))/c + t_1$ et $g(R_s, t_1) = g(R_b, t_2)$ avec $t_2 = (R_s(t_1) - Rb(t_2))/c + t_1$.

IV.2 Application des équations dans le cas d'un conteneur sphérique élastique

Pour éviter à ce stade tout problème de différentiation numérique pour g'', à la place de l'équation (5) qui modélise la réponse statique d'une coque sphérique soumise à une pression uniforme, un modèle de réponse dynamique de conteneur sphérique est utilisé. Cela permet d'assurer la continuité de la fonction R_s qui est alors obtenue par intégration. Pour simplifier les écritures, le rayon interne de la sphère est pris égal au rayon moyen de la coque sphérique. Cette approximation est justifiée car l'épaisseur de la coque est faible par rapport au rayon interne du conteneur.

Dans le cas d'une coque sphérique soumise à une pression uniforme, la courbure est constante et il n'y a des déplacements que dans la direction radiale. Les déformations sont donc calculées en utilisant l'approximation polynomiale de Reissner (1944) (38) :

$$\varepsilon_{\theta\theta} = \varepsilon_{1_{\theta\theta}} + \varepsilon_{2_{\theta\theta}}(r - R_s) + \varepsilon_{3_{\theta\theta}}(r - R_s)^2 \quad (38)$$

avec $\varepsilon_{1_{\theta\theta}}$ le coefficient de membrane, $\varepsilon_{2_{\theta\theta}}$ le coefficient de flexion, et $\varepsilon_{3_{\theta\theta}}$ le coefficient quadratique, rappelés dans le cas d'une coque sphérique dans (39) :

$$\varepsilon_{1_{\theta\theta}} = \frac{R_s - R_{s_0}}{R_{s_0}} \quad ; \quad \varepsilon_{2_{\theta\theta}} = -\frac{R_s - R_{s_0}}{{R_{s_0}}^2} \quad ; \quad \varepsilon_{3_{\theta\theta}} = \frac{R_s - R_{s_0}}{{R_{s_0}}^3} \tag{39}$$

En utilisant la loi de Hooke, les contraintes s'exprime comme (40) :

$$\sigma_{\theta\theta} = E\frac{1+\nu}{1-\nu^2}\varepsilon_{\theta\theta} = E\frac{1+\nu}{1-\nu^2}(R_s - R_{s_0})\left(\frac{1}{R_{s_0}} - \frac{(r-R_s)}{R_{s_0}^2} + \frac{(r-R_s)^2}{R_{s_0}^3}\right) \tag{40}$$

Le flux de membrane $N_{\theta\theta}$ peut alors être calculé en utilisant (41) :

$$N_{\theta\theta} = \frac{E(1+\nu)}{1-\nu^2}\left(e\varepsilon_{1_{\theta\theta}} + \frac{e^3}{12}\left(\varepsilon_{3_{\theta\theta}} + \frac{\varepsilon_{2_{\theta\theta}}}{R_{s_0}}\right)\right) \tag{41}$$

Finalement l'équation d'équilibre (42) permet d'obtenir l'équation de mouvement d'une coque sphérique soumise à une pression spatialement uniforme (43), ce qui permet de calculer $\dot{R}_s$ et R_s.

$$\frac{-2N_{\theta\theta}}{R_{s_0}} + P_s - P_{s_0} + \rho h\ddot{R}_s = 0 \tag{42}$$

$$-\rho_s e\ddot{R}_s + P_s - P_{s_0} - \frac{2E(1+\nu)}{1-\nu^2}\frac{(R_s - R_{s_0})}{R_{s_0}^2}\left(e + \frac{2e^3}{12R_{s_0}}\right) = 0 \tag{43}$$

Les équations fluides et structures sont enfin couplées en utilisant (30) pour calculer le terme P_s dans (43).

Vérification du modèle compressible de dynamique de bulle dans un réservoir élastique

L'équation classique de Keller-Miksis est équivalente à celle de Rayleigh-Plesset quand la vitesse du son dans le liquide tend vers l'infini (Keller et Miksis 1980). Donc il est d'abord vérifié que lorsque la vitesse du son dans le liquide est élevée, les deux modèles confinés prédisent les mêmes dynamiques de bulles. Pour cela, la Figure XV compare les rayons de bulles prédits dans un réservoir avec le modèle de Keller-Miksis confiné pour plusieurs valeurs de vitesse du son, et avec le modèle de Rayleigh-Plesset confiné. Il est observé qu'en augmentant la vitesse du son dans le liquide, le modèle de Keller-Miksis confiné converge vers le modèle de Rayleigh-Plesset confiné. Pour une vitesse du son de $c_l = 10000$ m.s^{-1} les résultats obtenus avec les deux modèles sont identiques.

Le développement d'un modèle de dynamique de bulle confinée est effectué pour prendre en compte l'interaction entre la bulle et le réservoir. La Figure XVI compare les dynamiques de bulles prédites dans un conteneur infiniment rigide et dans des conteneurs ayant différentes raideurs. Le modèle se comporte comme attendu : l'amplitude et la période des bulles augmentent quand la rigidité globale de la structure diminue.

La Figure XVII présente un exemple de comportement du modèle analytique compressible confiné pour une paroi en acier de 6 mm d'épaisseur, à $R_s = 2$ m du centre de la bulle, sur une période de battement de la bulle. La Figure XVII-(a) présente la propagation de l'onde initiale et ses réflexions successives sur les parois de la structure et de la bulle. La Figure XVII-(b) montre la variation du rayon de la structure. Il est intéressant de noter que les temps auxquels l'onde interagit avec la structure correspondent à des changements brusques dans la pression à

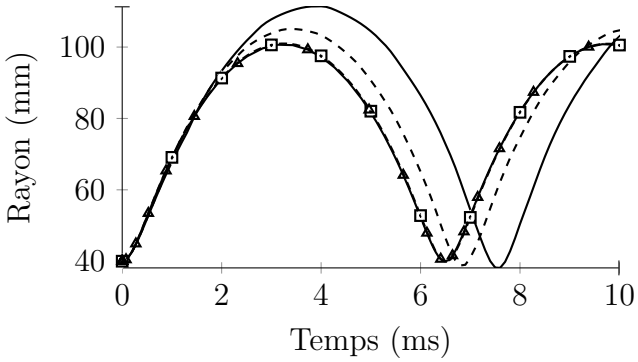

FIGURE XV – Rayons de bulles prédits dans un réservoir de rayon interne $R_s = 1$ m et d'épaisseur 6 mm d'acier avec le modèle de Keller-Miksis confiné avec $c_l = 1500$ m.s^{-1} (—), $c_l = 2500$ m.s^{-1} (- - -), $c_l = 10000$ m.s^{-1} (—□—) et avec le modèle de Rayleigh-Plesset confiné $c_l = \infty$ (—△—).

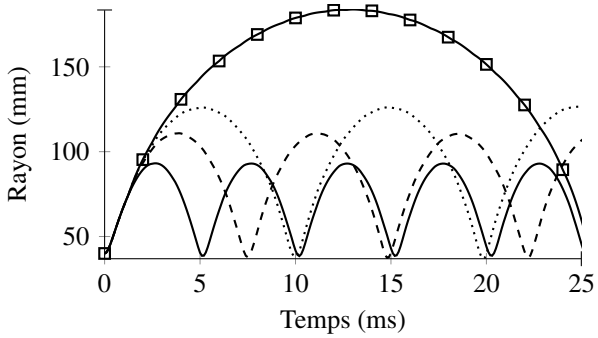

FIGURE XVI – Rayons de bulles prédits avec le modèle de Keller-Miksis dans des réservoirs de rayons internes $R_s = 1$ m rigide (—), d'épaisseur 6 mm en acier (- - -), en aluminium ($\cdot\cdot\cdot$), et en PMMA (—□—).

l'interface comme cela peut être observé sur la Figure XVII-(c). Il peut être noté qu'à la fin de la première période, ni la position de la paroi du réservoir ni les pressions appliquées à cette paroi ne retrouvent leurs valeurs initiales comme cela est le cas dans le modèle de Rayleigh-Plesset confiné.

Comparaison avec des simulations par éléments-finis de dynamiques de bulles dans des conteneurs élastiques

Les résultats obtenus avec le modèle de Keller-Miksis compressible confiné dans des réservoirs élastiques sont maintenant comparés à ceux obtenus par simulations éléments-finis. La Figure XVIII-(a) compare l'évolution des rayons de bulles dans trois conteneurs élastiques de rayons internes $R_s = 1$ m. La Figure XVIII-(b) compare les évolutions des rayons internes des réservoirs dans les mêmes cas. Les résultats obtenus dans tous les cas présentent un bon accord durant la première période de pulsation de la bulle. La différence maximale est obtenue pour le réservoir en PMMA (1% sur l'amplitude de la bulle et 3.5% sur sa période). Une différence de l'ordre de 5% est trouvée pour la réponse de la structure. Contrairement aux résultats typiquement obtenus avec le modèle de Rayleigh-Plesset confiné, les réponses des structures trouvées

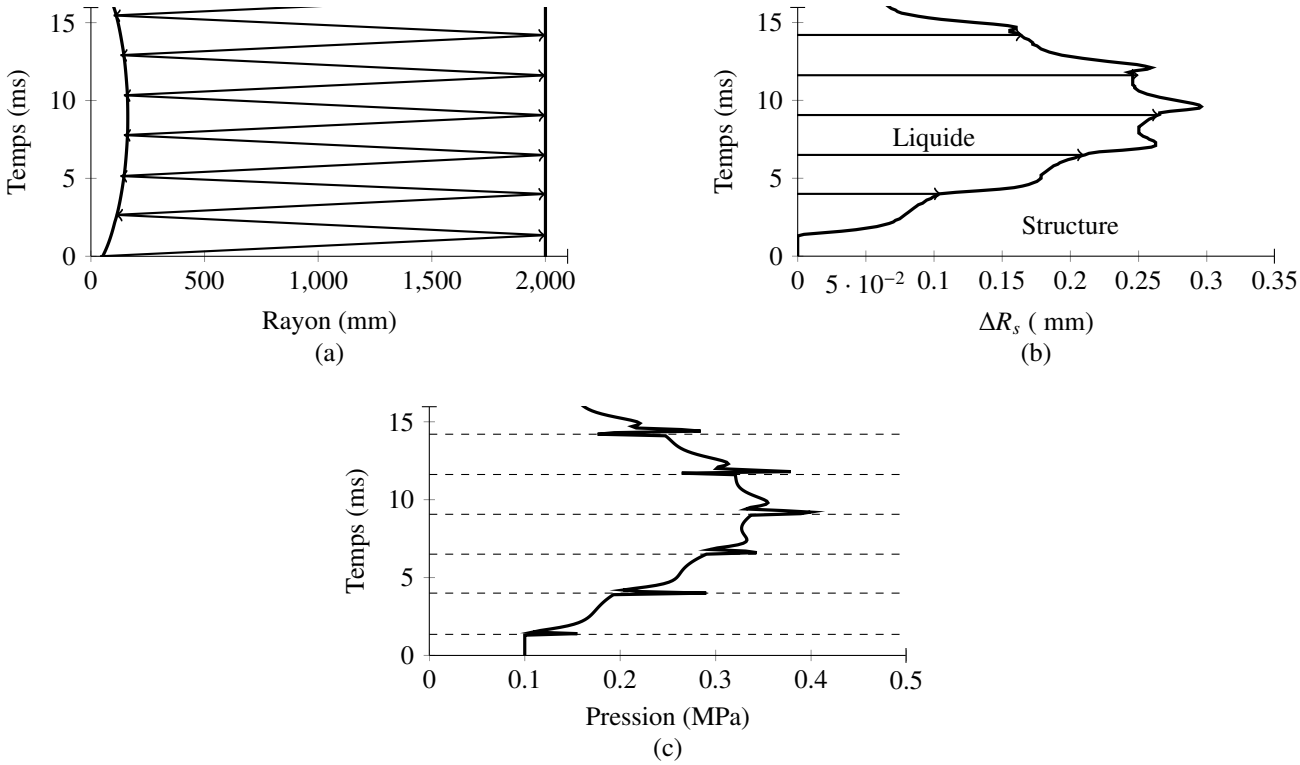

FIGURE XVII – Propagation du potentiel de vitesse initial dans le liquide (a) et variation du rayon de la structure (b), et pressions appliquées sur la structure (c) pour une bulle dans un réservoir élastique de rayon interne $R_s = 2$ m et d'épaisseur 6 mm en acier.

en utilisant le modèle de Keller-Miksis confiné oscillent d'une manière similaire à celles calculées par simulations éléments-finis.

Les Figures XVIII-(c) et (d) comparent les pressions aux interfaces de la structure et de la bulle calculées avec le modèle analytique de Keller-Miksis et la simulation éléments-finis. Les pressions prédites sur la surface de la structure sont en bon accord, en particulier lors de la première période de la bulle. Les pressions de bulle prédites en utilisant le modèle de Keller-Miksis confiné sont supérieures aux résultats éléments-finis, en particulier lors des rebonds de la bulle. Ceci est dû au fait que des rayons de bulle plus petits sont atteints au terme de l'implosion de la bulle dans le modèle de Keller-Miksis confiné. Il est possible que ce phénomène vienne d'un léger amortissement dans les simulations éléments-finis ou de l'hypothèse de propagation acoustique dans le modèle analytique. Cependant l'accord reste très bon, ce qui valide le modèle proposé de Keller-Miksis confiné dans un réservoir élastique.

Évaluation de l'amélioration dans les prédictions en utilisant le modèle de Keller-Miksis confiné

Dès lors que la version confinée du modèle de Keller-Miksis est validée pour l'analyse des dynamiques de bulles dans des réservoirs sphériques élastiques, l'amélioration en termes de prédiction apportée par ce modèle par rapport au modèle de Rayleigh-Plesset confiné peut être évaluée. Il a déjà été expliqué que pour des réservoirs très rigides le modèle de Rayleigh-Plesset

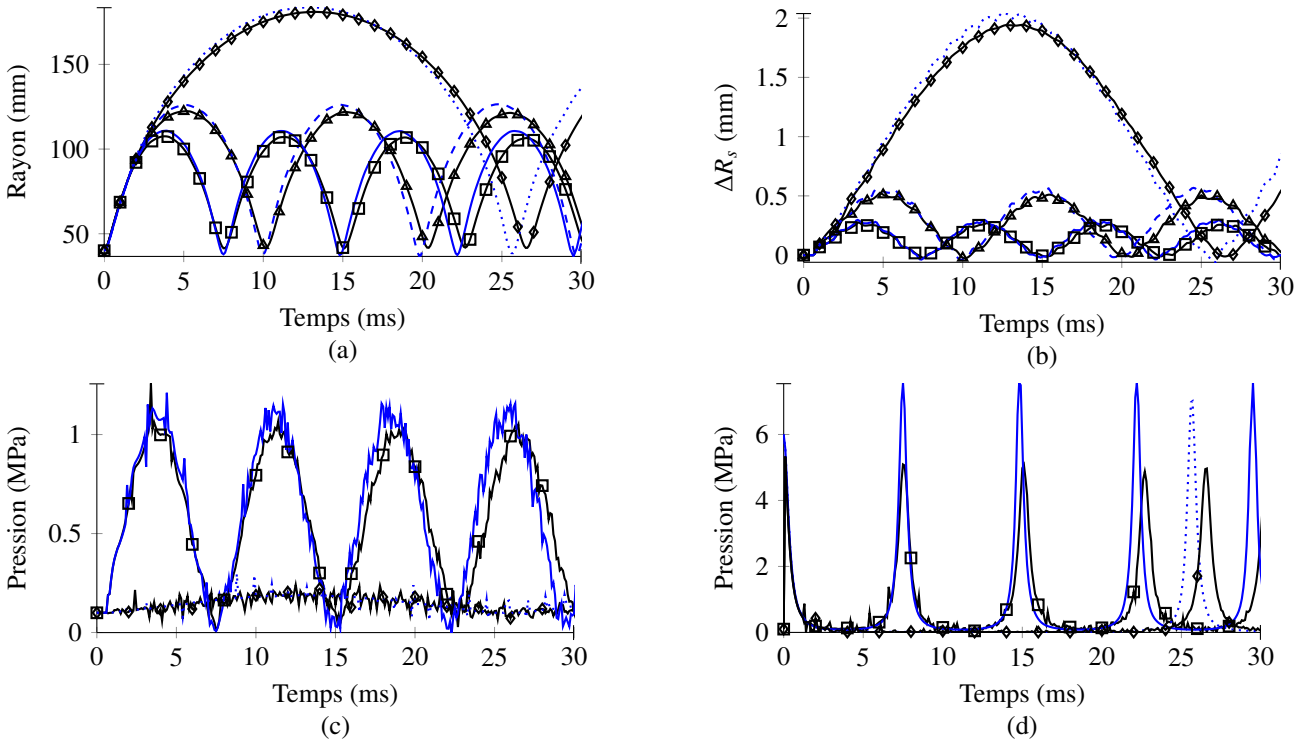

FIGURE XVIII – Rayons de bulles (a), rayons internes des réservoirs (b), pressions aux parois des structures (c) et des bulles (d) prédites en utilisant le modèle de Keller-Miksis confiné dans un réservoir de rayon interne $R_s = 1$m de 6 mm d'épaisseur en acier (——), en aluminium (- - -) et en PMMA (·····) et en utilisant des simulations éléments-finis dans un réservoir en acier (—□—), en aluminium (—△—) et en PMMA (—◇—).

confiné peut prédire des résultats non-physiques : dans cette partie seule une comparaison sur un cas n'étant pas trop rigide va être présentée pour étudier l'amélioration apportée par le modèle, en termes de prédiction de la dynamique de bulle, du mouvement de la paroi du réservoir et des chargements hydrodynamiques appliqués sur le réservoir.

La Figure XIX compare ces grandeurs dans le cas d'un réservoir élastique de rayon interne $R_s = 1$ m et de 6 mm d'épaisseur en acier. Le modèle de Rayleigh-Plesset confiné prédit des rayons plus petits que le modèle de Keller-Miksis ce qui est logique puisque la compressibilité du liquide doit mener à l'obtention d'un rayon de bulle plus important pour un même niveau de pression. Le modèle de Keller-Miksis confiné prédit des rayons de bulle plus proches de ceux obtenus avec la simulation éléments-finis que le modèle de Rayligh-Plesset (3% à la place de 10% en amplitude et inférieur à 1% à la place de 7% pour la période). De manière similaire, les courbes de pression et de rayon interne prédites avec le modèle de Keller-Miksis ont des formes très proches de celles prédites par éléments-finis, ce qui n'est pas le cas avec celles obtenues avec le modèle de Rayleigh-Plesset. La différence en termes d'impulsion appliquée à la structure durant la première période est aussi plus faible (moins de 1% à la place de 3.5% avec le modèle de Rayleigh-Plesset confiné). Le modèle de Keller-Miksis confiné constitue donc bien une amélioration du modèle de Rayleigh-Plesset confiné, amélioration pouvant s'avérer d'importance pour des cas plus sévèrement confinés, ou des carburants plus compressibles.

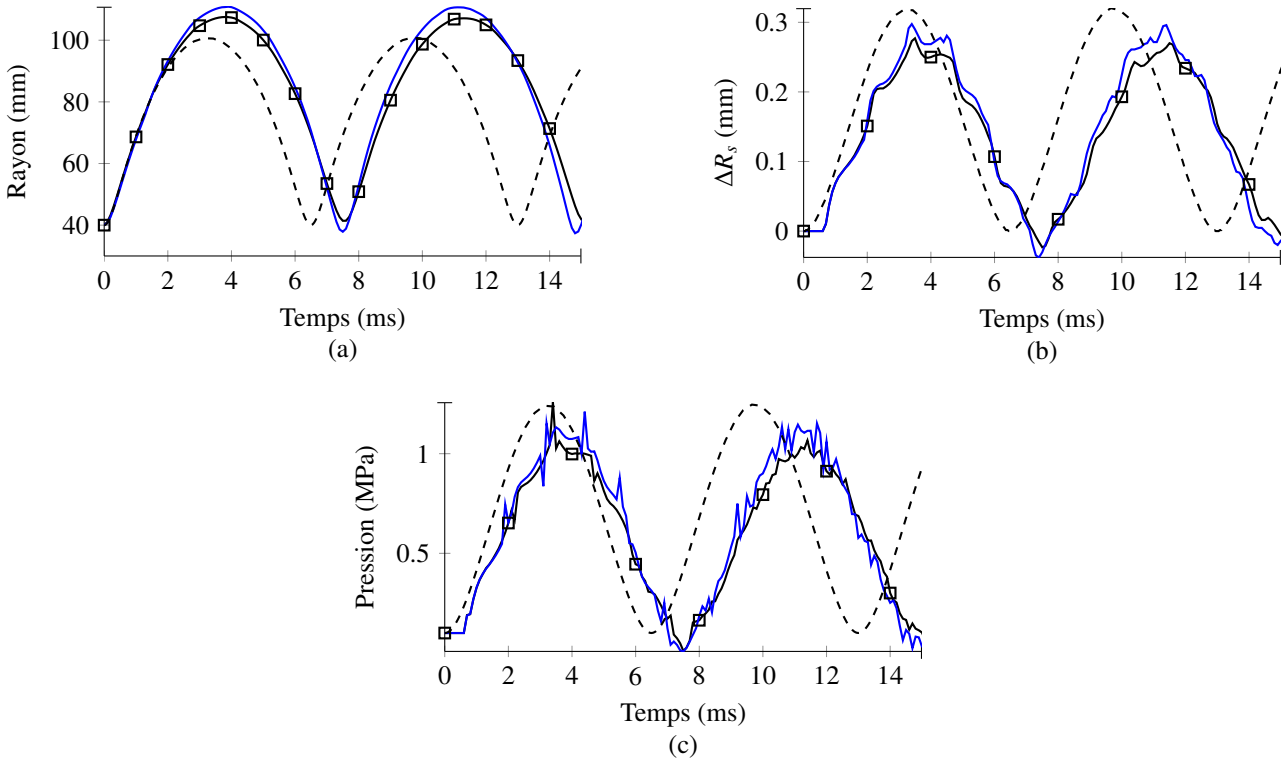

FIGURE XIX – Rayon de bulle (a), rayon interne du réservoir (b), pression aux parois de la structure (c) prédits en utilisant le modèle de Keller-Miksis confiné (——), le modèle de Rayleigh-Plesset confiné (- - -) et une simulation éléments-finis (—□—) dans un réservoir de rayon interne $R_s = 1$m de 6 mm d'épaisseur en acier.

V Conclusions et perspectives

Le travail de thèse présenté s'inscrit dans un axe de recherche visant à améliorer les connaissances et prédictions des chargements hydrodynamiques subis par les réservoirs de carburants lors d'impacts balistiques (coup de bélier hydrodynamique) pour améliorer la survivabilité des structures aéronautiques. Les modèles numériques les plus avancés ne permettent pas aujourd'hui encore de simuler le phénomène complet. De plus les modèles développés sont trop coûteux pour être utilisés lors de la conception ou de l'optimisation de réservoirs durant leur phase de développement. La recherche proposée a consisté à développer un modèle semi-analytique et des outils capables de simuler la séquence d'expansion et d'écroulement de la bulle de cavitation se produisant lors d'un coup de bélier hydrodynamique, et d'utiliser ce modèle pour déterminer les paramètres influant aux premier et second ordres sur les prédictions numériques des chargements hydrodynamiques lors de coups de bélier hydrodynamiques.

Pour parvenir à cet objectif une version modifiée de l'équation de Rayleigh-Plesset - qui décrit la dynamique d'une bulle de gaz sphérique dans un domaine de liquide infini - a été proposée pour inclure les effets de confinement du réservoir sur une dynamique de bulle. Ce modèle a été appliqué à deux essais de coup de bélier hydrodynamique : le premier dans un conteneur générique et le second dans un bassin. Un bon accord entre les résultats expérimentaux et numériques a été obtenu en calibrant le paramètre de confinement introduit dans les équations,

qui est lié à la rigidité du réservoir. Les résultats obtenus tendent à confirmer qu'une version confinée du modèle de Rayleigh-Plesset s'avère adaptée au premier ordre pour l'étude du coup de bélier hydrodynamique. Cependant restent quelques limitations à son utilisation prédictive, en particulier ce paramètre de confinement nécessite une calibration.

Pour lever ces limitations, la capacité de modèles analytiques élastiques linéaires à estimer la valeur du paramètre de confinement a été évaluée. Pour ce faire, le conteneur étudié expérimentalement est un assemblage parallélépipédique multi-matériaux donc non-sphérique : un modèle de plaques a été développé pour le représenter, et la relation entre les déformations de la structure et la pression appliquée sur ses parois a été réécrite pour calculer la variation de volume interne du réservoir. A noter qu'avec un telle écriture "volumique" des déformations du réservoir, toutes les géométries de conteneurs peuvent être considérées sous l'hypothèse que la pression appliquée aux parois est homogène. Finalement, les dynamiques de bulles prédites lorsque le paramètre de confinement est évalué analytiquement ou calibré ont été comparées. La différence dans les prédictions en utilisant les deux méthodes s'est avérée relativement faible (11% en amplitude et 33% pour le temps d'implosion). Cet accord satisfaisant tend à confirmer qu'un modèle analytique peut être intéressant pour dégrossir ce problème mécanique supposé hautement directionnel.

Cependant, le modèle de Rayleigh-Plesset proposé présente des limitations dues aux hypothèses sur lesquelles il est fondé. En particulier, la compressibilité du liquide peut influencer la dynamique des bulles confinées et les chargements hydrodynamiques associés. Pour déterminer dans quelle mesure ce facteur affecte la dynamique de bulles confinées, le modèle de Rayleigh-Plesset confiné a donc été comparé à des simulations éléments-finis explicites de croissance de bulles confinées. Une différence notable a été trouvée entre les dynamiques de bulles et les chargements hydrodynamiques prédits par les deux méthodes.

Pour prendre en compte l'effet de la compressibilité du liquide sur la dynamique de bulles confinées, un modèle semi-analytique de dynamique de bulles confinées a donc finalement été développé. Ce modèle est basé sur celui de Keller-Miksis, qui décrit la dynamique de bulles dans un domaine de liquide infini compressible, et associé à une formulation dynamique de la réponse élastique d'un conteneur sphérique basée sur l'approximation polynomiale de Reissner. La cohérence de ce modèle avec les résultats précédents a été vérifiée, puis il a de nouveau été validé par rapport à des simulations éléments-finis, ce qui a permis de démontrer l'amélioration apportée par le modèle de Keller-Miksis dans la prédiction des chargements hydrodynamiques par comparaison avec le modèle de Rayleigh-Plesset.

Pour faire le bilan du travail de thèse, une analyse critique des modèles par rapport à l'existant a été réalisée. Les conclusions sont principalement établies en comparaison avec des modélisations éléments-finis (Varas et collab. 2009b; 2012a; 2012b ; Artero-Guerrero et collab. 2013 ; Sareen et Smith 1996) car c'est la seule méthode décrite dans l'état de l'art qui permette de prédire une partie du phénomène de manière réaliste. Deux modèles semi-analytiques ont finalement été développés pour décrire la dynamique de bulles de gaz créées par impacts balistiques dans des réservoirs remplis de liquide. Contrairement au modèle proposé par Lee et collab. (1997a), la forme de la cavité est ici supposée sphérique, elle ne dépend pas du mouvement du projectile qui la génère, mais seulement de l'énergie cinétique initiale de ce projectile. Le fait de considérer une cavité sphérique présente plusieurs avantages. Cela permet d'abord de résoudre numériquement un modèle unidimensionnel, ce qui est efficace en termes de coût de calcul. De plus, l'analyse est plutôt jugée conservative puisque l'apparition d'une bulle sphérique est liée au retournement du projectile, phénomène pour lequel Bless et collab. (1976) ont relevé

des pressions plus intenses qu'en l'absence de retournement. Cette observation expérimentale semble être confirmée par les résultats du paragraphe 2, dans lequel la bulle prédite présente le même temps d'implosion mais une amplitude supérieure à celle observée expérimentalement. C'est un avantage important des modèles proposés puisque le retournement d'un projectile haute vitesse est un phénomène complexe à simuler, en particulier pour des projectiles qui ne peuvent pas être considérés rigides (voir Deletombe et collab. (2013)) pour lesquels il n'y avait pas de modèles analytiques. La phénoménologie du retournement d'un projectile rigide a certes été simulée par Sareen et Smith (1996) en utilisant une méthode éléments-finis, mais leurs résultats n'ont pas été comparés à des données expérimentales. La "non-rigidité" du projectile peut être ici prise en compte par un abattement sur l'énergie cinétique transmise au fluide.

Reste que ces modèles ont encore quelques limitations. Il ne sont pas capables de prédire parfaitement l'onde secondaire émise au terme de l'implosion de la bulle. De plus, même si le modèle de Keller-Miksis permet de traduire le mécanisme de propagation des ondes, le caractère unidimensionnel des modèles induit des limitations à leur utilisation, en particulier le conteneur est toujours supposé sphérique. Autre point : il a été montré qu'en considérant un conteneur sphérique de même rigidité globale qu'un conteneur d'une autre géométrie, il était possible d'obtenir une approximation intéressante de la dynamique de bulles créées par coups de bélier hydrodynamiques, mais seule une réponse élastique du réservoir est pour l'instant considérée, donc aucune non-linéarité (et donc dissipation structurale) n'est prise en compte (plasticité, rupture, ...), alors que cela est clairement observé expérimentalement (Deletombe et collab. 2013 ; Varas et collab. 2009a ; Lecysyn et collab. 2010).

Autre élément : ces modèles ne sont pas adaptés à l'analyse prédictive d'impacts dans des configurations présentant une surface libre, tel que l'impact dans la piscine hydrodynamique décrit dans Deletombe et collab. (2013), pour lequel un très bon accord a néanmoins pu être obtenu en calibrant le paramètre de confinement. Aucune solution n'a été proposée pour évaluer analytiquement la valeur de ce paramètre dans un tel cas. Il ne peut donc pas être utilisé pour l'analyse de réservoirs partiellement remplis. Cette limitation est relative car Varas et collab. (2009a) ont estimé (comme bien d'autres) que des pressions et des dommages plus importants étaient attendus pour des réservoirs entièrement remplis, ce qui laisse supposer qu'étudier un réservoir empli à 100% est également conservatif.

Enfin, il reste délicat à ce stade du développement d'utiliser ces modèles avec confiance pour le dimensionnement de réservoirs au coup de bélier hydrodynamique, en particulier à cause du manque de cas de validation expérimentale (sur conteneurs sphériques), et des limitations discutées précédemment. Néanmoins ces modèles peuvent donner une approximation intéressante des chargements hydrodynamiques appliqués sur le réservoir pendant la phase de cavitation. De plus, au delà du développement de ces modèles, la recherche a permis d'atteindre une meilleure compréhension du phénomène de coup de bélier hydrodynamique, en apportant des connaissances sur l'effet de la pression du gaz de la bulle (qui est négligeable), de la présence de vapeur (étant aussi négligeable) ou de la compressibilité du liquide sur la dynamique de bulles et les prédictions de chargements hydrodynamiques. Ceci constitue une amélioration significative dans le domaine, car comme cela est rappelé dans l'état de l'art, il n'y avait pas de modèles analytiques pour décrire la phase de cavitation dans un domaine borné, confiné et déformable.

Concernant les perspectives de ces travaux, plusieurs éléments/pistes de réflexion peuvent être mentionnés :

- premièrement, puisqu'un modèle analytique de dynamique de bulle confiné dans un liquide

compressible a été développé, il serait intéressant d'établir les limites du domaine de validité du précédent modèle de Rayleigh-Plesset (plus facile à utiliser),

- une validation expérimentale des modèles proposés serait forcément une étape importante pour augmenter la confiance dans cette approche, et permettre son utilisation pour le dimensionnement de réservoirs réels civils, aéronautiques ou militaires,
- puisque une des limitations de ces modèles est la géométrie sphérique des conteneurs et des bulles traités, les dynamiques de bulles quelconques dans des conteneurs non-sphériques pourraient être étudiées,
- enfin, le couplage de ces modèles analytiques avec des modèles éléments-finis de la structure, de la même manière qu'évoquée dans le paragraphe II.3, pourrait être mis en œuvre pour passer outre les limitations du modèle (structures sphériques élastiques).

Remerciements

L'auteur tient à remercier le Ministère de la Défense ainsi que la DGA pour leur support financier dans la réalisation de cette thèse. Il souhaite aussi remercier le Dr Daniel Fuster du CNRS/UPMC Université Paris 06, UMR 7190, le Dr Vincent Faucher du CEA et le Dr Bertrand Langrand de l'ONERA pour leurs précieux conseils, suggestions, et pour leur aide durant la réalisation de ces travaux, ainsi que Jacky Fabis de l'ONERA à l'origine de l'idée d'une analogie entre le phénomène de coup de bélier hydrodynamique et celui d'explosion sous-marine.

Introduction

In the event of an impact of high speed/high energy projectiles on liquid filled tanks, the container may suffer large hydrodynamic loads that could possibly rupture the entire structure. This impact scenario is referred to as hydrodynamic ram (HRAM).There is an insistent need for tools to model hydrodynamic effects that occur during a hydrodynamic ram for military but also civilian aircraft design (vulnerability requirement). In this context it is admitted that numerical modelling of hydrodynamic ram would allow to improve the survivability of structures with respect to this particular threat.

Pioneer studies on the subject were carried out by Morse and Stepka (1966); Stepka and Morse (1963); Stepka et al. (1964, 1965); Stepka (1966). They performed numerous experimental measurements during high speed projectile impacts on liquid filled tank. They identified the factors that affect the loading during a hydrodynamic ram event. These factors can be organised according to the three media: the projectile (shape, size, and material), the tank wall (the thickness, material, pre-stress, and protective structure) and the liquid properties. They tried to determine the influences of the different parameters on the survivability of tanks. However they could not clearly establish a correlation that would embrace the effects of all parameters.

The first numerical method used, that greatly simplifies the problem, is *the piston theory* to model the interaction between the fluid and the structure. This theory has been used by (Ball, 1974) to simulate tests results presented in (Ball, 1976). The numerical results obtained using this theory coupled with finite element codes was found to give displacements and strains inferior to the ones observed experimentally. The use of this theory was a first step toward a coupled resolution of the non-linear equations of the fluid and the structure. However this one dimensional approach underestimates the pressure transmitted to the structure walls during hydrodynamic ram events.

Lundstrom (1977) proposed the use of the Variable Image Method. In this method the pressure field is described as a potential function which satisfies the wave equation. This method permits to simulate bi-dimensional problems and to obtain a more realistic coupling between the fluid and the structure. However its use has not been very successful and is limited to geometrically simple cases.

Then Lagrangian finite element methods have been used, in particular by Kimsey (1980). He simulated in a realistic way the propagation of the shock wave and the drag of a cylindrical projectile that does not experience tumbling in a cylindrical container. Unfortunately the use of a Lagrangian formulation is not adapted to deal with the large deformations of the liquid during a hydrodynamic ram event. So these simulations have been limited to linear trajectories and to the first stages of the phenomena.

Varas et al. (2009a,b, 2012a,b) tested the impact and penetration of a high speed (600 and 800 m/s) spherical projectile in an aluminium tank. They recorded the evolution of the cavity

and the pressure measured at several positions in the tank. They also performed numerical simulations (ALE and SPH) and compared the computed results to the experimental ones. They obtained a good agreement in the bubble shape and dynamics and in the predicted pressure in the liquid. However they did not observe nor simulate the whole duration of the phenomenon and limited their studies to the drag and cavity growth stages. In addition they did not model any vaporisation process in their simulations and did not justify this assumption.

Deletombe et al. (2011, 2013) tested the impact of 7.62 mm NATO projectiles into a composite dummy tank and in a pool. In these tests the whole sequence of event of the bubble created in the wake of a tumbling projectile was recorded. In particular the bubbles created in the pool were particularly spherical. These tests furnished data for the validation of advanced numerical simulations of real projectile impacts in a tank and in a pool on the whole duration of the events. They concluded that none of the stages could be neglected for the sizing of structures because they could all induce significant impulse. However, due to the complexity of the numerical simulation of tumbling projectiles, these tests have not been simulated numerically.

A summary of these studies highlights that there exist numerical models capable of simulating the first stages of the phenomenon that have been validated against experimental data. Plus there exist experimental data on the whole sequence of events of a spherical bubble created in the wake of a projectile. However there are two main limitations: on the one hand no model has been proved capable of simulating hydrodynamic ram cavity dynamics during the whole sequence of events up to the collapse time[4]; on the other hand the approximations on the physics done in the more advanced models used in hydrodynamic ram simulations have not been justified, which raises questions on the validity of the model especially for the implosion stage for which it has not been validated.

It is in this context that this thesis work has been done. This research consists in developing an analytical model capable of simulating the expansion and collapse of the cavitation bubble for tumbling projectiles, and to use this model to determine the parameters that affect the predictions of hydrodynamic loads during hydrodynamic ram events.

First the research context and the state of the art of analytical and numerical modelling of the hydrodynamic ram phenomenon are introduced. To begin, a description of the hydrodynamic ram phenomenon is given with emphasis on the effect of two parameters: the tumbling of the projectile and the filling of the tank. Then the analysis of the state of the art shows the limitations of the current analytical and numerical models and hence the interest of developing a new model for the cavitation stage of this phenomenon. (Chapter 1)

Then the approach consists in estimating the error in the obtained solution when the gas behaviour is neglected in HRAM numerical simulations. For this the classic Rayleigh-Plesset equation has been applied to a set of chosen HRAM tests. This equation has been retained because it models a 1D single bubble dynamics in an infinite domain of liquid. To apply this equation, an original method based on an energetic criterion has been developed to determine the initial conditions needed in this equation. This criterion has been chosen to ensure the

[4] A preliminary study presented in Appendix A on the water entry of relatively low speed projectile ($10 m.s^{-1}$) shows that the cavity closing is a difficult stage to simulate using this type of tool even at relatively low impact speed.

energetic consistency of the model with respect to the tests. However the Rayleigh-Plesset equation models an infinite domain of liquid, which is not the case in the HRAM tests. A modification of this equation has then been proposed to include the effect of an elastic linear container on the predicted bubble dynamics. This version has been applied to the selected cases using a calibration of the confinement parameter (that defines the structure response). Finally this modified version of the Rayleigh-Plesset equation has been used to calculate the bubble dynamics with and without the gas behaviour in order to estimate the error obtained by doing such a simplification. The work presented in this chapter has been published in (Fourest et al., 2014). (Chapter 2)

The next step consists in evaluating the capability of linear elastic analytical model to estimate the numerical value of the confinement parameter in the modified Rayleigh-Plesset equation, that is calibrated in the previous chapter. This is done to validate the order of magnitude of the previously calibrated values. Firstly the numerical value of the proposed confinement parameter has been obtained by calibration on one of the previous HRAM cases. This value is calculated to obtain a reference for future comparisons. Then the numerical value of the confinement parameter is analytically calculated in two configurations. Firstly, it is calculated in an academic case when an elastic mono material spherical shell model is used for the structure. Then it is evaluated when an analytical plate model Timoshenko and Woinowsky-Krieger (1959) is used to model the linear behaviour of the multi-material orthorhombic test container. Finally the confinement parameter values and the bubble dynamics predicted when the confinement parameter is calibrated and evaluated with plate formulae are compared. The work presented in this chapter has been published in (Fourest et al., 2015c). (Chapter 3)

Once the order of magnitude of the calibrated and analytically evaluated confinement parameter have been compared, the next step is to compare the proposed confined Rayleigh-Plesset equation to a 1D bubble dynamics numerical model including the effect of compressibility and structure inertia. The objective of this comparison is to estimate the error in bubble dynamics and in hydrodynamic loads prediction when the liquid compressibility is neglected in HRAM bubble dynamics. Finite Element simulations have been run to obtain such a reference because it permits to perform simulations of bubble dynamics with the liquid compressibility and the structure inertia being modelled. First to determine the effect of the structure inertia the Rayleigh-Plesset model is compared to quasi-incompressible simulations (high speed of sound) to obtain the effect of this parameter alone. Then the Rayleigh-Plesset model is compared to compressible simulations. To achieve this, equivalent overpressure initial conditions are determined to have a domain of liquid at rest at the beginning to avoid introducing a bias in the study of the liquid compressibility effect. This work has been submitted as Fourest et al. (2015a).(Chapter 4)

The effect of the liquid compressibility on the confined bubble dynamics having been found significant in the previous chapter, it is chosen to develop an analytical confined bubble dynamics model that take its effects into account. First a formulation of this model is proposed. This formulation is based on the Keller-Miksis model that describes the dynamics of a gas bubble in an infinite domain of compressible liquid. This model is first developed for the case of a spherical rigid container, and its consistency is verified. Then the bubble radius and the pressure at the structure and bubble walls are compared to results obtained by finite element

simulations. Once the model has been validated in the case of a rigid container it has been developed for an elastic spherical container. For this a dynamic formulation of the container response based on Reissner's polynomial approximation is used. The consistency of this model is verified and it is compared with finite element simulations. Once the model is validated for an elastic spherical container, the bubble radii, structure wall movement and pressure at the structure wall predicted using the confined Rayleigh-Plesset and Keller-Miksis models are compared to evaluate the improvement in the predictions using the later one. This work has been submitted as Fourest et al. (2015d)(Chapter 5)

Then a general conclusion on the thesis work is given, and a critical analysis of the thesis work is given in comparison with existing models. Finally some outlooks of the thesis work are presented and briefly discussed.

Chapter 1

Context of the research and state of the art

Contents

1.1 Hydrodynamic Ram **41**

1.2 State of the art of Hydrodynamic Ram simulations **43**

1.2.1 Analytical models 43

1.2.2 Numerical models 45

This chapter introduces the context and the state of the art of analytical and numerical modelling of the hydrodynamic ram phenomenon. To begin a description of the hydrodynamic ram phenomenon is given with emphasis on the effects of two parameters: the tumbling of the projectile and the filling of the tank. Then the analysis of the state of the art shows the limitations of the current analytical and numerical models and hence the interest of developing a new model for the cavitation stage of hydrodynamic ram events.

1.1 Hydrodynamic Ram

The hydrodynamic ram phenomenon occurs during the penetration of a high speed/ high energy projectile or fragment in a liquid-filled tank. Ball (1985) described the hydrodynamic ram phenomenon in three stages: shock stage, drag stage and cavitation stage. To these stages numerous authors as (Varas et al., 2009a) added a possible projectile exit stage. These stages are illustrated in Figure 1.1. It is interesting to note that all experimental studies on the hydrodynamic ram phenomenon have been done on water filled containers, for security reasons, and that it is assumed by all authors that even if it is not the liquid used in real applications the properties of both liquids are not too different and that working on water filled containers gives insight on the behaviour of kerosene filled containers.

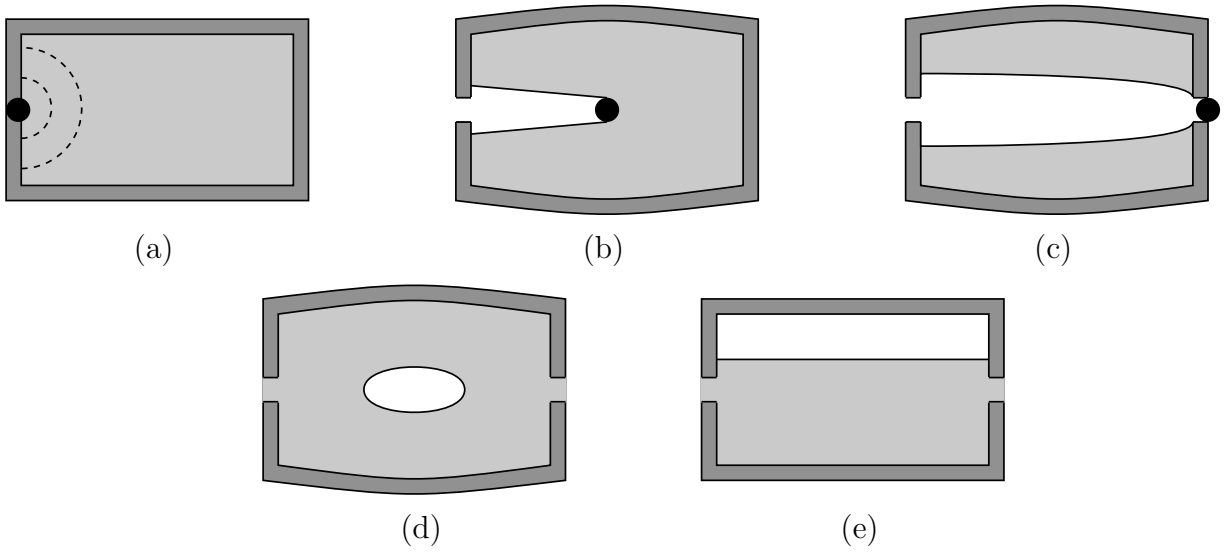

Figure 1.1 – Sketch of the stages of the hydrodynamic ram phenomenon: (a) shock stage, (b) drag stage, (c) exit stage, (d) cavity stage and (e) container after the hydrodynamic ram.

Shock stage: this stage starts when the projectile perforates the container and impacts the liquid. The first experimental observations of that phenomenon have been done by McMillen (1945) and McMillen and Harvey (1946) who studied the shock wave generated by the impact of steel spheres at high speed (from 610 $m.s^{-1}$ to 1500 $m.s^{-1}$) on a free water surface using a shadowgraph method. They observed that the projectile accelerates the liquid and generates an hemispherical shock wave centred on the impact point. They also observed that the projectile is quickly slowed down and that the shock wave speed rapidly converges to the speed of sound in the liquid. Same observations have been later made for impacts in liquid-filled containers and a spherical shock has been observed by Stepka et al. (1965) in a test in which the projectile is guided in a tube to the centre of the container. This wave is studied because it generates an impulsive loading of the structure in the vicinity of the impact point which may cause damages in the entry area (petalling, crack propagations,...). Later Disimile et al. (2009) observed that the pressure recorded during that stage is not always the more intense and that it depends on the projectile material (mass and impedance).

Drag stage: in this stage the projectile loses velocity when moving in the liquid due to the resistance opposed by the liquid. The kinetic energy lost by the projectile is transferred to the

liquid and sets it in motion. It generates a pressure pulse that propagates in the liquid and loads the container walls. May (1952) is the first to observe the movement of the cavity and its closure (surface sealing or deep sealing) for the impact of low speed projectiles (8 $m.s^{-1}$). Then Shi et al. (2000); Shi and Kume (2001, 2004); Shi and Takami (2001); Shi and Itoh (2009) made the same observations for the impact of higher speed projectiles (342 $m.s^{-1}$). Contrary to the shock phase, the liquid is set gradually in motion and not impulsionally. It results in lower pressure than in the shock stage but lasting a considerable longer time.

Cavitation stage: this stage occurs after the crossing of the projectile. During its crossing, the projectile transmits its velocity to the liquid and generates a cavity in its wake. Due to the high velocity of the impact, the cavity is not only filled with air but also with liquid vapour, especially when the wake of the projectile undergoes a sealing as in (Deletombe et al., 2013) contrary to (Varas et al., 2009a). This cavity oscillates while the liquid tries to reach its undisturbed state. This fluid movement and the resulting pressure might continue long after the exit of the projectile. During the implosion, of the cavity a secondary shock wave is emitted by the cavity and is reflected on the walls of the tank, which generates cavitation on the walls (see Deletombe et al. (2013)). This phenomenon might be another source of damage in the tank. Disimile et al. (2009) observed that the pressure peak emitted during this stage can be more intense that during the shock stage depending on the projectile mass (material). Then generally the cavity undergoes a fission due to its lack of sphericity which generates numerous gas bubbles during the rebound that follows the implosion. Then these bubbles continue to oscillate in the tank.

Exit stage: this stage starts when the projectile impacts the exit panel. Contrarily to the impact on the entry panel, the exit panel is pre-stressed or even already damaged. In a metallic tank a characteristic petalling damage is usually observed (Stepka, 1966).

There are several parameters that affect hydrodynamic ram phenomena such as those mentionned (Morse and Stepka, 1966; Stepka and Morse, 1963; Stepka et al., 1964, 1965; Stepka, 1966), which are related to the three media: the projectile (shape, size, and material), the tank wall (the thickness, material, and pre-stress, and protective structure) and the liquid properties. The effect of two others: the tumbling of the projectile and the filling percentage of the container are discussed hereafter.

Tumbling of the projectile: the tumbling of the projectile occurs because high speed/high energy projectiles are stable in air but not in water. The impact angle between the projectile and the tank wall strongly influences the occurrence and tumbling of the projectile (Sareen and Smith, 1996). Deletombe et al. (2013) presented impacts in water of non academic projectiles (7.62 mm NATO ammunition) at high speed (850 $m.s^{-1}$). They enlighten the differences in the cavity behaviour due to the tumbling of the projectile. When the projectile tumbles, it transmits more quickly its kinetic energy to the liquid. An extreme case of tumbling would be an instantaneous transfer which would lead to a spherical cavity similar to an underwater explosion. Contrarily, if a projectile does not tumble (as a spherical projectile), the transfer of kinetic energy is slower and it creates a more elongated projectile wake. These differences are illustrated in Figure 1.2. Indirectly this phenomenon may also affect the amount of projectile kinetic energy transferred to the liquid: a tumbling projectile may not have enough remaining

energy to perforate the exit wall while a non tumbling one would transmit less energy to the liquid. Bless (1979) observed that the pressure resulting from the impact of a tumbling projectile could be five times superior to the one recorded in a non tumbling case.

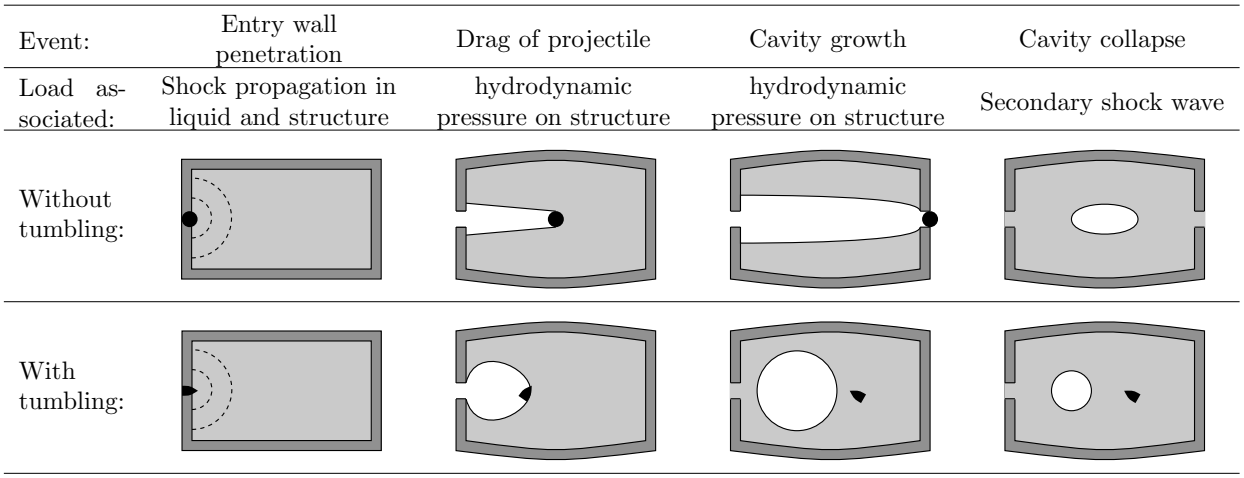

Figure 1.2 – General scenario of Hydrodynamic Ram event in liquid-filled tank for extreme cases of non-tumbling and of strongly tumbling projectiles.

Filling of the tank: another parameter that influences the severity of a hydrodynamic ram impact is the filling percentage of the container. Ballistic impacts on fuel tanks do not always occur when the container is fully filled. Varas et al. (2009a, 2012b) studied both experimentally and numerically the influence of this parameter for impacts of steel spheres on aluminium containers. They recorded in all cases the dynamics of the projectile and observed in all cases the residual deformations of the containers. They observed that during the impact of a projectile on a partially filled tank, the free surface of the liquid may impact with high velocity the tank wall and that there is a concentration of deformations in the areas close to the projectile trajectory. They found the maximal residual deformations for 100% filled tanks in all cases. However, the impact of the free surface might not always be negligible in function of the material that constitutes the tank walls.

In conclusion, according to this literature review, it can be concluded that a conservative approach would be to study the case of tumbling projectile in fully filled containers. Plus it would seem that the rate at which the projectile kinetic energy is transmitted to the liquid medium is an interesting parameter to discriminate tumbling and non-tumbling cases.

1.2 State of the art of Hydrodynamic Ram simulations

This section offers an overview of the state of the art of hydrodynamic ram simulations presented in the literature. This review is based on Varas (2009) and Abrate (2011) with addition of the most recent works.

1.2.1 Analytical models

Analytical models have been developed to deal with the water entry of projectile which is a phenomenon that is highly similar to the hydrodynamic ram phenomenon. Numerous analytical

studies have been done on the penetration of projectile at low speed (afew m.s^{-1}) as in (Scolan and Korobkin, 2003; Korobkin, 1994). However extension of these models to higher impact velocities and to hydrodynamic ram has not been done.

Projectile movement The only law used for the motion of rigid projectile for instance in (Varas et al., 2009a) is based on Newton's second law.

$$m_p \ddot{z_p} = -\frac{1}{2}\rho_l A C_d \dot{z_p}^2 \tag{1.1}$$

with z_p the depth of penetration, ρ_l the liquid density, A the projected area of the projectile and C_d its drag coefficient. Assuming a constant drag coefficient for a spherical projectile, the velocity of the projectile is found to decay exponentially.

$$\dot{z_p} = Ce^{-\beta z_p} \tag{1.2}$$

with $\beta = 3/4(\rho_l/\rho_p 2R_p)C_d$ for a spherical projectile of radius R_p and of density ρ_p. This exponential decay of the projectile velocity has been observed by numerous authors (Shi and Kume, 2001; Shi and Takami, 2001; Lecysyn et al., 2010). Lecysyn et al. (2010, 2009) also considered the case where the drag coefficient is a function of the Reynold's number:

$$C_d = \frac{24}{\mathrm{Re}} + \frac{3.73}{\mathrm{Re}^{0.5}} - \frac{4.83 \cdot 10^{-3}\mathrm{Re}^{0.5}}{1 + 3 \cdot 10^{-6}\mathrm{Re}^{1.5}} + 0.49 \tag{1.3}$$

These authors got good results using this type of model, however they were limited because they do not consider the forces that act on the projectile during the impact, plus they do not consider neither projectile tumbling nor its deformation which may largely influence its motion during the impact of a non academic ballistic projectile.

Shock and drag stage When a projectile impacts a water surface it generates a shock wave that propagates in the liquid. The initial shock pressure can be estimated by the shock polar technique in planar conditions. However, this method provides an overestimation since it does not take the attenuation due to the radial propagation into account. Then, during the drag stage the projectile generates a pressure pulse that propagates in the liquid. Lundstrom (1971) and later Lee et al. (1997b) developed analytical models for the pressure waves radiated during the impact of a high speed spherical projectile in an infinite domain of liquid. They use Newton's second law for the projectile motion and use it to calculate the rate of change of the kinetic energy with respect to the depth of penetration.

$$\frac{dE_p}{dz_p} = -m_p \dot{z_p} \frac{d\dot{z_p}}{z_p} = m - p\beta \dot{z_p}^2 \tag{1.4}$$

Then they relate the loss of the projectile kinetic energy to the energy stored in the liquid. They assumed that the fluid can be described thanks to a potential function ϕ that respects the wave equation $c^2\nabla^2\phi = \ddot{\phi}$ and used Bernoulli equation to relate the pressure in the fluid to its velocity. Plus they simplified the effect of a projectile by the action of distributed source points along the projectile trajectory.

Cavitation stage Even if numerous authors have been interested in the impact of various geometries on a free surface, only a few were interested in the motion of the cavity created in the wake of solids (May, 1952; Shi and Itoh, 2009) in particular for impact speed higher than 400 m.s^{-1} and lower than 1000 m.s^{-1}. Lee et al. (1997a) developed an analytical model to predict the dynamics of the cavity created in the drag of a high speed projectile. This model is very similar to (Lee et al., 1997b) as they used the velocity calculated in the liquid to obtain the movement of the cavity wall. However their model was only validated for low speed water entries and its use to hydrodynamic ram cases was limited because the effect of the container on the cavity motion was not modelled.

1.2.2 Numerical models

To solve the hydrodynamic ram phenomenon one has to solve the coupled problem of non-linear equations for the structure and for the fluid.

Piston theory The first method used is the *piston theory* developed by Ashley and Zartarian (1956), which simplifies greatly the liquid/structure interaction problem. This 1D theory models the container wall as an element of mass m, rigidity K and area A and gives the relations for its displacement w due to the applied pressure $P(t)$ as a differential equation.

$$m\ddot{w} + Kw = AP(t) \tag{1.5}$$

It models the pressure at the wall as the sum of the incident P_i and reflected P_r pressures. It assumes that the incident pressure is constant and the reflected one is approximated using Bernoulli equation, which gives (1.6) for the pressure.

$$P(t) = P_i - \rho_l \dot{\phi}_r(t) \tag{1.6}$$

with ρ_l the liquid density and ϕ_r the velocity potential reflected at the container wall. This equation expressed in terms of velocity potential is the basis of the piston theory. To obtain this form $\dot{\phi}_r$ must respect the wave propagation equation $c^2\nabla^2\phi = \ddot{\phi}$ with $\phi = \phi_i + \phi_r$. Then by equalling the velocity of the wall to the one in the fluid, the following expression is obtained:

$$P(t) = 2P_i + \rho c\dot{w} \tag{1.7}$$

This theory has then been used in (Ball, 1974) to simulate tests presented in (Ball, 1976). He coupled this model with finite element codes by using it to compute the pressure applied on the structural elements. The numerical results obtained using this theory give displacements and strains of the wall inferiors to the ones recorded experimentally. It was then concluded that the piston theory underestimates the pressures transmitted to the structure walls during a hydrodynamic ram event.

Variable Image Method Once the incapacity of the piston theory to reproduce experimental results has become clear, Lundstrom (1977) proposed the use of the *Variable Image Method* to predict the interaction between the liquid and the structure. In this method the pressure field is described using a potential function ϕ which satisfies the wave equation. Then the amplitude of the incident wave can be calculated from Bernoulli equation and can be used to calculate the reflected pressure using (1.8).

$$\phi_r = Q\tilde{\phi}_i \tag{1.8}$$

with ϕ_r the potential of the reflected wave, Q a function which varies in space and time in order for ϕ_r to satisfy the wave equation and $\tilde{\phi}_i$ is the speculated image of the potential of the incident wave with respect to the wall plane. Then using the Bernoulli equation, the expression of the particle velocity in the liquid ($u = \nabla\phi$) and the contour conditions between the liquid and the structure, the expression (1.9) for the pressure P can be obtained.

$$P = P_i + P_r = (1+Q)P_i - \rho\phi_i\frac{\partial Q}{\partial t} \tag{1.9}$$

In general the use of this method has not been very successful and the geometries that can be studied are limited. However this method permits to deal with 2D problems. So it resolves some of the approximations of the piston theory, by allowing a more realistic coupling between the liquid and the structure.

Lagrangian finite element simulations One of the first documented examples of numerical simulation of the complete phenomenon (interaction between the projectile, the liquid and the structure) has been done using explicit finite element simulations with a Lagrangian formulation by Kimsey (1980). This type of tool is classically used for the analysis of the dynamic behaviour of structures. This study simulates the propagation of the hemispherical shock wave and a part of the drag stage of a cylindrical projectile that does not tumble in a cylindrical container. The progression of the projectile in the liquid is allowed by erosion (deletion) of fluid elements that exceed a maximal strain criteria. However he could not simulate the complete crossing of the tank by the projectile due to large deformations in some elements that lead to a drop of the time step which is related in explicit finite element codes to the size of the smallest element. The deformations of the liquid elements is the main limitation of the use of Lagrangian finite element codes for hydrodynamic ram because they prevent simulating the whole phenomenon.

Deletombe and Malherbe (1998); Deletombe et al. (2003) proposed a method to deal with the tumbling of the projectile in Lagrangian formulation to limit the deformation of the mesh. This method uses the displacement of the projectile recorded experimentally to determine the drag coefficient of the projectile as a function of time. Then this function is used to reproduce this variation using a conical projectile which shape varies during the simulation. Even if it permits to deal with the tumbling of the projectile, the method needs experimental data, is limited to linear trajectories and has not been extensively validated. Finally, Lagrangian explicit finite element simulations are not adapted to simulate this phenomenon because of large deformations in the liquid during this type of impacts. This problem would not appear in Eulerian simulations in which the mesh is fixed.

More advanced methods for coupled fluid/structure problem Varas et al. (2009b, 2012a,b) performed simulations of steel sphere impacts in aluminium tanks using both Coupled Euler Lagrange and SPH (Smooth Hydrodynamics Particles) methods.

- In the coupled Euler Lagrange method the interaction is made between solids having Lagrangian mesh et fluids having Eulerian mesh in which the solids are fully immersed. This method has the advantages of both Lagrangian and Eulerian formulations because it is capable of dealing with large deformations of the fluids but keeps a good definition of the structure contours. They used this method with a bi-material law (air and water)

to allow the mixing of two fluids in an element, which enables the air to fill the cavity created by the projectile;

- The SPH method has been developed by Gingold and Monaghan (1977) and has since been applied in a variety of domains including hydrodynamics (Monaghan and Gingold, 1983). SPH is the first of a class of methods called meshfree methods. This method is often used to deal with large deformations of the medium as in Caleyron et al. (2013); Sauer (2010).

Using both methods, Varas et al. obtained good agreements between numerical and experimental results for the shock and drag stages. However they did not have experimental results for the cavitation phase and could not validate their models for this stage during which the lack of vaporisation might affect the dynamics of the cavity and the loads applied to the structure.

More recently Charles et al. (2012) proposed an attempt to simulate (Deletombe et al., 2013)'s tests. In this simulation, the projectile is not modelled, instead a direct injection of the energy as latent heat is done in a finite volume model for the fluids using a bi-phase law (water and its vapour). This methodology permits to simulate a growth and an implosion of the cavity. However, even if it is phenomenologically similar to the one observed experimentally, there are differences in the shapes of the cavity that might be due to the fact that the cavity dynamics in hydrodynamic ram event is governed by mechanical effects and replacing them by thermal cavitation induces a softening of the mechanical shock.

In conclusion, the available analytical or numerical models for prediction of the loads applied on the structure during a hydrodynamic ram phenomenon are very limited. The only models that have been proved to simulate part of this phenomenon with good agreement with experimental data are CEL finite element simulations and SPH ones. And the application of these models have been limited to the beginning of the cavitation stage for non-tumbling projectile impacts.

Chapter 2

Analysis of bubbles dynamics created by hydrodynamic ram in confined geometries using the Rayleigh-Plesset equation

Contents

2.1 Introduction **51**
2.2 Studied cases **53**
2.3 Rayleigh-Plesset modelling **55**
2.4 Confined Rayleigh-Plesset equation **58**
2.5 Discussion **62**
2.6 Conclusion **63**

The objective of this thesis work is to estimate the error in the obtained solution when the gas behaviour is neglected in HRAM numerical simulation. For this, the classic Rayleigh-Plesset equation has been applied to a set of chosen HRAM tests. This equation is retained because it models a 1D single bubble dynamics in an infinite domain of liquid. To apply this equation an original method based on an energetic criterion has been developed to determine the initial conditions needed in this equation. This criterion has been chosen to ensure the energetic consistency of the model with respect to the tests. However the Rayleigh-Plesset equation models an infinite domain of liquid, that is not the situation in the HRAM tests. A modification of this equation has then been proposed to include the effect of an elastic linear container on the predicted bubble dynamics. This version has been applied to the selected cases using a calibration of the confinement parameter (that defines the structure response). Finally this modified version of the Rayleigh-Plesset equation has been used to calculate the bubble dynamics with and without the gas presence in order to estimate the error obtained by doing such a simplification. This chapter has been published in T. Fourest, J.-M. Laurens, E. Deletombe, J. Dupas, and M. Arrigoni. Analysis of bubbles dynamics created by hydrodynamic ram in confined geometries using the rayleigh-plesset equation. *International Journal of Impact Engineering*, 73:66–74, 2014.

2.1 Introduction

In case of the impact of high speed/high energy projectiles through liquid filled tanks, the container may suffer large hydrodynamic loads that could possibly rupture the entire structure. This scenario is usually referred to as Hydrodynamic Ram (HRAM). The physical comprehension of the hydrodynamic effects that occur during a HRAM event is essential in the civilian domain as well as for the military aircraft design (vulnerability requirements). The physical comprehension of HRAM dynamics would in fact allow manufacturers to design better structures with respect to this particular threat.

The HRAM event is generally characterized in four stages described by Ball (1985): the shock stage, the drag stage, and the cavity growth and collapse stages. These stages and their associated loads are illustrated in Figure 2.1.

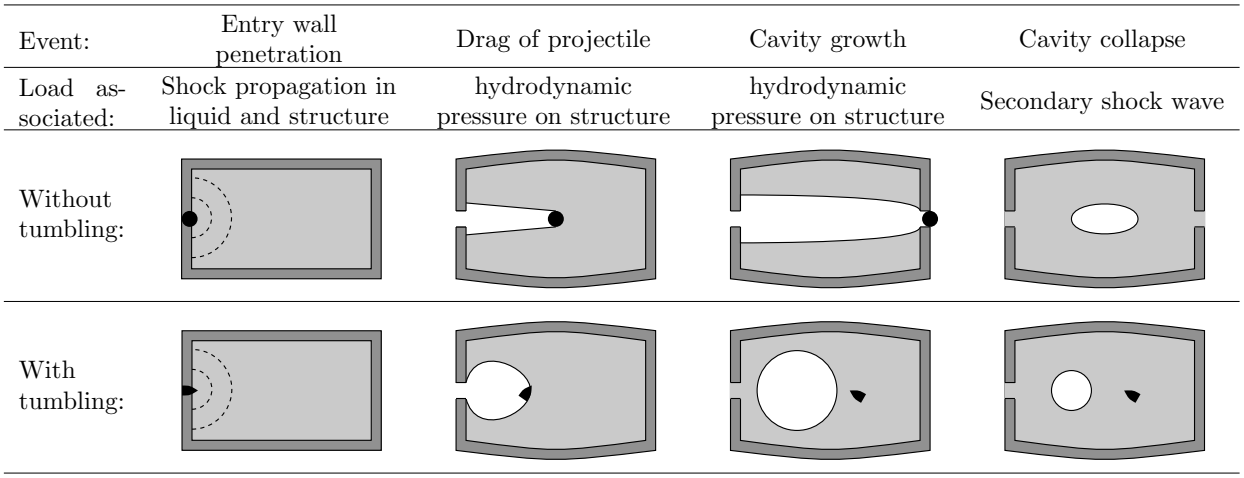

Figure 2.1 – General scenarios of Hydrodynamic Ram event in liquid-filled tanks for extreme cases of non-tumbling and of strongly tumbling projectiles.

The first experimental observations were conducted by McMillen (1945) and McMillen and Harvey (1946) who studied the shock waves and drag stage produced by the penetration of small steel spheres at high speed (610 m.s^{-1} to 1500 m.s^{-1}) into water using a shadowgraphy method. They were particularly interested in the liquid shock wave characteristics. They observed that the projectile was quickly slowed down by drag effects and that the shock wave velocity rapidly converged towards the speed of sound in the considered water.

Using high speed cameras (1900 frames/sec), May (1952) was the first author to observe the cavity motion, surface sealing and deep sealing (closure of the cavity occurring at the surface or under the surface of the liquid) phenomena induced by subsonic speed (8 m.s^{-1}) spheres entry into water. Shi et al. (2000); Shi and Kume (2001); Shi and Takami (2001); Shi and Kume (2004); Shi and Itoh (2009) made the same observations for supersonic speed in air (342 m.s^{-1}) water entry of bullets. More recently Deletombe et al. (2013) presented experiments of the impact in water of non-academic projectiles (7.62 mm NATO bullets) at ballistic speed (850 m.s^{-1}). The same stages of the HRAM event were observed during these experiments. They demonstrated the effect of the tumbling of projectiles on the cavity shape and dynamics.

The differences induced in the liquid behaviour due to the tumbling of the projectile are illustrated in Figure 2.1. Tumbling occurs because general high-speed/high-energy projectiles are stable in air but not in water. The impact angle of the projectile strongly influences the

occurrence and the intensity of the tumbling (Sareen and Smith, 1996), since the projectile possibly transmits its momentum to the liquid medium more quickly. The partition of the transferred energy between the drag and cavity growth stages depends on the shape, mass and velocity of the projectile and on the time of its possible tumbling. An extreme case would be an instantaneous transfer that would lead to a perfect spherical cavity bubble (as observed in underwater explosion). On the other hand, a projectile that does not tumble transfers its kinetic energy more slowly and creates a more elongated cavity shape in its wake. Bless (1979) observed that the pressure pulse resulting from the tumbling of the projectile could be five times more intense than the one observed in a case without tumbling.

The cavity growth is a complex stage that occurs during an HRAM phenomenon. Generally, during the water entry of a projectile, the drag highly contributes to the creation of the cavity. This cavity evolves to form a surface seal or a deep seal as in (Shi and Itoh, 2009). In both cases a cavity bubble is then created. This cavity may continue to grow if the momentum associated to the water is high enough to separate the fluid from the projectile and to continue its expansion, until it reaches a maximum and then eventually collapses. Deletombe et al. (2011) performed pressure measurements for 7.62 mm bullet impacts in water filled tanks, and observed higher pressures of shorter duration during the drag stage than during the cavity growth. Nevertheless they concluded that none of these stages could be neglected for the sizing of structures because they could both carry significant amounts of energy.

In the present paper the authors focus on the study of bubble dynamics created by tumbling projectiles, which is particularly difficult to correctly simulate with existing numerical tools. Deletombe and Malherbe (1998) and Deletombe et al. (2003) proposed an equivalent method to conduct studies with real projectiles. To the authors knowledge, the more advanced numerical simulations of this phenomenon presented in the open literature deal with non-deformable projectiles such as spheres in (Varas et al., 2009b, 2012a,b; Artero-Guerrero et al., 2013) or tumbling projectiles in (Sareen and Smith, 1996). These numerical studies either use Lagrange-Euler finite element methods or Smooth Particle Hydrodynamics methods. Anyway the whole sequence of the event up to the collapse of the cavity (that can take up to 30 ms) has not yet been simulated. In the present work it was decided to study this complex phenomenon by using an analytical approach. Pioneer studies on the subject were caried out by NASA researchers, principally Stepka and Morse (Morse and Stepka, 1966; Stepka and Morse, 1963; Stepka et al., 1964, 1965; Stepka, 1966). They identified the factors that affect the liquid loading during an HRAM event such as : projectile shape, size, material; tank wall thickness, material, and pre-stress; contained liquid properties, and tank wall protective structures. They tried to analyse the effects of the different parameters on the survivability of tanks, but they could not clearly establish a correlation that includes the effects of all the parameters. In fact, the phenomenon is complex and each HRAM stage needs to be analysed in detail. Lee et al. (1997b) investigated, both analytically and numerically, the shock waves generated by a body impacting and penetrating into water at high speed up to supersonic speed in the water. They also studied, both analytically and numerically, the cavity dynamics in the case of an impact without tumbling of the projectile in (Lee et al., 1997a). The present study focusses on the cavity growth and collapse stages, in the case of tumbling projectiles.

Recent experimental results, presented in (Deletombe et al., 2013), allow us to observe the evolution of bubbles created in the wake of tumbling projectiles. The bubble dynamics seems to be similar to those observed in underwater explosions in (Cole, 1945). The object of the present study is to discuss the applicability of the classical Rayleigh-Plesset (RP) equation

for bubble dynamics to model bubbles created by ballistic impacts on liquid-filled tanks that provoke HRAM events.

2.2 Studied cases

The Rayleigh-Plesset approach has been used for two cases : the first case is a 7.62 mm NATO ballistic impact in a generic EADS-IWF closed water-filled tank (tested within the frame of the EUCLID RTP 3.32 project). The second case is a ballistic shot in a large ONERA/DAAP pool. In both cases the impact is normal to the entry wall of the tank or free surface of liquid. These experiments are reported in (Deletombe et al., 2013). These two tests correspond respectively to a confined tank and a larger domain.

2.2.1 Description of the ballistic experiments

Only the general description of the cavity evolution is presented hereafter. For more details on the experimental tests, see (Deletombe et al., 2013). Figures 2.2 and 2.4 respectively show the cavity expansion observed in the pool test and in the tank test. Figure 2.3 shows the gas cloud and air ring that are observed at the end of the pool test. The pool dimensions are approximately 22x1.5x1.5 m^3 and the tank dimensions are 0.3x0.54x0.66 m^3.

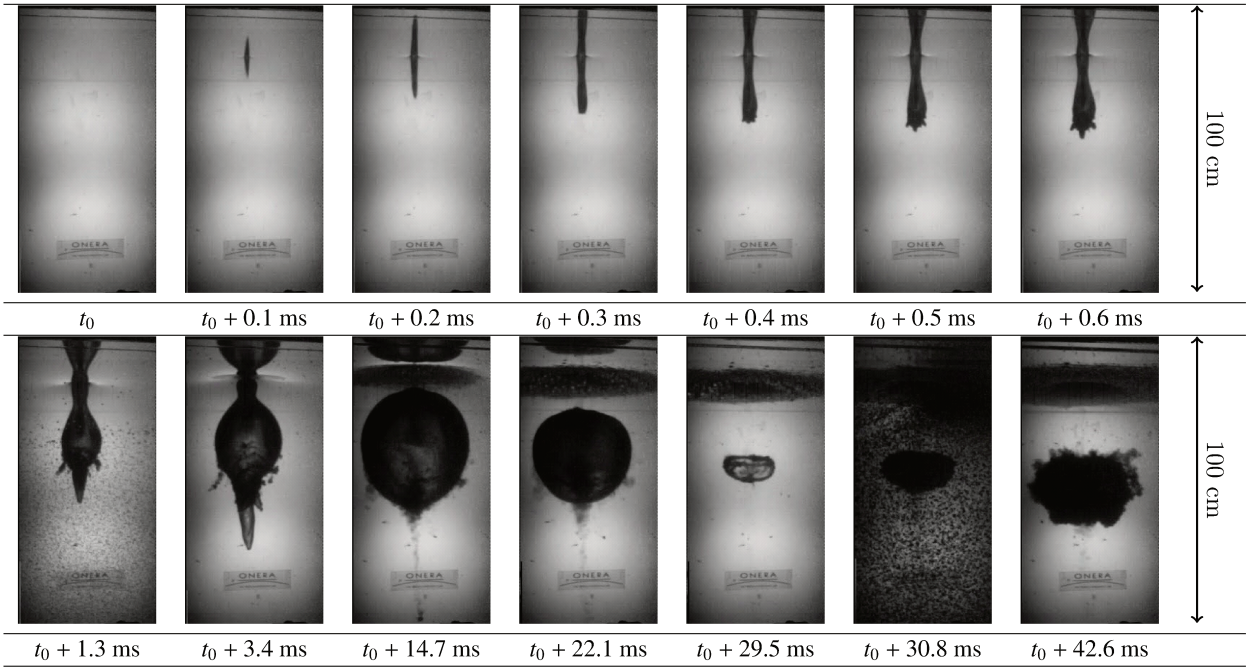

Figure 2.2 – Picture of cavity expansion in ONERA Pool obtained with visario camera (10 000 frames per second).

2.2.2 Exploitation of the test results for Rayleigh-Plesset simulation

The initial bubble radius and bubble interface velocity are obtained from the experimental videos using the same process as in (Deletombe et al., 2013). The only difference concerns the use of a second order approximation to calculate the bubble radius growth rate:

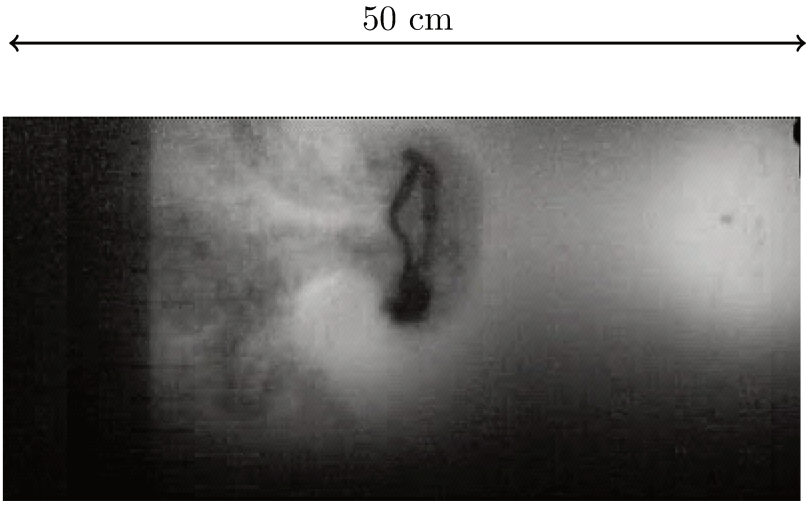

Figure 2.3 – Air ring observed at the end of the experiment in ONERA Pool obtained with a visario camera (10 000 frames per second).

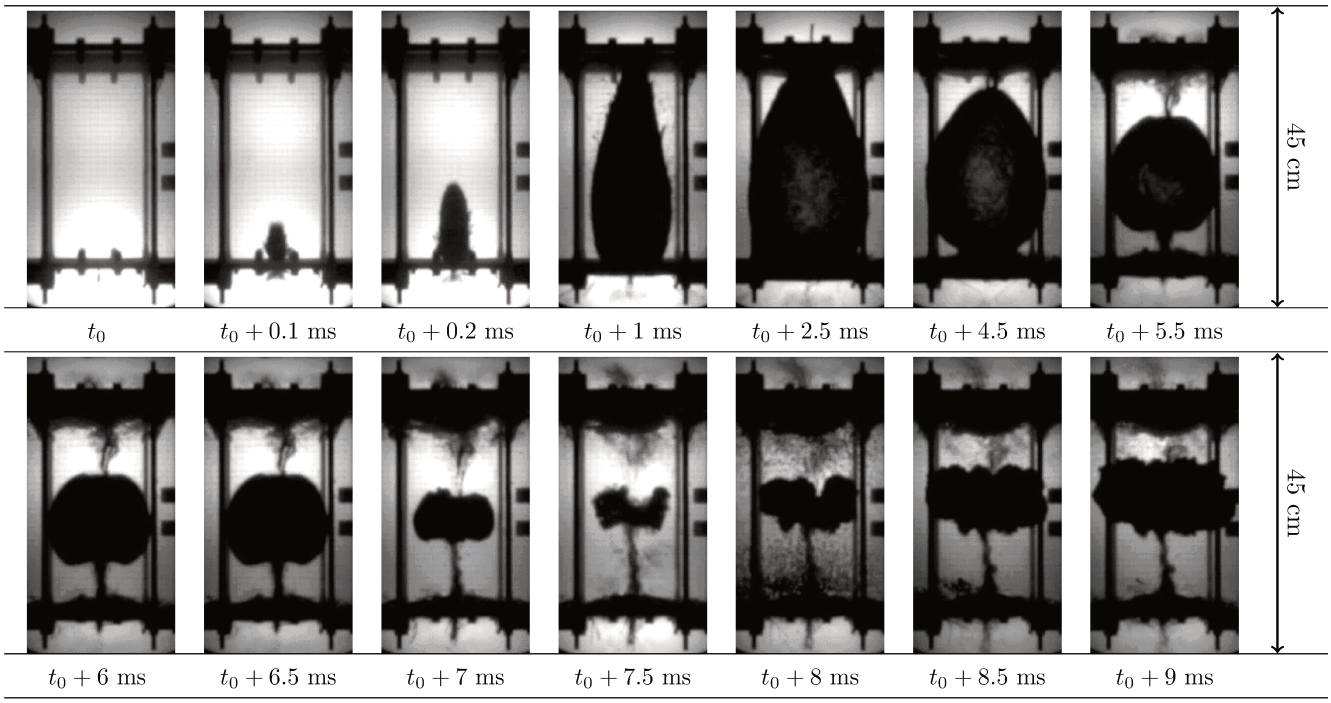

Figure 2.4 – Picture of cavity expansion in Airbus-Group Innovation caisson obtained with visario camera (10 000 frames per second).

1. an approximated elliptic 2D projected surface is estimated to cover the dark shades on the pictures, using a tool which then calculates this surface (pix^2);

2. the measured surface is converted into m^2, using the graduation grid (0.01x0.01 m for the composite box, and 0.05x0.1 m for the hydrodynamic pool);

3. the measured surface is used to calculate the radius of an equivalent disc, and the cavity bubble is given by the volume of the corresponding sphere;

4. the radius growth rate is calculated by using a second order polynomial approximation of the radius evolution during the first milliseconds of the phenomenon.

2.3 Rayleigh-Plesset modelling

A large amount of studies on bubble dynamics can be found in the literature. These studies could be useful to understand the physics of the cavity evolution process that is observed during HRAM events generated by the impact of projectiles in liquid filled containers. These studies began with Lord Rayleigh (1917) on the pressure prediction during the collapse of a spherical bubble, assuming that the surrounding liquid is incompressible and inviscid, and that surface tension forces are negligible. His work was extended by Plesset (1949), who derived the second-order non-linear ordinary differential equation for the time-dependent bubble radius evolution, which became the well known *Rayleigh-Plesset equation of bubble dynamics*. Improvements of this equation have been proposed by numerous authors, like by Keller and Miksis (1980), or extensions by Fujikawa and Akamatsu (1980), Prosperetti and Lezzi (1986) and Hauke et al. (2007). These improvements mainly concern effects that are important at the end of the collapse stage: liquid compressibility, thermal effects, and the effect of the non-equilibrium of vapour condensation.

The classical Rayleigh-Plesset equation for a single bubble dynamics has proven its efficiency in the physical analysis of bubble dynamics in various applications and for different bubble dimensions (cavitating flow, underwater explosion, ...). This equation is a simple and efficient model for the first approach of bubble expansion phenomena. The Rayleigh-Plesset equation is used here to discuss the influence of several physical parameters on HRAM bubble dynamics in the case of the ballistic impacts in the water filled tank and ONERA pool.

2.3.1 Derivation of Rayleigh-Plesset equation

To obtain this equation and use it to predict HRAM bubble dynamics, a spherical gas bubble in an infinite domain of liquid is considered (confinement effect is not investigated in this first part), and the following assumptions are made:

- incompressibility of the liquid;
- spherical deformation of the bubble interface;
- instantaneous energy transfer of kinetic energy of the bullet to the liquid;
- gravity effects are negligible;

- idealised case of zero mass transport across the bubble interface: as the transferred mass is small, the influence is negligible on large radius bubbles, which is the case here (0.2 m in pool, 0.12 m in tank);
- the dynamic viscosity and the surface tension effects are negligible due to the large dimensions of the bubbles. Viscous effects are supposed to be important for bubbles with a radius smaller than 10^{-3} m (Chapman and Plesset, 1971), but they are usually negligible when the bubble's radius is 10^{-1} m, or more;
- the pressure in the liquid at the bubble boundary is equal to the pressure inside the bubble;
- assumption of isothermal process since thermal effects are negligible for cavitation in water (Brennen, 1995)[1];
- in addition to the hypothesis classically used to obtain Rayleigh-plesset equation the presence of an initial amount of non-condensable gas (here air) is added, in a first approach its behaviour is assumed to be adiabatic.

The equation of mass conservation for a radial movement is expressed in spherical coordinates. It reduces due to the previous assumptions to (2.1).

$$r^2\dot{r} = R_b^2\dot{R}_b \tag{2.1}$$

where R_b is the radius of the bubble and $\dot{r}$ is the radial speed of the liquid at radius r.

Using the previous assumptions, the equation of conservation of momentum in the radial direction is reduced to (2.2).

$$\ddot{r} + \dot{r}\frac{\partial \dot{r}}{\partial r} + \frac{1}{\rho}\frac{\partial P}{\partial r} = 0 \tag{2.2}$$

Integrating (2.2) between $r = \infty$ and $r = R_b$, and using (2.1), the classical 3D Navier-Stokes equations reduces to the 1D spherical Rayleigh-Plesset equation for single bubble dynamics (2.3):

$$R_b\ddot{R}_b + \frac{3}{2}\dot{R}_b^{\,2} + \frac{P_\infty - P_b}{\rho} = 0 \tag{2.3}$$

Where R_b is the radius of the bubble, P_∞ is the pressure at $r = \infty$, P_b is the pressure in the bubble / at the liquid-gas interface , and ρ is the density of the liquid.

More details on the use of this equation related to underwater explosions can be found in (Brennen, 1995) and (Franc et al., 1995; Franc, 2007).

2.3.2 Application of Rayleigh-Plesset equation for HRAM events

In the case of bubbles created by HRAM events, it is proposed here to use the Rayleigh-Plesset equation in a non classical manner. To solve this differential equation, some initial conditions have to be set. Generally for classic cases of Rayleigh-Plesset applications, these initial conditions are $R_{b_0} \neq 0$, $P_{b_0} > P_\infty$, and $\dot{R}_{b_0} = 0$. In the present case $R_{b_0} \neq 0$, $P_{b_0} < P_\infty$,

[1]The influence of thermal effects for cavitation in aeronautic fuel materials is investigated in Appendix B.

Table 2.1 – Numerical values of the initial conditions used for Rayleigh-Plesset simulations of HRAM events.

Case	P_∞ (MPa)	P_{b_0} (MPa)	t_0 (ms)	R_{b_0} (mm)	$\dot{R}_{b_0}$ (mm/ms)	E_k (kJ)
Pool	$P_{atm} = 0.1$	$8.1 \cdot 10^{-3}$	0.5	41.9	86.8	3500
Tank	$P_{atm} = 0.1$	$P_{sat} = 2.23 \cdot 10^{-3}$	0.2	44.1	73.4	2900

and $\dot{R}_{b_0} \neq 0$, which means that the dynamics of the bubble is not created by an initial pressure difference between the bubble gas and the liquid at infinity but by momentum.

The initial conditions of the Rayleigh-Plesset equation determined from the ONERA experiments are linked to the initial time chosen for the analysis (when a bubble cavity reasonably appears). To choose the starting times for Rayleigh-Plesset simulations, energetic considerations are also used e.g. when the liquid initial kinetic energy in Rayleigh-Plesset equation is equal to the theoretical initial kinetic energy of the projectile that created the bubble (approximately 3.5 kJ in the pool and 2.9 kJ in the tank). It has been observed that it corresponded approximately to the beginning of the growth stage of the bubble cavity in the tests. As the energetic partition between the kinetic energy transferred to the liquid and the energy dissipated by the deformation of the projectile is not known, no dissipative phenomena are considered here: the whole projectile kinetic energy is assumed to be transferred to the liquid. The amount of kinetic energy of the liquid is calculated using the assumption of incompressibility of the liquid (2.4):

$$E_k = \frac{1}{2} \iiint_V \dot{r}^2 \rho \, \mathrm{d}V = 2\pi\rho R_b^3 {\dot{R}_b}^2 \tag{2.4}$$

Table 2.1 summarises the initial conditions used for the Rayleigh-Plesset simulation of the tank and pool cases. The initial air pressure in the pool bubble (after the wake has closed), $P_{b0} = 8.1.10^{-3}$ MPa, is calculated from the estimated volume of the "air ring" observed at the end of the experiment (Figure 2.3): $V_{ring} = 4.5.10^{-5}\,\mathrm{m}^3$. Since the video shows that the air ring volume seems to be time-independent, it is assumed to be at atmospheric pressure. Then assuming that the gas follows an adiabatic compression ($V_{ring}^{\gamma}.P_\infty = V_{b_0}^{\gamma}.P_{b_0}$) it is possible to estimate the initial pressure in the bubble. For the bubble in the tank, the amount of gas trapped in the wake of the projectile is not known, therefore the bubble is assumed to be initially only composed of air at the vapour saturation pressure (the beginning of the vaporisation process). Note that the mass transfer between the liquid and the vapour is assumed to be instantaneous. At the end of the collapse, a partial condensation occurs (Fujikawa and Akamatsu, 1980; Fujikawa et al., 1982): the small amount of remaining vapour is compressed and stops the inrushing liquid. This effect, which influences the minimal bubble radius that is reached (no full collapse) and the subsequent pressure waves, is neglected in the present work because the study only focuses on bubble dynamics prior to the final collapse. The minimum pressure in the bubble is thus equal to the pressure of vaporisation of the liquid which is assumed to be constant (at ambient temperature).

The Rayleigh-Plesset second order differential equation is numerically solved with a Runge-

Kutta fourth order method. The calculated radii are compared with the experimental ones in Figure 2.5. The liquid kinetic energy evolutions are presented in Figure 2.6.

Although the shapes show similarities, in both cases (pool and tank) the Rayleigh-Plesset equation predicts larger radii and longer oscillations than in experiments. As expected, the difference between experimental results and the Rayleigh-Plesset equation prediction is more important in the case of the impact in the small closed water-filled tank rather than in the case of the impact in the large pool. In both simulations the kinetic energy drops during the growth stage until it reaches zero value when the bubble radius is maximal and increases again during the collapse of the cavity. The initial kinetic energy is recovered at the end of the collapse stage since no dissipative phenomena are considered here.

Experimentally the bubble in the pool reaches a larger radius and collapses later than the bubble in the tank. This large difference does not appear in the Rayleigh-Plesset simulations. It is suggested in the present paper that the difference is due to the confinement effect (not considered in the standard Rayleigh-Plesset equation) that is much stronger in the tank experiment than in the pool case.

2.4 Confined Rayleigh-Plesset equation

2.4.1 Modification of RP equation to take confinement effect into account.

A modification of the Rayleigh-Plesset equation is proposed to take into account the confinement effect without changing the resolution method. Three modifications are proposed to model the confinement effect preserving the unidimensionnal character of the model, all the other assumptions are unchanged:

- the liquid domain is considered to be of finite dimensions;

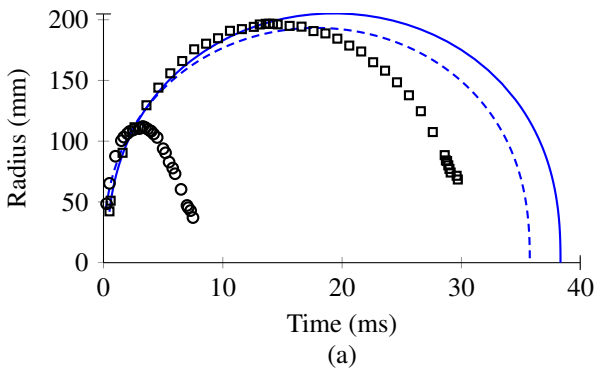

Figure 2.5 – Radius evolution in tank (o), and pool (□) tests and predicted with the Rayleigh-Plesset equation in the tank (- - -) and the pool (—).

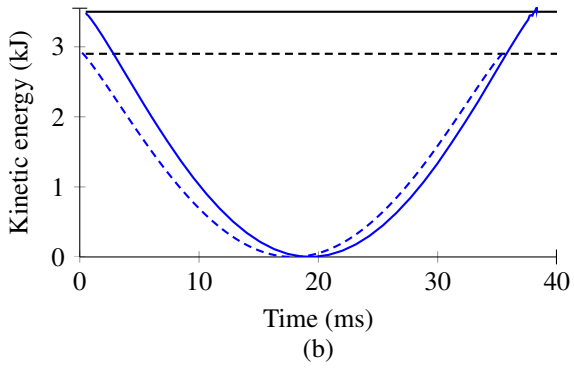

Figure 2.6 – Kinetic energy in liquid in tank (- - -), in pool (—) and theoretical initial kinetic energy of the projectile in tank test (- - -) and pool (—).

- the structural confinement effect is studied by introducing an elastic equivalent spherical shell in the analytical problem (Figure 2.7).

- the structure is assumed to be elastic, the material isotropic, and the material movement slow enough to neglect inertia and use static formulation.

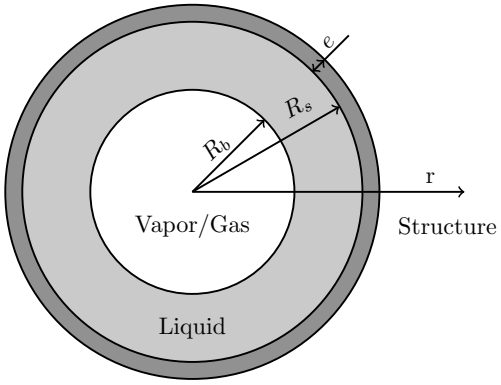

Figure 2.7 – Description of the system considered to take the confinement effect into account in Rayleight-Plesset equation.

It is considered that the centre of the bubble corresponds to the centre of the container. The initial external radii R_{s_0} of the liquid domains were defined as the radii that yield the same volume as the tested containers (respectively 50 m^3 for the pool and $7.7.10^{-2}$ m^3 for the tank). The same equations of continuity and conservation of momentum apply (2.1) and (2.2). The behaviour of the liquid is still assumed to be incompressible, hence the current radius of the elastic sphere R_s is related to the radius of the bubble (2.5):

$$R_s = (R_{s_0}^3 + R_b^3 - R_{b_0}^3)^{1/3} \tag{2.5}$$

Integrating (2.2) between R_s and R_b, using (2.1) and defining $\Lambda = R_b/R_s$, the same equation as in (Obreschkow et al., 2006) is found (2.6):

$$R_b\ddot{R}_b + \frac{3}{2}\dot{R_b}^2 + \frac{P_s(t) - P_b(t)}{\rho} - 2\dot{R_b}^2\Lambda - R_b\ddot{R}_b\Lambda + \frac{1}{2}\dot{R_b}^2\Lambda^4 = 0 \tag{2.6}$$

with P_s the pressure at the interface between the liquid and the structural sphere.

A similar equation to the Rayleigh-Plesset equation is obtained with the addition of three terms that vanish when $R_s = \infty$. In case of a spherical container, the structure can be modelled using the theory of elasticity on a spherical thick shell (2.7) (Figure 2.7):

$$P_s - P_{s_0} = (R_s - R_{s_0}).E.\left(\frac{(R_{s_0}+e)^3 - R_{s_0}^3}{R_{s_0}^3}\right)\left(\frac{2R_{s_0}^2}{2(1-2\nu)R_{s_0}^3 + (1+\nu)(R_{s_0}+e)^3}\right) \tag{2.7}$$

with E the Young Modulus, ν the Poisson ratio and e the shell thickness.

2.4.2 Confined Rayleigh-Plesset equation for bubble created by HRAM events

Clearly, the containers in the experiments are not spherical, and are made of several parts of different materials, the overall rigidity of which cannot be obtained with a monolithic elastic sphere of any of the single constitutive materials (the tank walls in the tests are bending, while an elastic sphere acts as a membrane).

In fact the relationship between the pressure applied to the structure and the deformation of the structure is a complex one. It depends on the container dimensions, materials, fixations, shape and on the bubble position. Obtaining this relationship would require the use of full 3D physical numerical simulations. Hence, the authors introduce a non-dimensional factor κ to obtain the simplest model for the spherical tank deformation (2.8) that replaces (2.7):

$$\frac{(P_s - P_{s_0})}{P_{s_0}} = \kappa \frac{(R_s - R_{s_0})}{R_{s_0}} \tag{2.8}$$

The kinetic energy in the liquid in (2.9) is calculated in the same way as in (2.4) considering a liquid domain of finite dimensions.

$$E_k = 2\pi\rho R_b^4 \dot{R_b}^2 \left(\frac{1}{R_b} - \frac{1}{R_s}\right) \tag{2.9}$$

As previously explained the starting time is chosen based on energetic considerations (initial liquid kinetic energy equal to theoretical initial kinetic energy of projectile). Table 2.2 summarises the initial conditions used for these simulations. Once the coefficient κ is calibrated, the experimental and numerical curves are globally in good agreement. Assuming a linear relationship between the internal pressure in the liquid and the radius evolution of the elastic sphere that is expected to represent the tested structures, the Rayleigh-Plesset equation enhanced with the confinement effect allows to describe the radius evolution observed in the case of the pool and in the case of the water-filled tank.

Table 2.2 – Numerical values of the initial conditions used for confined Rayleigh-Plesset simulations of HRAM events.

Case	P_{b_0} (MPa)	t_0 (ms)	R_{b_0} (mm)	$\dot{R}_{b_0}$ (mm/ms)	R_{s_0} (mm)	E_{k_0} (kJ)
Pool	$P_{b_0} = 8.1 \cdot 10^{-3}$	0.51	42.3	86.44	2200	3500
Tank	$P_{sat} = 2.23 \cdot 10^{-3}$	0.26 ms	48.5	70.6	264	2900

The radii evolution obtained in both cases with the modified Rayleigh-Plesset equation for several values of κ is shown in Figures 2.8 and 2.9. The coefficients κ have been calibrated to obtain good agreement in amplitude between the experimental radii from tests and those obtained numerically : $\kappa = 2200$ and $\kappa = 400$ for the pool and tank respectively.

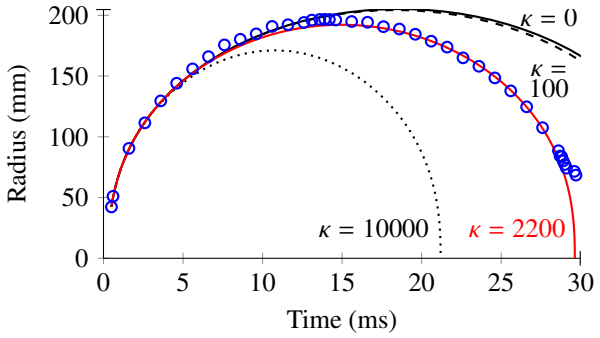

Figure 2.8 – Radius evolution in pool test (o), and calculated with RP with confinement effect with $\kappa = 0$ (—), $\kappa = 100$ (- - -), $\kappa = 10000$ (···), and with $\kappa = 2200$ (—).

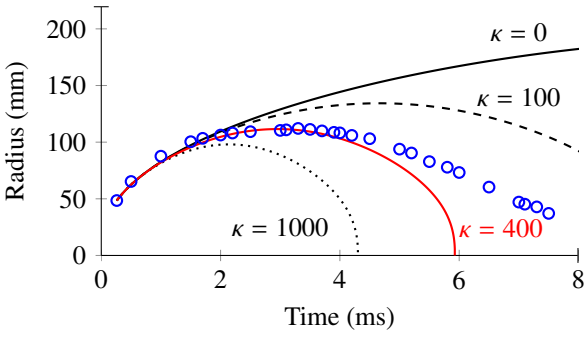

Figure 2.9 – Radius evolution in tank test (o), and calculated with RP with confinement effect with $\kappa = 0$ (—), $\kappa = 100$ (- - -), $\kappa = 1000$ (···), and with $\kappa = 400$ (—).

2.4.3 Influence of gas modelling in numerical simulations

The calibrated Rayleigh-Plesset equation with added confinement effect is then used to evaluate the influence of the bubble internal pressure on the bubble growth and decay to discuss the need to model the gas in Hydrodynamic Ram numerical simulations. This is first done by evaluating the differences induced by neglecting the gas medium ($P_b = 0$ in (2.6)). The amount of gas in the bubble can be evaluated for the bubble in the pool from the ring of gas at atmospheric pressure observed at the end of the experiment (see Figure 2.3 and 2.10). However in the tank case, the amount of initial gas is not known hence two extreme assumptions are investigated: the radius evolution is calculated assuming that the gas, at the initial time, is either at vapour saturation pressure, or at atmospheric pressure (Figure 2.11).

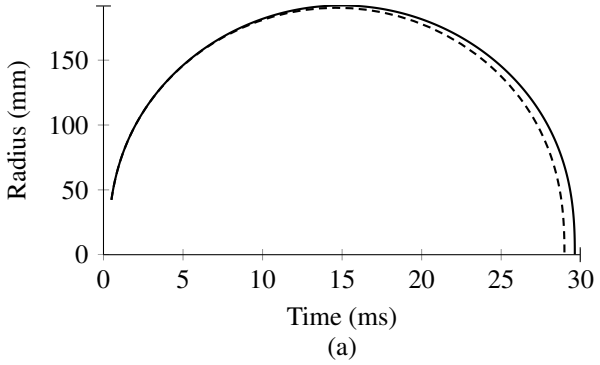

Figure 2.10 – Radius evolution predicted with the confined Rayleigh-Plesset model in pool with known initial pressure and air volume (—) and without i.e. $P_b = 0$ (- - -).

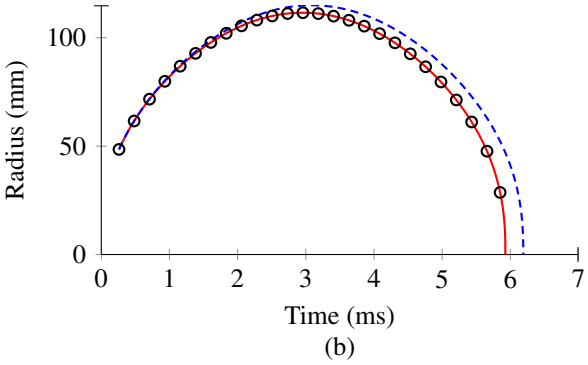

Figure 2.11 – Radius evolution predicted with the confined Rayleigh-Plesset model in tank with $P_b = P_{sat}$ (—), $P_b = 0$ (o) and with $P_{b_0} = P_{atm} = 0.1$ MPa (- - -).

Little influence of the bubble pressure is observed on the radius evolution in both cases. It has been verified that the confinement parameter κ is only slightly dependent on the initial bubble pressure P_{b_0} in the $[0, P_{atm}]$ interval of interest. The difference is less than 1% in terms of bubble amplitude and duration in the pool and 4% in the tank with the initial conditions $P_{b_0} = P_{atm}$ or $P_b = 0$. To illustrate the differences induced by neglecting the gas, it is chosen to focus on the

tank experiment. Figures 2.12 and 2.13 respectively show the evolution of the kinetic energy and applied pressure to the tank structure for the simulation cases presented in Figure 2.11. There is no great difference in kinetic energy regardless of the initial pressure, the duration being only a little longer for the case with $P_{b_0} = P_{atm}$. However, there is a noticeable difference in the applied pressure to the structure when $P_b = 0$ or $P_{b_0} = P_{atm}$ (here the difference is 0.1 MPa, i.e precisely P_{atm}). Comparing the impulse transmitted to the structure in each case (2.10), a difference of 12% is obtained between $Imp_{(P_b=0)} = 0.918$ N.s and $Imp_{(P_{b_0}=P_{atm})} = 1.040$ N.s.

$$Imp = \int_{t_0}^{t_{collapse}} 4\pi R_s^2 P_s dt \tag{2.10}$$

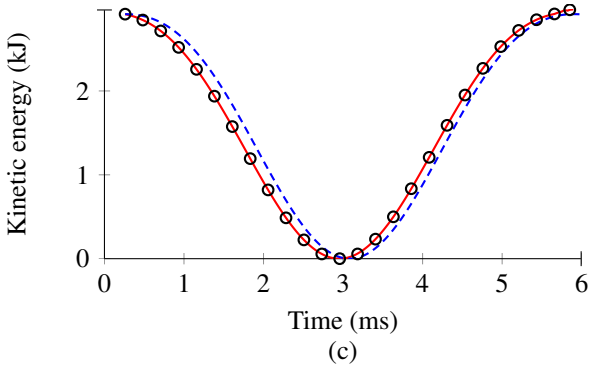

Figure 2.12 – Kinetic energy evolution predicted with the confined Rayleigh-Plesset model in tank with $P_b = P_{sat}$ (—), $P_b = 0$ (o) and with $P_{b_0} = P_{atm} = 0.1$ MPa (- - -).

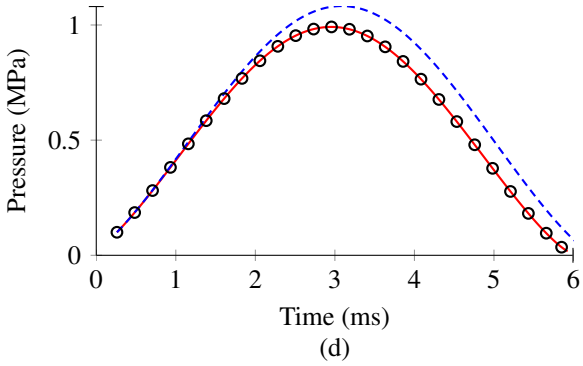

Figure 2.13 – P_s evolution predicted with the confined Rayleigh-Plesset model in tank with $P_{b_0} = P_{sat}$ (—), $P_b = 0$ (o) and with $P_{b_0} = P_{atm} = 0.1$ MPa (- - -).

Clearly one should be cautious to neglect the gas effect only if the initial pressure in the bubble is low, which can be reasonably assumed for the presently studied high speed impact and penetration of projectiles, as suggested by the recorded pressures in (Disimile et al., 2009).

2.5 Discussion

The results of the present paper tend to confirm the assumed similarities between the bubble dynamics in HRAM and the bubble dynamics in underwater explosions. The stages of bubble dynamics during HRAM events are also in agreement with those described in (Fuster et al., 2009) for other cavitation problems, that are: *expansion stage, deceleration stage, initial compression* (the *implosion, rebound and wave generation* are not investigated in the present study). The process of creation of bubbles is different (projectile impacts for HRAM events and detonations for underwater explosions), but the bubbles create liquid momentum in both cases. In the present study, the Rayleigh-Plesset bubble dynamics is initialised by the momentum of the incompressible liquid, not by the high initial pressure of the gas bubble. This approach is justified here since the bubble is created in the projectile wake and there is no reason for the experimental bubble gas pressure to be higher than the atmospheric pressure at the beginning of the growth stage. The bubble dynamics in HRAM events is then mainly due to the momentum transmitted from the projectile to the liquid. If explosive projectiles were studied as in

(Anderson et al., 1999), the bubble dynamics would be caused by the momentum transmitted from the projectile to the liquid and by high pressure / high temperature detonation products in the bubble: the pressure in the bubble would not be negligible and equations of state would be needed to model the bubble gas behaviour and surrounding water.

In the present study, the confinement in the modified Rayleigh-Plesset equation depends on two parameters : Λ and κ. The first one quantifies a correction of the Rayleigh-Plesset equation due to the finite geometries of the liquid domain. The second defines the resistance presented by the structure to the liquid expansion. The results obtained with the confined Rayleigh-Plesset equation seem to satisfactorily describe the bubble dynamics up to the beginning of the final collapse. At this time, the minimal radii predicted are a bit smaller than the experimental ones. Indeed the model used in the present study assumed spherical symmetry of the bubble and constant stiffness of the container, and reversible processes without energy dissipation, while in the experiments, dissipative phenomena occur in the liquid, the structure (as well as damage i.e loss of stiffness), and the projectile. Therefore it is suggested that these processes influence the bubble dynamics mainly at the end of the collapse stage.

The Rayleigh-Plesset equation is based on the hypothesis of the incompressibility of the liquid. To account for the liquid compressibility other models previously mentioned, as (Keller and Miksis, 1980) for small compressibility, or (Gilmore, 1952; Fujikawa and Akamatsu, 1980; Prosperetti and Lezzi, 1986; Hauke et al., 2007) for high compressibility can be used. These models also include effects such as non-equilibrium condensation of the vapour, heat conduction and temperature discontinuity at the bubble interface. All these effects influence the bubble dynamics during the final stage of the collapse and the subsequent waves emitted in the liquid, and should hence be considered in future studies.

2.6 Conclusion

In the present study the classic Rayleigh-Plesset equation for single bubble dynamics in a non-confined liquid domain has been modified to take the confinement effect of a container on the bubble dynamics into account. This equation has been applied to describe the dynamic of bubbles created during two HRAM events, one in a small tank and one in a larger pool. The experimental and numerical radii are in good agreement up to the ultimate collapse time.

The Rayleigh-Plesset equation enhanced with the confinement effect is used in the present study to determine the minimum "key parameters" that would be needed to perform more physically justified simulations of the HRAM hydrodynamic loads. The originality of the present research work compared with the few studies found in the open literature is that they deal with cavity motion created by constant shape projectiles, and most often only focus on the very first stages of HRAM (less than 1 ms). The present study does not consider cavity initiation but focuses on the effects of the container characteristics on cavity evolution up to 30 ms. The results of this study tend to indicate that bubbles created by ballistic impact in water-filled containers can be considered to follow a dynamic well described by the Rayleigh-Plesset equation once the confinement effect is taken into account. Further validation of the proposed method could be addressed by applying the modified Rayleigh-Plesset equation to experimental results obtained in spherical containers.

Subsequently, the influence of the presence of gas in the bubble is studied using the modified Rayleigh-Plesset equation. The study of the influence of the gas pressure in the bubble is of practical importance: neglecting the gas could allow easier finite element solving of HRAM phenomenon. Mono-phase numerical models could be faster and easier to run, even if mono-phase HRAM simulations present their own difficulties (see (Kimsey, 1980; Deletombe and Malherbe, 1998; Deletombe et al., 2003)). The main conclusion of the present research is that the pressure of the gas in the bubble seems to be of little influence on the bubble dynamics and on the hydrodynamic loads applied to the structure during the two experiments presented in (Deletombe et al., 2013), and probably for other HRAM events. But the proposed modified Rayleigh-Plesset model cannot be used to predict the loads applied on the container structure: the model needs to be initialised with experimental data, and the overall stiffness of the container cannot be explicitly calculated (except in case of spherical containers). Further efforts should then be made to experimentally validate the added confinement effect to the Rayleigh-Plesset equation or other models and solving methods applicable to general geometries (Finite Elements, Finite Volumes, ...) should be used to progress on the HRAM bubble dynamics understanding and prediction.

Acknowledgement

The authors would like to thank the French Ministry of Defence and DGA (French Armaments Procurement Directorate) for their financial support (in the thesis preparation and in the frame of EUCLID RTP3.32 and BaToLUS projects).

Chapter 3

Confined Rayleigh-Plesset equation for Hydrodynamic Ram analysis in thin-walled containers under ballistic impacts

Contents

3.1 Introduction **67**

3.2 Studied cases **68**

3.3 Confined Rayleigh-Plesset equation **70**

3.4 Application of the confined Rayleigh-Plesset equation for bubbles created by HRAM events **71**

3.5 Conclusion **76**

The objective of this part of the work is to evaluate the capability of linear elastic analytical models to estimate the numerical value of the confinement parameter in the modified Rayleigh-Plesset equation, that was calibrated in the previous chapter. This is done to validate the order of magnitude of the previously calibrated values. First the numerical value of the proposed confinement parameter has been obtained by calibration on one of the previous HRAM cases. This value is calculated to obtain a reference for future comparisons. Then the numerical value of the confinement parameter is analytically calculated in two configurations: in an academic case when an elastic mono material spherical shell model is used for the structure response; then when an analytical plate model is used to model the linear behaviour of the multi-material orthorhombic test container. Finally the confinement parameter values and the bubble dynamics predicted when the confinement parameter is calibrated and evaluated with plate formulae are compared which proved to reach a quite good correlation. This chapter has been published in T. Fourest, J.-M. Laurens, E. Deletombe, J. Dupas, and M. Arrigoni. Confined rayleigh-plesset equation for hydrodynamic ram analysis in thin-walled containers under ballistic impacts. *Thin− Walled Structures*, 86:67–72, 2015c.

3.1 Introduction

In the event of an impact of high speed/high energy projectiles on liquid filled tanks, the container may suffer large hydrodynamic loads that could possibly rupture the entire structure. This impact scenario is referred to as Hydrodynamic Ram (HRAM). The scenario is especially dangerous for thin walled structures that cannot be armoured due to weight penalty reasons. There is an insistent need for tools to model hydrodynamic effects that occur during a HRAM for military (vulnerability requirement) but also civilian aircraft design. Numerical modelling of HRAM dynamics would allow to improve the survivability of structures with respect to this particular threat.

The HRAM event is generally characterized by four stages, first described by Ball (Ball, 1985): the shock stage, the drag stage, the cavity growth and collapse stages. These stages and the associated loads are illustrated in Figure A.1.

Entry wall penetration	Drag of projectile	Cavity growth	Cavity collapse
Fluid shock	Drag pressure	Cavity growth pressure	Collapse fluid shock

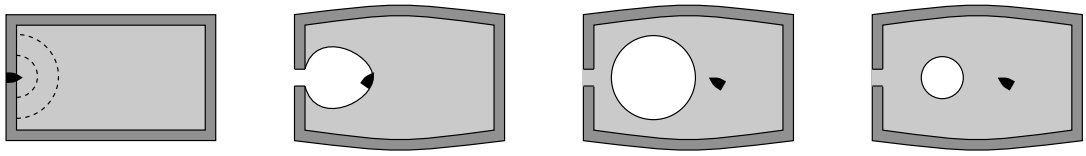

Figure 3.1 – General scenario of Hydrodynamic Ram event in liquid-filled tank for tumbling projectiles.

The first experimental observations on the subject were done by McMillen (1945) who recorded the shock waves and drag stage produced by the penetration of small steel spheres at high speed (610 m.s^{-1} to 1500 m.s^{-1}) into water by using a shadowgraphy method. He was particularly interested in the shock waves characteristics. He observed that the projectile is quickly slowed down by drag and that the shock wave rapidly decays to the speed of sound in water.

Shi et al. (2000) observed the cavity motion induced by a medium speed (342 m.s^{-1}) water entry of a bullet. More recently, Deletombe et al. (2013) presented experiments of the impact in water of non-academic projectiles (7.62 mm NATO bullet) at ballistic speed (850 m.s^{-1}). The same stages of water entry occurred during these experiments. They enlightened the effect of the tumbling of projectiles on the cavity shape during HRAM events.

During tumbling the projectile transmits its momentum more quickly to the liquid medium. An extreme case would be an instantaneous and homogeneous transfer that would lead to a spheric cavity bubble. On the other hand, a projectile that cannot tumble will transfer its kinetic energy more slowly and will create a more elongated cavity shape in its wake. Bless (1979) observed that the pressure resulting from the tumbling of the projectile could be five times greater to the one observed in a case without tumbling.

Generally, during the water entry of a projectile, the cavity created by the drag of the projectile will be enclosed by the surrounding free surface of the liquid, and a cavity bubble will then be created. After it has completed its growth, because of potential inertial effects this

cavity will eventually collapse. At the end of this collapse, another shock wave is emitted, that also strongly loads the structure. Deletombe et al. (2011) performed pressure measurements for 7.62 mm bullet impacts on water filled tanks, and observed greater pressures during the drag stage than during the cavity growth stage but in shorter times. They nevertheless concluded that none of these stages could be neglected for the sizing of structures because they could both induce significant impulse[1].

The present work focuses on the cavity growth and collapse stages in the case of tumbling projectiles. A conservative approach would be to design structures to counter this threat (higher pressure loads). However the tumbling of projectiles is particularly difficult to correctly simulate with available numerical tools. The most advanced numerical simulations of this phenomenon presented in the open literature deal with non-deformable projectiles (Varas et al., 2009b, 2012a,b; Artero-Guerrero et al., 2013; Sareen and Smith, 1996). These studies either use Lagrange-Euler finite element methods or particle type solutions. Anyway the whole sequence of events up to the collapse (that might take up to 30 ms) is not entirely simulated. In this paper another approach has been chosen that consists in studying this complex phenomenon with analytical equations. Pioneer studies on the subject were carried out by Stepka and Morse (Morse and Stepka, 1966; Stepka and Morse, 1963; Stepka et al., 1964, 1965; Stepka, 1966). They identified the factors that affect the loading during an HRAM event (projectile shape, size, material; tank wall thickness, material, and pre-stress; contained liquid properties, and tank wall protective structures), and tried to analyse the effects of the different parameters on the survivability of tanks, but they could not clearly establish a correlation that could embrace the effects of all parameters.

Recent experimental results, in particular those presented in (Deletombe et al., 2013), allow to observe the evolution of the bubble created in the wake of a tumbling projectile. The bubble dynamics seems to be comparable to the one observed during underwater explosions (Cole, 1945). These bubble dynamics were then described using a modified version of the Rayleigh-Plesset (RP) equation introducing a confinement effect of the container on the bubble expansion, that are presented in (Fourest et al., 2014). The object of the present study is to discuss[2] the confinement parameter which has been introduced in this confined version of the classic Rayleigh-Plesset equation for bubble dynamics, that is applied to bubbles created by ballistic impacts. At the moment the method is not developed in order to perform the sizing of containers but in order to evaluate the feasibility and relevance of this approach.

3.2 Studied cases

The Rayleigh-Plesset approach has been used to study the case of a 7.62 mm NATO ballistic impact at 850 m.s^{-1} in a generic Airbus-Group Innovations closed water-filled tank (tested within the frame of the EUCLID RTP 3.32 project)[3]. The impact is normal to the entry wall of the tank. This experiment is described in (Deletombe et al., 2013).

[1] As discussed in Chapter 1, it might also be mentioned that all stages carry a significant portion of the initial projectile kinetic energy.

[2] In facts the initial objective of this paper was to present a discussion on the confinement parameter. However since a good approximation of this parameter has been obtained using analytical plates formulae, the paper rather presents an analytical approach to evaluate the value of this parameter for a container of non-spherical geometry.

[3] Only the impact in the tank case is studied in this paper because the free surface in the pool impact case prevents the application of a similar approach to that case.

3.2.1 Description of the ballistic experiment

Only the general description of the cavity evolution is presented hereafter. For more details on the experimental test, see (Deletombe et al., 2013). Figure 3.2 shows the cavity expansion observed in the tested tank. The external dimensions of the tank are approximately 0.3x0.54x0.66 m^3.

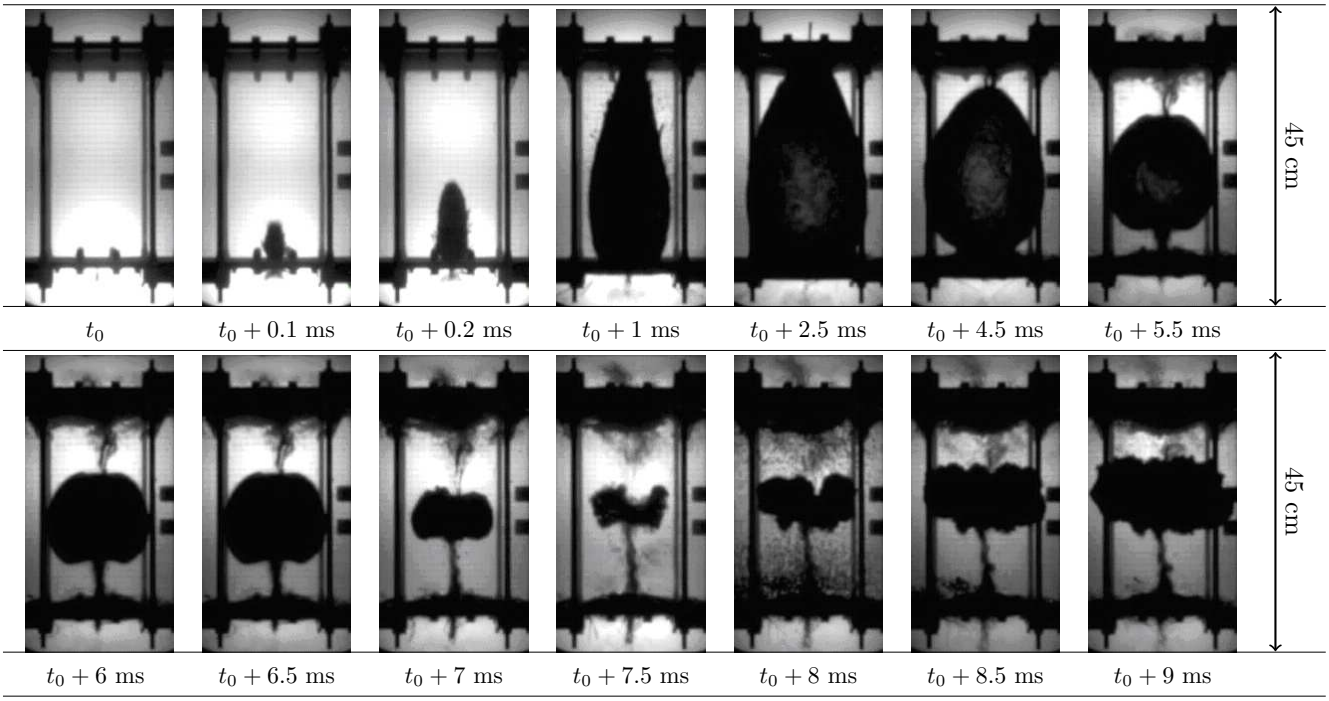

Figure 3.2 – Picture of cavity expansion in Airbus-Group Innovation caisson obtained with a visario camera (10 000 frames per second).

3.2.2 Use of the test results for Rayleigh-Plesset simulation

The initial bubble radius and bubble interface velocity are obtained from the experimental video using the same process as in (Deletombe et al., 2013). The only difference concerns the use of a second order approximation to calculate the bubble radius growth rate:

1. an approximated elliptic 2D projected surface is estimated to cover the dark shades on the pictures, using a tool which then calculates this surface (pix^2);

2. the measured surface is converted into m^2, using a graduation grid (0.01x0.01 m for the Airbus-Group Innovations box);

3. the measured surface is used to calculate the radius of an equivalent disc, and the cavity bubble is given by the volume of the corresponding sphere;

4. the radius growth rate is calculated by using a second order polynomial approximation of the radius evolution during the first milliseconds of the phenomenon.

3.3 Confined Rayleigh-Plesset equation

A large number of studies on bubble dynamics can be found in the literature. These studies began with Lord Rayleigh (1917) on the pressure prediction during the collapse of a spherical bubble, assuming that the surrounding liquid is incompressible and inviscid, and that surface tension forces are negligible. His work was extended by Plesset (1949), who derived the second-order non-linear ordinary differential equation for the time-dependent bubble radius evolution, which became the well known *Rayleigh-Plesset equation for bubble dynamics*. Improvements of this equation have been proposed by numerous authors, like Keller and Miksis (1980), or extensions by Fujikawa and Akamatsu (1980), Prosperetti and Lezzi (1986) and Hauke et al. (2007). These improvements mainly concern effects that are important at the end of the collapse stage: liquid compressibility, thermal effects, and the effect of the non-equilibrium of vapour condensation.

A modification of the classic Rayleigh-Plesset equation has been proposed in (Fourest et al., 2014) to account for confinement effects without changing the resolution method. To obtain this equation and use it to predict HRAM bubble dynamics, a spherical gas bubble in a spherical finite domain of liquid is first considered (see Figure 3.3), and the following assumptions are made:

- Spherical deformation of the bubble interface;
- Instantaneous energy transfer from kinetic energy of the bullet to the liquid;
- Gravity effects are negligible;
- An idealised case of zero mass transport across the bubble interface is considered;
- Dynamic viscosity and surface tension effects are negligible due to the large dimensions of the bubbles (Chapman and Plesset, 1971);
- An initial amount of non-condensable gas (here air) is considered, its behaviour is assumed to be adiabatic;
- The liquid domain is considered to be incompressible and of finite dimensions;
- An elastic structural confinement is added by means of a spherical shell.

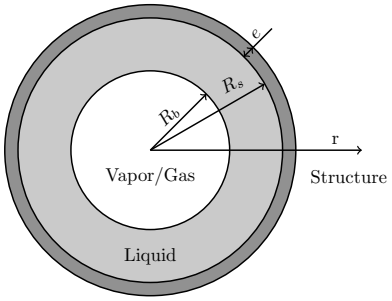

Figure 3.3 – Sketch of the system considered in the proposed confined Rayleigh-Plesset equation.

The equation of mass conservation for a radial movement is expressed in spherical coordinates and is reduced in view of the above assumptions to (3.1),

$$r^2\dot{r} = R_b^2\dot{R}_b \tag{3.1}$$

with R_b the radius of the bubble and $\dot{r}$ the radial speed of the liquid at radius r. Using the previous assumptions, the momentum equation in the radial direction is reduced to (3.2),

$$\ddot{r} + \dot{r}\frac{\partial \dot{r}}{\partial r} + \frac{1}{\rho}\frac{\partial P}{\partial r} = 0 \tag{3.2}$$

It is assumed that the centre of the bubble corresponds to the centre of the container. The initial external radius R_{s_0} of the liquid domain was defined as the radius that yields the same volume as the tested container ($7.7{\cdot}10^{-2}$ m^3). The behaviour of the liquid is assumed to be incompressible, hence the effective radius of the elastic sphere R_s is related to the radius of the bubble (3.3):

$$R_s = (R_{s_0}^3 + R_b^3 - R_{b_0}^3)^{1/3} \tag{3.3}$$

Integrating (3.2) between R_s and R_b, using (3.1) and defining $\Lambda = R_b/R_s$, the same equation as in Obreschkow et al. (2006) is found (3.4):

$$R_b\ddot{R}_b + \frac{3}{2}\dot{R}_b^{\,2} + \frac{P_s(t) - P_b(t)}{\rho} - 2\dot{R}_b^{\,2}\Lambda - R_b\ddot{R}_b\Lambda + \frac{1}{2}\dot{R}_b^{\,2}\Lambda^4 = 0 \tag{3.4}$$

with P_s the pressure at the interface between the liquid and the structural sphere. Λ defines a geometrical parameter with respect to the finite size of the considered fluid domains.

A similar equation to the Rayleigh-Plesset equation is obtained with the addition of three terms that vanish when $R_s = \infty$ (infinite medium).

Another relation between the pressure applied on the wall and the structural sphere response is needed. During an HRAM event the structure undergoes complex mechanisms such as plasticity and failure. In the present work the authors consider only elastic behaviour of the structure as a first step. Inelastic analysis would be considered after the relevance and validity of the proposed analytical model is enough substantiated. If the behaviour of the containers is assumed elastic and linear, a good approximation of the relationship is obtained by assuming proportionality between the variation of pressure on the sphere wall $P_s - P_{s_0}$ and the (small) variation of the internal volume of the sphere $V - V_0$. This coefficient of proportionality will hereafter be called confinement parameter, and denoted α[4] in (3.5),

$$P_s - P_{s_0} = \alpha.(V - V_0) \tag{3.5}$$

3.4 Application of the confined Rayleigh-Plesset equation for bubbles created by HRAM events

The initial conditions of the Rayleigh-Plesset equation determined from the ONERA experiment are linked to the initial time chosen for the analysis (when a bubble cavity reasonably appears).

[4]This change in the relation defining the confinement parameter in comparison to the previous chapter is done to allow the application of the confined Rayleigh-Plesset equation to non-spherical containers. The relation between α and κ is $\alpha = \kappa\left({}^1/_{4\pi}\right)\left(P_{s_0}/R_{s_0}^3\right)$. This relation is demonstrated in Appendix D.

To choose the starting time for Rayleigh-Plesset simulations, energetic considerations are used e.g. when the liquid initial kinetic energy in Rayleigh-Plesset equation is equal to the theoretical initial kinetic energy of the projectile that created the bubble (approximately 2.9 kJ in the tank). In (Deletombe et al., 2013) it is estimated that the projectile has lost 90% of its kinetic energy after 1 ms. As the energy partition between the kinetic energy transferred to the liquid and the energy dissipated by the deformation of the projectile is not known, no dissipative phenomena are considered here: the whole projectile kinetic energy is assumed to be transferred to the liquid. It has been observed that the chosen initial conditions corresponded approximately to the beginning of the growth stage of the bubble cavity in the test. The amount of kinetic energy of the liquid is calculated using the assumption of incompressibility of the liquid (3.6):

$$E_k = 2\pi\rho R_b^4 \dot{R_b}^2 \left(\frac{1}{R_b} - \frac{1}{R_s}\right) \tag{3.6}$$

3.4.1 Experimental calibration of α

First, before trying to obtain the numerical value of α from analytical formulae, its value is obtained by calibration means using the experimental results. This value is denoted α_{calib}.

The modified Rayleigh-Plesset equation is solved with a Runge-Kutta forth order method. During the experiment the bubble does not follow the standard Rayleigh-Plesset equation leading to a symmetric growth and decay. It is believed that the decay stage was affected by phenomena that are not modelled (damages and inertia effect). To obtain a good agreement during the growth stage between tests and results (in terms of radius amplitude of the bubble), a coefficient α_{calib} has been calibrated to 150 MPa.mm^{-3} (see Figure 3.4). Table 3.1 summarises the initial conditions used for this simulation.

Table 3.1 – Numerical values of the initial conditions used for the tank case in confined Rayleigh-Plesset simulations.

Case	P_{b_0} (MPa)	t_0 (ms)	R_{b_0} (mm)	$\dot{R}_{b_0}$ (mm.ms^{-1})	R_{s_0} (mm)	α_{calib} (MPa.mm^{-3})
Tank	$2.23 \cdot 10^{-3}$	0.26	48.5	70.6	264	150

3.4.2 Use of elasticity formula for the structure response

The results obtained by calibrating the coefficients α are found to be quite encouraging. The extent to which the numerical values of this coefficient can be predicted with analytical formulae is now investigated.

First the case of an "academic container" is examined. A spherical elastic container is used for this purpose. Obviously this model induces large differences with the real container. A mono-material spherical shell is used instead of a multi-material orthorhombic container assembled by metallic bolts.

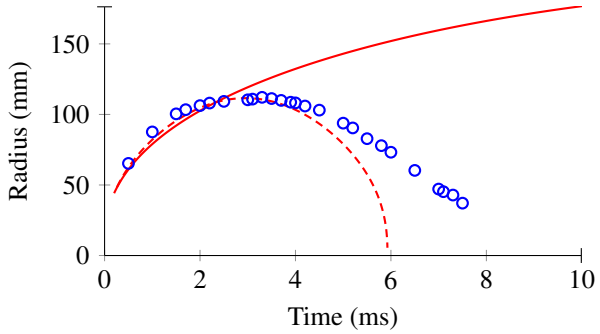

Figure 3.4 – Radius evolution in test (o), predicted with non-confined Rayleigh-Plesset equation (—) and with confined Rayleigh-Plesset (- - -) with α_{calib}.

However, this first approach is introduced for its practical interest in some industrial applications (e.g. civil liquid gas containers, space tanks). It will also be used in future works as a reference to compare with Finite Elements modellings.

Analytical value of α for spherical containers

In the case of a spherical container, the structure can be modelled using the theory of elasticity on a spherical shell. The numerical values of the coefficient α can be determined for this configuration, it will be denoted α_s in (3.7):

$$\alpha_s = \frac{E}{4\pi}.\left(\frac{(R_{s_0}+e)^3 - R_{s_0}^3}{R_{s_0}^3}\right).\left(\frac{2}{2(1-2\nu)R_{s_0}^3 + (1+\nu)(R_{s_0}+e)^3}\right) \tag{3.7}$$

The confinement parameters in (3.5) obtained with the structure being modelled as a monomaterial spherical elastic shell, have been computed for materials with contrasted mechanical characteristics (Tables 3.2). It appears that these values of alpha largely overestimate the calibration value.

Table 3.2 – Numerical values used for the calculation of the coefficient α_s for a V =0.3x0.54x0.66 m^3 tank (see Airbus-Group Innovation tank).

Tank material	E (MPa)	ν	e (mm)	α_s (MPa.mm^{-3})
OMC[a]	110000	0.3	6	$3.0 \cdot 10^4$
Plexiglass	2600	0.3	40	$5.1 \cdot 10^3$
Steel	210000	0.3	50	$3.4 \cdot 10^5$

[a]Organic Matrix Composite

As expected, none of the containers allows a good correlation with the experimental results. There is respectively a ratio of 34 between the calibrated value and the best one obtained by considering a PMMA spherical shell that yields the same volume than the tank.

Use of elastic plates formulae

The container used in the experiment is not spherical, and is an assembly of several parts with different materials (mainly six plates: two in OMC, two in PMMA, and two in steel). In this section the numerical value of the coefficient α is calculated with plates formulae. It will be denoted α_{plate}.

Plates formulae to obtain ΔV

The total variation of the container volume is obtained by adding the variation of volume allowed by the deformation of each panel of the symmetric tank: $\Delta V = 2(\Delta V_{plate_{OMC}} + \Delta V_{plate_{Steel}} + \Delta V_{plate_{PMMA}})$. The plates are considered to be embedded and submitted to a uniform pressure field.

The variation of volume allowed by a single panel (see Figure 3.6), is calculated using Timoshenko 's theory of plates and shells (3.8),

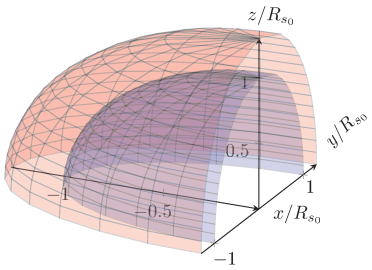

Figure 3.5 – Variation of volume for a quarter of the structural sphere submitted to uniform internal pressure before application of the pressure (blue) and after (red).

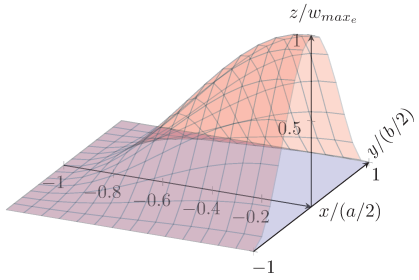

Figure 3.6 – Variation of volume for half of an embedded plate submitted to uniform pressure before application of the pressure (blue) and after (red).

$$\Delta V_{plate} = \iint_S w_{emb}.dS \tag{3.8}$$

The bending of each plate w_{emb} is calculated according to Timoshenko and Woinowsky-Krieger (1959) using (3.13) to (3.16) addends in (3.10 - 3.12) to obtain the terms in (3.9),

$$w_{emb} = w_{ss} + w_1 + w_2 \tag{3.9}$$

$$w_{ss} = \frac{4(P_w(t) - P_{w_0}).a^4}{\pi^5.D} \sum_{m=1,3,5...}^{\infty} \frac{(-1)^{(m-1)/2}}{m^5} cos\left(\frac{m\pi x}{a}\right) \left(1 - \frac{\beta_a tanh(\beta_a) + 2}{2cosh(\beta_a)} cosh\left(\frac{m\pi y}{a}\right) + \frac{1}{2cosh(\beta_a)} \frac{m\pi y}{a} sinh\left(\frac{m\pi y}{a}\right)\right) \tag{3.10}$$

Where a and b are the dimensions of the plate, and D is the stiffness of the plate to bending: $D = E.e^3/(12(1-\nu^2))$, $\beta_a = mb\pi/(2a)$ and $\beta_b = ma\pi/(2b)$.

$$w_1 = -\frac{a^2}{2\pi^2 D}\sum_{m=1,3,5...}^{\infty} E_m \frac{(-1)^{(m-1)/2}}{m^2 cosh(\beta_a)} cos\left(\frac{m\pi x}{a}\right) \left(\frac{m\pi x}{a} sinh\left(\frac{m\pi x}{a}\right) - \beta_a tanh(\beta_a) cosh\left(\frac{m\pi x}{a}\right)\right) \quad (3.11)$$

$$w_2 = -\frac{b^2}{2\pi^2 D}\sum_{m=1,3,5...}^{\infty} F_m \frac{(-1)^{(m-1)/2}}{m^2 cosh(\beta_b)} cos\left(\frac{m\pi y}{b}\right) \left(\frac{m\pi y}{b} sinh\left(\frac{m\pi y}{b}\right) - \beta_b tanh(\beta_b) cosh\left(\frac{m\pi y}{b}\right)\right) \quad (3.12)$$

with:

$$(M_y)_{y=\pm b/2} = \sum_{m=1,3,5...}^{\infty} (-1)^{(m-1)/2} E_m cos\left(\frac{m\pi x}{a}\right) \quad (3.13)$$

$$(M_x)_{x=\pm a/2} = \sum_{m=1,3,5...}^{\infty} (-1)^{(m-1)/2} F_m cos\left(\frac{m\pi y}{b}\right) \quad (3.14)$$

and:

$$\left(\frac{\partial w}{\partial y}\right)_{y=\pm b/2} + \left(\frac{\partial w_1}{\partial y} + \frac{\partial w_2}{\partial x}\right)_{y=\pm b/2} = 0 \quad (3.15)$$

$$\left(\frac{\partial w}{\partial x}\right)_{x=\pm a/2} + \left(\frac{\partial w_1}{\partial x} + \frac{\partial w_2}{\partial y}\right)_{x=\pm a/2} = 0 \quad (3.16)$$

Numerical value of α_{plate} for an orthorhombic tank

To obtain the numerical value of α_{plate} such as $\Delta P = \alpha \Delta V$, one needs to solve a system of partial differential equations, which requires a numerical resolution. First the variation of volume induced by an arbitrary variation of pressure of $P_s - P_{s_0} = 1$ MPa is calculated for each plate. The obtained numerical values are presented in Table 3.3.

Table 3.3 – Variation of volume authorised by the plates with respect to 1 MPa variation of pressure.

	Material	a (mm)	b (mm)	ΔV_{plate} (m^3)
Tank	OMC	540	660	$7.5{\cdot}10^{-3}$
	Plexiglass	300	540	$6.9{\cdot}10^{-5}$
	Steel	300	660	$6.0{\cdot}10^{-7}$

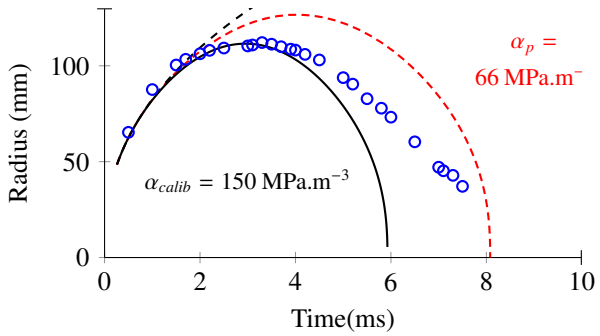

Figure 3.7 – Radius evolution in tank test (o) and predicted with the confined Rayleigh-Plesset model in tank with α_{plate} (- - -) and α_c (—).

Using (3.5) with $P_s - P_{s_0} = 1$ MPa, $\Delta V = 1.52{\cdot}10^{-2}$ m^3[5], the obtained numerical value for the confinement parameter is: $\alpha_{plate} = 66$ MPa.mm^{-3} for the tank case. It is found to be closer to the calibrated value which is $\alpha_{calib} = 150$ MPa.mm^{-3} than the one obtained with a spherical container ($\alpha_s = 5100$ MPa.mm^{-3}). The ratio in the tank case between the calibrated confinement parameter and the one calculated with the plates formulae is 2.27 instead of 34 with the spherical container. The bubble dynamics obtained with (3.4) using α_{calib} and α_{plate} are compared to the experimental one in Figure 3.7.

The prediction of the bubble dynamics obtained with α_{plate} is quite satisfactory (difference between the maximum radius is 11 %, and 33 % in collapse time) knowing that the model is only an approximation of the real container response. The plates in the real container are not perfectly embedded but bolted, there are extra reinforcements at the corners of the tank, the dimensions of the plates that effectively work in bending are not known and there are parts that are simply not modelled.

3.5 Conclusion

In the present study, the confinement in the modified Rayleigh-Plesset equation depends on two parameters : Λ and α. The first one quantifies a correction of the Rayleigh-Plesset equation due to the finite size of the liquid domain. The second defines the confinement effect caused by the structure against the liquid expansion.

In fact, this relationship between the pressure applied to the structure and the deformation of the structure is complex. It depends on the container dimensions, materials, fixations, shape and on the bubble position. Obtaining this relationship would require the use of full 3D physical numerical simulations. In the present study the authors examined the extent to which analytical formulae allow to predict the numerical value of the confinement parameter that is used in the Rayleigh-Plesset 1D model[6].

First the authors introduce a factor α to obtain the simplest relationship between the pressure applied on the container and its volumic deformation in the elastic domain. Assuming a linear relationship between the internal pressure in the liquid and the volume evolution of an

[5]The total variation of the internal volume is $\Delta V = 2(\Delta V_{plate_{OMC}} + \Delta V_{plate_{Steel}} + \Delta V_{plate_{PMMA}})$.

[6]Same remark as in the introduction, the paper proposes a method to estimate the confinement parameter for container of non-spherical geometry.

elastic spherical container, that is first used to represent the tested structures, the Rayleigh-Plesset equation enhanced with the confinement effect allows to well describe the radius evolution observed in the case of a water-filled tank by calibrating the proposed confinement parameter.

The authors then compare the experimentally calibrated value with the values calculated analytically by using an elastic formula on a mono-material spherical container with various single container materials, and with the value predicted by considering the variation of volume authorised by a multi-material orthorhombic container. It was not possible to obtain good numerical values with the mono-material spherical containers. In fact, the tank walls in the tests are bending, while an elastic sphere acts as a membrane. Eventually a better estimation of the value of this parameter is obtained using plates formulae in the tank case. The difference between the maximum bubble radius with calibrated and calculated confinement parameters is 11%, knowing that several aspects such as the fixations, inertia and the bubble position effects, were not included in these formulae. The analytical model has spherical symmetry, both in the container and in the fluid. The first results obtained with a spherical bubble on a real application case (ellipsoid cavity in an orthorhombic container) tend to demonstrate that an analytical approach could nevertheless give a rough approximation of such complex cases. Improvement in the prediction would be reached by taking the elliptic shape of the bubble into account as done in (Wang and Blake, 2010).

Further studies are currently carried out to experimentally validate the added confinement effect to the Rayleigh-Plesset equation in 1D conditions, and to numerically assess other models and solving methods applicable to general geometries (Finite Elements, Finite Volumes, ...) in order to be able to better understand and predict HRAM bubble dynamics.

Acknowledgement

This study has been carried out as part of the PhD thesis of the main author. The authors would like to thank the French Ministry of Defence and DGA (French Armament Procurement Directorate), for their financial support.

Chapter 4

Cross validation of analytical and finite element models for Hydrodynamic Ram loads prediction in thin walled liquid filled containers

Contents

4.1 Introduction **81**
4.2 Studied cases **83**
4.3 Confined Rayleigh-Plesset equation **83**
4.4 Quasi-incompressible confined bubble dynamics finite element simulations . **85**
4.5 Compressible confined bubble dynamics finite element simulations **88**
4.6 Discussion **93**
4.7 Conclusion **94**

Once the order of magnitude of the calibrated and analytically evaluated confinement parameter is compared, the next step has been to compare the proposed confined Rayleigh-Plesset equation to a 1D bubble dynamics model including the effect of compressibility and structure inertia. The objective of this comparison is to estimate the error in bubble dynamics and in hydrodynamic loads prediction when the liquid compressibility is neglected in HRAM bubble dynamics numerical simulations. Finite Element simulations have been chosen to obtain such a reference because it permits to perform simulations of bubble dynamics with the liquid compressibility and the structure inertia being modelled. First to determine the effect of the structure inertia the Rayleigh-Plesset model is compared to quasi-incompressible simulations (high speed of sound) to obtain the effect of this parameter alone. Then the Rayleigh-Plesset model is compared to compressible simulations. To achieve this, equivalent overpressure initial conditions (to initial bubble growth rate) are determined to have a domain of liquid at rest at the beginning to avoid introducing a bias in the study of the liquid compressibility effect. This chapter has been submitted in T. Fourest, J.-M. Laurens, E. Deletombe, M. Arrigoni, and J. Dupas. Cross validation of analytical and finite element models of hydrodynamic ram loads prediction in liquid filled thin-walled containers. *Journal of Fluids and Structures*, 59:285–296, 2015a.

4.1 Introduction

In the event of an impact of high speed/high energy projectiles on liquid filled tanks, the container may suffer large hydrodynamic loads that could possibly rupture the entire structure. This impact scenario is referred to as Hydrodynamic Ram. This scenario is especially dangerous for thin walled structures that cannot be armoured due to weight penalty reasons. There is an insistent need for tools to model hydrodynamic effects that occur during a Hydrodynamic Ram for military (vulnerability requirement) but also civilian aircraft design (safety reasons). Numerical modelling of Hydrodynamic Ram dynamics would allow to improve the survivability of structures with respect to this particular threat.

Generally, during the impact of a projectile in a large container, the cavity created by the drag of the projectile will be enclosed by the surrounding liquid, and a large bubble will be created as in (Deletombe et al., 2013; Disimile et al., 2009; Lecysyn et al., 2010). This bubble behaves in the same manner as gas bubbles generated by other means (Fourest et al., 2014). The stages of bubble dynamics during Hydrodynamic Ram events first described by Ball (1985) are in agreement with those described by Fuster et al. (2009) for other cavitation problems, i.e. *expansion stage, deceleration stage, initial compression, implosion, and rebound*. These oscillating bubble processes have been investigated for a long time. Extensive experimental and theoretical studies have been carried out on that subject, first motivated by the discovery that bubbles are a source of damage (erosion caused by cavitation (Philipp and Lauterborn, 1998), rupture due to underwater explosion (Cole, 1945), ...), and more recently for the beneficial aspect of cavitation (micro-surgery (Venugopalan et al., 2002; Vogel, 1997) and chemical reaction (Hauke et al., 2007)). In these phenomena two potential sources of damages have been identified in the literature. A collapsing bubble emits a shock wave in the liquid and if the bubble is near a solid boundary, it will develop a liquid jet (Plesset and Chapman, 1971; Lauterborn and Bolle, 1975; Chahine and Duraiswami, 1994). This jet originates from the opposite side to the solid boundary, penetrates through the bubble and impacts the solid boundary at high velocity.

There are two main differences between Hydrodynamic Ram bubbles and bubbles created by other means. Firstly, in Hydrodynamic Ram phenomena the bubble is generated in a closed container. This container is usually sufficiently small for the liquid medium not to be considered infinite, with sufficient distance between the bubble and each wall so that no hydrodynamic jet is formed towards the walls. However when bubbles are in a closed container, an additional cause of damage arises, that is the bursting of the container under the solicitation generated by the bubble growth (Deletombe et al., 2013). In the first approximation if the liquid is assumed incompressible, the container may suffer a large deformation in order to accommodate the gas bubble expansion (maximal radius of 120 mm for NATO bullet impacts at 850 $m.s^{-1}$ in Deletombe et al. (2013)).

Secondly, in Hydrodynamic Ram events the bubble is generated by projectile drag, hence it is dependent on the projectile parameters. Deletombe et al. (2013) presented experiments of the impact in water of non-academic projectiles (7.62 mm NATO bullets) at ballistic speed (850 $m.s^{-1}$). They enlightened the effect of the tumbling of projectiles on the cavity shape during Hydrodynamic Ram events. During tumbling the projectile transmits its momentum more quickly to the liquid medium. An extreme case would be an instantaneous and homogeneous transfer that would lead to a spheric cavity bubble. On the other hand, a projectile that cannot tumble will transfer its kinetic energy more slowly and will create a more elongated cavity shape in its wake as in Varas et al. (2009a). Bless (1979) observed that the pressure resulting from the tumbling of the projectile could be five times greater than the one observed in a

case without tumbling. Deletombe et al. (2011) performed pressure measurements for 7.62 mm bullet impacts on water filled tanks, and observed greater pressures during the drag stage than during the subsequent cavity growth stage but in shorter times. They nevertheless concluded that none of these stages could be neglected for the sizing of structures because they could both induce significant impulse.

The present work focusses on the cavity growth and collapse stages in the case of tumbling projectiles. However the tumbling of projectiles is particularly difficult to correctly simulate with available numerical tools. The most advanced numerical simulations of this phenomenon presented in the open literature deal with non-deformable projectiles (Varas et al., 2009b, 2012a,b; Artero-Guerrero et al., 2013; Sareen and Smith, 1996). These studies either use Lagrange-Euler finite element methods or particle type solutions. Anyway the whole sequence of events up to the collapse (that might take up to 30 ms) is not entirely simulated.

Another approach has been chosen in the present paper that consists of studying this complex phenomenon with analytical models. Pioneer studies on the subject were carried out by Morse and Stepka (1966); Stepka and Morse (1963); Stepka et al. (1964, 1965); Stepka (1966). They identified the factors that affect the structural loading during an Hydrodynamic Ram event. These factors can be organised with respect to the three media: the projectile (shape, size, and material), the tank wall (thickness, material, pre-stress, and protective structure) and the liquid properties. They tried to determine the effects of the different parameters on the survivability of tanks. However they could not clearly establish a correlation that could embrace the effects of all parameters. The present authors proposed an approach based on the classic Rayleigh-Plesset equation that describes the dynamics of a single gas bubble in an infinite liquid domain. The Hydrodynamic Ram bubble dynamics observed in Deletombe et al. (2013) were described using a modified version of the Rayleigh-Plesset equation introducing confinement effects of a spherical container on the bubble dynamics. This model has been applied to experiments presented in Deletombe et al. (2013) with the calibration of the structure response in Fourest et al. (2014). Then it has been applied to one of these tests with the structure response approximated using analytical plate formulae in Fourest et al. (2015c). The obtained results are promising, however this analytical model has not yet been validated against experiments or numerical simulations in 1D conditions, furthermore the model used in this approach is incompressible. The effect of liquid compressibility on unconfined bubble dynamics is known to be mainly important during collapse, where it dampens the amplitude of bubble rebounds (Fuster et al., 2011). However the effect of liquid compressibility during the first oscillation of confined bubbles is not well known.

The influence of a spherical container on the steady state motion of a gas bubble has been investigated in the literature (Lawrence and Kyekyoon, 1986). In the medical domain, studies can be found on bubbles oscillating in tubes (Jang et al., 2009; Oguz and Prosperetti, 1998; Coralic and Colonius, 2013) or between two planes (Leighton, 2011). Obreschkow et al. (2006) examined the influence of a closed spherical free surface on bubble dynamics by studying a bubble created in a water drop in microgravity, but to the authors' knowledge, the influence of a closed container on the transient bubble dynamics has not yet been investigated.

In the present study, the authors compare the proposed confined Rayleigh-Plesset equation with the numerical simulations of bubble dynamics with a finite element model including the effect of compressibility and structure inertia. The objective of this comparison is to estimate the error of the analytical Rayleigh-Plesset model in bubble dynamics to determine if a compressible confined analytical model is needed for predicting mechanical loads that occur during a Hydrodynamic Ram event. The present investigation focusses on the first oscillation of large

bubbles. The final collapse of bubbles is known to be a complex and unstable phenomenon, that often leads to the breaking of the spherical symmetry and to fission of the bubble (Frost and Sturtevant, 1986), but this stage remains a challenge to simulate numerically (Johnsen and Colonius, 2009; Popinet and Zaleski, 2002).

Finite element simulations have been chosen to obtain reference results because they permit to study bubble dynamics with the liquid compressibility and the structure inertia being modelled. Barras et al. (2012) proved that explicit finite element codes correctly predict the dynamics of a gas bubble in an infinite domain of liquid. The present research is organised in two steps. First quasi-incompressible finite element simulations are performed to quantify the error in the bubble dynamics prediction when the inertia of the structure is neglected (quasi-static response). Then results of compressible finite element simulations will be compared to results obtained with a confined version of the Rayleigh-Plesset equation.

4.2 Studied cases

The authors chose to study the dynamics of confined bubbles comparable to those observed in HRAM events, in terms of radius amplitude and collapse time. Figure 4.1 describes the considered problem. The containers are filled with liquid (here water) and contain a bubble of gas (here air) at their centres. It is chosen to study the dynamics of bubbles in three different spherical containers. An internal radius container of $R_{s_0} = 1$ m, a wall thickness of e = 6 mm of three materials (steel, aluminium and PMMA) are chosen. The characteristics of the three materials offer a variety of structure overall rigidity and hence a range of confined bubble dynamics.

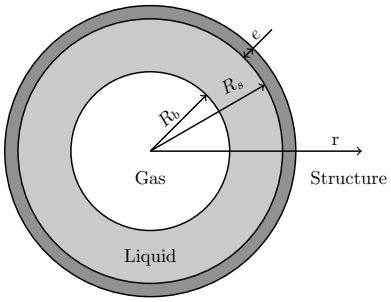

Figure 4.1 – Drawing of the system considered for the confined bubble dynamics simulations.

4.3 Confined Rayleigh-Plesset equation

Early studies on bubble dynamics began with Lord Rayleigh (1917) who examined the pressure prediction during the collapse of a spherical bubble, assuming that the surrounding liquid is incompressible and inviscid, and that surface tension forces are negligible. His work was extended by Plesset (1949), who derived the second-order non-linear ordinary differential equation for the time-dependent bubble radius evolution, which became the well known *Rayleigh-Plesset equation for bubble dynamics*. Improvements of this equation have been proposed by numerous authors, like Keller and Miksis (1980), or extensions in Fujikawa and Akamatsu (1980), Prosperetti and Lezzi (1986) and Hauke et al. (2007). These improvements mainly concern effects

that are important at the end of the collapse stage: liquid compressibility, thermal effects, and the effect of the non-equilibrium of liquid-vapour transformation.

A modification of the classic Rayleigh-Plesset equation has been proposed in Fourest et al. (2014) to account for confinement effects without changing the resolution method. To obtain this equation, a spherical gas bubble in a spherical finite domain of liquid is considered (see Figure 4.1), and the following assumptions are made:

- Spherical deformation of the bubble interface is assumed;
- Gravity effects are negligible;
- Idealised case of zero mass transport across the bubble interface is considered;
- Dynamic viscosity and surface tension effects are neglected for bubbles of this size (Chapman and Plesset, 1971);
- The behaviour of the air in the bubble is assumed adiabatic with $\gamma = 1.4$;
- The liquid domain is considered to be incompressible and of finite dimensions;
- An elastic structural confinement is added by means of a spherical shell.

The equation of mass conservation for a radial movement is expressed in spherical coordinates. It reduces, due to the previous assumptions to (4.1).

$$r^2 \dot{r} = R_b^2 \dot{R}_b \tag{4.1}$$

with R_b the radius of the bubble and $\dot{r}$ the radial speed of the liquid at radius r. Using the previous assumptions, the equation of conservation of momentum in the radial direction is reduced to (4.2).

$$\ddot{r} + \dot{r}\frac{\partial \dot{r}}{\partial r} + \frac{1}{\rho}\frac{\partial P}{\partial r} = 0 \tag{4.2}$$

It is considered here that the centre of the bubble corresponds to the centre of the container. The behaviour of the liquid is assumed to be incompressible, hence the current radius of the elastic sphere R_s is related to the radius of the bubble (4.3).

$$R_s = (R_{s_0}^3 + R_b^3 - R_{b_0}^3)^{1/3} \tag{4.3}$$

Integrating (4.2) between R_s and R_b, using (4.1) and defining $\Lambda = R_b/R_s$, the same equation as in Obreschkow et al. (2006) is found (4.4):

$$R_b\ddot{R}_b + \frac{3}{2}\dot{R}_b^{\,2} + \frac{P_s(t) - P_b(t)}{\rho} - 2\dot{R}_b^{\,2}\Lambda - R_b\ddot{R}_b\Lambda + \frac{1}{2}\dot{R}_b^{\,2}\Lambda^4 = 0 \tag{4.4}$$

with P_s the pressure at the interface between the liquid and the structural sphere and P_b the pressure in the bubble. Λ defines a geometrical parameter with respect to the finite size of the considered fluid domain.

A similar equation to the Rayleigh-Plesset equation is obtained with the addition of three terms that vanish when $R_s = \infty$ (infinite medium).

Another relation between the pressure applied on the wall and the structural sphere response is needed. If the container' s behaviour is assumed to be elastic and linear, a spherical container can be modelled using the theory of elasticity on a spherical thick shell (4.5) (Figure 4.1):

$$P_s - P_{s_0} = (R_s - R_{s_0}).E.\left(\frac{(R_{s_0}+e)^3 - R_{s_0}^3}{R_{s_0}^3}\right)\left(\frac{2R_{s_0}^2}{2(1-2\nu)R_{s_0}^3 + (1+\nu)(R_{s_0}+e)^3}\right) \quad (4.5)$$

with E the Young Modulus, ν the Poisson ratio and e the shell thickness.

4.4 Quasi-incompressible confined bubble dynamics finite element simulations

Finite element simulations of confined bubble dynamics were first performed in quasi-incompressible situation to obtain reference results to validate the proposed confined Rayleigh-Plesset model. It permits to estimate the error in bubble dynamics prediction when the inertia of the structure is neglected in the analytical model (use of quasi-static formulae). The finite element simulations were performed using the EUROPLEXUS explicit code, which was jointly developed by the CEA and the EU CRC-Ispra to accurately solve fast dynamic problems for coupled fluid/structure systems. It has been shown by Barras et al. (2012) that explicit finite element codes allow to simulate the dynamics of a gas bubble in an infinite domain of liquid with good agreement with analytical solution (Keller and Kolodner, 1956).

4.4.1 Description of the quasi-incompressible confined bubble problem

The initial conditions used for these simulations have been determined in Fourest et al. (2014) and used in Fourest et al. (2015c). They have been determined from a Hydrodynamic Ram test presented in Deletombe et al. (2013). These initial conditions are: $R_{b_0} = 48.5$ mm, $\dot{R}_{b_0} = 70.6$ m.s^{-1} and $P_{b_0} = 0$ MPa. To use this set of Rayleigh-Plesset initial conditions in finite element simulations an initial speed is applied to each node of the model to mimic the hypothesis of incompressibility. The initial radial speed is computed using equation (4.1). With these initial conditions the bubble dynamics is not created by an initial pressure difference between the bubble gas and the liquid at infinity but by initial liquid momentum. It has been shown in Fourest et al. (2014) that in such a case the initial pressure in the bubble has negligible effects on the bubble dynamics during the first oscillation. For this reason the bubble pressure is chosen to be zero in the confined Rayleigh-Plesset equation and only the water medium and the spherical structure are meshed in the finite element simulations. The air in the bubble is not meshed since in this attempt, it is assumed that the compressibility of the gas phase does not act in the bubble oscillation. The air surrounding the container is not meshed, but the atmospheric pressure is applied to the structure.

In view of the problem geometry axi-symmetric bi-dimensional simulations are performed. The mesh domain is reduced to a quarter with symmetry conditions being applied in the x and y direction. Arbitrary Lagrangian Eulerian (ALE) grid deformation is used for the water medium in order to keep a regular mesh during the calculation and avoid cells collapse around the bubble interface. ALE finite element methods permit to control the mesh grid independently from the

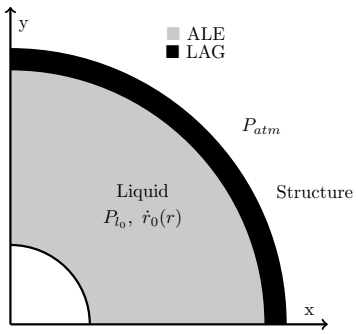

Figure 4.2 – Drawing of the considered problem in quasi-incompressible simulations

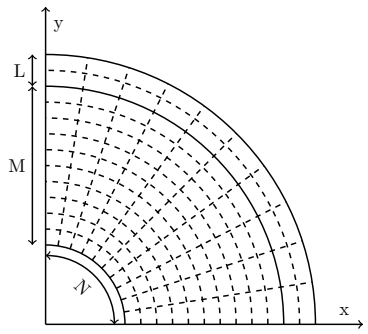

Figure 4.3 – Mesh principle for the liquid medium in quasi-incompressible simulations.

material grid (Souli et al., 2000). The bubble interface and the structure nodes displacements are defined Lagrangian. The sphericity of the bubble interface (free surface) is imposed in these simulations to avoid unstable phenomena to occur during collapse due to a small deviation in the mesh. The interaction between the structure and the liquid medium is established through conform meshing (common nodes). Figure 4.2 describes the considered problem.

4.4.2 Material Laws used in quasi-incompressible confined bubble dynamics simulations

It is known that no thermal effects affect bubble dynamics in water at ambient temperature (Brennen, 1995). Therefore the behaviour of the liquid is assumed to be isothermal. The equation of state used for the liquid is (4.6).

$$P_l = P_{l_0} + (\rho_l - \rho_{l_0})c_l^2 \tag{4.6}$$

where $P_{l_0} = 0.1$ MPa and $\rho_{l_0} = 1000$ kg.m^{-3} are the reference values for the pressure and density of the liquid. In the quasi-incompressible simulations the sound speed in the liquid is artificially elevated to $c_l = 10000$ m.s^{-1}.[1] This high value reduces the compressibility of the liquid to perform quasi-incompressible simulations at an acceptable numerical cost.

The containers are modelled using a linear elastic law. The Young modulus of materials is noted E, their density ρ, and their Poisson coefficient ν. Table 4.1 summarises the different values used for the simulations.

4.4.3 Convergence study for the quasi-incompressible simulations

The Finite Element models are made of 4 nodes axi-symetric elements. Figure 4.3 shows the parameters used in the definition of the mesh. N is the number of orthoradial elements, M the number of liquid elements in the radial direction and L the number of container elements

[1] It will be seen in Chapter 5 that this value is sufficient to be in a quasi-incrompressible case for a compressible analytical model. Plus it will be seen by comparing Table 4.2 to Table 5.1 that this value largely increase the computation time by reducing the time step.

Table 4.1 – Material numerical values used in the simulations.

Material	ρ (kg.mm^{-3})	E (MPa)	ν
Steel	$7.8{\cdot}.10^{-3}$	210000	0.3
Aluminium	$2.7{\cdot}10^{-3}$	70000	0.3
PMMA	$1.18{\cdot}10^{-3}$	2600	0.3

in the radial direction. Figure 4.4 shows the bubble radius vs. time curves for different mesh refinements. This study is performed in the case of the PMMA container, which develops the larger bubble radius.

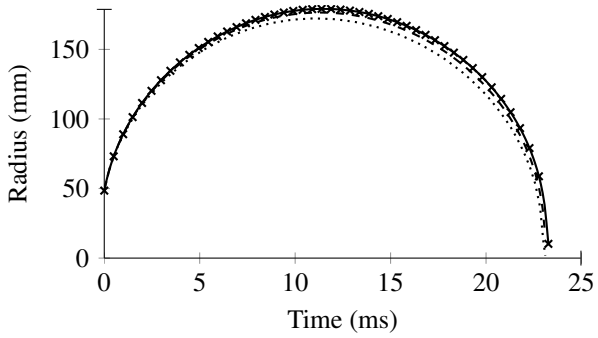

Figure 4.4 – Bubble radius vs. time results obtained with different mesh refinements NxMxL: 10x158x1 (····), 23x318x2 (- - -), 55x636x4 (—) and 110x1272x8 (x) in quasi-incompressible finite element simulations.

A good convergence is obtained for the 55x636x4 mesh refinement (<1% of relative error). For the following analyses the same mesh (55x636x4) will be used for the three materials. However it can be seen that the difference in bubble radius prediction using a coarser mesh is relatively small. The calculations have been performed on a cluster using 8 threads and the following performance Intel® Ivy-Bridge E5-2667v2 @ 3.3 GHz, 132 GB RAM, 10 GB swap. Table 4.2 presents the numerical cost of each simulation.

4.4.4 Simulation results of quasi-incompressible confined bubble dynamics

In the present section, numerical results obtained with the quasi-incompressible finite element simulations are compared with results obtained with the proposed confined Rayleigh-Plesset model. The confined Rayleigh-Plesset model is solved using a forth order Runge-Kutta method. Figure 4.5-(a) compares the radii time histories, Figure 4.5-(b) the liquid kinetic energy and Figure 4.5-(c) the movement of the internal structure radius during the first oscillation of the bubble of the finite element models and the confined Rayleigh-Plesset equation. The liquid kinetic energy E_k in the analytical model is given by equation (4.7).

Table 4.2 – Model features and calculation performances on Intel® Ivy-Bridge E5-2667v2 processors clocked at 3.3 GHz.

model	Elements	Nodes	Δt_0 (ms)	CPU time (s)
10x158x1	3180	336	$2.59{\cdot}10^{-3}$	52
23x318x2	17864	18240	$1.88{\cdot}10^{-4}$	2057
55x636x4	70400	71151	$9.58{\cdot}10^{-5}$	12398
110x1272x8	281600	283101	$4.79{\cdot}10^{-5}$	370663

$$E_k = 2\pi\rho_l R_b^4 \dot{R}_b^2 \left(\frac{1}{R_b} - \frac{1}{R_s}\right) \tag{4.7}$$

A very good agreement is found between the results obtained with the confined Rayleigh-Plesset model and the quasi-incompressible finite element simulations. Predictions of the bubble radius, liquid kinetic energy and movement of the internal wall of the container obtained with both methods are pretty similar. These results prove that in these examined cases, a dynamic description of the structure response (inertia effect) is not needed. The approximation of the structure response obtained using quasi-static formulae for the structure response proved to be satisfactory.

4.5 Compressible confined bubble dynamics finite element simulations

In this section compressible finite element simulations are performed in order to study the effect of liquid compressibility on confined bubble dynamics.

4.5.1 Description of the compressible confined bubble problem

New initial conditions have been chosen to simulate a bubble growth that is caused by initial overpressure in the bubble. This is a more standard case to simulate, moreover the domain of liquid is at rest at the beginning of the simulation so there is no bias in the study of compressibility effects. These initial conditions are the following: $R_{b_0} = 40$ mm, $\dot{R}_{b_0} = 0$ m.s^{-1} and $P_{b_0} = 6$ MPa.

The maximum of the unconfined bubbles radius predicted with these initial conditions is approximately the same as in the previous case. The standard theory (C.2) used in Lauterborn and Vogel (2013) gives the bubble energy E_b for a bubble in an infinite domain of liquid in function of its maximal volume. As the 4.4.1 and 4.5.1 cases have approximately the same maximal bubble radius they are energetically equivalent.

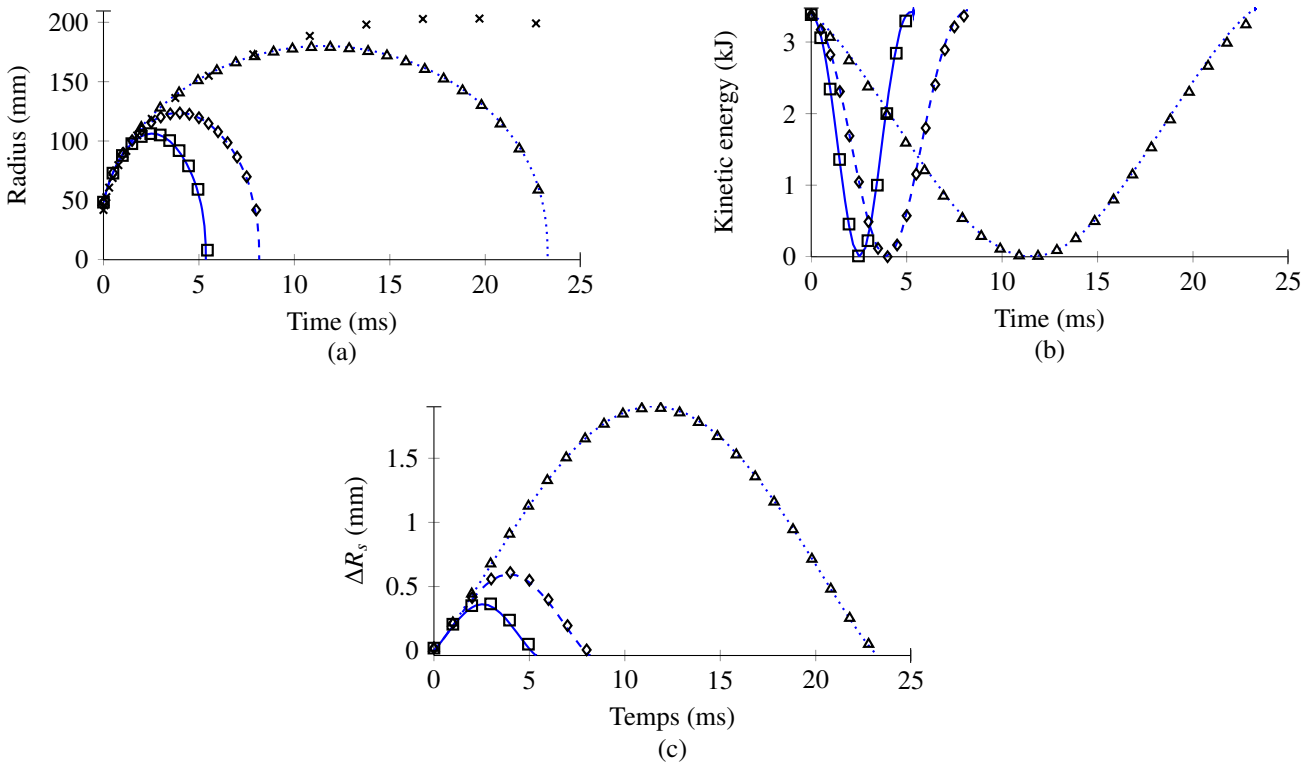

Figure 4.5 – Bubble radius (a), liquid kinetic energy (b) and movement of the internal container wall (c) for quasi-incompressible finite element simulation in steel (□), aluminium (◇) and PMMA (△) containers and for confined Rayleigh-Plesset resolution in steel (—), aluminium (- - -) and PMMA (···) containers. For reference the bubble radius evolution predicted with the unconfined Rayleigh-Plesset equation (x) are plotted in (a).

$$E_b = \frac{4\pi}{3}(P_l - P_{vap})R_{b_{max}}^3 \tag{4.8}$$

In this case the dynamic of the bubble is created by the initial difference in pressure between the gas in the bubble and the liquid. Contrary to the previous case in the finite element simulations, the whole problem is meshed (bubble, liquid and structure) to seaze the effect of the bubble gas relaxation. Again the air surrounding the container is not meshed, instead the atmospheric pressure is applied on the external face of the structure.

The problem is the same as in 4.4.1 except that an air domain has been added. The bubble interface (between liquid and air) and the structure nodes displacements are again defined Lagrangian and spherical. So there is no mixture between the air and water in the simulations. Figure 4.6 describes the considered problem.

Material laws used in compressible confined bubble simulations

The behaviour of the gas is assumed to be ideal and the state variables are linked by equation (4.9).

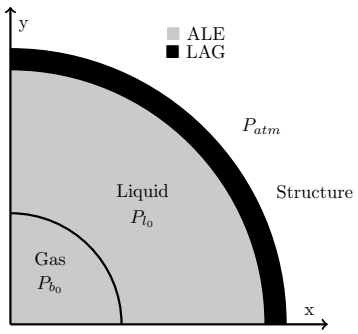

Figure 4.6 – Drawing of the considered problem in compressible confined bubble dynamics simulations

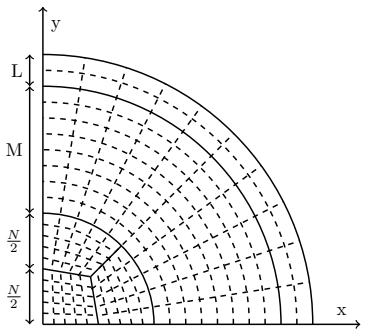

Figure 4.7 – Mesh principle in compressible confined bubble dynamics simulations.

$$P_g = P_{g_0} \left(\frac{\rho_g}{\rho_{g_0}} \right)^{n_g} \tag{4.9}$$

Here $P_{g0} = 0.1$ MPa and $\rho_{g0} = 1$ kg.m^{-3} are the reference values of gas pressure and density, and n_g is the polytropic exponent. $n_g = \gamma_g = 1.4$ is used, it corresponds to an adiabatic transformation. The liquid is assumed to follow the same equation of state (4.6) as in the previous case, except that this time $c_l = 1500$ m.s^{-1}. The structure material follows a linear elastic law.

4.5.2 Convergence study for the compressible simulations

Again the finite element models are made of 4 nodes axi-symetric elements. Figure 4.7 shows the parameters used in the description of the mesh. They are the same as in 4.4.3. Figure 4.8 shows the results of the convergence study. Again this study is performed in the case of the PMMA container.

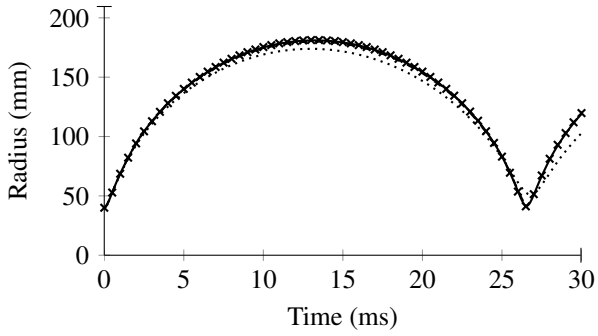

Figure 4.8 – Bubble radius vs. Time results obtained with different mesh refinements NxMxL: 10x158x1 (···), 23x318x2 (- - -), 55x636x4 (—) and 110x1272x8 (x) in compressible finite element simulations.

A satisfactory convergence is obtained for the 55x636x4 mesh refinement (<1% of relative error). For the following analyses the 110x1272x8 mesh will be used. Table 4.3 presents the numerical cost of each simulation.

Table 4.3 – Model features and calculation performances on Intel® Ivy-Bridge E5-2667v2 processors clocked at 3.3 GHz.

model	Elements	Nodes	Δt_0 (ms)	CPU time (s)
10x158x1	1675	1851	$6.41{\cdot}10^{-4}$	42
24x318x2	8136	8494	$2.53{\cdot}10^{-4}$	205
56x636x4	38248	38974	$1.03{\cdot}10^{-4}$	2938
110x1280x8	150865	152320	$5.16{\cdot}10^{-5}$	12842

4.5.3 Simulation results of compressible confined bubble dynamics

In the present section, numerical results obtained with the compressible finite element simulations are compared with results obtained with the proposed confined Rayleigh-Plesset model. First the confined bubble dynamics obtained with the finite element simulations are compared to the classic Keller and Miksis (1980) analytical compressible solution in an infinite domain of liquid (see Figure 4.9-(a)). Figure 4.9-(b) compares the radii time histories, Figure 4.9-(c) the liquid kinetic energy and Figure 4.9-(d) the movement of the internal structure radius of the bubble in the three containers with the finite element simulations and confined Rayleigh-Plesset equation.

The bubbles created in the spherical containers follow the same dynamics as the bubble in an infinite domain of liquid until approximately $t_1 = 1.25$ ms, i.e. the time needed for the initial wave to be reflected on the structure wall and return to the bubble interface. Subsequently the three bubbles have different dynamics. The maximal radius and collapse time of bubbles in the spherical containers are inferior to the one predicted in the unbounded case. Contrary to bubble dynamics predicted with the Keller-Miksis model, those created in the spherical containers present a small asymmetry between growth and decay stages. The velocity of the bubble interface during collapse is lower due to a slight energy dissipation as shown in Figure 4.9-(a).

The comparison between the bubble dynamics, in the Figures 4.9-(a) and 4.9-(b), predicted with the confined Rayleigh-Plesset equation and obtained with compressible finite element simulations shows that the confined Rayleigh-Plesset equation provides a good approximation of the first bubble oscillation with an error on the maximal radius below 6%. Moreover the liquid compressibility also modifies the collapse time, which is larger in compressible finite element simulations.

The comparison of the liquid kinetic energies, in Figure 4.9-(c), predicted with both methods shows that those computed with compressible simulation are largely lower than these predicted with the confined Rayleigh-Plesset equation for the same source (same initial overpressure). It is easily understandable since in compressible simulations the liquid domain is at rest initially. On the contrary in the confined Rayleigh-Plesset model, the liquid is instantaneously put globally

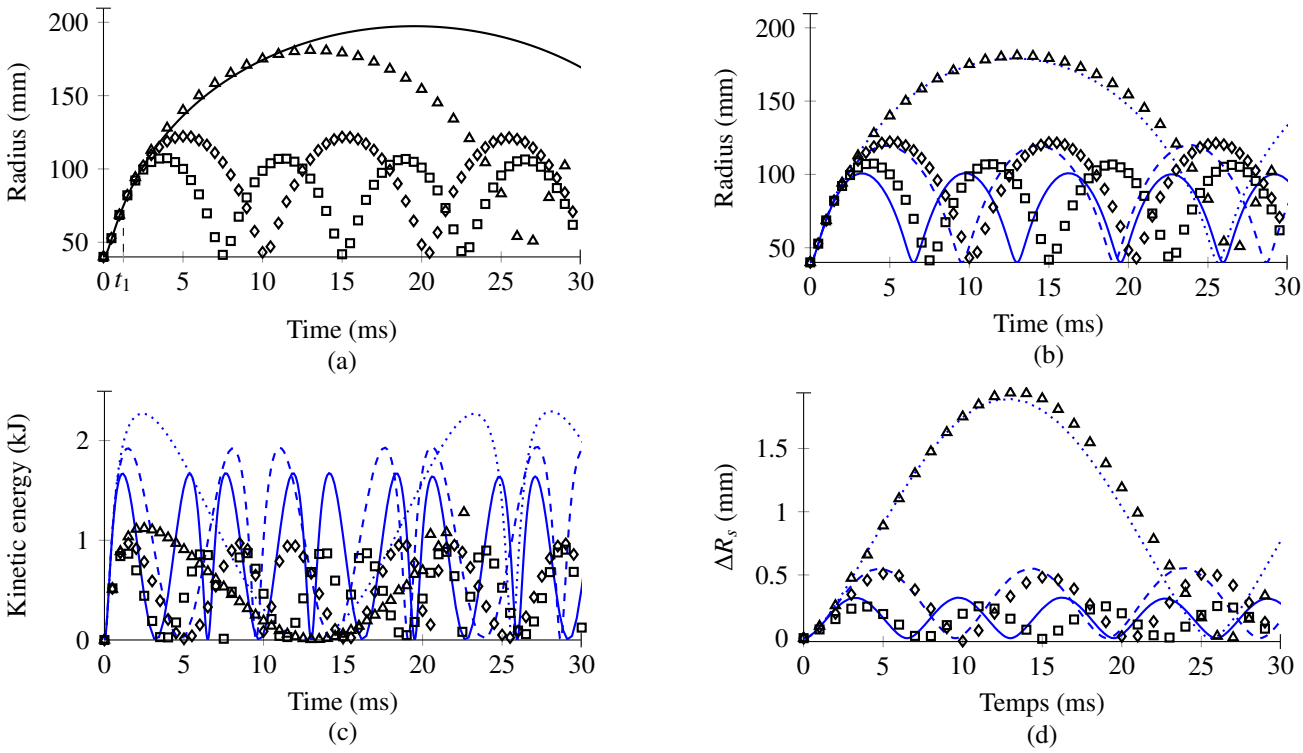

Figure 4.9 – Bubbles radii (a-b), liquid kinetic energy (c) and movement of the internal container wall (d) predicted using finite element simulations in steel (□), aluminium (◇) and PMMA (△) containers compared with (a) Keller-Miksis unconfined model (—) and (b) the confined Rayleigh-Plesset model in steel (—), aluminium (- - -) and PMMA (···) containers.

in motion. However, in the compressible simulations, the liquid kinetic energy seems to be less dependent on the container material.

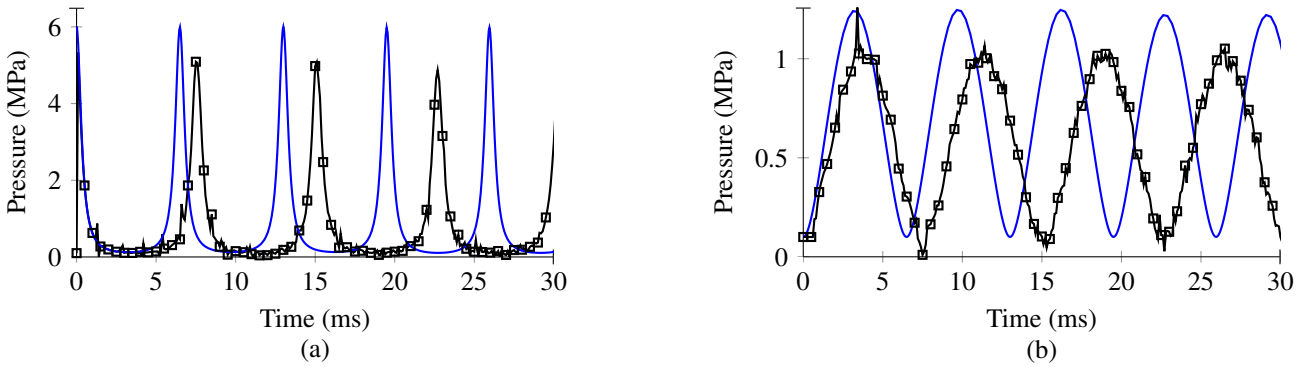

Figure 4.10 – Pressure applied onto the structure (a) and pressure at the bubble interface (b) predicted in the steel container with the confined Rayleigh-Plesset equation (—) and with the finite element simulation (—□—).

Figure 4.10 compares the pressure in the liquid at the bubble and structure interfaces for the steel container case. The pressure applied on the structure is of main interest in these simulations. This information is needed for the sizing of the structure with respect to the Hydrodynamic Ram phenomenon. It can be seen that the pressure prediction during the first

oscillation is good using the confined Rayleigh-Plesset in the case of the steel container. It predicts a slightly higher pressure during a smaller time. The predicted impulse transmitted to the structure (4.10) is $5.79{\cdot}10^4$ N.s instead of $5.60{\cdot}10^4$ N.s in compressible simulations i.e. to a 3.3% difference only. The same order of difference has been found for the three cases, however even if the approximation of the impulse obtained with the Rayleigh-Plesset equation is good, there is a significant difference between the pressure curves predicted with both methods.

$$Imp = \int_{t_0}^{t_{collapse}} 4\pi R_s^2 P_s dt \tag{4.10}$$

This result shows that if the bubble dynamics predicted with both methods are consistent, the confined Rayleigh-Plesset equation provides a correct approximation of the time dependent hydrodynamic loads applied on the structure. This results show that if the two bubble dynamics are in agreement the obtained prediction of the impulse with the confined Rayleigh-Plesset equation is be acceptable.

4.6 Discussion

In the finite element simulations the domain of liquid is bounded by a structure. By limiting the size of the domain of study with a structure, the simulation is freed of its dependency to the size of the domain modelled and the type of boundary conditions used in infinite bubble simulations, as shown in Barras et al. (2012). However the differences between confined bubble dynamics predicted with the confined Rayleigh-Plesset equation or complete finite element simulations might depend upon the size of the studied liquid container. The bubble period depends on the material used for the container as shown by the simulation results but it also depends on other parameters that have been set constant in the present study. Obviously the container thickness and dimensions change its overall rigidity and hence affect the bubble dynamics. But the container dimensions also determine the time when the bubble dynamics begins to be affected by the confinement, which is the time needed for the initial wave to be reflected by the structure and return to the bubble interface. For instance the bubble dynamics will not be affected by a very large container even if it is extremely rigid. This compressibility effects related to the time of travel of waves in the liquid are not modelled in the confined Rayleigh-Plesset equation for which a small soft container may be equivalent to a large rigid one.

However, for the Hydrodynamic Ram bubbles of interest here, the container sizes are usually relatively small in comparison to the distance travelled by the waves during the bubble periods. Hence it has been shown in Fourest et al. (2014, 2015c) that this model proved useful to study the first period of Hydrodynamic Ram bubble at first order. The results obtained with compressible finite element simulations in the present study confirm this conclusion. The hydrodynamic loads are reasonably well approximated using the confined Rayleigh-Plesset equation. However the confined Rayleigh-Plesset equation does not permit to predict the damping that occurs during the following oscillations when the bubble is assumed to remain spherical. But the first bubble period is of main interest for the sizing of aircraft fuel tanks.

4.7 Conclusion

In the present study, the authors examined the effects of liquid compressibility on the dynamics of bubbles in thin walled containers using a numerical approach with explicit finite element methods. The presented approach articulates in two steps.

First quasi-incompressible finite element simulations of confined bubble dynamics were performed for three spherical container materials (steel, aluminium and PMMA). The results of these simulations have been found to be in very good agreement with these obtained using the confined Rayleigh-Plesset equation proposed in Fourest et al. (2014). This comparison is performed to study the need of using a dynamic structure response in confined bubble predictions. On the one hand, in the confined Rayleigh-Plesset equation, the structure response is described by using an elastic formula, and a quasi-static response is used. On the other hand, in the finite element models the structure response includes the effect of the structure inertia. The agreement between these results shows that in the domain of the study a dynamic description of the structure response is not analytically needed. The approximation of the structure response obtained using quasi-static formulae for the structure response provides satisfying results. These comparisons also validate the implementation of the confined Rayleigh-Plesset equation and its resolution algorithm.

Then compressible finite element simulations of confined bubble dynamics were performed for the three container materials. By comparing the results of these simulations with predictions obtained with the confined Rayleigh-Plesset equation, the effect of liquid compressibility only was observed on confined bubble dynamics. The liquid compressibility has been found to affect the bubble maximal radius and its collapse time. The two approaches are in reasonable agreement during the first oscillation for the bubbles. Then for the steel container case the pressure on the structure has been compared between the analytical and finite element simulations. This information is needed for the sizing of structures with respect to the Hydrodynamic Ram phenomenon. The pressure prediction is in reasonable agreement and the impulses transmitted to the structure are consistent in both case (maximal difference of 3.35%). These results show that the confined Rayleigh-Plesset equation gives a useful first approximation of the time dependent hydrodynamic loads applied on structures during the first oscillation period of the bubble. However there is a significant difference between the pressure curves predicted with both methods, so if more detail on the hydrodynamic loads than the impulse is needed the Rayleigh-Plesset approximation may prove insufficient especially for fuels that are more compressible than water ($c_l \approx 1300$ m.s^{-1} for kerosene (Aldred, 1972)). Plus the domain sizes for which the confined Rayleigh-Plesset equation may be used have not been determined in this study and one should be cautious in its use.

Liquid compressibility effects was shown to influence the dynamics of confined bubbles. Finite element simulations have been successfully used to simulate the confined bubble dynamics in a compressible liquid. For the finite element simulations ALE formulation with the movement of the bubble interface defined as Lagrangian has been used. In this approach there is no mass transfer between the gazeous and the liquid phases and the deformation of each domain mesh is maintained homogeneous. However this approach may have some limitations in particular for large mesh deformations in 3D simulations. It would then be interesting to use a diffusive approach as in Barras et al. (2012). Moreover an analytical confined and compressible bubble dynamics model would be useful to predict the bubble dynamics and hydrodynamics loads applied on the containers more accurately. Further efforts will be made to develop such a model and to validate it with respect to finite element simulations.

Acknowledgement

This study has been carried out as part of the PhD thesis of the main author. The authors would like to thank the French Ministry of Defence and DGA (French Armament Procurement Directorate), for their financial support. The authors would also like to thank Dr Vincent Faucher from the CEA and Dr Bertrand Langrand from ONERA for their precious advise on the finite element simulations.

Chapter 5

Development and validation of a confined Keller-Miksis model for Hydrodynamic Ram loads prediction in liquid-filled containers.

Contents

5.1 Introduction **99**
5.2 Formulation of the Keller-Miksis model **100**
5.3 Application to a rigid wall case **103**
5.4 Application to an elastic wall case **107**
5.5 Discussion **113**
5.6 Conclusion and outlooks **114**

The effect of the liquid compressibility on the confined bubble dynamics having been found important in the previous chapter, it is decided to develop an analytical confined bubble dynamics model that takes its effects into account. First a formulation of this model is proposed. This formulation is based on the Keller-Miksis model that describes the dynamics of a gas bubble in an infinite domain of compressible liquid. This model is first developed for the case of a spherical rigid container, and its consistency is verified. Three homogeneous containers are considered. Each of them is made of single materials having distinguishable mechanical properties, respectively steel, aluminium and PMMA. Then the bubble radius and the pressure at the structure and bubble walls are compared to results obtained by finite element simulations. Once the model has been validated in the case of a rigid container it has been developed for an elastic spherical container. For this a dynamical formulation of the container response based on Reissner's polynomial approximation is used. The consistency of this model is verified and it is compared with finite element simulations. Once the model is validated for an elastic spherical container, the bubble radii, structure wall movement and pressure at the structure wall predicted using the confined Rayleigh-Plesset and Keller-Miksis models are compared to evaluate the improvement in the predictions using the later one. This chapter has been submitted in T. Fourest, J.-M. Laurens, V. Faucher, E. Deletombe, M. Arrigoni, and J. Dupas. Development and validation of a confined keller-miksis model for hydrodynamic ram loads prediction in liquid-filled containers. *Journal of Fluid Mechanics*, 2015d. (submitted).

5.1 Introduction

In the event of an impact of high speed/high energy projectiles on liquid filled tanks, the container may suffer large hydrodynamic load that could possibly rupture the entire structure. This impact scenario is referred to as Hydrodynamic Ram. This scenario is especially dangerous for thin walled structures that cannot be armoured due to weight penalty reasons. There is an insistent need for tools to model hydrodynamic effects that occur during a Hydrodynamic Ram for military (vulnerability requirement) but also civilian aircraft design (safety reasons). Numerical modelling of Hydrodynamic Ram would allow to improve the survivability of structures with respect to this particular threat.

Generally, during the impact of a projectile in a large container, the cavity created by the drag of the projectile will be enclosed by the surrounding liquid, and a large bubble will be created as in (Deletombe et al., 2013; Disimile et al., 2009; Lecysyn et al., 2010). Similarities are observed between HRAM bubbles and gas bubbles generated by other means (Fourest et al., 2014). The stages of bubble dynamics during Hydrodynamic Ram events first described by Ball (1985) are in agreement with those described by Fuster et al. (2009) for other cavitation problems, i.e. *expansion stage, deceleration stage, initial compression, implosion, and rebound.* Extensive experimental and theoretical studies have been carried out on that subject, first motivated by the discovery that bubbles are a source of damage (erosion caused by cavitation (Philipp and Lauterborn, 1998), severe loading due to underwater explosion (Cole, 1945), ...), and more recently for the beneficial aspect of cavitation (micro-surgery (Venugopalan et al., 2002; Vogel, 1997) and chemical reaction (Hauke et al., 2007)). In these phenomena two potential sources of damages have been identified in the literature. A collapsing bubble emits a shock wave in the liquid and if the bubble is near a solid boundary, it will develop a liquid jet (Plesset and Chapman, 1971; Lauterborn and Bolle, 1975; Chahine and Duraiswami, 1994). This jet originates from the opposite side to the solid boundary, penetrates through the bubble and impacts the solid boundary at high velocity.

There are two main differences between Hydrodynamic Ram bubbles and bubbles created by other means. Firstly, in Hydrodynamic Ram phenomena the bubble is generated in a closed container. This container is usually sufficiently small for the liquid medium not to be considered infinite, with sufficient distance between the bubble and each wall so that no hydrodynamic jet is formed towards the walls. However when bubbles are in a closed container, an additional cause of damage arises, that is the bursting of the container due to the solicitation generated by the bubble growth (Deletombe et al., 2013). In the first approximation if the liquid is assumed incompressible, the container may suffer a large deformation in order to accommodate the gas bubble expansion (maximal radius of 200 mm for NATO 7.62 mm bullet impacts at 850 $m.s^{-1}$ in (Deletombe et al., 2013)).

Secondly, in Hydrodynamic Ram events the bubble is generated by projectile drag, hence it is dependent on the projectile parameters. Authors enlightened in (Deletombe et al., 2013) the effect of the tumbling of projectiles on the cavity shape during Hydrodynamic Ram events. During tumbling, the projectile transmits its momentum more quickly to the liquid medium. An extreme case would be an instantaneous and homogeneous transfer that would lead to a spherical cavity bubble which is the case in underwater explosions. On the other hand, a projectile that cannot tumble will transfer its kinetic energy more slowly and will create a more elongated cavity shape in its wake as in (Varas et al., 2009a). Bless (1979) observed that the pressure resulting from the tumbling of the projectile could be five times greater than the one observed in a case without tumbling. Deletombe et al. (2011) performed pressure measurements

for 7.62 mm bullet impacts on water filled tanks, and observed greater pressures during the drag stage than during the subsequent cavity growth stage but in shorter times. They nevertheless concluded that none of these stages could be neglected for the sizing of structures because they could both induce a significant impulse.

The present study focusses on the cavity growth and collapse stages in the case of tumbling projectiles. However the tumbling of projectiles is particularly difficult to correctly simulate with available numerical tools. The most advanced numerical simulations of this phenomenon presented in (Varas et al., 2009b, 2012a,b; Artero-Guerrero et al., 2013; Sareen and Smith, 1996) deal with non-deformable projectiles. These studies either use Lagrange-Euler finite element methods or particle type solutions. Anyway the whole sequence of events up to the collapse (that might take up to 30 ms) is not entirely simulated.

Another approach has been chosen in the present study that consists in studying this complex phenomenon by using analytical models. Pioneer studies on the subject were carried out by Stepka and Morse (Morse and Stepka, 1966; Stepka and Morse, 1963; Stepka et al., 1964, 1965; Stepka, 1966). They identified the factors that affect the structural loading during Hydrodynamic Ram events. These factors can be organised with respect to the three media: the projectile (shape, size, and material), the tank wall (thickness, material, pre-stress, and protective structure) and the liquid properties. They tried to determine the effects of the different parameters on the survivability of tanks. However they could not clearly establish a correlation that could embrace the effects of all parameters. Fourest et al. (2014) proposed an approach based on the classic Rayleigh-Plesset equation that describes the dynamics of a single gas bubble in an infinite liquid domain. The Hydrodynamic Ram bubble dynamics observed in (Deletombe et al., 2013) were described using a modified version of the Rayleigh-Plesset equation introducing confinement effects of a spherical container on the bubble dynamics. This model has been applied to experiments presented in (Deletombe et al., 2013) with the calibration of the structure response in (Fourest et al., 2014). Then it has been applied to one of these tests with the structure response being approximated using analytical plate formulae in (Fourest et al., 2015c). The obtained results are promising, however the model used in this approach is incompressible. The effect of liquid compressibility on unconfined bubble dynamics is known to be mainly important during collapse, where it dampens the amplitude of bubble rebounds (Fuster et al., 2011). However, the effect of liquid compressibility during the first oscillation of confined bubbles is not well known. Furthermore it is clear that for very stiff containers the confined Rayleigh-Plesset equation might lead to non-physical results due to the liquid incompressibility.

To solve these issues, the authors propose a confined version of the Keller and Miksis (1980) model in the present paper. The model was developed for two cases of containers: rigid and elastic. For each configuration the self-consistency of the model was verified and the model is compared against finite element simulations. Finite element simulations have been chosen to obtain reference results because they permit to study bubble dynamics with the liquid compressibility being modelled, as in Barras et al. (2012). Finally the improvement in the hydrodynamic loads prediction using this model will be quantified in an elastic spherical tank case.

5.2 Formulation of the Keller-Miksis model

Early studies on bubble dynamics began with Lord Rayleigh (1917) who examined the pressure prediction during the collapse of a spherical bubble, assuming that the surrounding liquid is in-

compressible and inviscid, and that surface tension forces are negligible. His work was extended by Plesset (1949), who derived the second-order non-linear ordinary differential equation for the time-dependent bubble radius evolution, which became the well known *Rayleigh-Plesset equation for bubble dynamics*. Improvements of this equation have been proposed by numerous authors, in particular Keller and Miksis (1980) to include the effect of liquid compressibility on the bubble dynamics and to study the propagation of the wave emitted during the collapse.

A modification of the standard Rayleigh-Plesset equation has been proposed in Fourest et al. (2014) to account for confinement effects without changing the resolution method. The objective of the present study is to propose an improvement of this model by taking liquid compressibility into account in an analytical confined bubble dynamic model.

5.2.1 Basic fluid mechanics equations

This model is based on the Keller and Miksis (1980) model which is a modification of the Keller and Kolodner (1956) model to include the effect of a convergent liquid velocity potential on the bubble dynamics. The Keller-Miksis model is presented hereafter. It is here written under the following assumptions:

- Spherical deformation of the bubble interface (no fission of the bubble);
- Gravity effects are negligible;
- Dynamic viscosity and surface tension effects are negligible;
- The bubble is at the centre of a spherical container of internal radius R_s;
- No cavitation is considered at the structure/liquid interface,
- Assumption of adiabaticity.

The velocity of the bubble interface must be equal to the velocity of the fluid at the bubble surface, which gives (5.1),

$$\dot{R}_b = \frac{\partial \phi(R_b, t)}{\partial r} \tag{5.1}$$

The velocity potential ϕ, the pressure P, and the liquid density ρ_l must satisfy the equations of conservation of mass (5.2), the Navier-Stokes equation (5.3) and the equations of states (5.4) (here the perfect gas law),

$$\frac{\partial \rho_l}{\partial t} + \frac{\partial \phi}{\partial r}\frac{\partial \rho_l}{\partial r} + \rho_l \left(\frac{\partial^2 \phi}{\partial r^2} + \frac{2}{r}\frac{\partial \phi}{\partial r} \right) = 0 \tag{5.2}$$

$$\rho \left(\frac{\partial}{\partial t}\frac{\partial \phi}{\partial r} + \frac{\partial \phi}{\partial r}\frac{\partial^2 \phi}{\partial r^2} \right) + \frac{\partial P}{\partial r} = 0 \tag{5.3}$$

$$P_b = P_{b_0} \left(\frac{R_{b_0}}{R_b} \right)^{3\gamma} \tag{5.4}$$

5.2.2 Simplifications introduced in the Keller-Miksis model

The Navier-Stokes equation (5.3) is integrated with respect to r from r to infinity, which gives (5.5),

$$-\dot{\phi}-\frac{1}{2}\frac{\partial\phi}{\partial r}^2+\int_r^\infty\frac{dP}{\rho_l}=0 \tag{5.5}$$

Next (5.5) is differentiated with respect to t with $\frac{\partial P}{\partial t}=\frac{\partial P}{\partial\rho_l}\frac{\partial\rho_l}{\partial t}=c^2\frac{\partial\rho_l}{\partial t}$ where $c^2=\frac{\partial P}{\partial\rho_l}$ and c is the speed of sound.

$$\frac{\partial^2\phi}{\partial t^2}+\frac{\partial\phi}{\partial r}\frac{\partial^2\phi}{\partial t\partial r}+\frac{c^2}{\rho_l}\frac{\partial\rho_l}{\partial t}=0 \tag{5.6}$$

Then (5.2) is used in (5.6) to eliminate $\partial\rho_l/\partial t$, and divided by c^2 to obtain (5.7),

$$\frac{1}{c^2}\frac{\partial^2\phi}{\partial t^2}-\frac{\partial^2\phi}{\partial r^2}-\frac{2}{r}\frac{\partial\phi}{\partial r}=\frac{1}{\rho}\frac{\partial\rho_l}{\partial r}\frac{\partial\phi}{\partial r}-\frac{1}{c^2}\frac{\partial\phi}{\partial r}\frac{\partial^2\phi}{\partial t^2} \tag{5.7}$$

The Keller-Miksis equation is written under the assumption that for a nearly incompressible fluid c^2 is large and $\partial\rho/\partial r$ is small and that $\partial\phi\ \partial r$ and $\partial^2\phi\ \partial t^2$ have finite values. It leads to the classic wave propagation equation (5.8),

$$\frac{1}{c^2}\frac{\partial^2\phi}{\partial t^2}-\frac{\partial^2\phi}{\partial r^2}-\frac{2}{r}\frac{\partial\phi}{\partial r}=0 \tag{5.8}$$

For simplification ρ_l is set constant in (5.5) which gives (5.9) for the expression of pressure in the liquid:

$$P(r,t)=P_\infty-\rho_l\left(\frac{\partial\phi}{\partial t}+\frac{1}{2}\frac{\partial\phi^2}{\partial r}\right) \tag{5.9}$$

5.2.3 Derivation of the Keller-Miksis differential equation

$\Delta(R_b)$ is defined in (5.10) as the pressure difference divided by ρ_l.

$$\Delta(R_b)=\frac{P_b-P_\infty}{\rho_l}=-\frac{\partial\phi}{\partial t}-\frac{1}{2}\frac{\partial\phi^2}{\partial r} \tag{5.10}$$

In the Keller-Miksis model ϕ respects the wave equation (5.8), hence it can be written in (5.11) as the sum of a converging and diverging velocity potential.

$$\phi=\frac{f(t-r/c)}{r}+\frac{g(t+r/c)}{r} \tag{5.11}$$

Subsequently equation (5.11) is used in (5.10) and in (5.1) to obtain (5.12) for R_b where f do not appears,

$$R_b\Delta(R_b)-cR_b\dot{R}_b=c\phi(R_b,t)-\frac{1}{2}R_b\dot{R}_b^{\,2}-2\dot{g}(t+\frac{R_b}{c}) \tag{5.12}$$

Finally (5.12) is derived with respect to time and (5.10) is used to eliminate $\partial\phi/\partial t$, which leads to the Keller-Miksis standard equation (5.13).

$$-\ddot{R}_b R_b(\dot{R}b-c) = \frac{1}{2}\dot{R}_b{}^3+\dot{R}_b\Delta(R_b)-c\left(\frac{3}{2}\dot{R}_b{}^2-\Delta(R_b)\right)+R_b\dot{R}_b\Delta'(R_b)+2\left(1+\frac{\dot{R}_b}{c}\right)g''\left(t+\frac{R_b}{c}\right)=0 \tag{5.13}$$

5.2.4 Determination of g

To solve this differential equation the function $g(t+R_b(t)/c)$ must be expressed. This function will be used to account for confinement effects of a container on the bubble dynamics. First we need to calculate f and f' that are expressed in (5.14) and (5.15) by combination of (5.1) and (5.10) at $r = R_b$.

$$f(R_b,t) = -R_b^2\dot{R}_b+\frac{R_b^2}{c}\left(\Delta(R_b)+\frac{\dot{R}_b{}^2}{2}\right)-g(R_b,t)+\left(\frac{2R_b}{c}g'(R_b,t)\right) \tag{5.14}$$

$$f'(R_b,t) = -R_b\Delta(R_b)-g'(R_b,t)-\frac{1}{2}R_b\dot{R}_b{}^2 \tag{5.15}$$

Initially $g = g' = 0$ then for $t > (R_{s_0}-R_{b_0})/c$, that is the time needed of the initial velocity potential to reach the structure surface, g' is expressed using (5.1) and (5.11) at $r = R_s$, which gives (5.16). g is obtained by numerical integration of g' and g'' by the numerical differentiation of g' with suitable care, in order to limit the accumulation of residual error.

$$g'(Rs,t) = R_s c\left(\dot{R}_s+\frac{1}{R_s^2}(f(R_s,t)+g(R_s,t))+\frac{1}{R_s c}f'(R_s,t)\right) \tag{5.16}$$

The relations between f and g at the bubble and structure surfaces are obtained using the wave equation (5.8), which leads to $f(R_b,t_1) = f(R_s,t_2)$ with $t_2 = (R_s(t_2)-Rb(t_1))/c+t_1$ and $g(R_s,t_1) = g(R_b,t_2)$ with $t_2 = (R_s(t_1)-Rb(t_2))/c+t_1$.

5.3 Application to a rigid wall case

It was decided to simulate an air bubble growth that is caused by an initial gas overpressure. The domain of liquid is at rest at the beginning of the simulation hence there is no bias in the study of compressibility effects. The initial conditions are the following: $R_{b_0} = 40$ mm, $\dot{R}_{b_0} = 0$ m.s^{-1} and $P_{b_0} = 6$ MPa to compare with previous reference cases. These initial conditions produce bubble dynamics comparable to dynamics observed during HRAM events. The first case of interest is the case of a bubble inside a spherical rigid container. In that case the velocity of the structure wall is zero, which leads to (5.17):

$$\begin{cases} R_s = R_{s_0} \\ \dot{R}_s = 0 \end{cases} \tag{5.17}$$

Firstly the self-consistency of the model is examined and the results obtained with the Keller-Miksis model are compared with results obtained by finite element simulations since it has been shown in (Barras et al., 2012) that explicit finite element codes allow to simulate a similar case. The finite element simulations were performed using the EUROPLEXUS explicit

code, which is jointly developed by the CEA and the EU CRC-Ispra to accurately solve fast dynamic problems for coupled fluid/structure systems.

5.3.1 Verification of the consistency of analytical models for rigid containers

The confined Keller-Miksis model is solved using an Euler method with a fixed time step $\Delta t = 10^{-5}$ ms. The standard Keller-Miksis equation is equivalent to the Rayleigh-Plesset equation when the liquid speed of sound tends to infinity (Keller and Miksis, 1980). Unfortunately this verification cannot be carried out for this case since the confined Rayleigh-Plesset equation cannot be used in a rigid container: due to the liquid incompressibility hypothesis an increase in the bubble radius can only occur simultaneously with an increase in the structure radius. However Figure 5.1 shows the comparison between bubble dynamics predicted with the confined Keller-Miksis equation in a rigid $R_s = 1$ m spherical container and predicted using the confined Rayleigh-Plesset equation for several container rigidities. The material parameters used are summarised in Table 5.2. The confined Rayleigh-Plesset equation in a spherical elastic container is given by (5.18). For more details on the derivation of this model please refer to Fourest et al. (2014).

$$\begin{cases} R_b\ddot{R}_b + \frac{3}{2}\dot{R}_b{}^2 + \frac{P_s(t) - P_b(t)}{\rho} - 2\dot{R}_b{}^2\left(\frac{R_b}{R_s}\right) - \ddot{R}_b\left(\frac{R_b^2}{R_s}\right) + \frac{1}{2}\dot{R}_b{}^2\left(\frac{R_b}{R_s}\right)^4 = 0 \\ P_s - P_{s_0} = (R_s - R_{s_0}).E.\left(\frac{(R_{s_0}+e)^3 - R_{s_0}^3}{R_{s_0}^3}\right)\left(\frac{2R_{s_0}^2}{2(1-2\nu)R_{s_0}^3 + (1+\nu)(R_{s_0}+e)^3}\right) \end{cases} \tag{5.18}$$

with E the Young Modulus, ν the Poisson ratio and e the shell thickness.

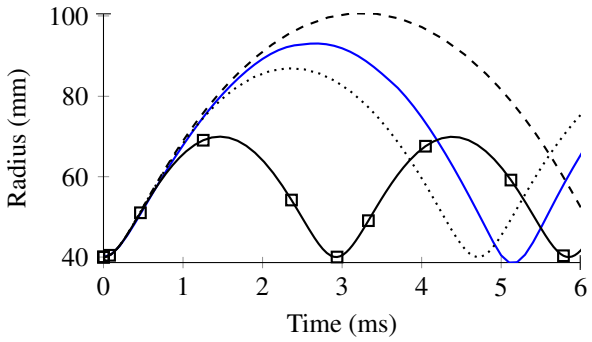

Figure 5.1 – Bubble radius predicted using the confined Keller-Miksis equation in a spherical rigid container (—) and predicted with the confined Rayleigh-Plesset equation in a 6 mm thick (- - -), 15 mm thick (·····) and 60 mm thick (⊸) $R_s = 1$ m steel container.

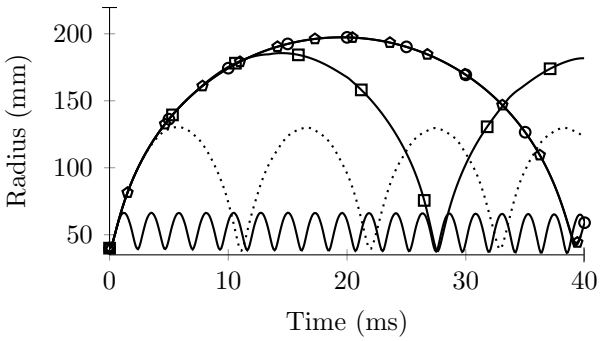

Figure 5.2 – Bubble radius predicted using the confined Keller-Miksis equation in several spherical rigid containers of internal radius R_s. $R_s = 0.5$ m (—), $R_s = 2$ m (·····), $R_s = 5$ m (⊸), $R_s = 50$ m (⊸) and $R_s = \infty$ (⊸).

The bubble predicted in the 6 mm thick steel spherical container using the confined Rayleigh-Plesset equation has larger oscillations than those predicted in the rigid container, however the

bubbles in the 15 mm and 60 mm thick steel spherical containers have lower oscillations than in the rigid container. This is obviously not possible but it was already known that for containers with high rigidity the confined Rayleigh-Plesset equation could lead to non-physical results. By taking the liquid compressibility into account the confined Keller-Miksis equation solves this problem.

Figure 5.2 shows the bubble radius versus time for several internal radius R_s of the spherical rigid container. As expected larger containers lead to larger bubble radius. For very large containers the predicted bubble dynamics is equivalent to the one predicted using the unconfined Keller-Miksis equation. Moreover contrary to the unconfined Keller-Miksis, the confined equation does not present a damping of the bubble amplitude at each rebound due to the liquid wave emitted outward. In this model this wave is eventually reflected by the structure and continues to interact with the bubble. The Keller-Miksis model is based on the hypothesis that the veloc-

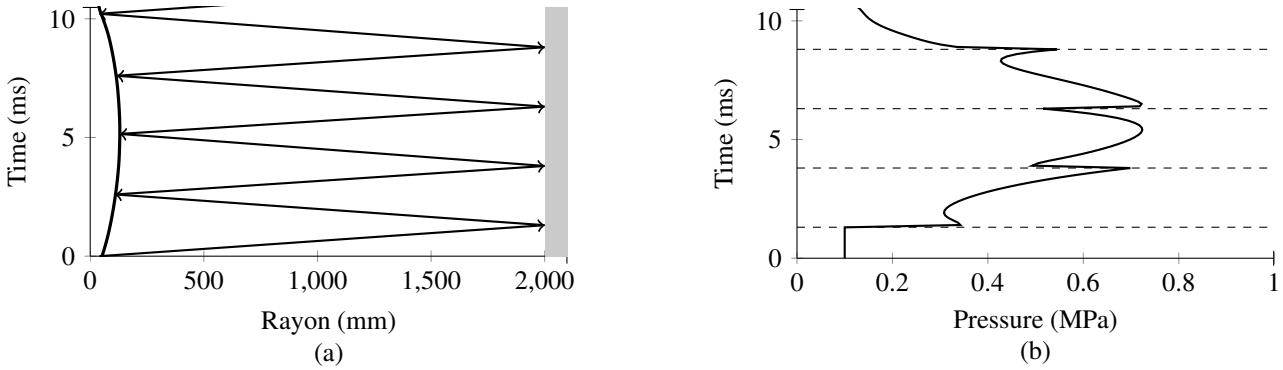

Figure 5.3 – Propagation of the initial liquid velocity potential within the liquid (a) and correspondence with change in the pressure onto the structure (b) for a bubble in a $R_s = 2$ m rigid container.

ity potential propagates at the speed of sound. Figure 5.3 shows an example of the behaviour of the model for a rigid wall at $R_s = 2$ m of the bubble centre. The bubble radius reaches a maximal value of approximately 150 mm. Figure 5.3-(a) presents the propagation of the initial wave and its subsequent reflections on the structure and bubble walls. It can be noted that when this wave interacts with the structure surface it corresponds to changes in the pressure at this interface (see Figure 5.3-(b)). As expected, the interaction between the structure and the bubble growth is effectively caught through the velocity potential propagation.

5.3.2 Finite element modelling

Due to the geometry of the problem, axi-symmetric bi-dimensional simulations are performed. The mesh domain is reduced to a quarter with symmetry conditions being applied in the x and y directions. Arbitrary Lagrangian Eulerian (ALE) grid deformation is used for the water medium in order to keep a regular mesh during the calculation and avoid excessive cell deformations collapse around the bubble interface. ALE finite element method allows to control the mesh grid independently from the material grid (Souli et al., 2000). The bubble interface and the structure nodes displacements are defined in a Lagrangian manner. The sphericity of the bubble interface (free surface) is imposed in these simulations to avoid unstable phenomena to occur during collapse due to a small deviation in the mesh, and hence permit the study of several

bubble periods. The interaction between the structure and the liquid medium is established through conform meshing (common nodes). Figure 5.4 describes the considered problem.

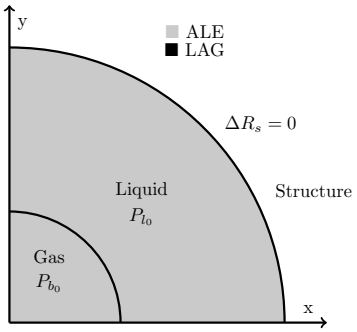

Figure 5.4 – Sketch of the considered problem for simulations of bubble dynamics inside a rigid container.

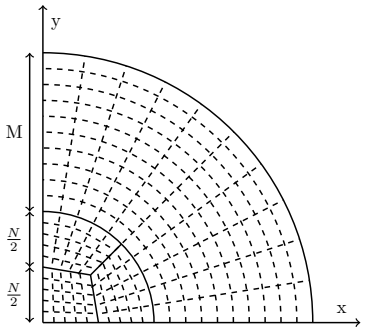

Figure 5.5 – Mesh principle for simulations of bubble dynamics inside a rigid container.

Material laws used in confined bubble simulations

It is assumed that no thermal effects affect bubble dynamics in water at ambient temperature (Brennen, 1995). Hence the behaviour of the liquid is assumed to be isothermal. The equation of state used for the liquid is (5.19) with $c_l = 1500$ m.s^{-1}, $P_{l_0} = 0.1$ MPa and $\rho_{l_0} = 1000$ kg.m^{-3}. The gas follows the ideal gas law (5.4) with $\gamma = 1.4$ for air as a diatomic gas.

$$P_l = P_{l_0} + (\rho_l - \rho_{l_0})c_l^2 \tag{5.19}$$

Convergence study for the rigid container case

The finite element models are made of 4 nodes axi-symetric elements. Figure 5.5 shows the parameters used in the description of the mesh. N is the number of orthoradial elements and M the number of liquid elements in the radial direction. Figure 5.6 shows the bubble radius versus time curves for different mesh refinements. This study is performed for $R_s = 1$ m.

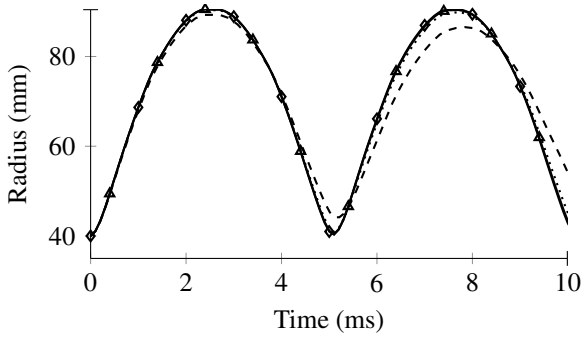

Figure 5.6 – Bubble radius vs time results obtained with different mesh refinements NxM: 10x159 (—), 24x318(—□—), 56x640 (—△—), 110x1280 (—◇—).

A satisfying convergence is obtained for the 56x640 mesh refinement (<1% of relative error with the 110x1280). For the following analyses N=56 will be used. Table 5.1 presents the numerical cost of each simulation for 10 ms of simulated time.

Table 5.1 – Model features and calculation performances on Intel® Ivy-Bridge E5-2667v2 processors clocked at 3.3 GHz.

model	Elements	Nodes	Δt_0	CPU time
10x158	1665	1840	$6.41{\cdot}10^{-4}$ ms	28s
24x318	8088	8444	$2.53{\cdot}10^{-4}$ ms	2min31s
56x636	38024	38746	$1.03{\cdot}10^{-4}$ ms	25min
110x1280	149985	151432	$5.16{\cdot}10^{-5}$ ms	11h40min

5.3.3 Comparison of the confined Keller-Miksis and finite element simulations for bubbles in rigid containers

The results obtained with the confined Keller-Miksis model in a rigid container are compared to those obtained by finite element simulations. Figure 5.7 compares the radius versus time evolution for a bubble in three containers of internal radius $R_s = 0.5$ m, 1 m and 2 m. Figure 5.8 compares the pressure at the bubble and structure surfaces calculated with the confined Keller-Miksis and finite element model for a $R_s = 1$ m rigid container. The results obtained in all cases are in a fairly good agreement. The radii predicted with the finite element models were found to be slightly inferior in terms of amplitude and period duration to the one predicted with the confined Keller-Miksis model. The same tendency is observed for the predicted pressure, in particular the pressure in the bubble obtained with the finite element model during the first rebound is inferior to prediction of the analytical model. It is attributed to the fact that the analytical model does not consider hydrodynamic decay (compression and tension wave propagate at the same velocity). Nevertheless the two models are in very good agreement which validates the proposed confined Keller-Miksis model in a rigid spherical container.

5.4 Application to an elastic wall case

Now that the confined Keller-Miksis model has been validated for bubbles in a rigid container, the case of bubbles in an elastic container is examined. Instead of eq. (5.18) that models the static response of a spherical shell submitted to uniform internal pressure, a dynamic response model is used for the spherical structure. This is done to ensure the continuity of the function R_s that is obtained by numerical integration. For reasons of simplification the internal radius of the sphere is used as the mean surface of the shell. It is justified since the shell thickness is largely inferior to the shell internal radius.

In the case of a spherical shell the curvature is constant and displacement only occurs in the radial direction. The strains are calculated using Reissner's polynomial approximation (Reissner, 1944) (5.20).

$$\varepsilon_{\theta\theta} = \varepsilon_{1_{\theta\theta}} + \varepsilon_{2_{\theta\theta}}(r - R_s) + \varepsilon_{3_{\theta\theta}}(r - R_s)^2 \tag{5.20}$$

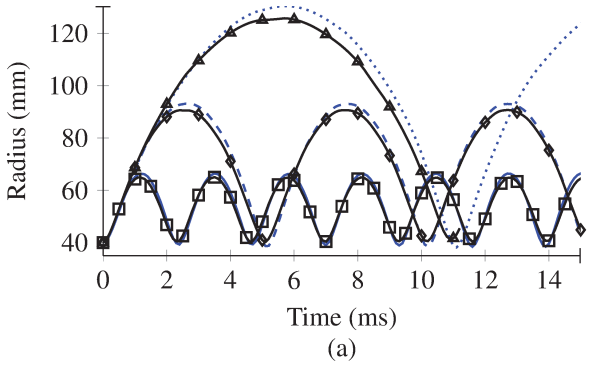

Figure 5.7 – Bubble radius predicted using the confined Keller-Miksis equation in a $R_s = 0.5$ m (——), $R_s = 1$ m (- - -) and $R_s = 2$ m (·····) rigid containers and obtained by ALE finite element simulations in $R_s = 0.5$ m (—□—), $R_s = 1$ m (—◆—) and $R_s = 2$ m (—▲—) spherical rigid containers.

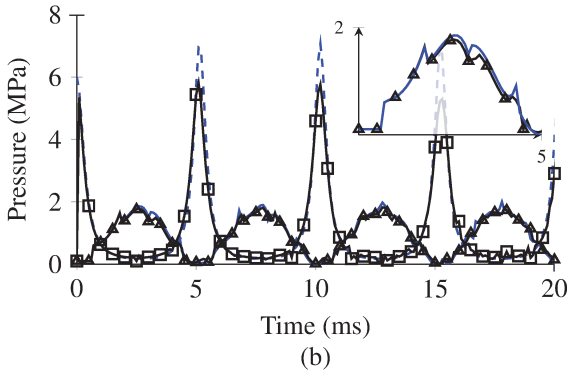

Figure 5.8 – Pressure at the bubble and structure interfaces predicted using Keller-Miksis equation (——) and (- - -) and obtained by ALE finite element bubble growth simulation (—□—) and (—▲—).

with $\varepsilon_{\theta\theta}$ the membrane coefficient, $\alpha_{\theta\theta}$ the bending coefficient and $\beta_{\theta\theta}$ the quadratic coefficient, given in the case of a spherical shell in (5.21),

$$\varepsilon_{1_{\theta\theta}} = \frac{R_s - R_{s_0}}{R_{s_0}} \quad ; \quad \varepsilon_{2_{\theta\theta}} = -\frac{R_s - R_{s_0}}{{R_{s_0}}^2} \quad ; \quad \varepsilon_{3_{\theta\theta}} = \frac{R_s - R_{s_0}}{{R_{s_0}}^3} \tag{5.21}$$

Using Hooke's law the following stresses are found in (5.22),

$$\sigma_{\theta\theta} = E\frac{1+\nu}{1-\nu^2}\varepsilon_{\theta\theta} = E\frac{1+\nu}{1-\nu^2}(R_s - R_{s_0})\left(\frac{1}{R_{s_0}} - \frac{(r-R_s)}{R_{s_0}^2} + \frac{(r-R_s)^2}{R_{s_0}^3}\right) \tag{5.22}$$

Then the membrane flux $N_{\theta\theta}$ can be calculated using (5.23):

$$N_{\theta\theta} = \frac{E(1+\nu)}{1-\nu^2}\left(e\varepsilon_{1_{\theta\theta}} + \frac{e^3}{12}\left(\varepsilon_{3_{\theta\theta}} + \frac{\varepsilon_{2_{\theta\theta}}}{R_{s_0}}\right)\right) \tag{5.23}$$

Finally, using the equilibrium equation (5.24) it is possible to obtain the equation of motion of a spherical shell submitted to spatially uniform pressure (5.25) which permits to calculate $\dot{R}_s$ and R_s.

$$\frac{-2N_{\theta\theta}}{R_{s_0}} + P_s - P_{s_0} + \rho h\ddot{R}_s = 0 \tag{5.24}$$

$$-\rho_s e\ddot{R}_s + P_s - P_{s_0} - \frac{2E(1+\nu)}{1-\nu^2}\frac{(R_s - R_{s_0})}{R_{s_0}^2}\left(e + \frac{2e^3}{12R_{s_0}}\right) = 0 \tag{5.25}$$

The fluid and structure equations are coupled using (5.9) to calculate the term P_s in (5.25).

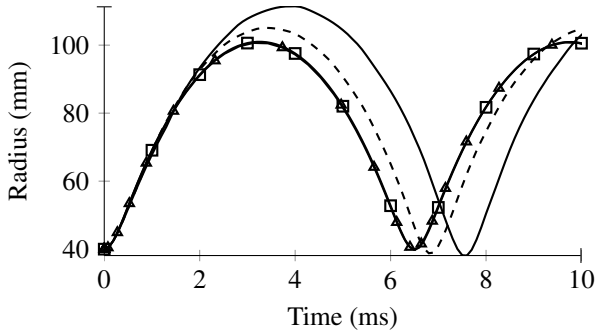

Figure 5.9 – Bubble radius vs. time in a $R_s = 1$ m 6 mm thick steel spherical container predicted with the confined Keller-Miksis equation with $c_l = 1500$ m.s^{-1} (—), $c_l = 2500$ m.s^{-1} (- - -), $c_l = 10000$ m.s^{-1} (—□—) and the confined Rayleigh-Plesset equation with $c_l = \infty$ (—△—).

5.4.1 Verification of the consistency of analytical models for elastic containers

The classic Keller-Miksis equation is equivalent to the Rayleigh-Plesset equation when the liquid speed of sound tends to infinity (Keller and Miksis, 1980). Therefore it will be first verified that when the speed of sound in the liquid is chosen high, both confined models predict the same bubble radius evolution. Figure 5.9 compares the bubble radius predicted in a 6 mm thick steel spherical container with the Keller-Miksis for several values of the sound speed to the radius predicted in the same container using the confined Rayleigh-Plesset equation. It can be observed that by increasing the sound speed in the liquid the confined Keller-Miksis converges to the confined Rayleigh-Plesset model. For a sound speed of $c_l = 10000$ m.s^{-1} the results obtained using both models are virtually identical.

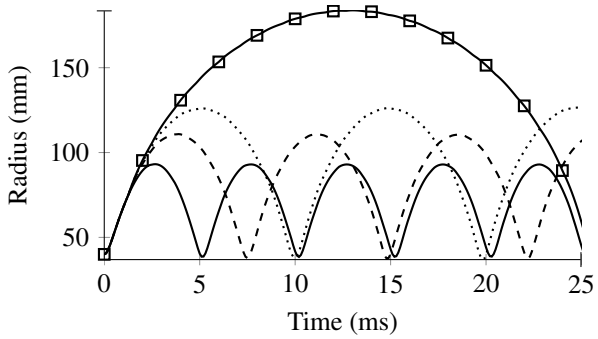

Figure 5.10 – Bubble radius vs. time predicted with the confined Keller-Miksis equation in $R_s = 1$ m rigid (——), 6 mm thick steel (- - -), aluminium (·····), PMMA (—□—) spherical containers.

The development of confined bubble dynamics models is carried out to take the interaction between the bubble and the structure into account. Figure 5.10 compares the predicted bubble dynamics in a rigid container and in several containers of different overall rigidity. The model

behaves in the expected way, the bubble amplitude and period increase while the overall rigidity of the container decreases.

Figure 5.11 shows an example of the behaviour of the model for a 6 mm thick steel wall at $R_s = 2$ m of the center of the bubble for one period of the bubble. Figure 5.11-(a) recalls the propagation of the initial wave and its subsequent reflections on the structure and bubble walls. Figure 5.11-(b) is a zoom of Figure 5.11-(a) at the deformable structure surface. It can be noted that the times at which the wave interacts with the structure surface correspond to changes in the pressure at this interface that can be seen in Figure 5.11-(c). The pressure observed in this case differs from the one in Figure 5.3-(b): there is a quick increase of the pressure at times when the initial wave interacts with the structure wall. However this increase is rapidly compensated by the structure deformation, hence no large discontinuities in the pressure response are observed in this case. As expected the pressure found at the surface in this elastic case is less than the one obtained for the same source in a rigid container in Figure 5.3-(b). It can also be noted that at the end of the period neither the structure wall position nor the pressure applied to it reach the initial value.

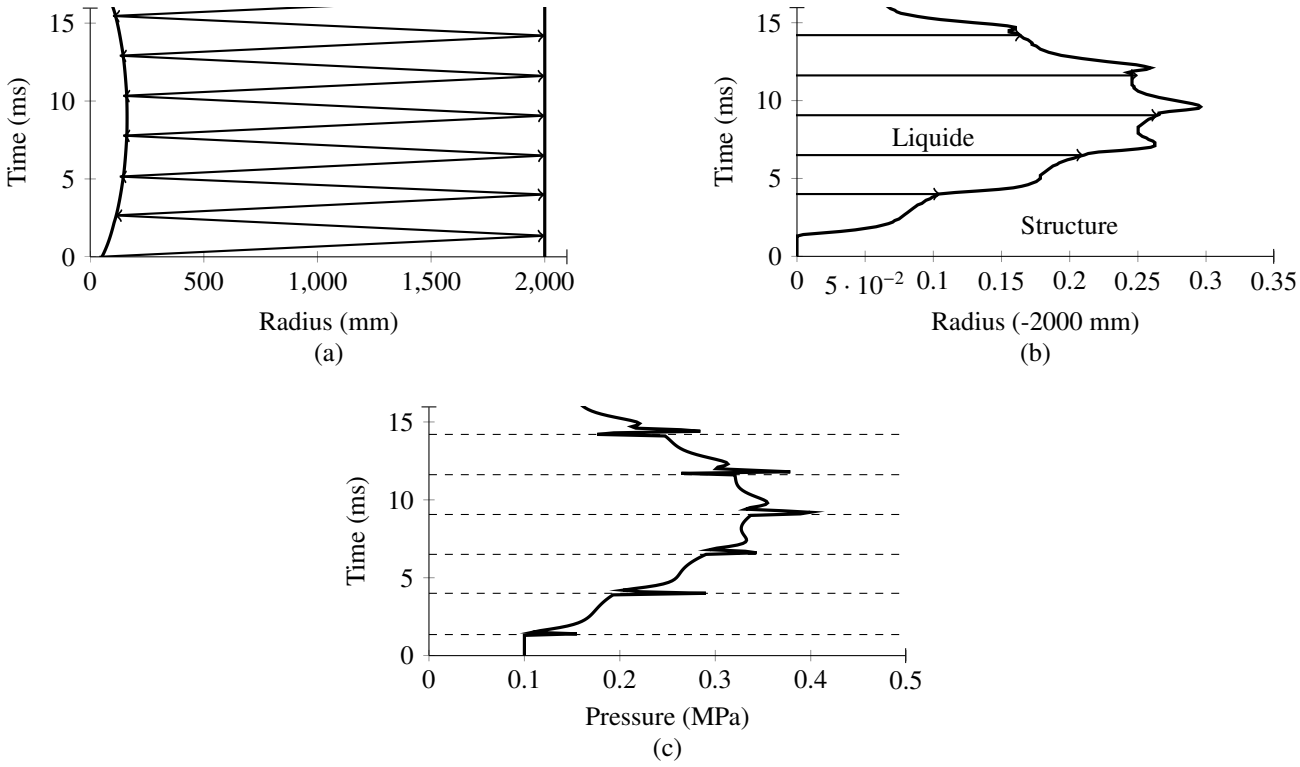

Figure 5.11 – Propagation of the initial liquid velocity potential within the liquid (a) and correspondence with change in the structure internal radius (b) and in the pressure at the structure wall (c) for a $R_s = 2$ m 6 mm thick steel container.

5.4.2 Comparison of the confined Keller-Miksis and finite element simulations for bubbles in elastic containers

Finite element modelling of the elastic case

The problem is the same as in Section 5.3.2 except that an external spherical structure has been added. The bubble interface (between liquid and air) and the structure nodes displacements are again defined Lagrangian and spherical. So there is no mixture between the air and water in the simulations. Figure 5.12 describes the considered problem.

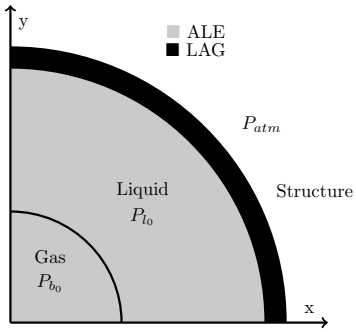

Figure 5.12 – Sketch of the considered problem for bubbles dynamics simulations in an elastic containers.

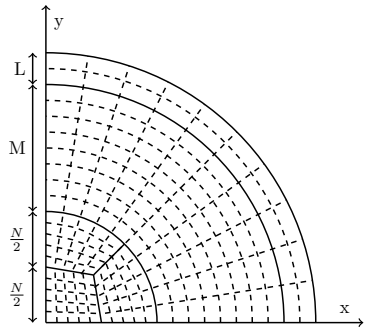

Figure 5.13 – Mesh principle for bubble dynamics simulations in an elastic containers.

Material laws used in confined bubble simulations

The liquid and gas are assumed to follow respective equations of state (5.19) and (5.4). The containers are modelled using a linear elastic law. Table 5.2 summarises the different material values used for the simulations.

Table 5.2 – Material numerical values used in the simulations.

Material	ρ_s (kg.mm^{-3})	E (MPa)	ν
Steel	$7.8{\cdot}.10^{-3}$	210000	0.3
Aluminium	$2.7{\cdot}10^{-3}$	70000	0.3
PMMA	$1.18{\cdot}10^{-3}$	2600	0.3

Convergence study for bubble dynamics in an elastic container

Again, the finite element models consist of 4 nodes axi-symetric elements. Figure 5.13 shows the parameters used in the description of the mesh. N is the number of orthoradial elements, M the number of liquid elements in the radial direction and L the number of container elements in the radial direction. A convergence study has been performed for a bubble in a $R_s = 1$ m 6 mm thick steel container. The conclusions reached are the same than in Section 5.3.2, therefore the details are not presented here. Satisfying convergence is obtained for the 56x640x4 mesh

refinement (<1% of relative error with the 110x1280x8). Therefore, the 56x640x4 models will be used for the following analyses.

Simulation results

The results obtained with the confined Keller-Miksis model in elastic containers are compared to those obtained with finite element simulations. Figure 5.14-(a) compares the radius versus time evolution for a bubble in three elastic containers of internal radius $R_s = 1$ m. Figure 5.14-(b) compares the predicted internal radius of the spherical structure in the same cases. The results obtained in all cases are in a fairly good agreement during the first period of bubble pulsation. The maximum difference in bubble dynamics is obtained for the bubble in the PMMA container (1% in bubble amplitude and 3.5% in bubble period). The same order of deviation is found for the structure response. Contrary to results that are usually obtained with the confined Rayleigh-Plesset equation the response of the structure (which has a smooth movement in Rayleigh-Plesset simulations) found using the confined Keller-Miksis equation oscillates in a similar manner than the one calculated using finite element simulations. Figure 5.14-(c) and (d) compares the pressure at the structure and bubble surfaces calculated using the confined Keller-Miksis and finite element model for $R_s = 1$ m elastic containers. The pressure predicted on the structure surface is in good agreement for both cases especially during the first bubble period. As in Figure 5.8 the bubble pressure predicted using the Keller-Miksis model is higher during the rebound than the one predicted using finite element simulations. This is due to the fact that lower bubble radii are reached during collapse in the Keller-Miksis model possibly due to small damping in the finite element simulations. Nevertheless the two models are in very good agreement which validates the proposed confined Keller-Miksis model in an elastic spherical container.

5.4.3 Evaluation of the improvement in prediction using the confined Keller-Miksis model

Now that the confined version of the Keller-Miksis equation for bubbles in an elastic container has been validated with respect to finite element simulations, the improvement obtained by using this equation instead of the confined Rayleigh-Plesset equation is examined. It has already been shown that for very rigid containers the confined Rayleigh-Plesset equation can lead to non-physical results. Therefore only one comparison on a not too rigid case will be presented hereafter to illustrate the obtained improvement in the bubble dynamics, structure movement and hydrodynamic load predictions using the confined Keller-Miksis model instead of the Rayleigh-Plesset equation. Figure 5.15 compares the bubble dynamics and pressure on the structure for a bubble in an elastic spherical container. The confined Rayleigh-Plesset equation predicts lower bubble radius which is logical since the liquid compressibility is expected to allow a larger bubble radius for the same pressure level. The Keller-Miksis model predicts a bubble radius closer to the results obtained by finite element simulations than the Rayleigh-Plesset equation (3% instead of 10% in amplitude and $< 1\%$ instead of 7% in period). Similarly the pressure and internal structure radius curves predicted using the Keller-Miksis equation have a very similar shape than those obtained by finite element simulations, which is not the case for Rayleigh-Plesset. The difference in the impulsion transmitted to the structure during the first oscillation is lower ($< 1\%$ instead of 3.5% with the confined Rayleigh-Plesset equation). This

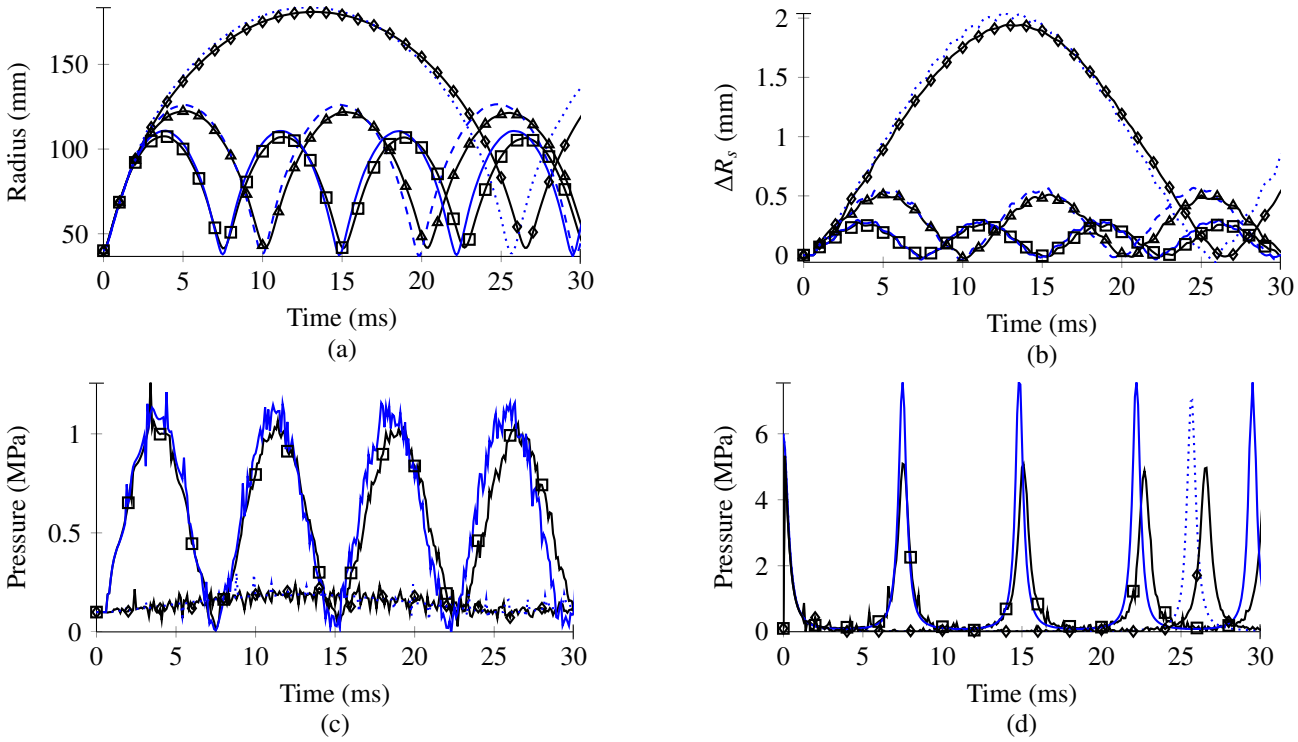

Figure 5.14 – Bubble radius (a), container internal radius variation (b), pressure at structure wall (c) and at the bubble interface (d) predicted using the confined Keller-Miksis equation in $R_s = 1$m steel (——), aluminium (- - -) and PMMA (·····) containers and obtained by ALE finite element simulations in steel (—□—), aluminium (—△—) and PMMA (—◇—) containers.

difference would of course increase if more compressible fluids ($c_l \approx 1300$ m.s^{-1} for kerosene (Aldred, 1972)) were examined. Therefore the confined Keller-Miksis equation proves to be closer to the finite element solution than the confined Rayleigh-Plesset equation.

5.5 Discussion

In the present study the Keller and Miksis (1980) equation has been used to predict the dynamics of gas bubbles in spherical containers. It is a logical use for this model, even if this equation was derived by considering an infinite domain of liquid and is mostly used in that case: it was initially developed to predict the response of a bubble submitted to an harmonic solicitation, typically a gas bubble in a vibrating vessel. In the present study the model is used for its initial application but instead of assuming the form of the harmonic pressure field in the liquid and deducing the converging velocity potential from this assumption, the converging velocity potential is found by considering the response of the structure. In the present study two cases have been studied: rigid and elastic containers on which the only load applied is derived from the bubble dynamics. However it is also possible to apply this equation for the initial purpose by considering a structure wall having an imposed harmonic movement. It would then require no assumption on the liquid pressure profile, but only on the frequency and amplitude of the structure vibrations.

In all calculations performed in the present study the liquid has been considered inviscid

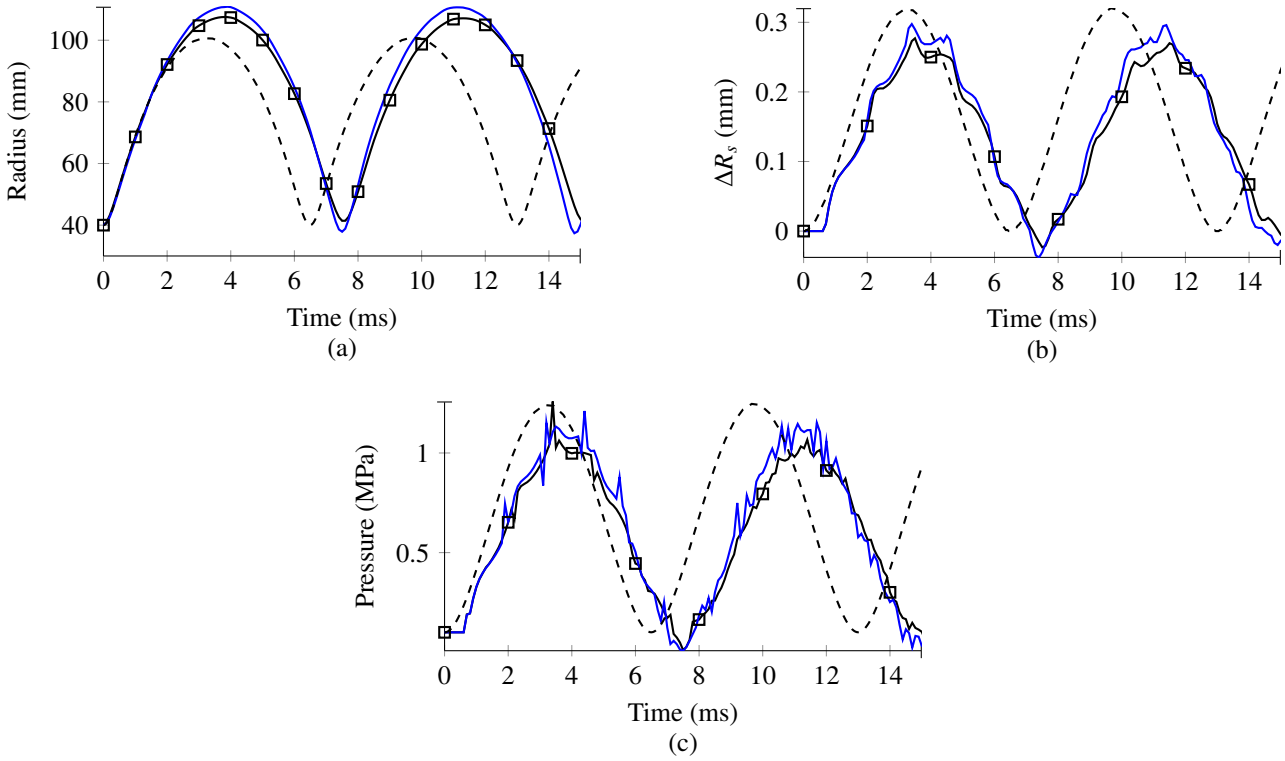

Figure 5.15 – Bubble radius (a), container internal radius variation (b) and pressure at structure wall (c) predicted in a R_s = 1m 6 mm thick steel container using the confined Keller-Miksis equation (——), the confined Rayleigh-Plesset equation (- - -) and obtained by ALE finite element simulations (—□—).

due to the large dimensions of the bubbles considered in the calculation. However the liquid viscosity and surface tension may be added by modifying the boundary condition at the bubble wall. Moreover the Keller-Miksis model uses an acoustic approximation and is expected to be most accurate when all liquid velocities are small compared to the velocity of sound in the liquid. However this approximation is found to be in good agreement with the numerical data. The predictions of this model might still be improved by changing this approximation to an extrapolation of the acoustic theory: the Kirkwood-Bethe hypothesis (summarised in Cole (1945)). It assumes that all quantities propagate at the speed $\dot{r}+c$ instead of c. This hypothesis is used in the Gilmore (1952) model in which it is found to be accurate for bubble wall velocities up to 2.2 times the sonic velocities for which the acoustic approximation seems unlikely to produce accurate results. Hence improvement in the bubble prediction for high growing rate bubbles may be obtained by using the Kirkwood-Bethe equation in a similar model than the one proposed in the present study.

5.6 Conclusion and outlooks

In the present study the classic Keller and Miksis (1980) equation that models the dynamics of a single gas bubble in an infinite domain of liquid assuming a constant liquid speed of sound has been used to take the confinement effects of a spherical container on the bubble dynamics into account. To this end the function g that represents the convergent part of the velocity

potential in the liquid has been used. A limit condition has been written in terms of velocity potential to link this function to the divergent potential that reaches the structure. This model has been developed for two cases of containers: rigid and elastic containers. In both cases the consistency of the analytical model has been assessed, and it has been compared to finite element simulations.

Concerning the consistency of the analytical model it has been verified that:

- contrary to the confined Rayleigh-Plesset model it does not predict non-physical results for high rigidity (or rigid) containers;
- the predicted bubble radius and period increase with the container size until it reaches the unconfined Keller-Miksis results for large containers;
- in an elastic container the confined Keller-Miksis model is equivalent to the confined Rayleigh-Plesset one for high sound speed (10000 $m.s^{-1}$);
- the predicted bubble radius and period increase while the overall rigidity of the container decreases.

In all studied cases a very good agreement has been found between the results obtained using the confined Keller-Miksis model and finite element simulations. The maximum difference in bubble dynamics is obtained for the bubble in the PMMA container (1% in bubble amplitude and 3.5% in bubble period). A good agreement in the pressure prediction is found, curves predicted with both methods have the same shape and variations on the pressure have very little effect on the impulse transmitted to the structure ($< 1\%$). These good agreements validate the development of the confined Keller-Miksis equation. The Keller-Miksis model allows to obtain very similar results in a time that is largely inferior (a few minutes for 40 ms of simulations against approximately 1 hour using finite element simulations), this computation time saving would allow the use the Keller-Miksis model in an optimisation process during the sizing of structure with respect to HRAM.

Finally the improvement in bubble dynamics and hydrodynamic load predictions achieved by developing this equation has been examined by comparing the confined Keller-Miksis to the confined Rayleigh-Plesset equation and to results obtained by finite element simulations. The Keller-Miksis model predicts a bubble radius closer to the results obtained with finite element simulations that the Rayleigh-Plesset one (3% instead of 10% in amplitude and $< 1\%$ instead of 7% in period). Moreover the difference in the impulsion on the structure during the first oscillation has been found to be lower ($< 1\%$ instead of 3.5%). However the obtained predictions with the confined Rayleigh-Plesset are reasonably accurate in this case. Moreover in terms of structure sizing the Rayleigh-Plesset is conservative since its predicts a slightly higher pressure and structure movement. Further studies have to be carried out to determine the domain of validity of the confined Rayleigh-Plesset equation with respect to the confined Keller-Miksis solution.

Acknowledgement

This study has been carried out as part of the PhD thesis of the main author. The authors would like to thank the French Ministry of Defence and DGA (French Armament Procurement Directorate), for their financial support. The authors would also like to thank Dr Daniel Fuster

from the CNRS/UPMC Université Paris 06, UMR 7190 for his very valuable suggestions on the method to solve this problem.

General conclusion and outlooks

The context of the thesis consists in improving the knowledge and the predictions of hydrodynamic loads applied on liquid tanks during ballistic impacts (Hydrodynamic Ram) to improve the survivability of aircraft structures. The most advanced numerical models still cannot fully and accurately simulate the whole phenomenon. Plus these models are too expensive to be used for optimisation or even design purpose during the tank development stage (Tilhac et al., 2012; Deletombe et al., 2012). The proposed study consists in developing an analytical model capable of simulating the expansion and collapse of the gas bubble generated by the projectile entry and tumbling, and to use this model to determine the parameters that affect the predictions of hydrodynamic loads during hydrodynamic ram events.

To achieve this objective, a modified version of the Rayleigh-Plesset equation - that describes the dynamics of a single gas bubble in an infinite domain of liquid - has been proposed to take confinement effect of the container on the bubble dynamics into account. This model has been applied to two hydrodynamic ram tests, one in a small container and one in a large pool, by calibrating a confinement parameter that is related to the structure rigidity a good agreement has been obtained with the bubble dynamics observed experimentally. Then the influence of the gas behaviour on the bubble dynamics has been studied using this model by comparing the bubble dynamics, liquid kinetic energy and structure wall pressure between simulations with and without gas. It was concluded that the influence of the gas on the bubble dynamics and on the hydrodynamic loads is negligible up to the collapse of the bubble. Plus the results obtained tend to confirm that the confined version of the Rayleigh-Plesset model is adapted to the study of hydrodynamic ram events, however there are some limitations: in particular the confinement parameter that is related to the rigidity of the container needs to be calibrated.

Then the capability of linear elastic analytical models to estimate the numerical value of the confinement parameter in the modified Rayleigh-Plesset equation is evaluated. However the studied container in the test is a multi-material orthorhombic container. In order to use a plate model of the container, the relationship between the structure deformations and the pressure applied on its walls has been rewritten to consider the variation of the internal volume of the container. In this way, various geometries of container can be studied under the assumption that the pressure applied on the container walls is homogeneous. Finally the confinement parameter values and the bubble dynamics predicted when the confinement parameter is calibrated and evaluated with plate formulae have been compared. The differences in terms of bubble prediction using both methods are relatively small (11% in amplitude and 33% in collapse time) knowing that the confinement parameter has been calibrated to have the same bubble amplitude than in the test and that the coefficient that is evaluated analytically gives the same period. This good agreement tends to confirm that a 1D analytical model is interesting to study this possibly highly directional phenomenon at first order.

However the proposed Rayleigh-Plesset model has some limitations due to the hypothesis on which it is based. In particular, the liquid compressibility may influence the confined bubble dynamics and the predicted hydrodynamic loads. To determine the extend to which this factor affects the confined bubble dynamics the proposed confined Rayleigh-Plesset equation is compared to explicit finite element simulations of confined bubbles growth. The finite element model differs from the confined Rayleigh-Plesset model by two aspects: the liquid compressibility and the dynamical response of the structure (inertia effect). First to determine the effect of the structure inertia, the Rayleigh-Plesset model is compared to quasi-incompressible simulations (high speed of sound) to obtain the effect of inertia alone. It has been found that in the domain of study, the structure inertia has very little influence on the bubble dynamics and hence can be neglected. To study the effect of the liquid compressibility, equivalent overpressure initial conditions have been chosen to have a domain of liquid at rest in the beginning of the bubble growth. A difference in the bubble dynamics and in the hydrodynamic loads predicted by both methods due to the liquid compressibility is found.

So, to take the effect of liquid compressibility on the confined bubble dynamics into account an analytical confined bubble dynamics model is developed. This model is based on the Keller-Miksis model that describes the dynamics of a gas bubble in an infinite domain of compressible liquid. This model has been first developed for the case of a spherical rigid container, and its consistency with previous results has been verified. Then the bubble radius and the pressure at the structure and bubble walls are compared to results obtained by finite element simulations. Once the model has been validated in the case of a rigid container it has been developed for an elastic spherical container. For this a dynamic formulation of the container response based on Reissner's polynomial approximation is used. The consistency of this model is verified and it is compared with finite element simulations. Once the model is validated for an elastic spherical container, the bubble radii, structure wall movement and pressure at the structure wall predicted using the confined Rayleigh-Plesset and Keller-Miksis models are compared. An improvement in the predictions has been found in the predictions using the later one.

To assess this thesis work, a critical analysis of the proposed models, with respect to existing models is done. The following observations are done in comparison to advanced finite element or SPH simulations (Varas et al., 2009b, 2012a,b; Artero-Guerrero et al., 2013; Sareen and Smith, 1996) since it is the only methods described in the state of the art that have the ability to predict parts of this phenomenon with accuracy. In this thesis work two analytical models have been proposed to describe the dynamics of gas bubbles created by ballistic impacts in liquid-filled containers. Unlike the model proposed by Lee et al. (1997a), the shape of the cavity is assumed to be spherical and does not depend on the motion of the projectile that generates it, but only on the initial kinetic energy of the projectile. Considering a spherical cavity has several advantages. It permits to solve numerically a 1D problem which is computationally cost efficient. Plus, the analysis is conservative since the case of a spherical bubble is related to the occurrence of tumbling of the projectile for which Bless et al. (1976) recorded more intense pressure. This seems to be confirmed by the results in Fourest et al. (2015c) where the predicted bubble in the container has the same collapse time but has larger amplitude than the one observed experimentally. So the unidimensional character of the model is an important advantage because the tumbling of high velocity projectiles is a complex phenomenon for which there is no analytical model available especially for projectiles that cannot be considered rigid (see Deletombe et al. (2013)). The phenomenology of the tumbling of a rigid projectile has been simulated by Sareen and Smith (1996) using finite element simulations but the projectile

motion has not been compared to experimental data.

However the proposed analytical model has some limitations compared to other existing ones. It is not capable of simulating the propagation of the initial shock and the wave emitted at the final collapse of the bubble. Plus the unidimensional character of the model induces some limitations for its application. In particular the container is assumed to be spherical. It has been shown that considering a spherical container, that has the same overall rigidity as a container of another geometry, permits to have an interesting approximation of the bubble dynamics created during hydrodynamic ram events. However only an elastic response of the container has been modelled. So, no non-linearity is considered in the structure response because this model does not consider the accumulation of non-linearity (plasticity, damages, rupture ...) as it is observed experimentally (Deletombe et al., 2013; Varas et al., 2009a; Lecysyn et al., 2010). The non-linear behaviour of the spherical container may be analytically taken into account but it would only be relevant for the analysis of impacts in spherical containers. In fact, the developed models apply to an intermediary case between two extreme cases. The case of an underwater explosion inside a container, with very high pressure during a very small time, in which the behaviour of the container can be described using analytical models for shell fragmentation (Mott, 1947; Grady, 2006). And the case of a gas bubble with a pressure relatively small with respect to the yield stress of the material, and quasi-static pressure evolution, in which the linear theory of wave propagation apply. Another limitation is that the model is not fitted for the predictive analysis of bubble dynamics where there is a free surface like for the impact in the pool in Deletombe et al. (2013). In this case a very good agreement has been found for the bubble dynamics using the confined Rayleigh-Plesset model by calibrating the response. However no solution has been proposed to evaluate analytically the confinement parameter in such a case with to the presence of a free surface. So this model cannot be used to study impacts in a partially filled container. However Varas et al. (2009a) recorded greater pressures for fully filled cases than for partially filled ones, which suggests that studying a 100% filled container is a conservative approach.

Due to the lack of experimental validation and to some limitations discussed before it is difficult, at this stage of the development, to use the Rayleigh-Plesset model for the sizing of structures. However this model can give an interesting approximation of the hydrodynamic loads applied to the container during the cavitation stage. Plus, the proposed Keller-Miksis model fixes some of the issues of the Rayleigh-Plesset model by considering wave propagation effects in the liquid, which permits for instance to study several bubble oscillations if no bubble fission is considered. Plus, beyond the development of the models, the thesis work had permitted to gain more insight on the hydrodynamic ram phenomenon, by better knowing the influence of the gas pressure and liquid compressibility on the hydrodynamics loads for instance, or on the pressure field in the liquid on simplified cases. This is a great improvement because, as discussed in the state of the art description there were no analytical models developed for the cavity stage in a container at the beginning of this research work.

Concerning the outlooks of this work, several points can be mentioned:

- First, now that a confined analytical bubble model has been developed for a bubble in a compressible liquid, it would be very valuable to investigate the domain of validity of the Rayleigh-Plesset model versus the Keller-Miksis one,

- Then, an experimental validation of the proposed models would be an important step to

increase the confidence in these models, towards their use for the sizing of structures. The Appendix C presents the first work done in this direction during the thesis,

- As one of the important limitations of the model is the use of a spherical structure, the dynamics of spherical bubble inside non-spherical containers should be studied to relate the modification in the bubble dynamics to the container shape,
- And also, the coupling of these models with finite element models for the structure, in the same manner than done in (Fourest et al., 2015c) using analytical plate formulae, might be used to deal with the limitations of the spherical elastic structure model.

Appendix A

Study of the capabilities of an ALE bi-material fluid simulation for solving cavity expansion and collapse during an Hydrodynamic Ram event

During the thesis a preliminary study has been done on the capacity of ALE bi-material fluid simulation to solve cavity expansion and collapse during an Hydrodynamic Ram event. The aim of this feasibility study was to determine whether an ALE solver using bi-material fluid permits a qualitative simulation of all the phases of the HRAM event, in particular the final collapse, that has not been simulated in the literature. It was chosen to study a relatively small speed impact to observe if in that case a collapse of the bubble could be observed. This work as been presented in T. Fourest, J. Dupas, E. Deletombe, J.-M. Laurens, and M. Arrigoni. Study of the capabilities of an ale bi-material fluid simulation for solving cavity expansion and collapse during an hydrodynamic ram event. In $13^{ème}$ *Colloque national en calcul des strutures*, May 2013.

In the field of aircraft safety, the vulnerability considerations are of utmost importance. The study of the effects identified as important factors in aircraft vulnerability implies solving the fluid/structure interaction problem which has been for the past decades, one major focus of research. In particular during ballistic impacts on fuel filled tanks, the phenomenon referred as Hydrodynamic Ram (HRAM) can occur.

During the impact of a projectile on a liquid filled tank, the kinetic energy of the projectile is transferred to the fluid in the form of thermal energy (tangential friction) and of kinetic energy (drag). This transfer gives rise to several phenomena. The HRAM is generally characterized by five phases (see Figure A.1) : the shock phase ($t = 0$ ms), the drag phase ($t = 0.2$ ms), the surface closure (its time of occurrence is not easily determined in this experiment), the cavity oscillation phase ($t = 2.5$ *to* 6.5 ms), and the potential exit phase (that does not appear in this experiment). Those phases could induce important loads on the tank structure with potentially destructive results.

The physics of the problem are quite complex when dealing with "non-trivial geometry" high speed deformable projectiles. It depends on many highly non-linear aspects (fluid, material, geometry, etc) that no analytical model or expert predictions can anticipate. Thus, the use of reliable numerical simulations appears necessary to correctly take this threat into account at

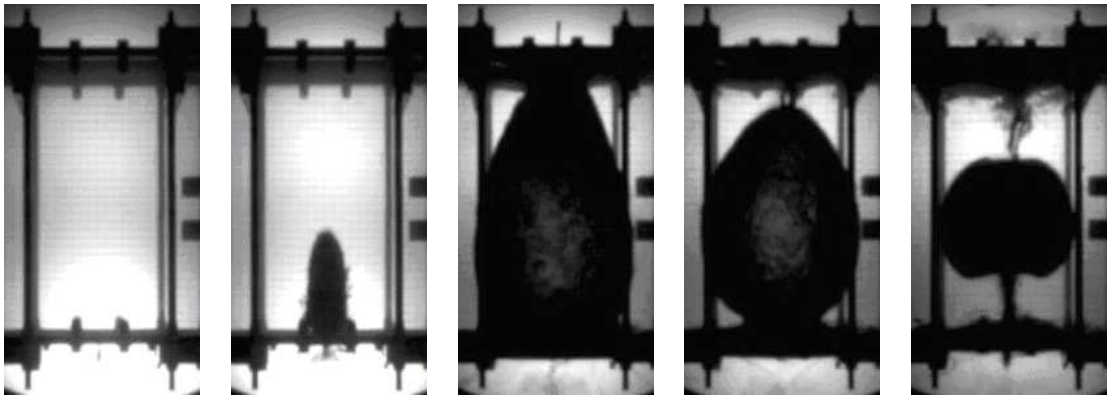

t_0	t_0+ 0.2 ms	t_0+ 2.5 ms	t_0+ 4.5 ms	t_0+ 6.5 ms

Figure A.1 – ONERA ballistic test of 7.62 mm ammunition at 850 $m.s^{-1}$ on a generic AIRBUS-Group Innovation tank (Deletombe et al., 2011).

the design stage.

A.1 State of the art of HRAM modelling

In the studies carried out at ONERA, the numerical simulation of the cavity oscillations (growth and collapse) is of particular interest. The aim is to demonstrate that the ability to qualitatively and quantitatively simulate the oscillations of the cavity during HRAM events is necessary to determine the structural loads in general cases of ballistic impact on liquid filled structures. This part summarises the state of the art of the HRAM modelling, presented in the open literature.

The first numerical studies of the complete phenomenon (projectile, liquid and gas phase and structure) were conducted using Lagrangian explicit finite elements in the seventies Kimsey (1980). These studies focused on the simulation of the propagation of the shock wave and the drag phase. This was achieved by deleting fluid elements that exceed a maximum deformation criterion. It clearly shows that this method did not permit to accurately represent the cavity growth and collapse due to the erosion of fluid elements and to the simple equation of states used for the fluid.

Improvements of this method were proposed by using classical Lagrangian explicit finite elements in Deletombe and Malherbe (1998); Deletombe et al. (2003). In these studies, the fluid elements were not discarded but were supposed to flow smoothly around the projectile. Unfortunately, the simulated time was very short due to the fluid mesh deformation which greatly limited simulation versus experimental comparisons.

More recently, new numerical methods were used to try to simulate the hydrodynamic ram phenomenon. The main studies in this area have been carried out by Varas et al. (2009b, 2012b,a); Artero-Guerrero et al. (2013). They presented results in which they demonstrated the capabilities of a commercial explicit finite element software (LS-Dyna) to simulate the shock phase, drag phase and the beginning of the cavity expansion phase generated by the impact of an indeformable sphere without tumbling, in an aluminium water filled tank. These different phases involve different time steps are actually minimized by the smallest one. To deal with the very large amount of deformation in the fluid during HRAM events, they used

both an Coupled Euler Lagrange (CEL) solver with "bi-material" fluid and a mesh free Smooth Particles Hydrodynamics (SPH) approach. For the CEL simulation, they used an Eulerian mesh composed of two zones, the first one full of water and the second empty (air is not modelled in the simulation); multi-material elements were used to allow the water to fill the void elements. Both formulations appear to be able to qualitatively simulate the shock phase, the drag phase and the beginning of the cavity growth phase. Nevertheless they concluded that the CEL solver is more efficient than the SPH method to simulate the phenomenon in terms of computation time.

In the open literature no numerical simulations of HRAM events are performed up to the time of cavity closure, and the following evolution of the cavity bubble has still not be approached.

A.2 Importance of the cavitation phase simulation

The cavitation phase is the more complex phase and the least understood of the phases that occur during the HRAM phenomenon. Generally, during the water entry of a projectile, the wake created by the drag of the projectile separate from the surface, either by a surface seal or by a deep seal (closing that occurs under the surface of the fluid) as could be seen in Shi and Itoh (2009). In both cases a cavity bubble will be created. This cavity may continue to expand if the momentum associated with the velocity field is sufficiently high to separate the flow from the projectile and to continue to expand the cavity. Anyway the cavity will eventually collapse.

In his experiments, Disimile et al. (2009) found that greater pressures would occur either during the drag phase or during the cavitation phase depending on the projectile's material (mass). Deletombe et al. (2011) performed the same type of pressure measurements for 7.62 mm bullet impacts on water filled tanks; he observed greater pressure during the drag phase than during the cavitation phase but during a shorter time period. He concluded that none of those phases could be neglected in the dimensioning of structure because they could both carry a significant amount of energy. The energy partition between the drag phase and cavitation growth also depends on the shape of the projectile, on the time of its eventual tumbling and on its material (mass) (Disimile et al., 2009).

A.3 Numerical simulation of the water entry of the projectile

The aim of this study is to determine the capability of a CEL solver with an Eulerian (air + water) fluid multi-material law to simulate the growth and collapse of cavities created by ballistic impacts on fluid filled tanks. Hence the correct simulation of the cavity closure is of key importance. During the closure of the cavity the phenomenon changes from the drag of a projectile in liquid to the evolution of a bubble of gas in the same liquid. The time of closure determines the amount of gas trapped in the bubble. The amount of gas is an important quantity, that influences the following behaviour of the bubble and the intensity of the pressure pulses emitted during the collapse of the gas bubble.

The complete simulation of the penetration of a high speed projectile in water filled tanks is a very complex task. In the present study great simplifications were made in order to concentrate on the cavity formation in the wake of the projectile and its closure. Firstly the water entry

of a projectile is considered here instead of impacts on water filled tanks. The confinement effect of the tank is also studied, without taking its penetration by the projectile into account (a pre-pierced tank is used). In addition, due to great numerical instabilities in a bi-phasic simulation of high speed projectiles impacts, observed by Thevenet (2009), and because the observation of cavity closure in high speed projectiles impacts on fluid filled tanks is not clear, impacts at lower speed are examined in this study. It is assumed that the process of closure of the cavity is the same regardless of the speed of the projectile and that only its content evolves with speed due to a drop in cavity pressure that leads to the vaporisation of the water during cavity growth. The classic water entry experiment at low speed compared to ballistic speeds (10.6 $m.s^{-1}$) presented by May (1952), has been identified to fullfil the above conditions. In experiments presented by Shi and Itoh (2009), the same type of cavity closing is observed for non-spherical projectiles at 350$m.s^{-1}$. And even though it is not clear, it seems that in the ballistic speed (850 $m.s^{-1}$) water entry of an ammunition experiment carried out at ONERA and presented in Charles et al. (2012), the cavity closure respects the same scenario.

A.4 Finite Element model

The simulation of the HRAM phenomenon has been performed using the EUROPLEXUS explicit research code, which has been developed by the French CEA and the EU CRC-ISPRA to accurately solve fast dynamic problems for coupled fluid/structure systems. It enables the use of multi-material fluids in CEL solvers.

A.4.1 Description

Due to the symmetry of the problem and in order to reduce calculation time, an axisymmetric calculation is used to simulate these experiments. A CEL solver is used. In Europlexus, the Eulerian part is defined as ALE without any grid motion. Thus the mesh consists of two Eulerian fluid zones, water and air and of a Lagrangian projectile and tank. The projectile is a sphere of 1 inch (≈12.5 cm) diameter. Each fluid material mesh is composed of two parts, a fine part for the interaction (1 mm side square elements) with the projectile, and a second part where the mesh becomes coarser at a further distance from the projectile. In May's simulation experiment, the fluid domain is assumed to be of infinite dimensions. Absorbing boundaries conditions have been used to prevent wave reflection that would disturb the simulation. As the upward jet in May's experiment proved to be dependent on gravity effects, the gravity acceleration is taken into account in our simulation.

A.4.2 Material laws

Fluid model

The Europlexus code permits the modelling of the behaviour of a liquid-gas mixture. This mixture is assumed to be homogeneous and includes two phases. Modelling the air material permits to take the depression in the wake of the projectile and the variation of the bubble pressure into account.

The behaviour of the gas is assumed to be perfect and the state variables are linked by the

following equation:

$$P_g = P_{g_0} \left(\frac{\rho_g}{\rho_{g_0}} \right)^{n_g} \tag{A.1}$$

Here P_{g0} and ρ_{g0} are the initial values of gas pressure and density, and n_g is the polytropic exponent. This exponent may be an arbitrary real number. The value $n_g = 1$ corresponds to an isothermal transformation while $n_g = \gamma_g$ corresponds to an adiabatic transformation.

The liquid is assumed to be compressible and isothermal. The equation of state is the following one:

$$P_l = P_{l_0} + (\rho_l - \rho_{l_0}) c_l^2 \tag{A.2}$$

Here P_{l_0} and ρ_{l_0} are the initial values, and c_l the sound speed is assumed constant. It is also possible to take the viscosity of the liquid μ_l into account with this bi-phasic law.

This law is used in ALE or Eulerian formulation; the mixture in the elements is modelled with a volume of fluid approach. The interface between the fluids is not defined, and the content of the elements is calculated using the mass fraction in gas x_l and liquid x_g.

$$x_l + x_g = 1 \tag{A.3}$$

Projectile and tank model

The projectile and tank are modelled using a simple linear elastic law as the projectile does not undergo notable damages at this speed of impact (10.6 m.s^{-1}). The Young modulus of steel is noted E its density ρ, and its Poisson coefficient ν.

Numerical values used

The table A.1 presents the numerical values used in the following simulations.

Table A.1 – Numerical values used for the water entry simulation

	ρ (kg.mm^{-3})	c_l (m.s^{-1})	E (MPa)	ν	P_0 (MPa)	μ_l (Pa.s)	n_g
Steel	$7.72 \cdot 10^{-3}$	-	$2.01 \cdot 10^5$	0.26	-	-	-
Water	$1 \cdot 10^{-3}$	1500	-	-	0.1	$1.006 \cdot 10^{-3}$	-
Air	$1 \cdot 10^{-6}$	-	-	-	0.1	-	$\gamma_g = 1.4$

A.4.3 Fluid structure interaction

In the Europlexus code it is possible to model fluid structure interactions using a formulation based on Lagrange multipliers. In this case, suitable fluid structure interaction constraints are written between the fluid and the structure velocities, and are imposed exactly (and costly) (in an implicit manner) by the Lagrange multipliers method.

A.5 Results

A.5.1 May's experiment (water entry 10.6 m.s^{-1})

Figures A.2 and 4 show the comparison between the experimental results and the simulation. The comparison is carried out at the same depth of penetration of the sphere in the liquid.

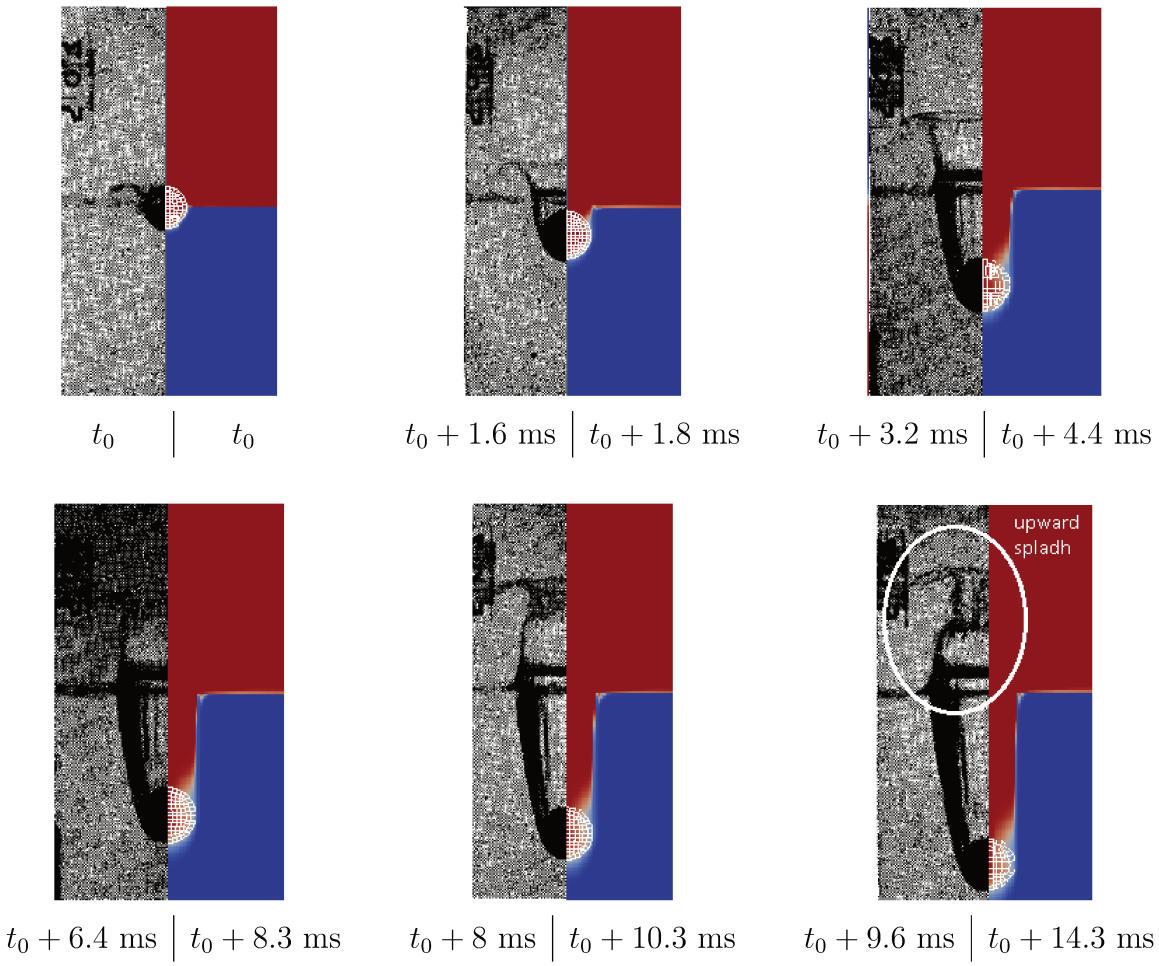

Figure A.2 – Comparison of the cavity shape between the experimental shape and mass fraction of gas calculated in the simulation (Blue : $x_g = 0$, Red: $x_g = 1$)

At first similarity could be observed in the drag created cavity shape between experiment and simulation, however the projectile is more decelerated in the simulation than in the experiment. It has been observed in this study that it is probably due to the fluid mesh size and that the drag of the projectile in the liquid could be better represented by decreasing this size. However a thinner mesh density would lead to very long calculation times particularly in three dimensional calculations, therefore the convergence in mesh size has not been examined in the present study.

In May's experiments the surface closure of the cavity created by the projectile comes from the upward splash that closes above the water level. In this simulation no upward splash appears. In the simulation no closure of the drag created cavity is observed and would lead to difficulties to perform a simulation of the ballistic speed water entry of the projectile. It is obvious that if the cavity does not close, no bubble would be properly created and the cavity growth and collapse phases would not occur in the simulation, and as explained previously

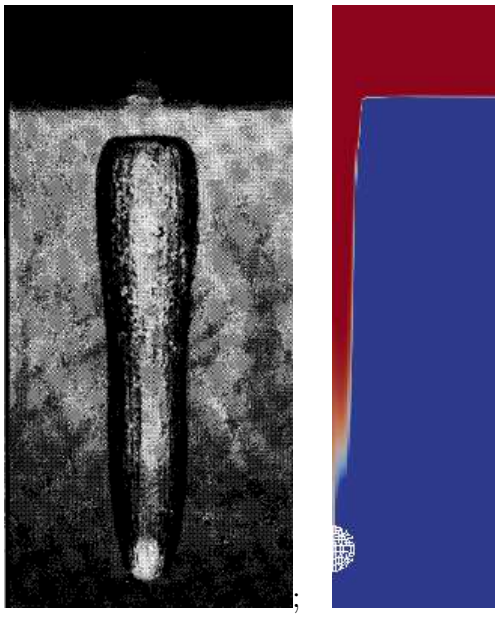

Figure A.3 – Photograph taken shortly after the cavity pulled away from the surface and the simulation result at the same depth of penetration of the sphere (Blue : $x_g = 0$, Red: $x_g = 1$)

those phases should be taken into account in the dimensioning of the structure.

A.5.2 Water entry with confinement tank

It is difficult to observe the process of the closure of the wake cavity during a ballistic impact as little information on this subject is available. The simulation aims to observe the influence of the presence of the tank walls on the cavity closure scenario. The speed of penetration is still 10.6 m.s^{-1}. Figure A.4 shows the cavity evolution observed in the simulation.

The confinement due to the tank influences the cavity closure scenario. The pressure wave reflected from the tank walls tends to compress the cavity in the wake of the projectile; this leads to a surface seal of the cavity that would occur around 20 ms after the impact where the opening is 4 mm large. In this simulation, complete closure is not reached, it has been verified with another simulation (not shown here) that this is due to the limit condition on the symmetry axis, and that this problem does not occur when using three dimension simulations.

A.6 Conclusion

The capabilities of an CEL bi-material solver to simulate high speed water entry have been examined in this study through the simulation of a classic experiment at slow speed (10.6 m.s^{-1}) compared to the ballistic speed in May's experiment. The simulation of this experiment has shown that the actual Coupled Euler Lagrange solver with bi-material fluid law, does not permit to numerically simulate the closing of the cavity created in the wake of a projectile in the case of a free surface and infinite medium, but it does permit the simulation of the closing of the wake cavity in the case of tank penetration due to its confinement. It would be interesting to determine the lack of any confinement effect in May's experiment, but the dimensions of the

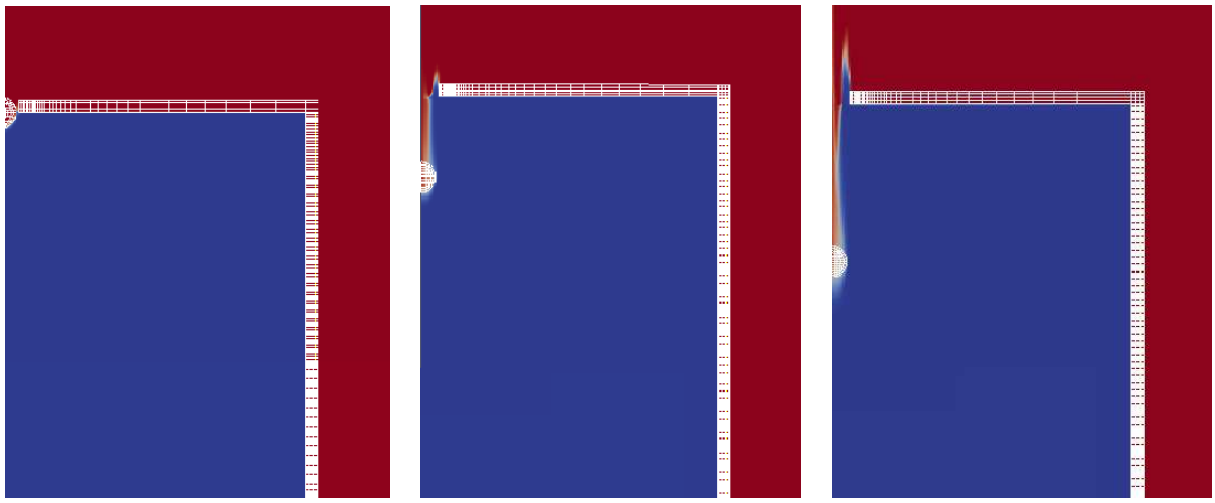

t_0 $t_0 + 15$ ms $t_0 + 67$ ms

Figure A.4 – Cavity evolution in a fluid filled tank penetration simulation (10.6 m.s^{-1}), mass fraction of gas calculated in the simulation (Blue : $x_g = 0$, Red: $x_g = 1$).

water container used for the experiment are not presented in his paper. It is also believed that even at a low speed impact (10 m.s^{-1}) the closure of the cavity might be governed by surface tension effects and not by gravity acceleration. A further study should be carried out to take this phenomenon into account for water entry.

This study demonstrates that the closure of wake cavity can be achieved for a liquid filled tank penetration simulation using an CEL bi-material solver. This is an important problem since correctly simulating the closing of the surface is of key importance to the study of the cavity oscillations phase created by ballistic impacts in water. However, difficulties have been observed in the simulation of high speed projectile penetration in water. The simulation stopped due to a rapid drop of the elemental time step to ensure the convergence of the pressure calculation in the wake of the projectile. It is believed that the computed drop in pressure in the wake cavity at this speed of impact is not physical and that it would be limited by the vaporisation of the fluid medium that is not taken into account in this simulation. New material laws which take the liquid vaporisation into account, should be developed to avoid these difficulties. Only then will it be possible to compare the time of cavity closing and the evolution of the cavitation bubble in the tank between simulation and experiment.

A.7 Acknowledgement

This study has been carried out as part of the PhD thesis of the main author. The authors would like to thank the French Ministery of Defense and DGA (French Armament Procurement Directorate), for their financial support in the thesis preparation.

Appendix B

Thermal effects in cavitation

In all the experimental tests presented in the literature, the impacts have been done on water-filled tank. It is generally assumed that studying a hydrodynamic ram in a water filled tank gives insight on this phenomenon in fuel-filled tank. However when it comes to the modelling of this phenomenon it is not clear if differences in the behaviour between water and fuel materials would modify the needed models. Among these differences the effect of possible thermal effects in fuel cavitation that does not occur in water cavitation are investigated in this appendix.

According to classical thermodynamics, the cavitation represents the crossing of the saturation curve from the liquid phase to the vapour phase. This happens when the pressure is lower than the vapour pressure, that is a function of the liquid temperature. Usually, only a small amount of heat is needed to generate a large volume of vapour, so the vaporisation is assumed isothermal. However, in certain case the heat transfer needed for this change of phase is large enough that a significant drop in the local temperature T_c of the liquid is achieved with respect to the temperature of the liquid far from the cavity T_∞. Then this local drop in the liquid temperature results in a drop in the vapour pressure, that facilitates the vaporisation process. The difference in temperature $T_\infty - T_c$ is called thermal delay in cavitation because generally this phenomenon results in longer time for the oscillation of the bubble. It also results according to Grazia De Giorgi et al. (2010) in larger bubble radius. It is clear that if this phenomenon influences the bubble dynamics, it also influences the hydrodynamic loads applied on the structure during this phenomenon. So it is important to determine if this phenomenon occurs for cavitation in aeronautic fuel materials in order to take it into account if it does.

B.1 Characteristics of usual aeronautic fuel materials

In this study two fuel materials used in aeronautics are investigated the Jet-A which is one of the most common fuel used in civilian aeronautic and an aviation gasoline which is more rarely used but has quite different characteristics. The behaviours of these liquids are compared to the ones of water for which there is no thermal effect in cavitation at $T = 273\,^\circ$K and of hydrogen at $T = 22\,^\circ$K for which there is large thermal effect (Brennen, 1995). A large number of numerical values of liquid thermal properties are summarized in Tables B.1 and B.2. The characteristics are extracted from the Handbook of Aviation Fuel Properties (1983);Shepherd et al. (1997, 2000); Woodrow and J.N. (1997) for the fuel properties, from Franc et al. (1995) for the water properties and from Jensen et al. (1980) for the hydrogen properties.

Table B.1 – Numerical values of liquids thermal properties at the studied temperature (Part 1).

Liquid	T (^oK)	ρ_l $(kg.m^{-3})$	ρ_v $(kg.m^{-3})$	ν_l $(mm^2.s^{-1})$	S $(N.m^{-1})$
Water	293	1000	$17.2.10^{-2}$	1.007	0.0728
Jet-A	293	810	$17.7.10^{-2}$	1.75	0.023
Av. Gas.	293	700	0.81	0.65	0.020
Hydrogen	22	69	2.01	0.017	2.10^{-3}

Table B.2 – Numerical values of liquids thermal properties at the studied temperature (Part 2).

Liquid	T (^oK)	L_{ev} $(kJ.kg^{-1})$	c_{pl} $(kJ.kg^{-1}.K^{-1})$	k_l $(W.m^{-1}.K^{-1})$
Water	293	2454.3	4.182	0.6
Jet-A	293	363	1.95	0.115
Av. Gas.	293	387	2.23	0.115
Hydrogen	22	447	11	0.12

B.2 Indicator of thermal effects

It is shown in this thesis that the dynamics of the cavity bubble created in the wake of a projectile can be modelled using a Rayleigh-Plesset type equation. The rigorous method to solve the bubble dynamics with thermal effects require to solve simultaneously the Rayleigh-Plesset equation and the equation of heat diffusion. However, in first approach it is common to rely on thermal effects indicators for bubbles dynamics analysis, that are related to the Rayleigh-Plesset equation (Brennen, 1995; Grazia De Giorgi et al., 2010). Two classic ones are used to estimate the importance of thermal effects on hydrodynamic ram bubble dynamics. The first one is ΔT, which is the temperature drop required for the vaporisation of a unit volume of vapour, and Σ, that is defined by Brennen (1995) in relation with a characteristic time at which thermal effects become as important as the other terms in the Rayleigh-Plesset equation, which means that the change of temperature during cavitation really influences the bubble dynamics.

$$\Delta T = \frac{\rho_v L_{ev}}{\rho_l C_{pl}} \tag{B.1}$$

$$\Sigma = \frac{\rho_v^2 L_{ev}^2}{\rho_l^{3/2} c_{pl}^{1/2}.T.k^{1/2}} \tag{B.2}$$

The numerical values of these indicators are presented in Table B.3 for the liquids studied in the present work.

Table B.3 – Numerical values of ΔT and Σ for the different liquids at the studied temperature.

Liquid	T (^oK)	ΔT (^oK)	Σ ($m.s^{3/2}$)
Water	293	0.01	3.84
Jet-A	293	0.004	0.41
Av. Gas.	293	0.36	1131
Hydrogen	22	1.18	$1.76.10^6$

The numerical values of ΔT and Σ for the Jet-A material are inferior to the ones of the water, so it indicates that there is no thermal effect for cavitation in the Jet-A material, which is the most common fuel material for aeronautic civilian applications. So the use of impacts in water-filled tanks as references to study the hydrodynamics ram phenomenon in fuel container seems justified from this viewpoint. However there may be some thermal effect for the cavitation in the Aviation Gasoline fuel for which the value is higher than for water but lower than for hydrogen. So one should be caution when using a model that does not take the thermal effects into account to model a ballistic impact in this liquid.

Appendix C

Confinement effects of a spherical container on the dynamic of a single bubble created by optic cavitation

A preliminary experimental study has been done on the transient dynamic of a single bubble created by laser induced cavitation in a spherical container filled with distilled water. To study this phenomenon, optic cavitation tests have been done in two containers. First in a large aquarium to obtain reference data, then in a small PMMA spherical container to observe confinement effects of the container on the bubble dynamics. The bubbles dynamics obtained in both cases are compared.

C.1 Experimental setup

To investigate the confinement effects of a spherical container on a single bubble dynamics, two set of experiments have been performed. First, optical cavitation tests have been done in a large aquarium in order to obtain reference results (without confinement effect). Then optical cavitation tests have been done in a small PMMA (Poly(methyl methacrylate)) spherical container in which confinement effects are expected.

This section contains information about the experimental setup used for bubble generation. It also explains how the measurements of bubble radius evolution created by laser breakdown is made. The sketch of the experimental devices used for the tests is shown in Figure C.1.

During these tests a laser pulse is emitted and focused in a container, either in a small PMMA sphere or in a large aquarium, both filled with clean distilled water.

C.1.1 Laser source

The tests have been performed using ENSTA-Bretagne/LBMS Q-switched Quanta-Ray Pro 350-10 modified Nd:Yag laser. Its wavelength is 532 nm, the maximal energy level is approximately 800 mJ and it delivers a pulse of approximately 9 ns at full width and half diameter (FWHD), the beam diameter is about 14 mm. To obtain a better pulse to pulse stability the laser is operated at maximal energy and its beam is attenuated by filters.

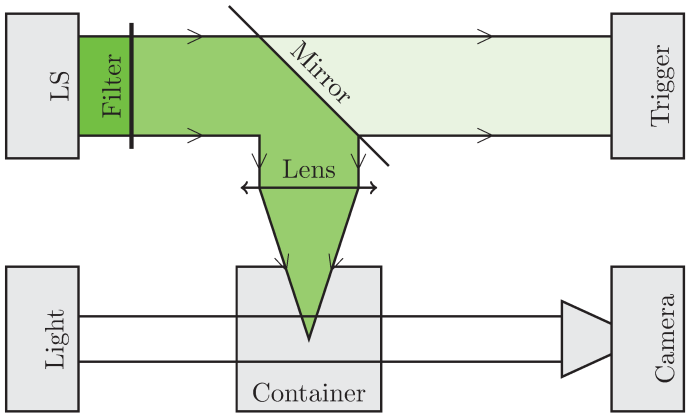

Figure C.1 – Sketch of the experimental setup for optic cavitation experiments

C.1.2 Optical system

The laser beam is reflected using a mirror: 99.5 % of the beam goes in direction of the lens and 0.5 % in direction of a photodiode used as trigger for the high speed camera. The beam is focussed at the center of the container using a 5 cm focal length lens. This length has been chosen as a compromise to avoid optical breakdown in the air and to prevent interaction between the beam and the container.

C.1.3 Containers description

Two different containers have been used in the experiments: an aquarium of 120x190x380 mm^3 with glass walls and a small PMMA spherical container. Description of the spherical container is given in Figure C.2. The spherical container was obtained by assembly of two half-spheres. The spherical container internal radius is $R_s = 6.55$ mm, its thickness $e = 3$ mm. A meplat was made on the spherical container to limit the optical deformations due to the container curvature. The meplat diameter is $D_m = 7$ mm. A hole of diameter $D_h = 7$ mm was drilled in the sphere in order to prevent the laser beam to interact with the sphere wall. The upper side of the sphere was closed with a glass plate.

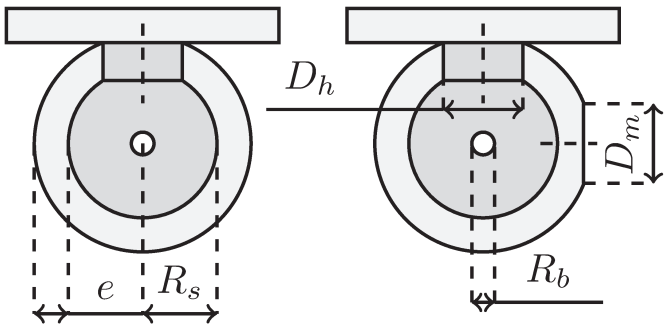

Figure C.2 – Sketch of the PMMA sphere used in the optic cavitation experiments.

C.1.4 High-speed camera and lighting system

A APX-Photron high-speed camera has been used to record the radius evolution of the bubbles in the containers. A 80 W LUMINUS CBM 360 high luminosity LED positioned behind the sphere was used to provide sufficient light to obtain an exposure time compatible with the use of the camera at 100 000 frames per second.

C.1.5 Millimetric grid

Preliminary to the tests, a transparent grid was positioned in the containers, in order to obtain the conversion between the image pixels and the distance in the container (see Figure C.3).

(a) (b)

Figure C.3 – Millimetric grid positioned in the plexiglass spherical container (a) and aquarium (b) before the tests.

C.2 Experimental results

When a high-power laser pulse is focused in a transparent media (such as water), the medium becomes opaque to the laser radiation as soon as a certain irradiance threshold is attained Noack and Vogel (1999). This phenomenon is due to the formation of a plasma, also known as laser breakdown in water. It is followed by a rapid heating of the material in the focal volume, that leads to an explosive expansion and the emission of a shock wave. This explosive expansion is in case of laser breakdown in water, a cavitation bubble. The dynamics of which is the matter of interest in the present work.

In all the tests presented, only a single bubble was created. For the bubbles created in the spherical container, the distance between the bubble centre and the container centre d_c is evaluated from the images, numerical values are presented in Table C.1. Examples of bubble dynamics in the aquarium and in the spherical container are respectively shown in Figures C.4 and C.5. In both cases the bubble is the dark shape that is near the centre of the images. In the spherical container, the bubble is unfortunately behind a little drop of water, and a default of the container can be observed on the right of the bubble. However these problems could be overcame during the post-treatment of the images and do not affect the results. In both cases, the bubble created is non-spherical at the beginning but fairly good sphericity is attained during the growth and decay of the bubbles.

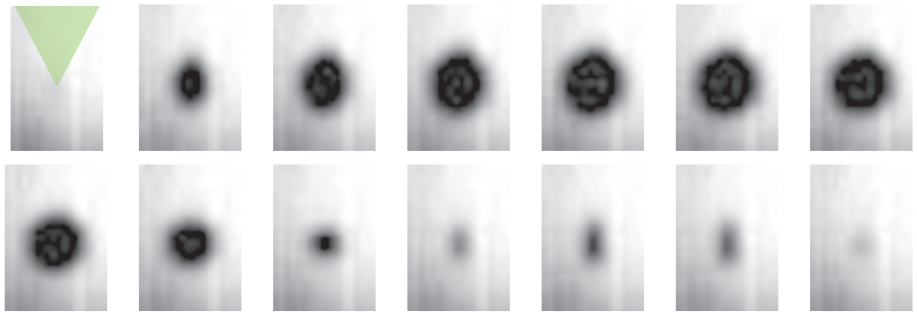

Figure C.4 – Dynamic of a vapour bubble created by optic cavitation in a large aquarium filled with water obtained with high speed camera (100000 frames per second, original images size is 128x32 pixels). The bubble is created with a 9 ns Nd:Yag laser with wavelength of 532 nm. The series starts at breakdown, the interframe is 30 μs.

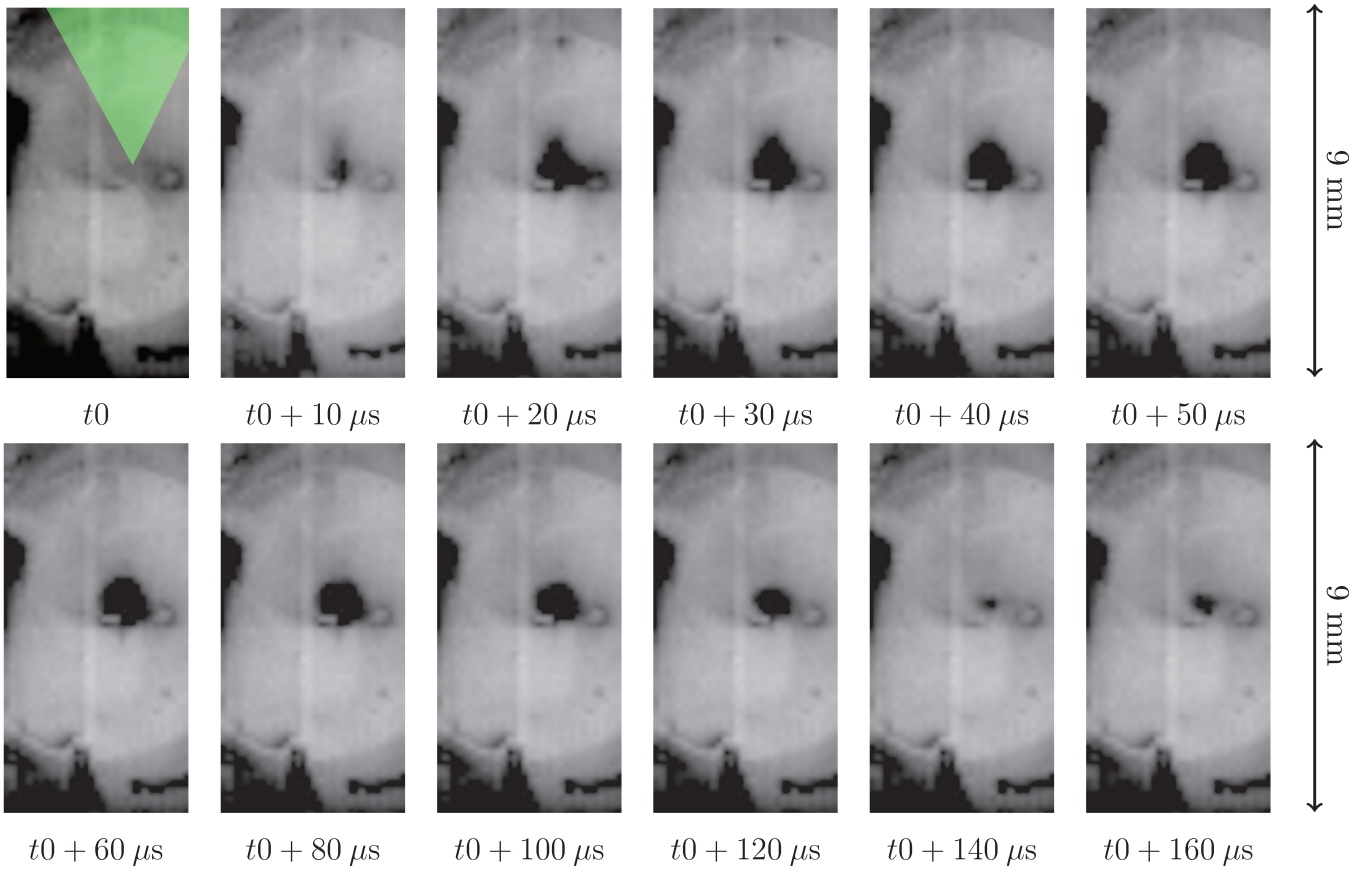

Figure C.5 – Dynamic of a vapour bubble created by optic cavitation in a spherical container of 13.1 mm internal diameter, filled with water obtained with high speed camera (100000 frames per second, original images size is 128x32 pixels). The bubble is created with a 9 ns Nd:Yag laser with wavelength of 532 nm. The series starts at breakdown.

C.2.1 Time history of bubble radius

The bubble radii are obtained from the experimental videos (see Figures C.4 and C.5), using the following method.

1. an approximated elliptic 2D projected surface is estimated to cover the dark shades on the pictures, using a tool which then calculates this surface (pix^2);
2. the measured surface is converted into mm^2, using the millimetric graduation grid. The optical distortion of the bubble images in the spherical container proved to be sufficiently low at the centre of the container (due to the meplat) that it is not possible to observe it with the images resolution, so no correction is applied to the images;
3. the measured surface is used to calculate the radius of an equivalent disc;

The experimental bubble radii are presented in Figure C.6. The bubble dynamics observed are found to be quite reproducible up to the collapse time (approximately 0.3 ms for the bubble in the aquarium and approximately 0.13 ms in the sphere). The numerical values of the maximal bubble radii and collapse time for all tests are reported in Table C.1.

The collapse time in all tests is known in an interval of 10^{-2} ms (time between two images). The bubble maximal radii obtained with the videos in the aquarium are in agreement with classic theory (C.1) in Lauterborn and Vogel (2013), the numerical values are summarised in Table C.1.

$$R_{max_{th}} = 1.09 \left(\frac{P_{stat} - P_{vap}}{\rho_l} \right)^{\frac{1}{2}} T_c \tag{C.1}$$

with R_{max} the maximal radius of the bubble, $P_{stat} = 0.1$ MPa the ambient pressure, $P_{vap} = 0.00233$ MPa the vapour pressure, ρ_l the liquid density and T_c half the collapse time.

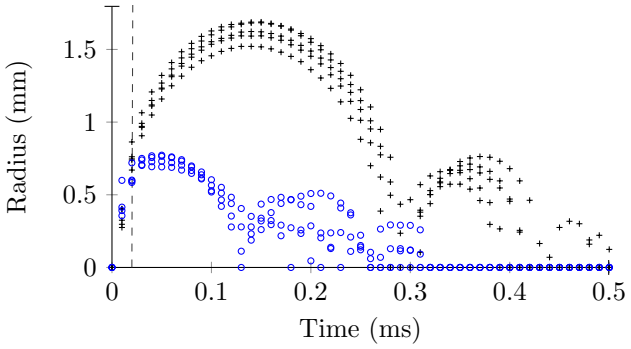

Figure C.6 – Experimental bubble radius time histories for bubbles created by optic cavitation in a 120x190x380 mm^3 aquarium (+) and in a 13.1 mm internal diameter spherical container (o).

After the collapse the bubble dynamics is not reproducible. Bubble collapse is known to be a complex and unstable phenomenon, that might lead to fission of the bubble Frost and Sturtevant (1986), that would explain the low reproducibility of the bubble dynamics after collapse. However, with the images resolution, it is not possible to observe if fission effectively occurs. In the present work, only the bubbles behaviour prior to collapse is investigated.

The bubbles created in the spherical container seem to follow the same dynamics than the one in the aquarium until approximately $t_1 = 2{\cdot}10^{-2}$ ms, then confinement effects modify the

bubble dynamics. The time for the initial shock wave to propagate and return to the bubble wall is approximately of $9{\cdot}10^{-3}$ ms, so it would appear that the time at which the bubble behaviour is modified is of the same order than the time needed for the initial shock wave to be reflected and return to the bubble wall. Then the maximal radius and collapse time of bubbles created in the spherical container are inferior to the ones obtained in the unbounded case. Contrary to bubbles created in the aquarium, the ones created in the spherical container do not respect the classic symmetry between growth and decay stages (see Figure C.6). There is small asymmetry: difference between the maximal radius time and half collapse time is approximately of 10^{-2} ms (7.5 %).

Table C.1 – Summary of the data of interest for optic cavitation tests in the aquarium and spherical container filled with water.

	Test nb	E_B (mJ)	$R_{max_{exp}}$ (mm)	$R_{max_{th}}$ (mm)	$2T_c$ (ms)	d_c (mm)
Aquarium	7	1.64 ± 0.06	1.68 ± 0.28	1.59 ± 0.02	$0.295 \pm 5{\cdot}10^{-3}$	
	8	1.49 ± 0.06	1.62 ± 0.28	1.54 ± 0.02	$0.285 \pm 5{\cdot}10^{-3}$	
	10	1.64 ± 0.06	1.69 ± 0.28	1.59 ± 0.02	$0.295 \pm 5{\cdot}10^{-3}$	
	16	1.32 ± 0.06	1.52 ± 0.28	1.48 ± 0.02	$0.275 \pm 5{\cdot}10^{-3}$	
	19	1.64 ± 0.06	1.59 ± 0.28	1.59 ± 0.02	$0.295 \pm 5{\cdot}10^{-3}$	
Sphere	4	$1.59^{+3.39}_{-1.24}$	0.73 ± 0.17		$0.135 \pm 5{\cdot}10^{-3}$	0.18
	5	$0.38^{+1.32}_{-0.33}$	0.75 ± 0.17		$0.135 \pm 5{\cdot}10^{-3}$	0.52
	17	$0.30^{+1.14}_{-0.27}$	0.70 ± 0.17		$0.125 \pm 5{\cdot}10^{-3}$	0.62
	18	$0.24^{+0.98}_{-0.22}$	0.66 ± 0.17		$0.135 \pm 5{\cdot}10^{-3}$	0.62

For non confined bubbles (here bubbles in the aquarium), the classic theory also permits to evaluate the energy that participates to the bubble growth knowing its maximal volume (C.2).

$$E_B = \frac{4\pi}{3}(P_{stat} - P_{vap})R^3_{max_{th}} \tag{C.2}$$

For confined bubbles the previous equation cannot be applied because the pressure far in the liquid does not remain constant. To estimate the bubble energy, the bubbles kinetic energy is calculated at the first instants (the potential energy in the liquid being small at the beginning of the bubble growth) recorded during the tests using (C.3). The time derivative of the bubble radius is obtained by centred finite difference method. The numerical values are reported in Table C.1.

$$E_k = 2\pi\rho\dot{R}_b^2 R_b^3 \left(1 - \frac{R_b}{R_s}\right) \tag{C.3}$$

The obtained energy numerical values are slightly inferior in the spherical container to the ones obtained for bubbles in the aquarium. It is comprehensible since the kinetic energy is calculated for the first instant available and the temporal discretisation obtained with the camera does not permit to obtain a precise estimation of bubble radius time derivative.

C.3 Conclusion

In the present study, optic cavitation tests have been done in two containers. First in a large aquarium to obtain reference data, then in a small PMMA spherical container to observe confinement effects of the container on the bubble dynamics. At the very beginning bubbles created in the small spherical container behave as the ones created in the aquarium. Then confinement effects develop and modify the behaviour of the bubbles in the spherical container: their maximum radii and collapse times are inferior to the ones of unbounded bubbles (in the aquarium). So an influence of the container on the bubble dynamics has been highlighted in these preliminary tests.

In the present work, the confinement effects of a spherical container on the dynamic of a bubble has been investigated experimentally. Laser breakdown has been chosen to generate bubbles in liquid filled containers, it bears the advantages of being easily repeatable and of leaving the liquid domain free for the bubble to develop. However this method induces difficulties due to the time scale (and low energy) at which bubbles develop compared to larger bubbles that are generated by other means (underwater explosion, spark generation, ...).

In the presented experiments the structure response could not be recorded, due to the speed of the phenomenon and to the small deformations of the container. The structure response is an important parameter for the physical comprehension of this phenomenon. The structure effects on the bubble dynamics proved to be quite important. The presence of a structure seems to break the symmetry in bubble behaviour between the growth and decay stages. It can be seen in the experimental results that the bubble response in the spherical container does not differ from the one in the aquarium from the beginning. It confirms that wave propagation (hence liquid compressibility) plays an important role in this phenomenon.

In fact for these tests the structure has been chosen quite rigid to ensure confinement effects. It would be interesting for further model validation to obtain reference data with softer structures for which the structure response would be easier to record. It would permit to obtain an experimental reference both for the bubble and structure dynamics.

Appendix D

Demonstration of the relation between κ and α

In Chapter 2 the relation between the pressure applied on the container and its deformation in the modified Rayleigh-Plesset equation has been written as (D.1) in a non-dimensional form. This led to a non dimentional parameter κ, related to the structure overall rigidity, that has been called the confinement parameter. Then, in Chapter 3, this relation has been rewritten as (D.2) to include the variation of the internal volume of the structure to obtain a more general relation (applicable to non-spherical containers), this time it was written as a dimensional equation, and the confinement parameter has been called α in this case. The relation between these two parameter is demonstrated in this appendix.

$$\frac{P_s - P_{s_0}}{P_{s_0}} = \kappa \frac{R_s - R_{s_0}}{R_{s_0}} \tag{D.1}$$

$$P_s - P_{s_0} = \alpha(V - V_0) \tag{D.2}$$

Equation (D.2) is rewritten in function of the container radius in (D.3).

$$P_s - P_{s_0} = \alpha \frac{4\pi}{3}(R_s^3 - R_{s_0}^3) \tag{D.3}$$

which can be modified as (D.4) to isolate $R_s - R_{s_0}$,

$$P_s - P_{s_0} = \alpha \frac{4\pi}{3}(R_s - R_{s_0})(R_s^2 + R_s R_{s_0} + R_{s_0}^2) \tag{D.4}$$

Then, by replacing the pressure difference in (D.4) by the one in (D.1) and by considering that $R_s = R_{s_0} + \Delta R_s$ with $\Delta R_s << R_{s_0}$, the relation (D.5) is found between κ and α.

$$\alpha = \kappa \left(\frac{1}{4\pi}\right)\left(\frac{P_{s_0}}{R_{s_0}^3}\right) \tag{D.5}$$

List of Figures

I Scénarios généraux de coups de bélier hydrodynamiques dans les cas extrêmes de non-retournement du projectile et de retournement violent du projectile. 3
II Images de la cavité créée lors de l'impact d'un projectile 7.62 mm à 850 m.s^{-1} dans la piscine hydrodynamique 8
III Image du torque d'air (en noir) observé à la fin de l'essai d'impact d'un projectile 7.62 à 850 m.s^{-1} dans la piscine hydrodynamique. 9
IV Images de la cavité créée lors de l'impact d'un projectile 7.62 mm à 850 m.s^{-1} dans le réservoir AIRBUS-Group Innovation. 9
V Description du système considéré pour prendre en compte les effets de confinement dans l'équation de Rayleigh-Plesset. 10
VI Évolution du rayon de bulle dans la piscine, expérimentale et calculée avec le modèle de Rayleigh-Plesset confiné pour plusieurs valeurs du paramètre de confinement. 14
VII Évolution du rayon de bulle dans le réservoir, expérimentale et calculée avec le modèle de Rayleigh-Plesset confiné pour plusieurs valeurs du paramètre de confinement. 14
VIII Variation du volume interne d'un quart de conteneur sphérique et de la moitié d'une plaque encastrée soumis à une pression uniforme. 16
IX Évolution du rayon de bulle expérimentale et prédite avec le modèle de Rayleigh-Plesset confiné avec α_{calib}, α_p et $\alpha = 0$ (- - -). 18
X Schéma du problème considéré dans les simulations compressibles de dynamique de bulles confinées. 20
XI Principe de maillage dans les simulations compressibles de dynamique de bulles confinées. 20
XII Rayon de la bulle en fonction du temps obtenu pour plusieurs raffinements du maillage NxMxL dans les simulations compressibles. 21
XIII Comparaison des rayon de bulles, de l'énergie cinétique du liquide et du mouvement de la paroi interne entre le modèle éléments-finis et les modèles analytiques de Keller-Miksis non-confiné et de Rayleigh-Plesset confiné. 21
XIV Comparaison des pressions dans la bulle et appliquées sur la paroi de la structure entre le modèle éléments-finis et le modèle analytique de Rayleigh-Plesset confiné. 23
XV Rayons de bulles prédits dans un réservoir de rayon interne $R_s = 1$ m et d'épaisseur 6 mm d'acier prédits avec le modèle de Keller-Miksis confiné pour plusieurs valeurs de la vitesse du son dans le liquide et prédit avec le modèle de Rayleigh-Plesset confiné. 28
XVI Rayons de bulles prédits avec le modèle de Keller-Miksis dans des réservoirs de rayons internes $R_s = 1$ m rigide et ayant différentes rigidités. 28

XVII Propagation du potentiel de vitesse initial dans le liquide (a) et variation du rayon de la structure (b), et pressions appliquées sur la structure (c) pour une bulle dans un réservoir élastique de rayon interne $R_s = 2$ m et d'épaisseur 6 mm en acier. . . 29
XVIII Rayons de bulles (a), rayons internes des réservoirs (b), pressions aux parois des structures (c) et des bulles (d) prédites en utilisant le modèle de Keller-Miksis confiné et des simulations éléments-finis dans des réservoirs de rayons internes $R_s = 1$m pour plusieurs rigidités du réservoir. 30
XIX Rayon de bulle, rayon interne du réservoir et pression à la paroi de la structure prédits en utilisant le modèle de Keller-Miksis confiné, le modèle de Rayleigh-Plesset confiné et une simulation éléments-finis dans un réservoir de rayon interne $R_s = 1$m de 6 mm d'épaisseur en acier. 31

1.1 Sketch of the stages of the hydrodynamic ram phenomenon 41
1.2 General scenario of Hydrodynamic Ram event in liquid-filled tank for extreme cases of non-tumbling and of strongly tumbling projectiles. 43

2.1 General scenarios of Hydrodynamic Ram event in liquid-filled tanks for extreme cases of non-tumbling and of strongly tumbling projectiles. 51
2.2 Picture of cavity expansion in ONERA Pool obtained with visario camera (10 000 frames per second). 53
2.3 Air ring observed at the end of the experiment in ONERA Pool obtained with a visario camera (10 000 frames per second). 54
2.4 Picture of cavity expansion in Airbus-Group Innovation caisson obtained with visario camera (10 000 frames per second). 54
2.5 Radius evolution in tank and pool tests and predicted with the Rayleigh-Plesset equation. 58
2.6 Liquid kinetic energy predicted with the Rayleigh-Plesset equation in the tank and pool and theoretical initial kinetic energy of the projectile in tank and pool tests. 58
2.7 Description of the system considered to take the confinement effect into account in Rayleight-Plesset equation. 59
2.8 Pool test: experimental radius evolution and calculated with the Rayleigh-Plesset model with confinement effect for several values of the confinement parameter. . . 61
2.9 Tank test: experimental radius evolution and calculated with the Rayleigh-Plesset model with confinement effect for several values of the confinement parameter. . . 61
2.10 Radius evolution predicted with the confined Rayleigh-Plesset model in pool with known initial pressure and air volume and without i.e. $P_b = 0$. 61
2.11 Radius evolution predicted with the confined Rayleigh-Plesset model in tank with with $P_b = P_{sat}$, $P_b = 0$ and with $P_{b_0} = P_{atm} = 0.1$ MPa. 61
2.12 Kinetic energy evolution predicted with the confined Rayleigh-Plesset model in tank with $P_b = P_{sat}$, $P_b = 0$ and with $P_{b_0} = P_{atm} = 0.1$ MPa. 62
2.13 P_s evolution predicted with the confined Rayleigh-Plesset model in tank with $P_{b_0} = P_{sat}$, $P_b = 0$ and with $P_{b_0} = P_{atm} = 0.1$ MPa. 62

3.1 General scenario of Hydrodynamic Ram event in liquid-filled tank for tumbling projectiles. 67
3.2 Picture of cavity expansion in Airbus-Group Innovation caisson obtained with a visario camera (10 000 frames per second). 69
3.3 Sketch of the system considered in the proposed confined Rayleigh-Plesset equation. 70

3.4 Radius evolution in test, predicted with non-confined Rayleigh-Plesset equation and with confined Rayleigh-Plesset with α_{calib}. 73
3.5 Variation of volume for a quarter of the structural sphere submitted to uniform internal pressure before application of the pressure and after. 74
3.6 Variation of volume for half of an embedded plate submitted to uniform pressure before application of the pressure and after. 74
3.7 Radius evolution in tank test and predicted with the confined Rayleigh-Plesset model in tank with α_{plate} and α_c. 76

4.1 Drawing of the system considered for the confined bubble dynamics simulations. . 83
4.2 Drawing of the considered problem in quasi-incompressible simulations 86
4.3 Mesh principle for the liquid medium in quasi-incompressible simulations. 86
4.4 Bubble radius vs. time results obtained with different mesh refinements in quasi-incompressible finite element simulations. 87
4.5 Comparison of bubble radius, liquid kinetic energy and movement of the internal container wall for quasi-incompressible finite element simulations and confined Rayleigh-Plesset equation. 89
4.6 Drawing of the considered problem in compressible confined bubble dynamics simulations 90
4.7 Mesh principle in compressible confined bubble dynamics simulations. 90
4.8 Bubble radius vs. Time results obtained with different mesh refinements in compressible finite element simulations. 90
4.9 Comparison of the bubbles radii, liquid kinetic energy and movement of the internal container wall for compressible finite element simulations and Keller-Miksis and the confined Rayleigh-Plesset analytical models. 92
4.10 Comparison of the pressure applied onto the structure and at the bubble interface for compressible finite element simulations and confined Rayleigh-Plesset equation. 92

5.1 Bubble radius predicted using the confined Keller-Miksis equation in a spherical rigid container (—) and predicted with the confined Rayleigh-Plesset equation in a 6 mm thick (- - -), 15 mm thick (·····) and 60 mm thick (—□—) $R_s = 1$ m steel container. 104
5.2 Bubble radius predicted using the confined Keller-Miksis equation in several spherical rigid containers of internal radius R_s. $R_s = 0.5$ m (—), $R_s = 2$ m (·····), $R_s = 5$ m (—□—), $R_s = 50$ m (—○—) and $R_s = \infty$ (—○—). 104
5.3 Propagation of the initial liquid velocity potential within the liquid (a) and correspondence with change in the pressure onto the structure (b) for a bubble in a $R_s = 2$ m rigid container. 105
5.4 Sketch of the considered problem for simulations of bubble dynamics inside a rigid container. 106
5.5 Mesh principle for simulations of bubble dynamics inside a rigid container.
5.6 Bubble radius vs time results obtained with different mesh refinements NxM: 10x159 (—), 24x318(—□—), 56x640 (—△—), 110x1280 (—◇—). 106

5.7 Bubble radius predicted using the confined Keller-Miksis equation in a $R_s = 0.5\,\mathrm{m}$ (——), $R_s = 1\,\mathrm{m}$ (- - -) and $R_s = 2\,\mathrm{m}$ (·····) rigid containers and obtained by ALE finite element simulations in $R_s = 0.5\,\mathrm{m}$ (—□—), $R_s = 1\,\mathrm{m}$ (—◇—) and $R_s = 2\,\mathrm{m}$ (—△—) spherical rigid containers. 108
5.8 Pressure at the bubble and structure interfaces predicted using Keller-Miksis equation (——) and (- - -) and obtained by ALE finite element bubble growth simulation (—□—) and (—△—). 108
5.9 Bubble radius vs. time in a $R_s = 1$ m 6 mm thick steel spherical container predicted with the confined Keller-Miksis equation with $c_l = 1500$ m.s^{-1} (—), $c_l = 2500$ m.s^{-1} (- - -), $c_l = 10000$ m.s^{-1} (—□—) and the confined Rayleigh-Plesset equation with $c_l = \infty$ (—△—). 109
5.10 Bubble radius vs. time predicted with the confined Keller-Miksis equation in $R_s =$ 1 m rigid (——), 6 mm thick steel (- - -), aluminium (·····), PMMA (—□—) spherical containers. 109
5.11 Propagation of the initial liquid velocity potential within the liquid (a) and correspondence with change in the structure internal radius (b) and in the pressure at the structure wall (c) for a $R_s = 2$ m 6 mm thick steel container. 110
5.12 Sketch of the considered problem for bubbles dynamics simulations in an elastic containers. 111
5.13 Mesh principle for bubble dynamics simulations in an elastic containers. 11
5.14 Bubble radius (a), container internal radius variation (b), pressure at structure wall (c) and at the bubble interface (d) predicted using the confined Keller-Miksis equation in $R_s = 1$m steel (——), aluminium (- - -) and PMMA (·····) containers and obtained by ALE finite element simulations in steel (—□—), aluminium (—△—) and PMMA (—◇—) containers. 113
5.15 Bubble radius (a), container internal radius variation (b) and pressure at structure wall (c) predicted in a $R_s = 1$m 6 mm thick steel container using the confined Keller-Miksis equation (——), the confined Rayleigh-Plesset equation (- - -) and obtained by ALE finite element simulations (—□—). 114

A.1 ONERA ballistic test of 7.62 mm ammunition at 850 m.s^{-1} on a generic AIRBUS-Group Innovation tank (Deletombe et al., 2011). 122
A.2 Comparison of the cavity shape between the experimental shape and mass fraction of gas calculated in the simulation. 126
A.3 Photograph taken shortly after the cavity pulled away from the surface and the simulation result at the same depth of penetration of the sphere. 127
A.4 Cavity evolution in a fluid filled tank penetration simulation (10.6 m.s^{-1}), mass fraction of gas calculated in the simulation. 128

C.1 Sketch of the experimental setup for optic cavitation experiments 134
C.2 Sketch of the PMMA sphere used in the optic cavitation experiments. 134
C.3 Millimetric grid positioned in the plexiglass spherical container and aquarium before the tests. 135
C.4 Dynamic of a vapour bubble created by optical cavitation in a large aquarium filled with water obtained with high speed camera. 136
C.5 Dynamic of a vapour bubble created by optical cavitation in a spherical container of 13.1 mm internal diameter, filled with water obtained with high speed camera. . 136

C.6 Experimental bubble radius time histories for bubbles created by optical cavitation in a 120x190x380 mm^3 aquarium and in a 13.1 mm internal diameter spherical container. 137

List of Tables

I Valeurs numériques des conditions initiales utilisées pour les simulations des coups de bélier hydrodynamiques avec l'équation de Rayleigh-Plesset confinée. 13
II Variation de volume autorisée par les plaques pour une variation de pression de 1 MPa. 17
III Informations sur les modèles et performances des calculs compressibles sur un calculateur Intel® Ivy-Bridge E5-2667v2 ayant une fréquence d'horloge de 3.3 GHz. 22

2.1 Numerical values of the initial conditions used for Rayleigh-Plesset simulations of HRAM events. 57
2.2 Numerical values of the initial conditions used for confined Rayleigh-Plesset simulations of HRAM events. 60

3.1 Numerical values of the initial conditions used for the tank case in confined Rayleigh-Plesset simulations. 72
3.2 Numerical values used for the calculation of the coefficient α_s for a V =0.3x0.54x0.66 m^3 tank (see Airbus-Group Innovation tank). 73
3.3 Variation of volume authorised by the plates with respect to 1 MPa variation of pressure. 75

4.1 Material numerical values used in the simulations. 87
4.2 Model features and calculation performances on Intel® Ivy-Bridge E5-2667v2 processors clocked at 3.3 GHz. 88
4.3 Model features and calculation performances on Intel® Ivy-Bridge E5-2667v2 processors clocked at 3.3 GHz. 91

5.1 Model features and calculation performances on Intel® Ivy-Bridge E5-2667v2 processors clocked at 3.3 GHz. 107
5.2 Material numerical values used in the simulations. 111

A.1 Numerical values used for the water entry simulation 125

B.1 Numerical values of liquids thermal properties at the studied temperature (Part 1). 130
B.2 Numerical values of liquids thermal properties at the studied temperature (Part 2). 130
B.3 Numerical values of ΔT and Σ for the different liquids at the studied temperature. 131

C.1 Summary of the data of interest for optic cavitation tests in the aquarium and spherical container filled with water. 138

Bibliography

Handbook of aviation fuel properties. Technical Report ADA132106, Coordinating Research Council, 1983.

S. Abrate. Hull slamming. *Applied Mechanics Reviews*, 64(6):1003–1037, November 2011.

J. Aldred. *Manual of Sound Recording*. Fountain Press, London, 1972.

C.E. Anderson, T.R. Sharron, J.D. Walker, and C.J. Freitas. Simulation and analysis of a 23-mm hei projectile hydrodynamic ram experiment. *International Journal of Impact Engineering*, 22:981–997, 1999.

J.A. Artero-Guerrero, J. Pernas-Sánchez, D. Varas, and J. López-Puente. Numerical analysis of cfrp fluid-filled tubes subjected to high-velocity impact. *Composite Structures*, 96:286–297, 2013.

H. Ashley and G. Zartarian. Piston-theory–a new aerodynamic tool for the aeroelastician. *Journal of the Aeronautical Sciences*, 23:1109, 1956.

R.E. Ball. *Aircraft fuel tank vulnerability to hydraulic ram: modification of the Northrup finite element computer code BR-1 to include fluid-structure interaction. Theory and user manual for BR-1*, July 1974.

R.E. Ball. Structural response of fluid containing tank to penetrating projectiles (hydraulic ram) - a comparison of experimental and analytical results. Technical Report NPS-57Bp75101, Naval Postgraduate School, 1976.

R.E. Ball. *The fundamental of aircraft combat survability analysis and design*. AIAA, 1985.

G. Barras, M. Souli, N. Aquelet, and N. Couty. Numerical simulation of underwater explosions using an ale method. the pulsating bubble phenomena. *Ocean Engineering*, 41:53–66, 2012.

S.J. Bless. Fuel tank survivabilty for hydrodynamic ram induced by high-velocity fragments. part i experimental result and desigh summary. Technical Report AFFDL-TR-78-184, Part I, University of Dayton Research Institute, 1979.

S.J. Bless, J.P. Barber, P.F. Fry, and Newman R.K. Studies of hydraudynamic ram induced by high velocity spherical fragment simulator. Technical Report AFML-TR-77-11, University of Dayton Research Institute, Dayton, Ohio, USA, 1976.

C.E. Brennen. *Cavitation and bubble dynamics*. Oxford University Press, 1995.

A. Caleyron, A. COmbescure, V. Faucher, and S. Potapov. Sph modeling of fluid-solid interaction for dynamic failure analysis of fluid-filled thin shells. *Journal of Fluids ans Structures*, 39:126–153, 2013.

G.L. Chahine and R. Duraiswami. Boundary element method for calculating 2-d and 3-d underwater explosion bubble behaviour in free water and near structures. Technical Report NSWCDD/TR-83/44, NSWC Weapons Research an Technology Department, 1994.

R.B. Chapman and M.S. Plesset. Thermal effects in the free oscillation of gas bubbles. *ASME J. Basic Eng.*, 93:373–376, 1971.

A. Charles, E. Deletombe, and J. Dupas. A numerical study on cavity expansion in water : Hydraulic ram under ballistic impacts. In *International Conference on Structures Under Shock and Impact*, Kos, Greece, September 2012.

R.H. Cole. *Underwater Explosions*. Priceton University Press, Priceton, 1945.

V. Coralic and T. Colonius. Shock-induced collapse of a bubble inside a deformable vessel. *European Journal of Mechanics - B\Fluids*, 40:64–74, 2013.

E. Deletombe and B. Malherbe. Fluid-structure simulation of hydraulic ram pressure in fuel tanks. In Civil-Comp Press, editor, *Advances in computational Structural Mechanics*, pages 271–281, Edinburgh, Scotland, 1998.

E. Deletombe, D. Delsart, J. Dupas, J.L. Charles, and J.F. Sobry. Methodology for f.e. resolution of coupled fluid/structure problems. In *International Crashworthiness and Design Symposium 2003*, 2003.

E. Deletombe, J. Fabis, and J. Dupas. Vulnerability of a/c fuel tanks with respect to hydrodynamic ram pressure. interpretation of 7.62 mm experiments. In *Colloque National en Calcul des Structures (CSMA)*, Giens, France, 2011.

E. Deletombe, J. Dupas, and T. Fourest. Numerical optimisation of composite fuel tanks subject to a 7.62 mm bullet hydraulic ram event using a loose fluid/structure coupling scheme. In *ECCOMAS*, Bourges, France, 2012.

E. Deletombe, J. Fabis, J. Dupas, and J.M. Mortier. Experimental analysis of 7.62 mm hydrodynamic ram in containers. *Journal of Fluids and Structures*, 37:1–21, 2013.

P.J. Disimile, L.A. Swanson, and N. Toy. The hydrodynamic ram pressure generated by spherical projectiles. *International Journal of Impact Engineering*, 36(6):821–829, 2009.

T. Fourest, J. Dupas, E. Deletombe, J.-M. Laurens, and M. Arrigoni. Study of the capabilities of an ale bi-material fluid simulation for solving cavity expansion and collapse during an hydrodynamic ram event. In $13^{ème}$ *Colloque national en calcul des strutures*, May 2013.

T. Fourest, J.-M. Laurens, E. Deletombe, J. Dupas, and M. Arrigoni. Analysis of bubbles dynamics created by hydrodynamic ram in confined geometries using the rayleigh-plesset equation. *International Journal of Impact Engineering*, 73:66–74, 2014.

T. Fourest, J.-M. Laurens, E. Deletombe, M. Arrigoni, and J. Dupas. Cross validation of analytical and finite element models of hydrodynamic ram loads prediction in liquid filled thin-walled containers. *Journal of Fluids and Structures*, 59:285–296, 2015a.

T. Fourest, J.-M. Laurens, E. Deletombe, M. Arrigoni, and J. Dupas. Développement et validation de modêles de dynamique de bulles confinées pour la simulation du coup de bélier hydrodynamique dans les réservoirs de carburants. *Comptes Rendus Mecanique*, 2015b. (submitted).

T. Fourest, J.-M. Laurens, E. Deletombe, J. Dupas, and M. Arrigoni. Confined rayleigh-plesset equation for hydrodynamic ram analysis in thin-walled containers under ballistic impacts. *Thin− Walled Structures*, 86:67–72, 2015c.

T. Fourest, J.-M. Laurens, V. Faucher, E. Deletombe, M. Arrigoni, and J. Dupas. Development and validation of a confined keller-miksis model for hydrodynamic ram loads prediction in liquid-filled containers. *Journal of Fluid Mechanics*, 2015d. (submitted).

J.P. Franc. The rayleigh-plesset equation: a simple and powerfull tool to understand various aspects of cavitation. *Fluid dynamics of cavitation and cavitating turbopumps, CISM Courses and lectures*, 496:1–41, 2007.

J.P. Franc, F. Avellan, B. Belahadji, J.Y. Billard, L. Brianǫn Marjollet, D. Fréchou, D.H. Fruman, A. Karimi, J.L. Kueny, and J.M. Michel. *La Cavitation, mécanisme*. Presse Universitaire de Grenoble, Grenoble, France, 1995.

D. Frost and B. Sturtevant. Effects of ambient pressure on the instability of a liquid boiling explosively at the superheat limit. *ASME Journal of Heat Transfer*, 108:418–424, 1986.

J. Fujikawa, T. Akamatsu, J. Yahara, and H. Fujioka. Studies of liquid-vapour phase change by a shock tube. *Applied Scientific Research*, 38:363–372, 1982.

S. Fujikawa and T. Akamatsu. Effects of the non-equilibrium condensation of vapour on the pressure wave produced by the collapse of a bubble in liquid. *Journal of Fluid Mechanics*, 97(03):481–512, 1980.

D. Fuster, G. Hauke, and C. Dopazo. Parametric analysis for a single collapsing bubble. *Flow Turbulence Combus*, 82:25–46, 2009.

D. Fuster, C. Dopazo, and G. Hauke. Liquid compressibility effects during the collapse of a single cavitation bubble. *J. Acoust. Soc. Am.*, 129(1), 2011.

F.R. Gilmore. The growth or collapse of a spherical bubble in viscous compressible liquid. Technical Report 26-4, California Institute of Technology, 1952.

R.A. Gingold and J.J. Monaghan. Smoothed particle hydrodynamics: Theory and application to non-spherical stars. *Monthly notices of the royal astronomical society*, 181:375–389, 1977.

D.E. Grady. *Fragmentation of Rings and Shells*. Springer, 2006.

M. Grazia De Giorgi, D. Bello, and A. Ficarella. Analysis of thermal effects in a cavitating orifice using rayleigh equation and experiments. *Journal of Engineering for Gas Turbines and Power*, 132(9), 2010.

G. Hauke, D. Fuster, and C. Dopazo. Dynamics of a single cavitating and reacting bubble. *Physical review*, 2007.

N.W. Jang, S.M. Gracewski, B. Abrahamsen, T. Buttaccio, R. Halm, and D. Dalecki. Natural frequency of a gas bubble in a tube: Experimental and simulation results. *Journal of the Acoustical Society of America*, 126(1):EL34–EL40, July 2009.

J.E. Jensen, W.A. Tuttle, R.B. Stewart, H. Brechna, and A.G. Prodell. Brookhaven national laboratory selected cryogenic data notebook, volume i, section i-ix. Technical Report BNL 10200-R, Vol. I, Brookhaven National Laboratory, 1980.

E. Johnsen and T. Colonius. Numerical simulations of non-spherical bubble collapse. *Journal of Fluid Mechanics*, 629:231–262, juin 2009.

J.B. Keller and I.I. Kolodner. Damping of underwater explosion bubble oscillations. *Journal of Applied Physics*, 27(10), 1956.

J.B. Keller and M. Miksis. Bubble oscillations of large amplitude. *J. Acoust. Soc. Am.*, 68: 628–633, 1980.

K.D. Kimsey. Numerical simulation of hydrodynamic ram. Technical Report ARBRL-TR-02217, US Army Ballistic Research Laboratory, Aberdeen, Maryland, USA, 1980.

A.A Korobkin. Blunt-body penetration into a slightly compressible liquid. *In: Proceedings of 20th Symposium on Naval Hydrodynamics*, 3:179–186, 1994.

W. Lauterborn and H. Bolle. Experimental investigations of cavitation-bubble collapse in the neighbourhood of a solid boundary. *Journal of Fluid Mechanics*, 72(Part 2), 1975.

W. Lauterborn and A. Vogel. Shockwave emission by laser generated bubbles. *SHOCKWAVES*, 8:67–103, 2013.

S.M. Lawrence and K. Kyekyoon. Motion of a gas bubble inside a spherical liquid container with a vertical temperature gradient. *Journal of fluid Mechanics*, 176:521–531, 1986.

N. Lecysyn, A. Bony-Dandrieux, L. Aprin, F. Heymes, P. Slangen, G. Dusserre, L. Munier, and C. Le Gallic. Experimental study of hydraulic ram effects on a liquid storage tank: Analysis of overpressure and cavitation induced by a high-speed projectile. *Journal of hazardous materials*, 178(1):635–643, 2010.

Nicolas Lecysyn, Aurélia Dandrieux, Frédéric Heymes, Laurent Aprin, Pierre Slangen, Laurent Munier, Christian Le Gallic, and Gilles Dusserre. Ballistic impact on an industrial tank: Study and modeling of consequences. *Journal of hazardous materials*, 172(2):587–594, 2009.

M. Lee, R.G. Longoria, , and D.E. Wilson. Cavity dynamics in high-speed water entry. *Physics of FLuids*, 9(3):540–550, 1997a.

M. Lee, R.G. Longoria, and D.E. Wilson. Ballistic waves in high-speed water entry. *Journal of Fluids and Structures*, 11:819–844, 1997b.

T.G. Leighton. The inertia terms in equations of motion for bubbles in tubular vessels or between plates. *Journal of the Acoustical Society of America*, 130(50):3333–3338, November 2011.

E.A. Lundstrom. Fluid dynamic analysis of hydrolic ram. Technical Report NWC TP 5227, Naval Weapons Center, China Lake, California, USA, 1971.

E.A. Lundstrom. Fluid/structure interaction in hydrolic ram. In *Proceedings of the Hydrodynamic Ram seminar*, pages 223–230, May 1977.

A. May. Vertical entry of missiles into water. *Journal of applied physics*, 23(12), 1952.

J.H. McMillen. Shock wave pressure in water produced by impact of small sphere. *Physical review*, 46(9), 1945.

J.H. McMillen and E.N Harvey. A spark shadowgraphic study of body waves in water. *Journal of Applied Physics*, 17(7), 1946.

J.J. Monaghan and R.A. Gingold. Shock simulation by the particle method {SPH}. *Journal of Computational Physics*, 52(2):374 – 389, 1983. ISSN 0021-9991.

C.R. Morse and F.S. Stepka. Effect of projectile size and material on impact fracture of walls of liquid-filled tanks. Technical Report TN D-3627, NASA, Cleveland, Ohio, USA, 1966.

N.F. Mott. Fragmentation of shell cases. *Proceedings of the Royal Society*, A189(300–308), 1947.

J. Noack and A. Vogel. Laser-induced plasma formation in water at nanosecond to femtosecond time scales: Calculation of thresholds, absorbtion coefficients, and energy density. *Journal of quantum electronics*, 35(8):1156–1167, 1999.

D. Obreschkow, P. Kobel, N. Dorsaz, A. de Bosset, C. Nicollier, and M. Farhat. Cavitation bubble dynamics inside liquid drops in microgravity. *Physical Revue Letter*, 97, 2006.

H.N. Oguz and A. Prosperetti. The natural frequency of oscillation of gas bubbles in tubes. *Journal of the Acoustical Society of America*, 1998.

A. Philipp and W. Lauterborn. Cavitation erosion by single laser-produced bubbles. *Journal of Fluid Mechanics*, 361:75–116, 4 1998. ISSN 1469-7645.

M.S. Plesset. The dynamics of cavitation bubbles. *Journal of applied mechanics*, 16:277–282, 1949.

M.S Plesset and R.B. Chapman. Collapse of an initially spherical vapor cavity in the neighbourhood of a solid boundary. *Journal of Fluid Mechanics*, 47:283–290, 1971.

S. Popinet and S. Zaleski. Bubble collapse near a solid boundary: a numerical study of the influence of viscosity. *Journal of Fluid Mechanics*, 464, 8 2002.

A. Prosperetti and A. Lezzi. Bubble dynamics in a compressible liquid. part 1. first order theory. *Journal of Fluid Mechanics*, 168:457–478, 1986.

L. Rayleigh. On the pressure developed in a liquid during the collapse of a spherical cavity. *Philosophical Magazine Series 6*, 34(200):94–98, 1917.

E. Reissner. On the theory of bending of elastic plates. *Journal of Mathematics and Physics*, 23(184), 1944.

RTP 3.32. Euclid contract-B-00009 EUROPA-TA-103.091.

A.K. Sareen and M.R. Smith. Evaluation of an analytical tool for ballistic dynamics simulation. In *MSC User's Conference*, 1996.

M. Sauer. Simulation of high velocity impact in fluid-filled containers using finite elements with adaptive coupling to smoothed particle hydrodynamics. *International Journal of Impact Engineering*, 38:511–520, 2010.

Y.-M Scolan and A.A Korobkin. Energy distribution from vertical impact of a three-dimensional solid body onto the flat free surface of an ideal fluid. *Journal of Fluids and Structures*, 17 (2):275–286, 2003.

J.E. Shepherd, J.C. Krok, and Lee J.J. Jet a explosion experiements: Laboratory testing. Technical Report FM97-5, Graduate Aeronautical Laboratories, California Institute of Technology, 1997.

J.E. Shepherd, C.D. Nuyt, and Lee J.J. Flash point and chemical composition of aviation kerosene (jet a). Technical Report FM99-4, Graduate Aeronautical Laboratories, California Institute of Technology, 2000.

H.H. Shi and M. Itoh. High-speed photography of supercavitation and multiphase flows in water entry. In *Proceedings of the 7th International Symposium on Cavitation*, Ann Arbor, Michigan, USA, August 2009.

H.H. Shi and M. Kume. An experimental research on the flow field of water entry by pressure measurements. *Physics of fluid*, 13(1), 2001.

H.H. Shi and M. Kume. Underwater acoustics and cavitating flow of water entry. In *ACTA MECHANICA SINICA*, volume 20, 2004.

H.H. Shi and T. Takami. Hydrodynamic behavior of underwater moving body after water entry. In *ACTA MECHANICA SINICA*, volume 17, pages 35–44, 2001.

H.H. Shi, M. Itoh, and T. Takami. Optical observation of the supercavitation induced by high-speed water entry. In *ASME Journal of Fluids Engineering*, volume 122, pages 806–810, 2000.

M. Souli, A. Ouahsine, and L. Lewin. Ale formulation for fluid−structure interaction problems. *Computer Methods in Applied Mechanics and Engineering*, 190(5-7):659–675, 2000.

F.S. Stepka. Projectile-impact-induced fracture of liquid-filled, filament-reinforced plastic or aluminium tanks. Technical Report TN D-3456, NASA, Cleveland, Ohio, USA, 1966.

F.S. Stepka and C.R. Morse. Preliminary investigation of catastrophic fracture of liquid-filled tanks impacted by high velocity particles. Technical Report D-1537, NASA, Cleveland, Ohio, USA, 1963.

F.S. Stepka, R.P. Dengler, and C.R. Morse. Investigation of catastrophic fracturing and chemical reactivity of liquid-filled tanks when impacted by projectiles of high velocity. Technical Report TM x-52063, NASA, Cleveland, Ohio, USA, 1964.

F.S. Stepka, C.R. Morse, and R.P. DengZey. Investigation of the characteristics of pressure waves generated in water filled tanks impactes by high-velocity projectiles. Technical Report TN D-3143, NASA, Cleveland, Ohio, USA, 1965.

P. Thevenet. Impact balistique d'une balle otan 7.62 sur réservoir : expérimentation et simulation du coup de bélier. In *19 ème Congrès Français de Mécanique*, 2009.

A.-L. Tilhac, E. Deletombe, and J. Dupas. Aircraft fuel tank design against hydrolic ram - an optimisation exercise. In *22th Military aspects of Blast and Shock Conference*, Bourges, France, 2012.

S. Timoshenko and S. Woinowsky-Krieger. *Theory of plates and shells*. McGraw-Hill Book Company, 1959.

D. Varas. *Estudio experimental y numerico del comportamiento de tanques integrados de combustible frente a impacto de alta velocidad*. PhD thesis, Universidad Carlos III de Madrid, 2009.

D. Varas, R. Zaera, and J. López-Puente. Experimental analysis of fluid-filled aluminium tubes subjected to high-velocity impact. *International Journal of Impact Engineering*, 36:81–91, 2009a.

D. Varas, R. Zaera, and J. López-Puente. Numerical modelling of the hydrodynamic ram phenomenon. *International Journal of Impact Engineering*, 36:363–374, 2009b.

D. Varas, J. López-Puente, and R. Zaera. Numerical analysis of the hydrodynamic ram phenomenon in aircraft fuel tanks. *AIAA JOURNAL*, 50(7):1621–1630, 2012a.

D. Varas, R. Zaera, and J. López-Puente. Numerical modelling of partially filled aircraft fuel tanks submitted to hydrodynamic ram. *Aerospace Science and Technology*, 16:19–28, 2012b.

V. Venugopalan, A. Guerra, K. Nahen, and Vogel A. Role of laser-induced plasma formation in pulsed cellular microsurgery and micromanipulation. *Physical revue letters*, 88(7), 2002.

A. Vogel. Nonlinear absorption: intraocular microsurgery and laser lithotripsy. *Physics in Medicine and Biology*, 42:895–912, 1997.

Q.X. Wang and J.R. Blake. Non-spherical bubble dynamics in a compressible liquid part 1. travelling acoustic wave. *Journal of Fluid Mechanics*, 659:191–224, 2010.

J.E. Woodrow and Seiber J.N. The laboratory characterisation of fuel vapor under simulated flight conditions. Technical Report NTSB12-97-SP-0255, Center dor Environemental Sciences and Engineering, 1997.

Development and validation of bubble dynamics models for Hydrodynamic Ram event in fuel tanks simulations

The context of the thesis consists of improving the knowledge and the predictions of hydrodynamic loads applied on fuel tanks during ballistic impacts (Hydrodynamic Ram) to improve the survivability of aircraft structures. The most advanced numerical models still cannot simulate the entire phenomenon. Moreover, these models are too expensive to be used for optimisation or for design purposes during the tank development stage. The proposed study consists of developing an analytical model capable of simulating the expansion and collapse of the cavitation bubble and to use it to determine the parameters that influence the consecutive hydrodynamic loads.

The state of the art hydrodynamic ram problem is first presented. In the second chapter, the Rayleigh-Plesset model is modified to include the stiffness effect of a spherical container on the described bubble dynamics, when neglecting the presence of the bubble gas on the hydrodynamic loads. This model is applied to hydrodynamic ram test cases, by calibrating a confinement parameter which is related to the structure rigidity. The next step, presented in the third chapter evaluates the capacity of an elastic linear analytical model (plate formulae) to provide the value of the confinement parameter. A good agreement is found with the calibrated value in the previous chapter, which validates the method to get this parameter and suppress the need for experimental calibration. In the fourth chapter, the incompressible Rayleigh-Plesset model is compared to explicit finite element simulations to determine the influence of the liquid compressibility and structural inertia on the dynamics of confined bubbles. Then, in the fifth chapter an analytical model for confined bubbles in a compressible liquid is developed. A formulation based on the Keller-Miksis model is proposed. The relevance of this model is verified and it is validated again with respect to finite element simulations. Then the improvement of hydrodynamic loads predictions using this model is estimated by comparison with the Rayleigh-Plesset model. Finality a critical analysis of the thesis work and some outlooks are given.
Keywords: Hydrodynamic ram, Rayleigh-Plesset equation, Finite element simulations

---

Développement et validation de modèles de dynamique de bulles pour la simulation du coup de bélier hydrodynamique dans les réservoirs de carburants

La thèse s'inscrit dans un axe de recherche visant à améliorer les connaissances et prédictions des chargements hydrodynamiques subis par les réservoirs de carburant lors d'impacts balistiques (coup de bélier hydrodynamique) pour améliorer la survivabilité de la structure. Les modèles numériques les plus avancés ne permète toujours pas de simuler le phénomène complet. De plus les modèles développés sont trop coûteux pour être utilisés lors d'optimisations de réservoirs durant la phase de conception. L'étude proposée consiste à développer un modèle analytique capable de simuler la séquence d'expansion et d'éfondrement de la bulle de cavitation et d'utiliser ce modèle pour déterminer les paramètres influant sur les chargements hydrodynamiques lors de coups de bélier hydrodynamiques.

La problématique du phénomène de coup de bélier hydrodynamique et l'état de l'art sont présentés dans le premier chapitre du mémoire. Dans le deuxième chapitre, le modèle de Rayleigh-Plesset est modifié pour prendre en compte l'effet de confinement d'un réservoir sphérique sur la dynamique d'expansion de la bulle en négligeant la présence du gaz dans la cavité dans les prédictions des chargements hydrodynamiques. Ce modèle a été appliqué à des cas expérimentaux de coup de bélier, en calibrant un paramètre de confinement lié à la rigidité de la structure. L'étape suivante, présentée dans le troisième chapitre, consiste à évaluer la capacité d'un modèle analytique linéaire élastique (de type plaque) à estimer la valeur du paramètre de confinement. Un bon accord est trouvé entre cette valeur et celle calibrée précédemment, ce qui valide la méthode d'estimation de ce paramètre et supprime la nécessité de la calibration expérimentale. Dans le quatrième chapitre le modèle incompressible de Rayleigh-Plesset est comparé à des simulations explicites éléments finis pour déterminer les effets de l'inertie de la structure et de la compressibilité du liquide sur la dynamique des bulles confinées. Enfin dans le cinquième chapitre un modèle analytique de dynamique de bulles confinées, dans un liquide compressible, est développé et validé. Pour cela une formulation basée sur l'équation de Keller-Miksis est proposée. La pertinence de ce modèle est vérifiée puis il est validé par rapport à des simulations éléments finis, ce qui permet d'estimer l'amélioration apportée par le modèle de Keller-Miksis dans la prédiction des chargements hydrodynamiques par comparaison au modèle de Rayleigh-Plesset. Finalement une analyse critique du travail de thèse et des perspectives sont donnés.

Mots-clés : Coup de bélier hydrodynamique, équation de Rayleigh-Plesset, Simulations éléments finis